

Kapitel 4: Gasturbine

1. Beschreibung des Gasturbinenprozesses
2. Flugtriebwerk
3. Gasturbinenkühlung
4. Variation des GT-Prozesses mit IPSEpro
5. STIG und HAT Gasturbine
6. A Study of Humidified Gas Turbines for Short-Term Realization in Midsized Power Generation – Part 1
7. Gas Turbine Inlet Cooling (GTW-Handbook 2010)
8. Heavy Duty vs. Aeroderivative
9. Gas Turbine Combustion
10. Market Drivers of Electric Power Gas Turbines: Reasons for the Revolution
11. Simple Cycle Prices (GTW Handbook 2016-17)
12. Gas Turbine Models (GTW Handbook 2016-17)
13. GE Power Systems Gas Turbine Products
14. LMS100: 46 % in Simple Cycle
15. First H System Gas Turbine Planned for Baglan
16. GE: New Air-Cooled H-Class
17. Mercury 50 introduces high efficiency recuperation to stationary gas turbines
18. Alstom Gas Turbines
19. Alstom GT24/GT26 Technology
20. Siemens SGT5-8000H
21. Alstom/Siemens Gasturbinen: Daten
22. Performance Benefits Using Siemens Advanced Compressor Cleaning System
23. Mikrogasturbine
24. State of direct fuel cell/turbine systems development (2004)
25. Performance comparison of three solid oxide fuel cell power systems (2013)
26. An optimal configuration for a solid oxide fuel cell-gas turbine (SOFC-GT) hybrid system based on thermo-economic modelling (2017)



Institute for
Thermal Turbomachinery
and Machine Dynamics



Graz University of Technology
Erzherzog-Johann-University

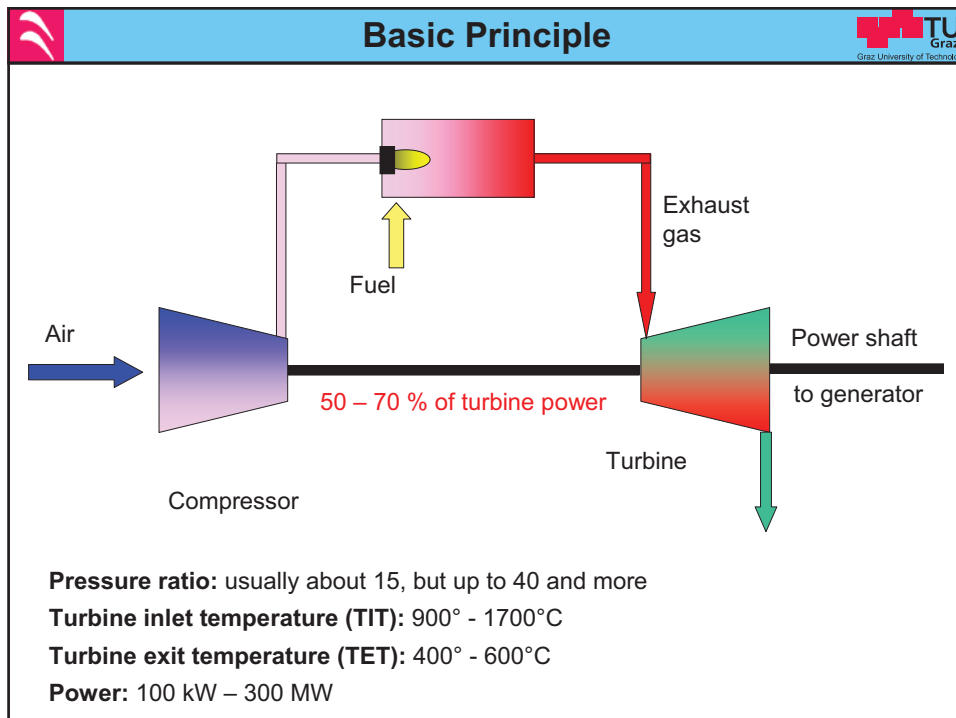
Gas Turbine Technology

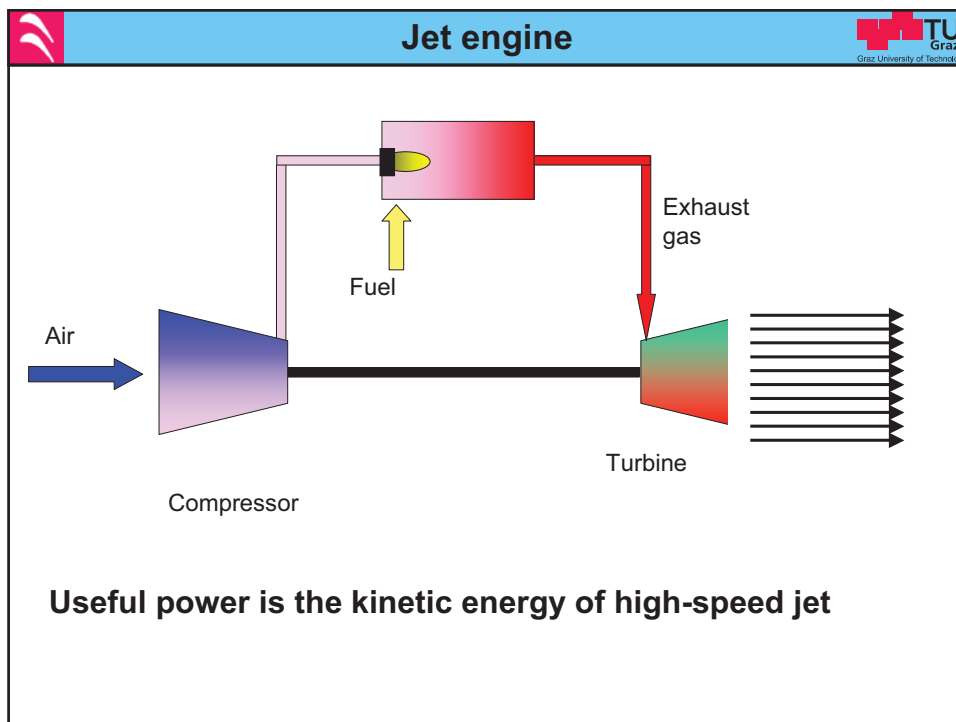
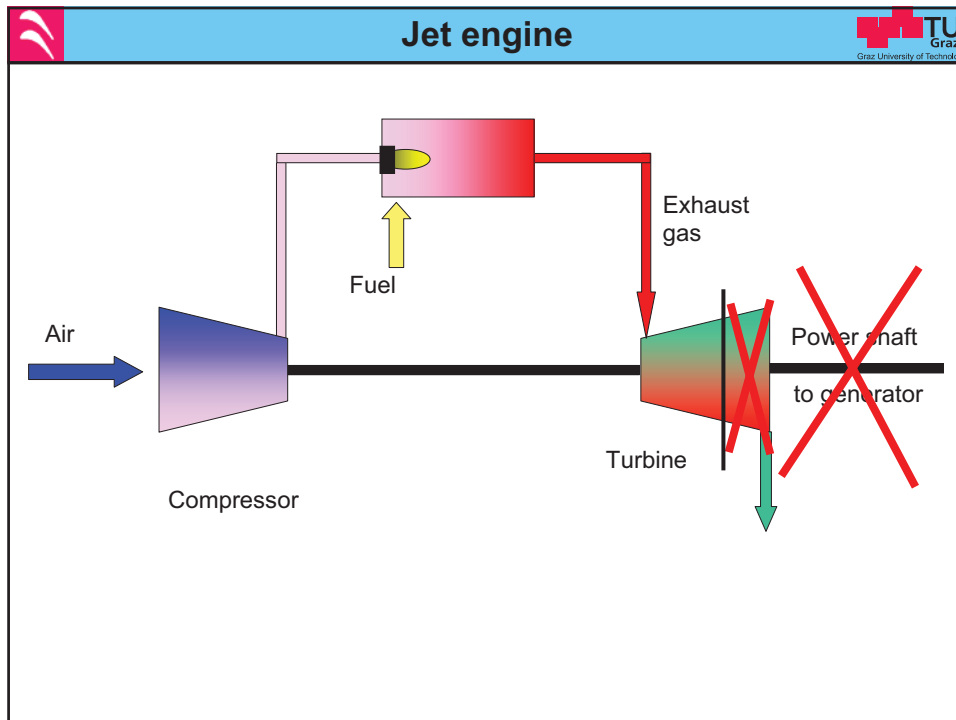
Lecture at the
Department of Aerospace Engineering
Middle East Technical University
Ankara, April 2008

Wolfgang Sanz

Institute for Thermal Turbomachinery and Machine Dynamics
Graz University of Technology
Austria

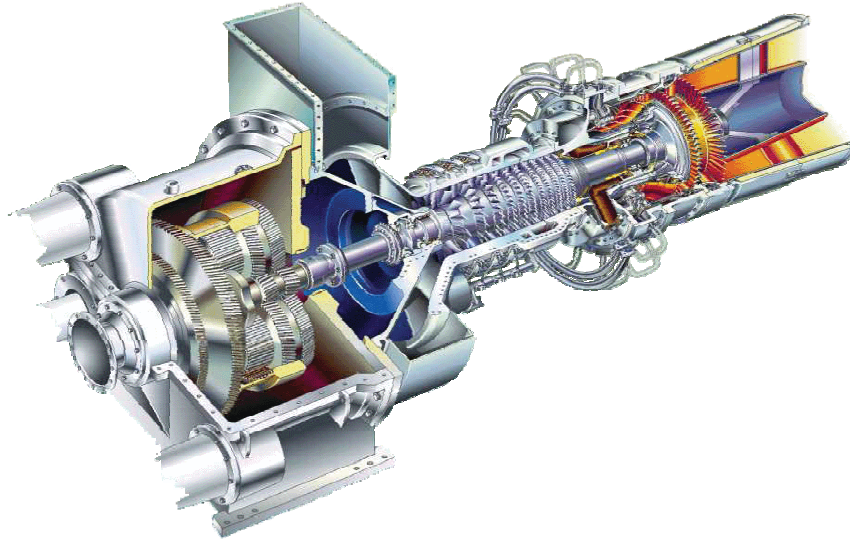
>>MIDDLE EAST TECHNICAL UNIVERSITY



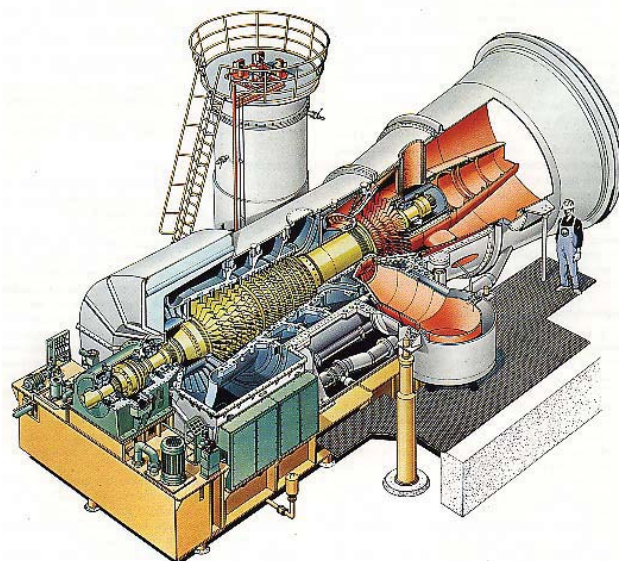




Stationary Gas Turbine



Stationary Gas Turbine

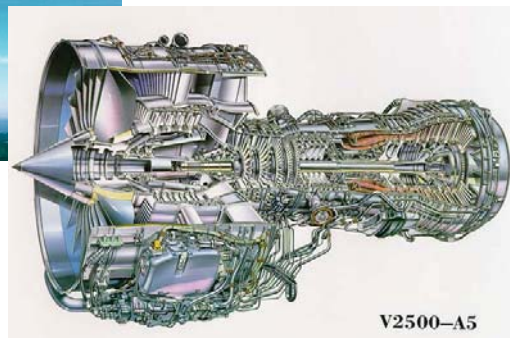


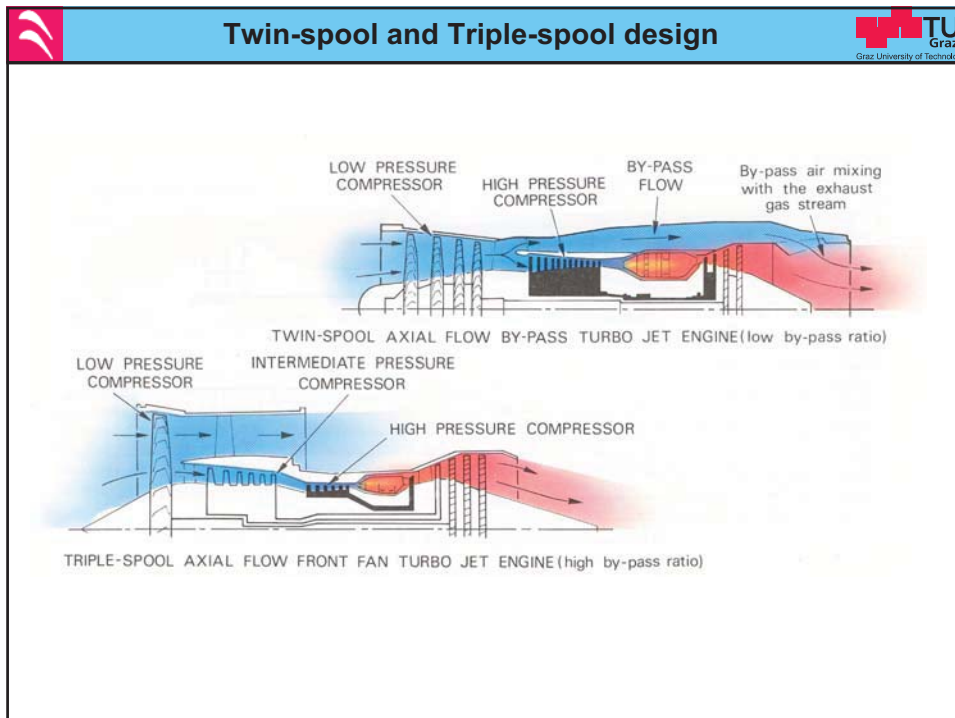



Silo-type combustion chamber




Aero Engine








Gas turbine history



- 18th century: First patents of John Barber, Dumpell and Bresson
- 1902: Moss (USA) built a gas turbine with „negative“ output
- 1904: Stolze (Germany) hot air turbine, not successful
- In 1930s: heat resistant steels, aerodynamic knowledge -> modern design
- In Switzerland Escher-Wyss, BBC and Sulzer built gas turbines up to 20 MW power with TIT of 650°C
- Strong impetus from the development of jet engines during and after WWII
- Since 1950: jet engine became dominant propulsion system
- Since 1960: strong development of stationary gas turbines, at the beginning mostly modified jet engines

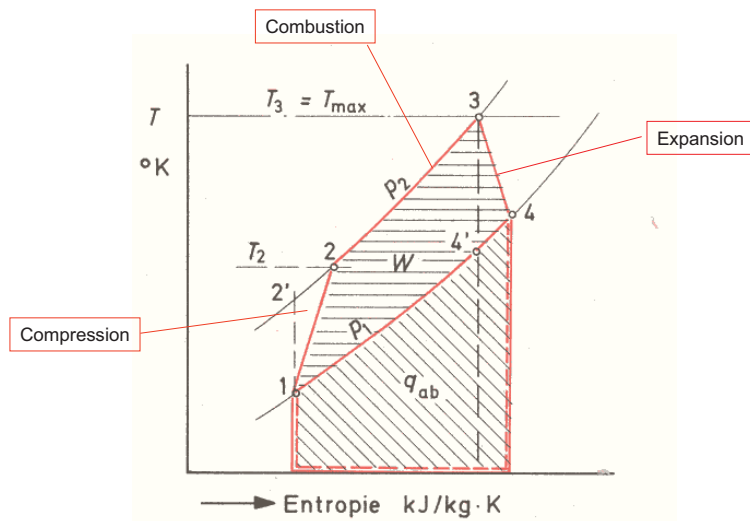


The world's first industrial gas turbine set – Neuchatel, Switzerland (1939-2002)

Source: Alstom



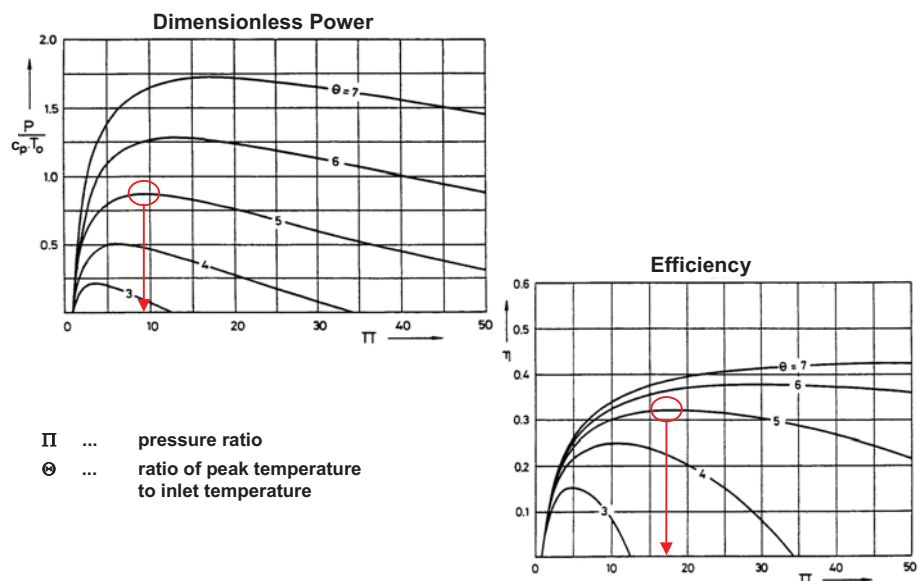
T-s diagram of gas turbine process

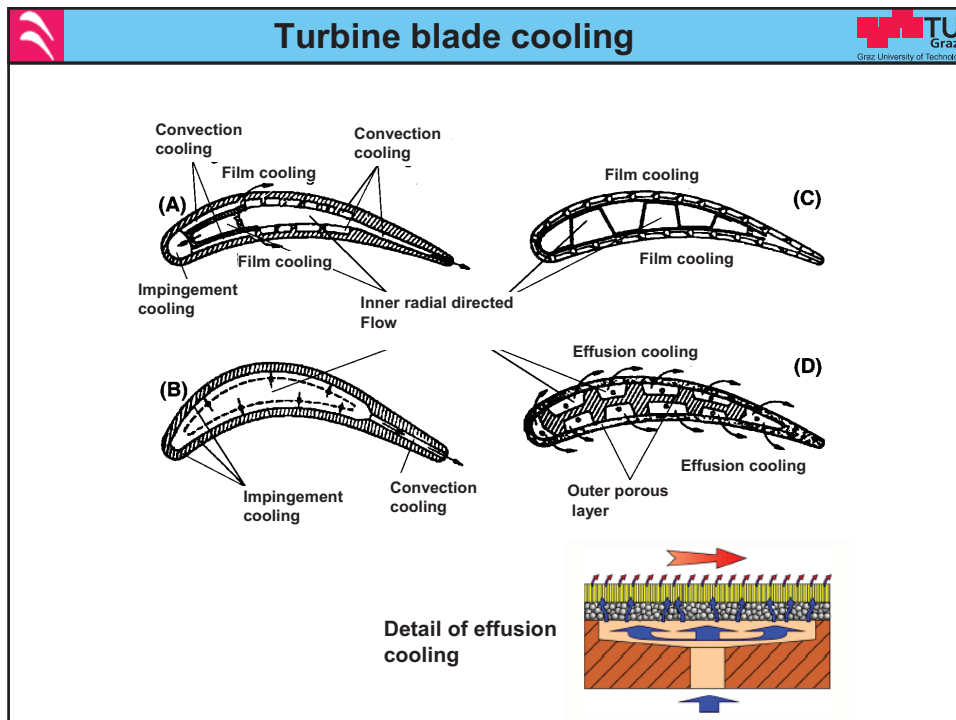
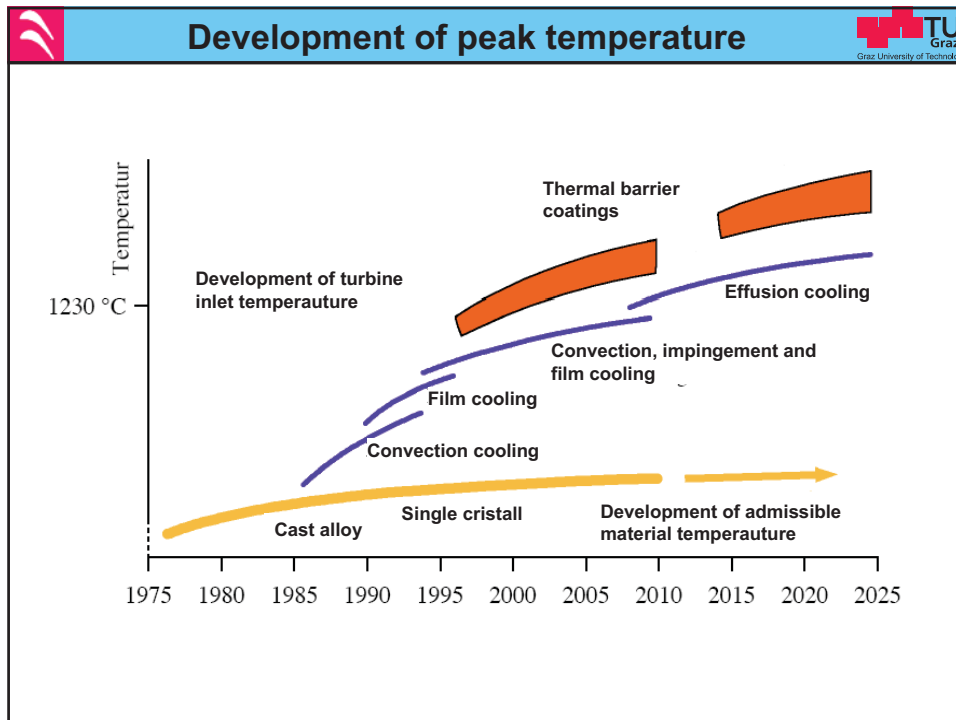


Enthalpy difference is higher between 3 and 4 than between 1 and 2 !



Characteristics of gas turbine process







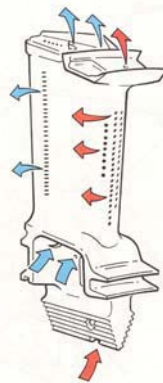
Turbine blade cooling



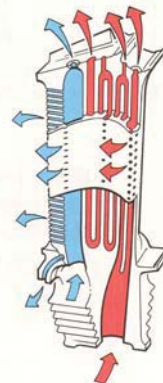
■ L.P. cooling air ■ H.P. cooling air



SINGLE PASS,
INTERNAL COOLING
(1960's)



SINGLE PASS,
MULTI-FEED
INTERNAL COOLING
WITH FILM COOLING
(1970's)



QUINTUPLE PASS,
MULTI-FEED
INTERNAL COOLING
WITH EXTENSIVE
FILM COOLING



Cooled turbine blade

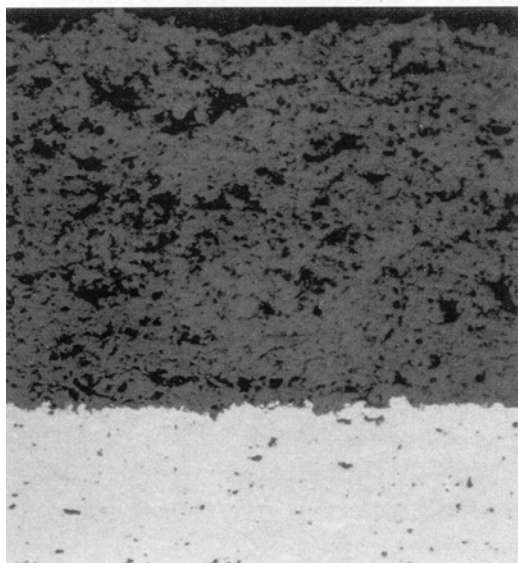




Overheated Turbine Blades



Thermal barrier coatings



APS ceramic thermal
barrier coating (ZrO_2)
with an intermediate
adhaerance layer

Surface temperature can
be reduced by 300K

Source: Werner Stamm, Siemens PG, Turbinenschaufeln mit Keramikbeschichtung, Technik in Bayern, Sept, Okt.2006, S. 12-13



Optimisation by controlled solidification



Quelle: Cerjak



Optimisation by controlled solidification

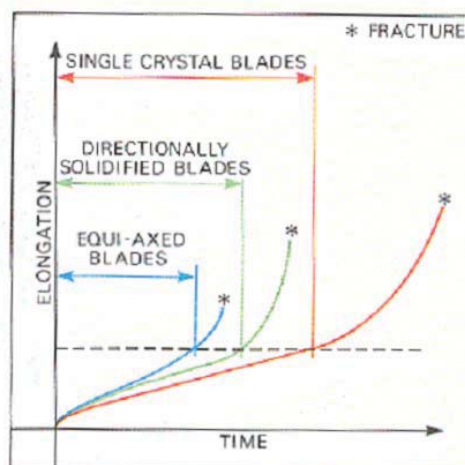
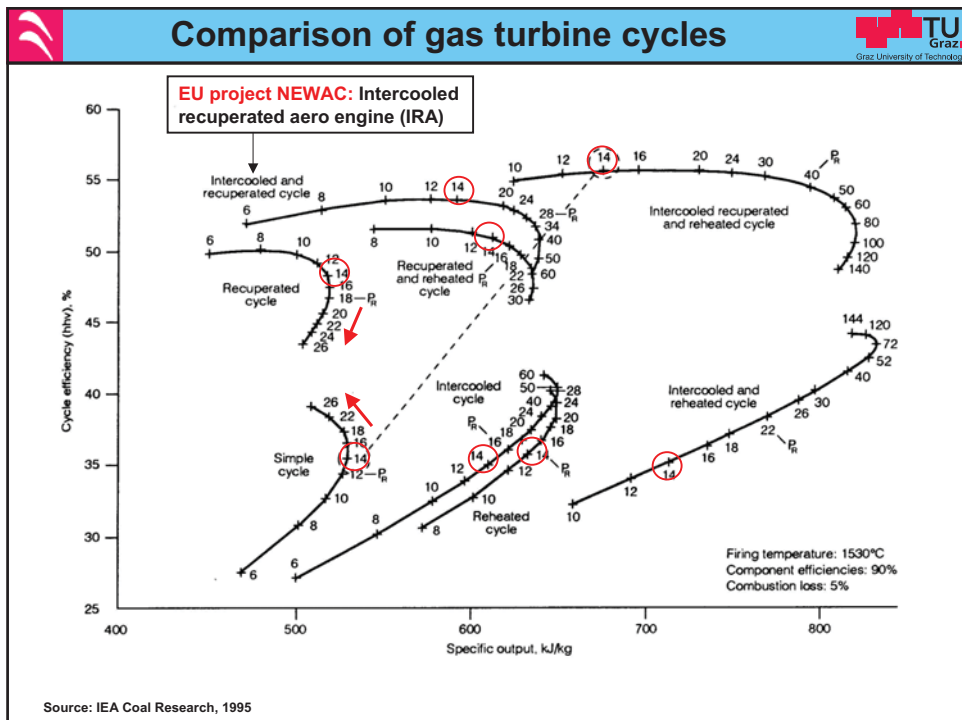
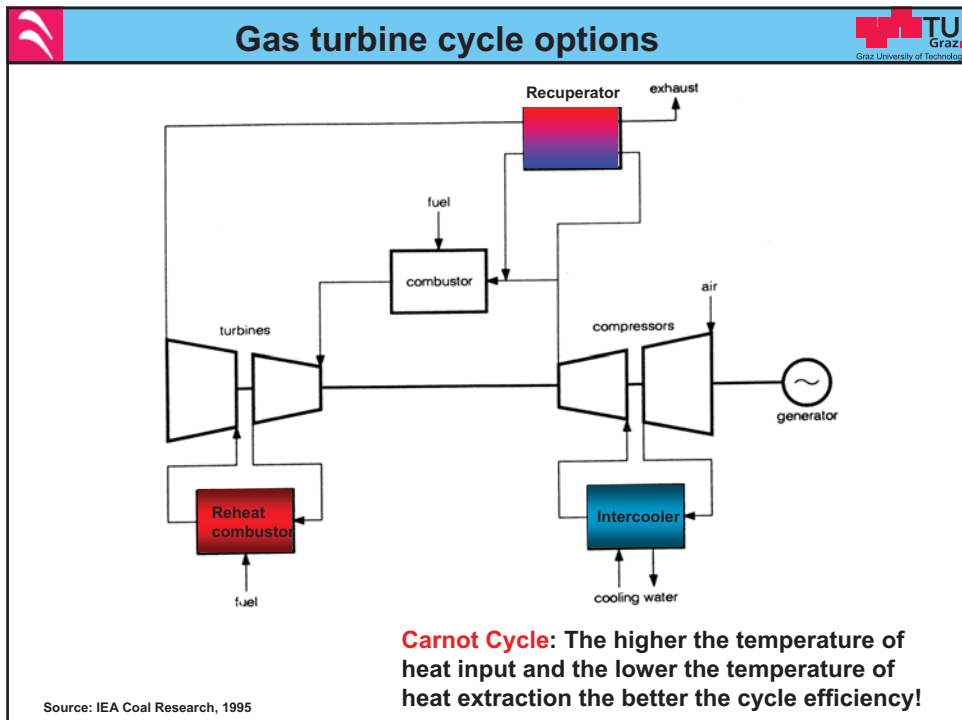
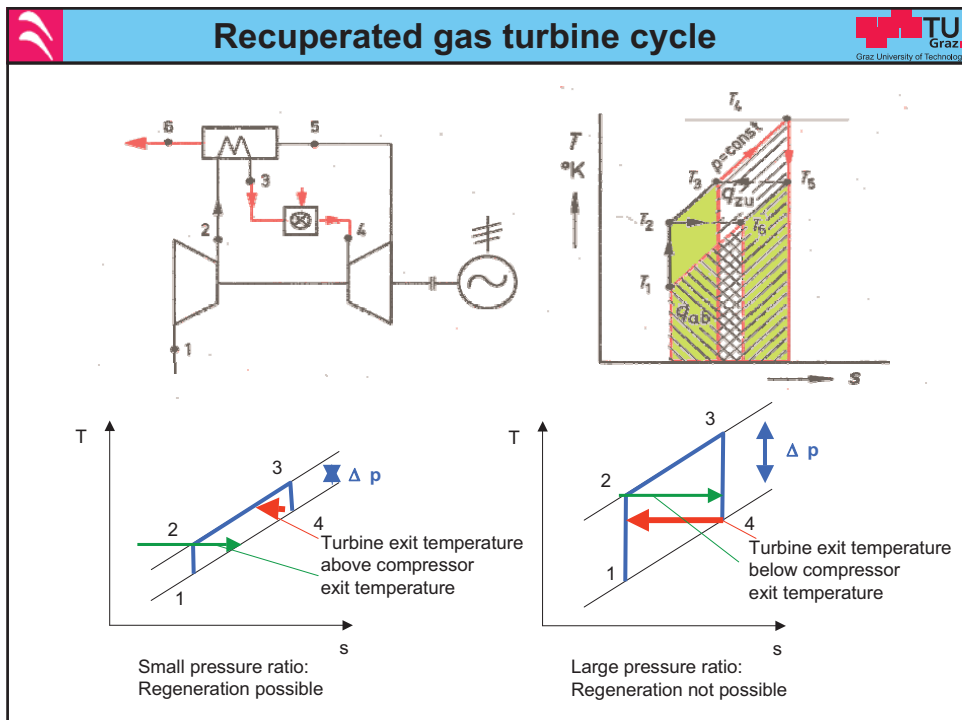
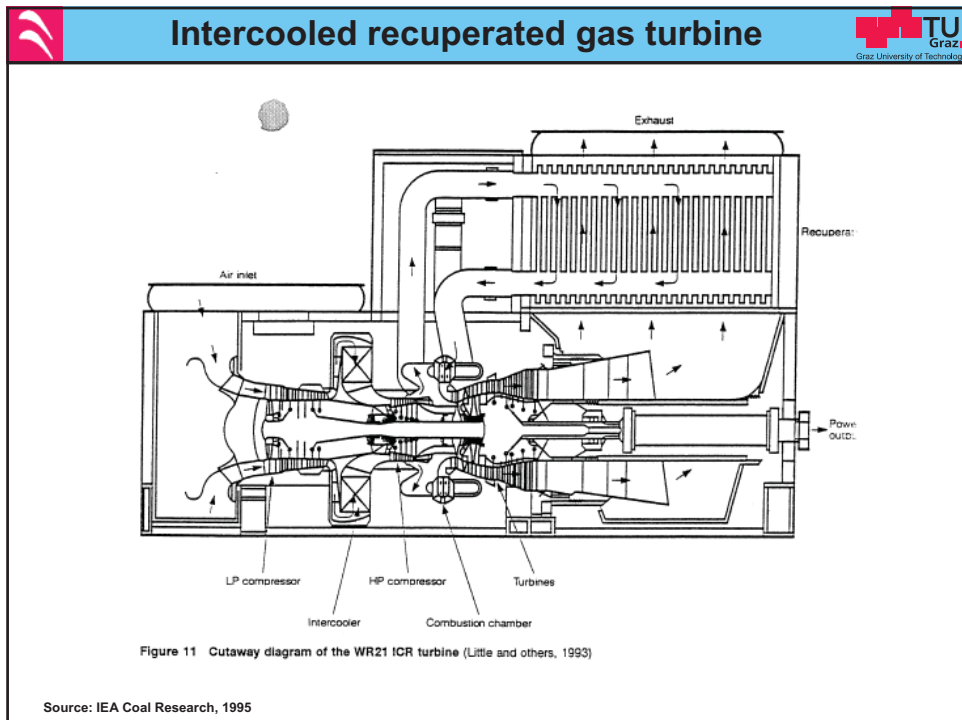


Fig. 5-13 Comparison of turbine blade life properties.







Intercooled gas turbine

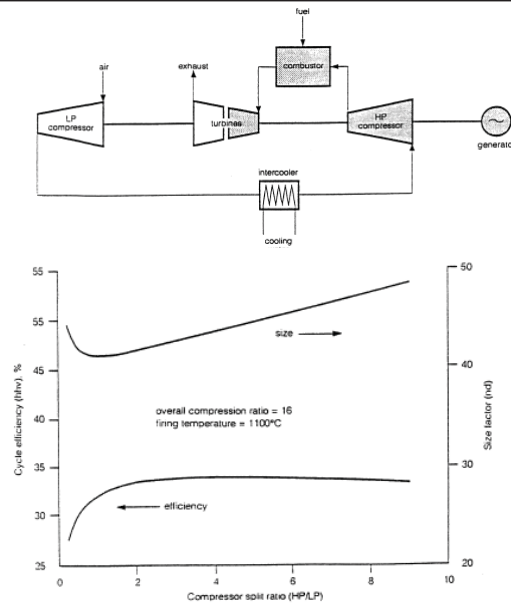


Figure10 Effect of compressor split ratio



Gas Turbines

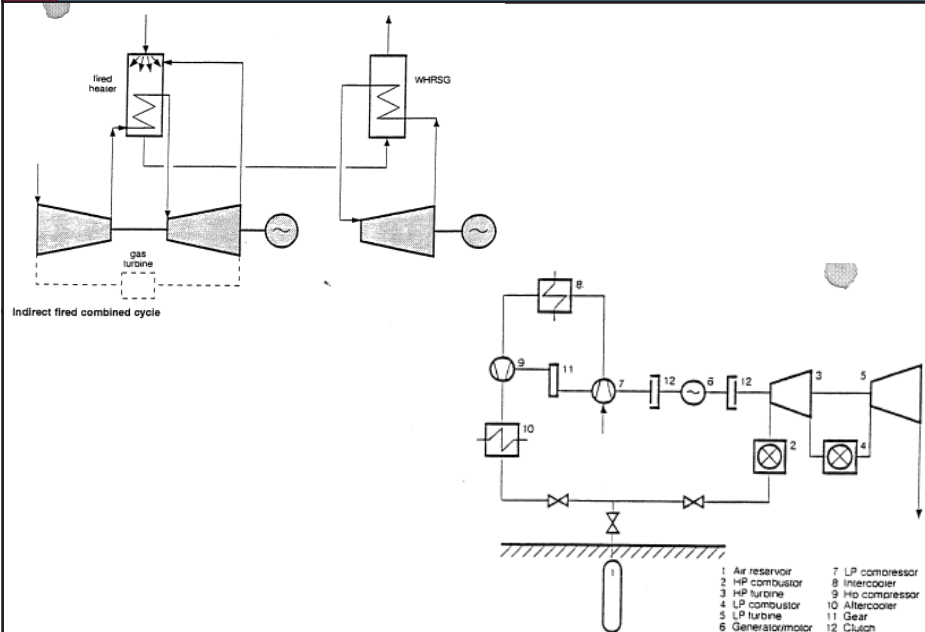
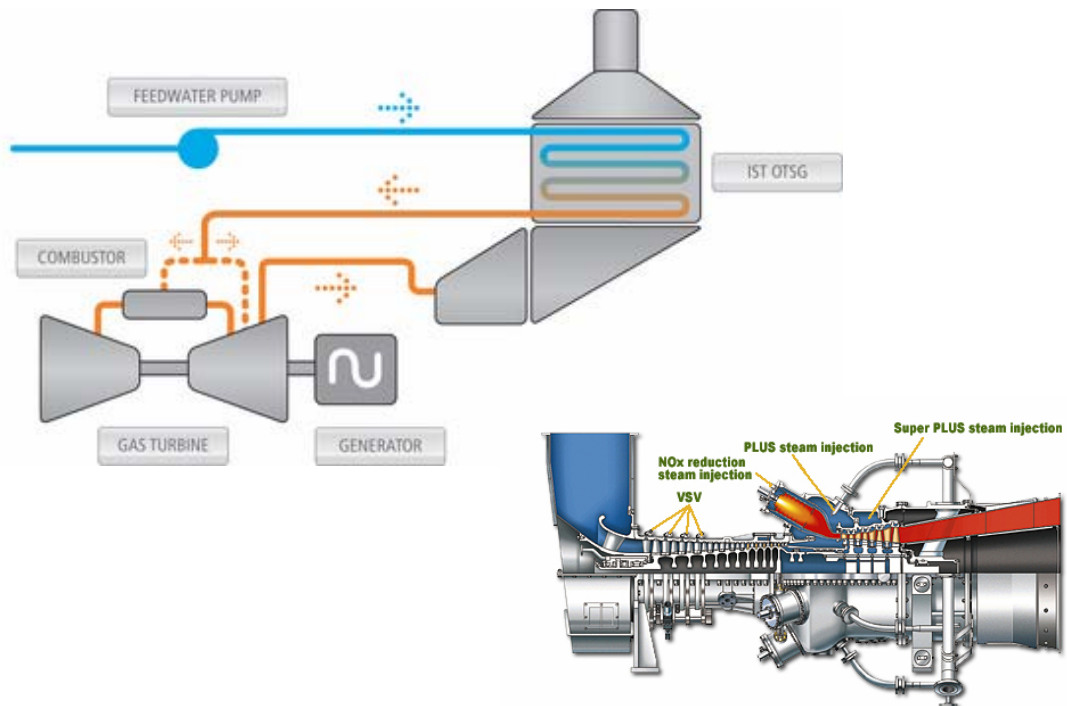


Figure 17 Compressed air energy storage flow diagram (Weber, 1976)



Steam Injected Gas Turbine (STIG)

STIG cycle takes waste heat from the gas turbine, converts water into steam and then injects this steam into the gas turbine (water treatment)



Source: www.otsg.com

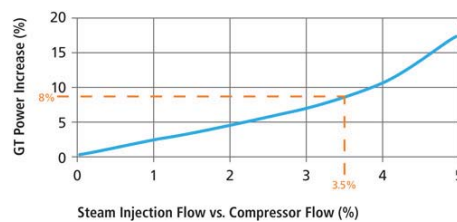
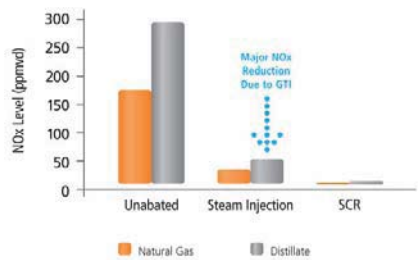
Steam-Injected Kawasaki M7A-01ST Gas Turbine



Steam Injected Gas Turbine (STIG)



- Steam/air flow ratio up to 0.2
- Power can be nearly doubled
- Efficiency increase by 15% - points
- NO_x emissions are reduced by up to 80%
- Less investment costs than CC plant
- Suitable for small power output (- 100 MW)
- High efforts for water treatment
- 5 – 10 % steam flow allowed for many models without adaptations



Source: www.otsg.com



HAT (Humidified Air Turbine)

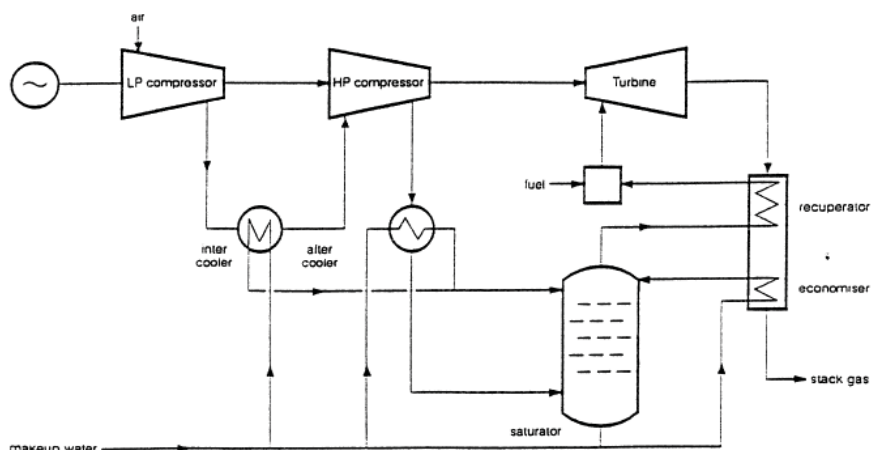


Figure 15 HAT cycle flow diagram (Morton and Rao, 1989)

Michael A. Bartlett
Mats O. Westermarck

Department of Chemical Engineering and
Technology/Energy Processes,
The Royal Institute of Technology,
SE-100 44 Stockholm, Sweden

A Study of Humidified Gas Turbines for Short-Term Realization in Midsized Power Generation—Part I: Nonintercooled Cycle Analysis

Humidified Gas Turbine (HGT) cycles are a group of advanced gas turbine cycles that use water-air mixtures as the working media. In this article, three known HGT configurations are examined in the context of short-term realization for small to midsized power generation: the Steam Injected Gas Turbine, the Full-flow Evaporative Gas Turbine, and the Part-flow Evaporative Gas Turbine. The heat recovery characteristics and performance potential of these three cycles are assessed, with and without intercooling, and a preliminary economic analysis is carried out for the most promising cycles.
[DOI: 10.1115/1.1788683]

Introduction

Humidified Gas Turbine (HGT) cycles are a group of advanced gas turbine cycles that have been studied as an alternative to the combined cycle and reciprocating engines for power generation. HGT cycles can be classified as gas turbine cycles that utilize water-air mixtures as the working fluid through the expander. Water vapor is obtained from evaporative processes in the cycle, for example, a heat recovery boiler, a humidification tower, or through water injection into the working fluid. As the expander flow increases without increasing the compressor flow, higher specific power outputs and efficiencies are achieved than those for the simple gas turbine cycle.

Many variations of the HGT have arisen, for example, the humid air turbine (HAT) cycle, the Steam Injected Gas Turbine (STIG) cycle, the Cheng cycle, the recuperated water injection (RWI) cycle, and the Evaporative Gas Turbine (EvGT) cycle. The main advantages identified with HGT cycles are electrical efficiencies similar to the combined cycle (CC) with higher specific power outputs [1–3] and significantly higher total efficiencies in combined heat and power (CHP) applications [4,5]. Furthermore, because the HGT cycles do not require a steam turbine for the bottoming cycle, specific investment costs (\$/kW_e) are significantly lower than those for the CC [6]. Rydstrand, Westermarck, and Bartlett [4] showed this to be especially true in combined heat and power applications due to the HGT's superior total efficiencies. Short start-up times and good load following characteristics have been reported [3,7] in addition to very low NO_x emissions with the use of only a diffusion burner [3]. Given this combination of characteristics, the focus of HGT commercialization falls naturally on distributed generation, peak-load plants, and industrial-sized applications (1–80 MW_e). Above this size, the flexibility and low investment costs of the HGT cycles become less important in the face of the mature performance and market position associated with large combined cycle.

The steam-injected gas turbine cycle uses exhaust gas heat to raise steam in a boiler that is then injected into the working fluid.

This configuration has been investigated thoroughly in the literature, with Larsson and Williams [8] and Tuzson [9] presenting good overviews. In 1978, Cheng patented the Cheng cycle [10], a variation on the steam-injected cycle, which has since been commercialized based on the Allison 501 KM gas turbine. Kellerer and Spangenberg [7] report on operating experience from such a plant in Munich. Other gas turbine cycles with varying degrees of steam injection have been commercialized by General Electric, Aquarius, and Kawasaki. Macchi and Poggio [11] and dePaepe and Dick [12] have addressed water recovery systems for steam-injected cycles.

Evaporative gas turbine cycles can be defined as cycles which evaporate water directly into the working fluid. Water injection, i.e., spraying fine, warm droplets into the working fluid, was proposed by Gasparovic and Stapersma [13] and was further studied and developed by Mori et al. [14], and Fruttschi and Plancherel [15]. Nakamura et al. [16] first patented an evaporative cycle which utilizes a humidification tower instead of direct water injection to evaporate the water. Fluor Daniel, Inc. investigated the humid air turbine (HAT) cycle [1,17], which also features a humidification tower instead of water injection, and patented some variations [18]. Amongst others, Chiesa et al. [19], Eidensten et al. [20], Stecco et al. [21], Rosén [22], and Yan, Eidensten, and Svedberg [23] have evaluated different configurations of evaporative gas turbine cycles.

In Sweden, evaporative gas turbine (EvGT) system studies were initiated at the Royal Institute of Technology (KTH) and Lund Institute of Technology (LTH), leading to the formation of the EvGT Consortium with industry and the Swedish Energy Agency in 1993. This consortium has concentrated on cycles with humidification towers for evaporation and has demonstrated the EvGT-technology for the first time in Lund, Sweden. A small-scale (600-kW_e) pilot plant was constructed with a humidification tower and recuperator, and later complemented with an after-cooler. Agren et al. [24], Lindquist [3], Bartlett and Westermarck [25], Dalili and Westermarck [26], and Thern, Lindquist, and Torrisson [27] have addressed different aspects of the EvGT pilot plant, including performance, operation characteristics, air and water quality, water recovery, humidification, and modeling.

Economic and technical simulation studies of midsize plants (70–80 MW) are also included in the EvGT project [6,28] along with application studies. Rydstrand, Westermarck, and Bartlett [4] investigated natural gas-fired humidified gas turbines in district

Contributed by the International Gas Turbine Institute (IGTI) of THE AMERICAN SOCIETY OF MECHANICAL ENGINEERS for publication in the ASME JOURNAL OF ENGINEERING FOR GAS TURBINES AND POWER. Paper presented at the International Gas Turbine and Aeroengine Congress and Exhibition, Atlanta, GA, June 16–19, 2003, Paper No. 2003-GT-38402. Manuscript received by IGTI, October 2002; final revision, March 2003. Associate Editor: H. R. Simmons.

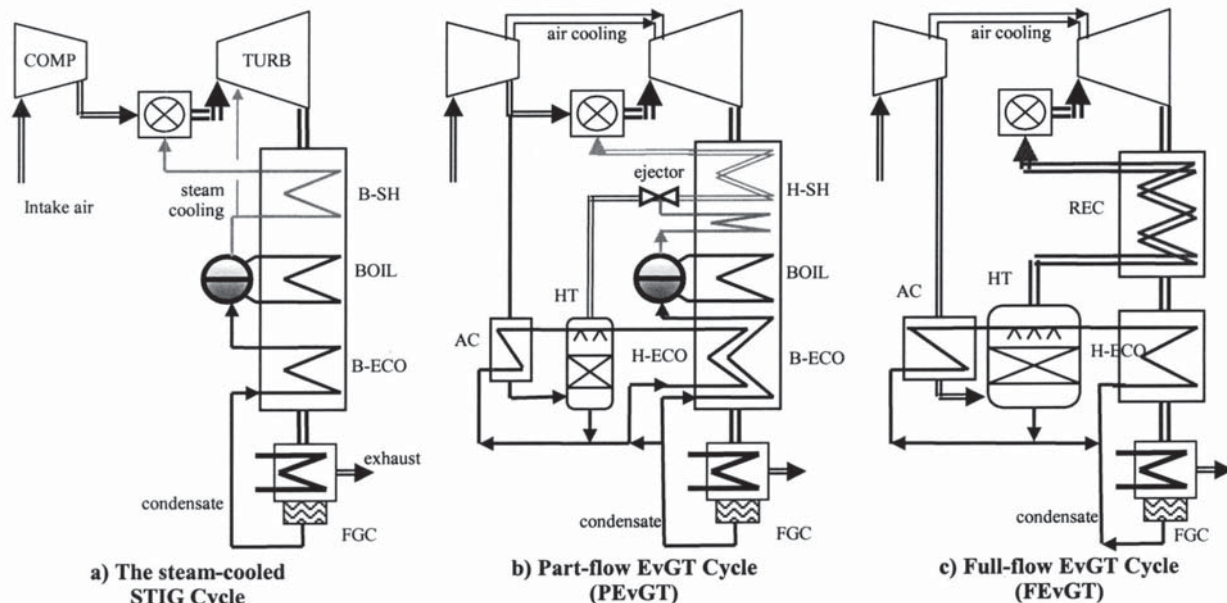


Fig. 1 Cycle layout of the nonintercooled HGT concepts to be studied

heating applications, while Bartlett et al. [29] examined cofired humidified cycles, also in district heating applications. Simonsson et al. [30] presented an analysis of EvGT cycles for industrial cogeneration using waste heat sources.

One important concept to arise from the EvGT project is the part-flow EvGT cycle (PEvGT), whereby only a fraction of the compressor air is used in the humidification tower. Westermarck patented the concept [31] and Agren [2] first introduced it to the literature. The authors studied this configuration with varying part-flow ratios for an industrial and an aeroderivative core engine and found that the optimal part-flow lies within the range 10–30% [2]. These studies, however, should be extended to a general thermodynamic and economic comparison with competing HGT concepts in power generation.

Scope

This two-paper series aims to identify the short-term thermodynamic and economic potential of HGT cycles with newly designed gas turbine machinery under 80 MW_e. An analysis is presented of three HGT concepts—the steam-injected cycle, the full-flow EvGT (FEvGT) cycle, and the PEvGT cycle—with and without intercooling. Favorable conditions for the different HGT concepts and configurations are identified and promising cycles are extracted for economic analysis. This paper, Part I, presents the background to the modeling and a thermodynamic analysis of the nonintercooled cycles, while the following paper, Part II, presents

a thermodynamic analysis of intercooled HGT cycles (HGT-IC) and an economic comparison of the alternatives [36].

Outline of the HGT Cycles for Analysis

The STIG Cycle. In the STIG cycle, shown in Fig. 1(a), steam is raised in a heat recovery steam generator (HRSG) and then injected into the working fluid after the compressor. Feed water preheating occurs in an economizer (B-ECO), evaporation in a boiler (BOIL), and high temperature heat recovery in a superheater (B-SH). Water vapor in the flue gas can be recovered in a flue gas condenser (FGC), then treated and recycled to the HRSG, making the cycle water self-sufficient. As the boiler is

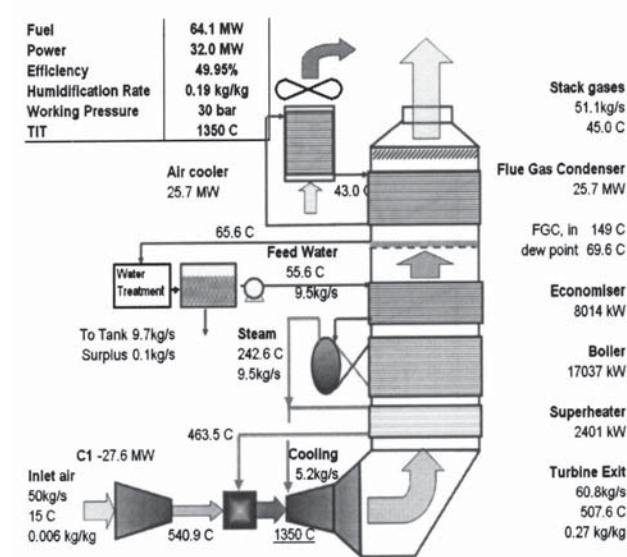


Fig. 2 STIG cycle used for the cost of electricity (CoE) analysis in Part II

Table 1 Core engine characteristics

Inlet conditions	ISO
Inlet flow	50 kg/s
Compressor inlet ΔP	1%
Compressor isentropic efficiency	0.9
Intercooler ΔP (Part II cycles only)	2%
Compressor outlet ΔP	1%
Combustion chamber ΔP	3%
Turbine polytropic efficiency	0.87
Turbine exit ΔP	1.8%

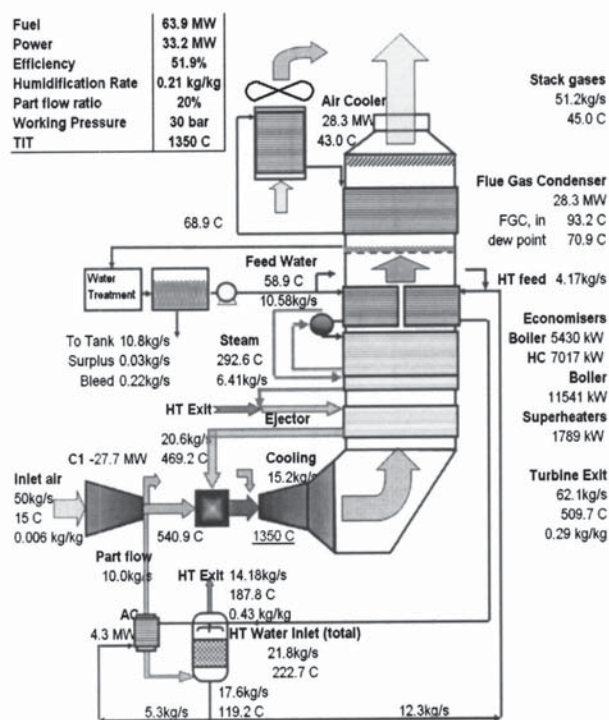


Fig. 3 PEvGT cycle used for the CoE analysis in Part II

limited to one pressure, superheated-STIG cycles typically have difficulty accessing low-quality heat and the flue gas can leave the HRSG at quite high temperatures. One way to increase heat recovery is to introduce steam cooling where slightly superheated steam is used to cool the gas turbine components instead of com-

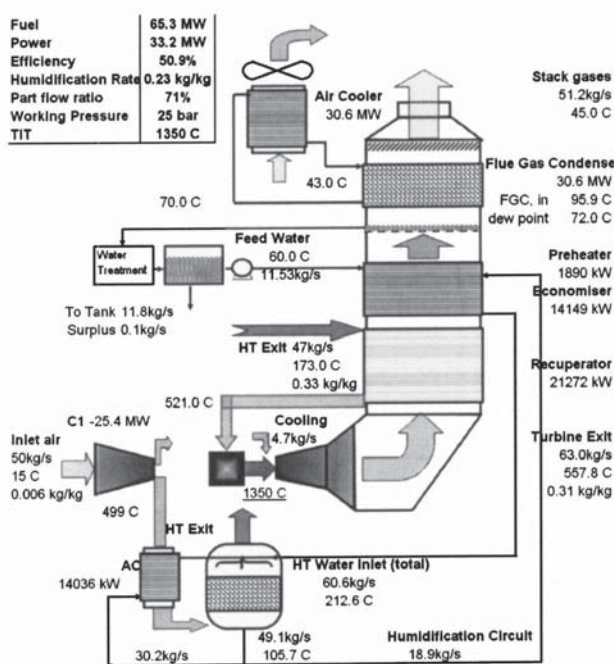


Fig. 4 FEGT cycle used for the CoE analysis in Part II

Table 2 Pressure losses in the different HGT cycles

Area	STIG	PEvGT	FEvGT
Flue gas	3%	4%	7% ^a
HC	—	0 ^b	5%
BC	c	c	—

^arecuperator $\Delta P=6\%$ [32].

^b a steam ejector is used to overcome the pressure loss in the humidification circuit.

5 bar overpressure is used to compensate for steam circuit pressure losses and the ejector.

Table 3 The modeling characteristics of cycle areas

Area	Item	Applicable cycle	Modeling characteristic	Value
Boiler circuit	B-ECO	STIG, PEvGT	Outlet sub cooling	10K
	BOIL	STIG, PEvGT	Pinch at drum	15K
	B-SH	STIG, PEvGT	Effectiveness ^a	85%
	H-SH			
Humidification circuit	H-ECO	PEvGT, FEvGT	Cold approach temperature	15K
	AC	PEvGT, FEvGT		
	IC	PEvGT, FEvGT		
	H-FWPH	PEvGT, FEvGT	Hot approach temperature	15K
	HT	PEvGT, FEvGT	Minimum driving force ($t - t_{ad}$)	4K
Recuperator	REC	FEvGT	Effectiveness ^a	90%
Water recovery	WRU	All	Self-supporting temperature	—

^aThe effectiveness quoted is the enthalpy effectiveness. This expresses the heat transferred as a percentage of complete, ideal heat exchange.

pressed air. This decreases the amount of steam for superheating, allowing more boiling and feed water preheating, thus increasing the amount of heat recovered.

The FEvGT Cycle. Instead of boiling the water separately, the EvGT cycle raises water vapor through evaporating water directly into the working medium in a humidification tower. In what is called the FEvGT concept in this article [see Fig. 1(c)], the entire compressor outlet passes through the humidification circuit, where it is cooled and humidified before being reheated and introduced to the combustion chamber. A primary surface recuperator (REC) is usually suggested for high-temperature heat recovery. The evaporation duty is extracted using an economizer (H-ECO) and an aftercooler (AC). In the humidification tower (HT), simultaneous mass and heat transfer takes place. Water heated to slightly below the boiling point is distributed across a packed bed where it is brought into countercurrent contact with compressed air. As the vapor pressure of the water exceeds the partial pressure

Table 4 The core engine parameters

Parameter		Values
CDP	Compressor discharge pressure (bar)	20, 25, 30, 35
TIT	Firing temperature (°C)	1200, 1350, 1500

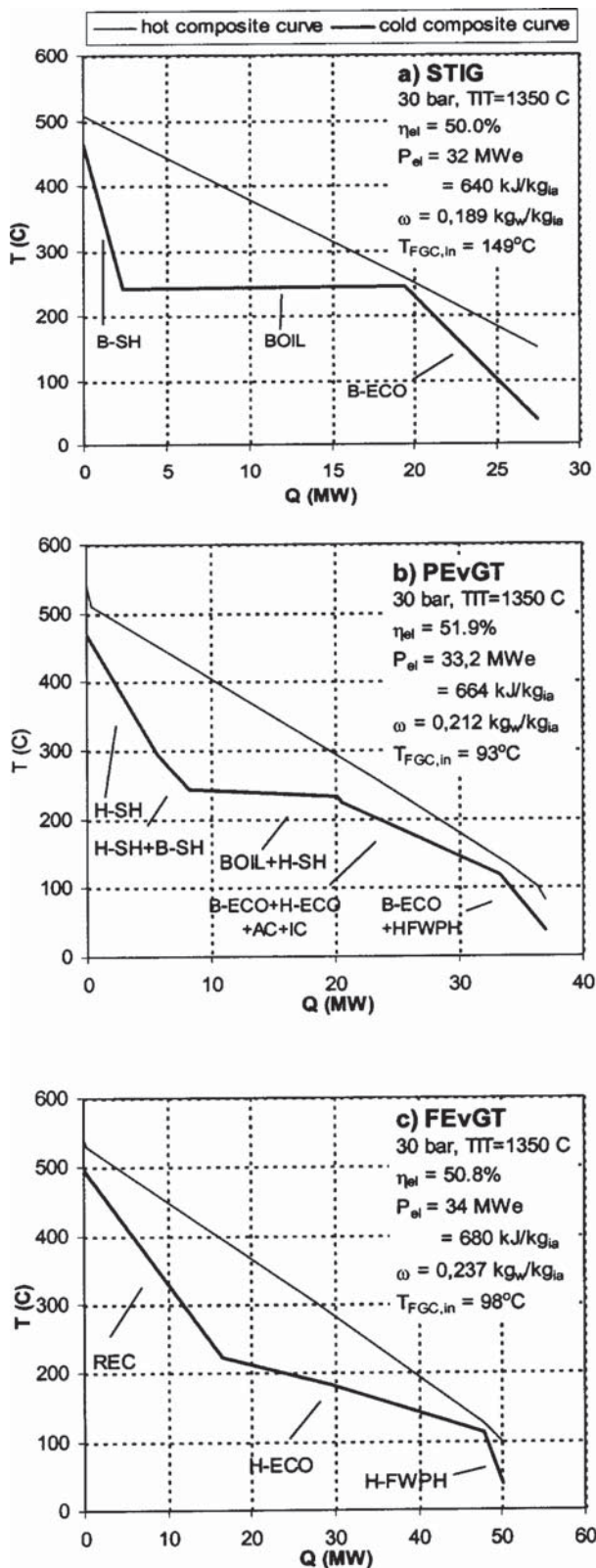


Fig. 5 Composite curves of the nonintercooled HGT cycles

of water in the air, evaporation takes place. This diabatic process takes most of the heat for evaporation from the water film, cooling the water as it flows down the tower. Hence a cold exit water stream from the HT is obtained, which can act effectively as an internal heat sink.

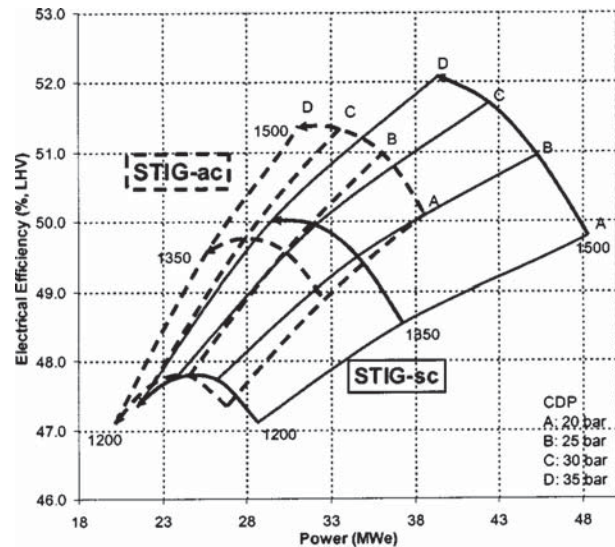


Fig. 6 Comparison of the performance maps of the air-cooled (ac) and steam cooled (sc) STIG cycle

The PEvGT Cycle. Ågren [2] presented and investigated the PEvGT concept introduced by Westermark [31]. The guiding principle of this concept is to reduce the heat exchange area and pressure drop penalties compared to a full-flow configuration while achieving the same heat recovery. To achieve this, only a part of the compressor outlet is extracted, cooled, humidified, reheated, and reinjected. The PEvGT cycle is illustrated in Fig. 1(b) and can be seen to combine features of the STIG and FEvGT cycle in one cycle. Like the STIG cycle, a HRSG is used to raise superheated steam, utilizing flue gas heat above the system boiling point. To fully exploit the heat remaining below the boiling point, a humidification tower with a part-flow from the compressor is used. Hence, the humidifier's purpose in this cycle is akin to the low-pressure boiler in a CC. The humidified part-flow is then heated with, or parallel to, the steam in a humid air superheater (H-SH). As the water vapor content is very high in the H-SH, excessive surface areas will not be required, nor the transition to a recuperator. Other PEvGT cycle configurations have been studied:

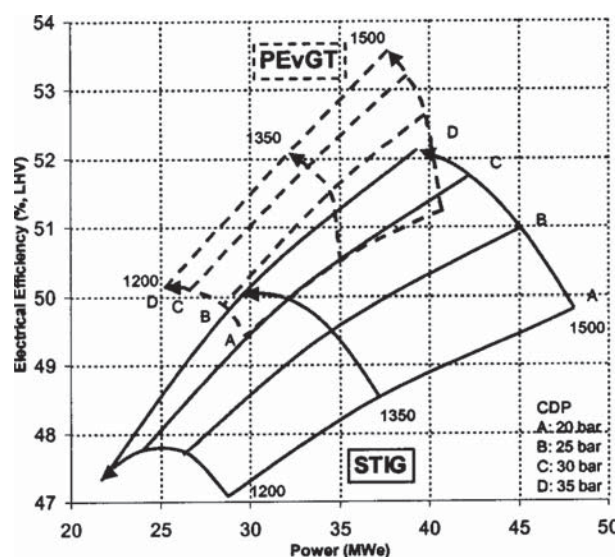


Fig. 7 The performance maps of the nonintercooled STIG and PEvGT cycles

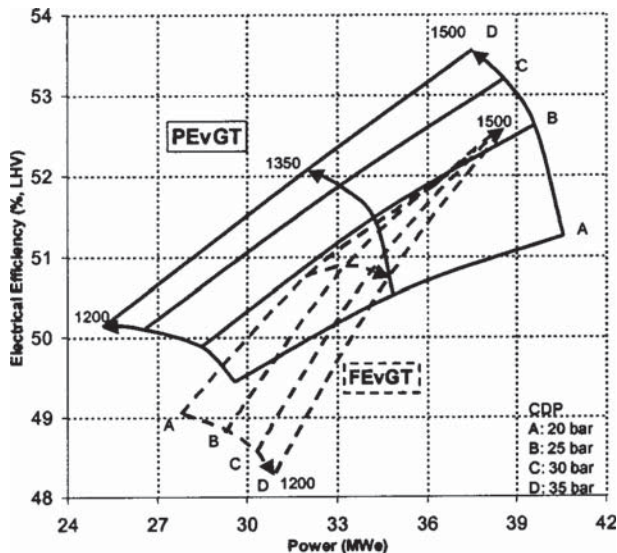


Fig. 8 The performance maps of the nonintercooled FEvGT and PEvGT cycles

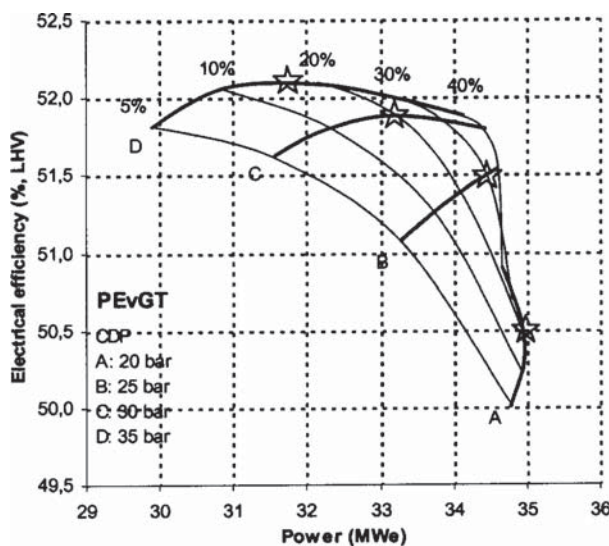


Fig. 9 The performance map of the nonintercooled PEvGT cycles for varying working pressures and part flows at a constant firing temperature of 1350°C

Table 5 Approach temperature and pressure drop sensitivity of the HGT cycles

Cycle	Config-uration	Base η_{el}	$\Delta \eta_{el}$ (% abs.)		
			Low Δt	Low HC Δp	Low flue gas Δp
STIG-sc	30 bar 1350°C	50	+0.4	...	+0.2
PEvGT	35 bar 1350°C	52.1	+0.4	...	+0.2
FEvGT	25 bar, 1350°C	50.9	+0.75	+0.3	+0.3

first with a recuperator and two-stage humidifier but no boiler, and second with a recuperator, humidifier and boiler [2]. However, we have chosen to study the concept in Fig. 1(b) due to its simplicity. As an improvement over past configurations, we suggest using a steam ejector instead of a booster fan to overcome the pressure drop caused by the humidification process and heat exchangers.

Modeling the Cycles

The parameters for the cycle simulation have been chosen to represent current gas turbine technology in the midsize range. Furthermore, the heat exchangers and the humidification tower are modeled with somewhat conservative parameters so that their dimensions and costs are reasonable. GATECYCLE is used to model the gas turbine, heat exchangers, and cycle performance. The humidification tower and flue gas condensers are modeled using in-house programs linked with GATECYCLE through MS Excel.

The cycle can be divided into four areas: the core engine, the boiler circuit, the humidification circuit, and water recovery. Each section is discussed below and refers to both Parts I and II.

The Core Engine. The core engines for the different HGT cases are assumed to be purpose-built for humidified operation, i.e., they operate at their design point with a flow imbalance. The design constant is a compressor capacity of 50 kg/s air at ISO conditions. Consequently, the size of the turbine expander varies between cases following the degree of humidification, giving a cycle power output of 30–50 MWe. As the heat exchange network is modeled conservatively, giving good driving forces and low costs, the thermodynamic data presented in the results may be scaled directly to smaller gas turbine cycles (5–15 MWe) without adjusting the heat exchange network. However, the lower firing temperatures and pressures presented in this article are perhaps more applicable to smaller core engines. Table 1 outlines the constants used to model the core engine.

HGT cycles have cooling media other than the compressor air available, for example, saturated steam or cool humid air from the humidification tower. For reasons outlined in the section entitled “Results and Discussion,” the STIG cycle presented is steam cooled, while the evaporative cycles are cooled with compressor air. The cooling flow to the nozzle (stator) of the turbine is determined by GATECYCLE using the metal temperature of the turbine blades as expressed in Eq. (1). The reference parameters are taken from previous simulations [2]. The cooling flow to the rotor is set as equal to the cooling flow to the nozzle, a conservative assumption as rotor cooling flows are usually less than nozzle flows.

$$M_{cool} = M_{cool,ref} \left(\frac{C_{p,ref}}{C_p} \right)_{cool} \left(\frac{C_p}{C_{p,ref}} \right)_{gas} \left(\frac{\left(\frac{T_g - T_{metal}}{T_g - T_{cool}} \right)}{\left(\frac{T_g - T_{metal}}{T_g - T_{cool}} \right)_{ref}} \right)^{1.1}, \quad (1)$$

where M is the cooling flow rate, C_p is the specific heat, T is the temperature, and subscripts gas denote inlet gas value, cool denotes cooling gas value, and ref denotes the value at the reference condition.

While Eq. (1) is limited as heat transfer properties are not accounted for, it was judged to be more realistic than other GATECYCLE options. Typical cooling flows are given in the flow sheets contained in Figs. 2–4 and Figs. 6–9 in Part II [36].

The Heat Recovery Circuits. The boiler circuit (BC) is classified as the section of the HGT cycle which raises steam for delivery to the combustion chamber, in other words, the HRSG. This includes the B-ECO, the BOIL, and the superheaters (B-SH and H-SH).

The humidification circuit (HC) is the heat recovery section that delivers energy to the humidification process. This consists of the

HT, aftercooler (AC), humidification circuit economizer (H-ECO), and feed water preheater (H-FWPH). An intercooler is also included in paper II.

Table 2 shows the pressure drops resulting from the heat recovery systems, while Table 3 shows the performance characteristics of these items. The water flows through the AC, intercooler (IC), and H-ECO were adjusted such that the water outlet temperature was 10 K subcooled compared to the humidification tower pressure.

Humidification Model. While GATECYCLE contains a humidification tower model, which satisfactorily performs overall energy and mass balances, it does not check the internal conditions of the tower packing. Therefore, the model may converge on inoperable conditions where a point in the packing actually contravenes equilibrium. As such an in-house humidification tower model is integrated into the cycle calculations through a link with MS Excel for performance and dimensioning. The model is based on working-line theory common in unit operations [33,34] and uses a humid air properties model that account for nonideal mixing effects [35]. Importantly, the model has been experimentally verified for use with packed-bed and tubular humidifiers [26]. A description of this model can be found in Agren [2] and Dalili and Westermark [26].

Parameter Study

Currently, there is a push for higher working pressures and firing temperatures for industrial midsize gas turbines. The parameters for this study are chosen to reflect these trends and are presented in Table 4. It was deemed infeasible to increase the working pressure beyond 35 bar without intercooling.

The optimal part-flow ratio in the PEvGT cycle will also vary with each core engine parameter. Agren [2] showed that the probable optimum lies at lower part-flow ratios. Therefore, the part-flow ratio (ψ) in the PEvGT cycle is varied from 5–40%. Note that ψ is defined as the mass fraction of compressor intake air that is lead to humidification circuit.

Results and Discussion

This section examines and compares the performance of the nonintercooled HGT cycles. The results for the intercooled HGT cycles and a final economic analysis may be found in paper II.

Heat Recovery Comparison. Before analyzing the response of the HGT cycles to changes in pressure and the firing temperature, it is important to appreciate the nature of each cycle's heat recovery system. Figure 5 presents composite curves produced from the simulations at 30 bar and a combustor outlet of 1350°C. These curves show the amount and nature of the heat transferred in the cycle, including the aftercooler and flue gas. Composite curves are obtained through adding the $m \cdot c_p$ values of all the heat sources or heat sinks for a temperature region, respectively, and multiplying the sum by the temperature change in that region.

Examining the three diagrams, it is clear that the FEvGT transfers the most heat between the streams (50 MW), nearly twice the amount of the STIG cycle (27 MW) and 35% more than the PEvGT (37 MW). This reflects the extra heat transfer required in the FEvGT's humidification circuit to cool and heat the entire airflow from the compressor in the aftercooler and recuperator. As the PEvGT passes only a fraction of the compressed air through the HC, it requires less heat transfer for this purpose. The STIG cycle has no humidification circuit. Importantly, the FEvGT cycle (16.6 MW) has seven times as much gas-gas heat transfer as the STIG (2.4 MW) and double that of the PEvGT (8.3 MW). Therefore, due to the amount of heat exchange in the FEvGT and the domination of gas-gas heat transfer therein, the FEvGT will require considerably more heat exchange area than either the STIG or the PEvGT.

It is important to note the different strategies to utilize low temperature heat in the different HGT cycles. It is these strategies

which in turn have a critical consequence on the choice of turbine cooling media. In the STIG cycle, steam cooling is used to recover more low temperature heat. By decreasing the amount of steam for superheating, the amount of water that may be boiled and preheated is increased. For example, switching to steam cooling for the STIG cycle in Fig. 5(a) decreased the flue gas exit temperature from 167 to 150°C. The effect of this on the STIG performance is significant, as shown in Fig. 6. In the evaporative cycles, the humidification tower already allows the recovery of practically all the useful heat contained in the exhaust. Consequently, switching to direct steam- or humid air-cooling will not lower the flue gas temperature further, nor benefit the cycle efficiency greatly. Hence direct air-cooling was chosen for the evaporative cycles and direct steam-cooling was chosen for the STIG cycle.

The recovery of low temperature heat in the humidifier affords the PEvGT cycle 1.9% points more efficiency than the STIG cycle at an increased power density. The FEvGT cycle, however, only gains 0.8% points due to the pressure and temperature loss (the humid air enters the combustor colder than the compressor air) associated with the humidification process.

The Performance Maps. Figures 7–9 present the performance maps of the nonintercooled HGT cycles. As with all performance maps presented in this article, they show the power output versus the electrical efficiency of the cycle. The specific power output (kJ/kg_{ia}) is gained by multiplying the power output value (MW_{e}) by 20 (constant intake air flow for all cycles). The isobars [constant compressor discharge pressure (CDP)] and isotherms (constant firing temperature) outline an area in the map for each type of cycle. Only the optimal PEvGT cycles are considered, see the next section for details on this choice. It is useful to keep in mind the example composite curves in Fig. 5 when interpreting these maps.

In Fig. 7, the STIG cycle exhibits substantial increases in both specific power and efficiency with an increasing firing temperature. Increases in the turbine inlet temperature (TIT) imply a higher turbine outlet temperature (TOT), which allows more flue gas heat to be recovered by the single-pressure HRSG. Hence, more steam expands in the turbine and therefore the efficiency and specific power output increase. Increases in the compressor discharge pressure also lead to higher efficiencies, but with falling specific power outputs. The higher efficiencies are attributable to more work being extracted from the steam when at higher working pressures. However, because the TOT sinks with increases in the pressure, steam generation falls, and an efficiency maximum is therefore found on the isotherms (constant TIT and increasing CDP).

The PEvGT area can be considered a projection of the STIG area into a smaller region at higher electrical efficiencies (see Fig. 7). This projection is especially marked when there are significant amounts of heat left by the HRSG that the humidification tower in the PEvGT can utilize, i.e., at low turbine outlet temperatures. As the PEvGT can utilize low temperature heat, the efficiency maxima on the isotherms lie at much higher pressures than the STIG cycle because water vapor generation does not decrease as markedly with increases in the CDP. Compared to the STIG cycle, the specific power increases with an increased TIT are more moderate. The higher temperature of the turbine outlet, which follows a higher TIT, is mainly utilized for increased superheating and efficiency gains in the PEvGT rather than water vapor generation and power gains, as in the STIG cycle. Furthermore, steam cooling gives the STIG cycle an advantage in specific power (see Fig. 6).

The FEvGT area, Fig. 8, resides mostly within the PEvGT area and is a twisting, narrow, and steep surface. The isotherms show that the FEvGT efficiency only improves with pressure increases when the TIT is high. This is because a positive difference is required between the turbine outlet and compressor outlet temperatures for the recuperator to contribute positively to the effi-

ciency. This factor is also reflected in the marked efficiency increase along the isobars with an increasing TIT, which increases the TOT and hence the recuperator's impact. Unlike both the STIG and PEvGT cycles, the specific power of the FEvGT increases with the CDP, albeit marginally. This is attributable to the balance between the humidifier and recuperator. As the working pressure increases, the TOT decreases while the temperature out of the humidifier increases. Hence the recuperator recovers proportionately less flue gas heat at higher CDPs, allowing more humidification and therefore an increased power output. From Fig. 8, we can conclude the FEvGT has a lower efficiency than the PEvGT at CDPs over 25 bar and only a marginally better efficiency at a lower power output at lower CDPs.

Optimizing the PEvGT Cycle. Figure 9 shows the performance map of the PEvGT cycles (nonintercooled) at a constant firing temperature of 1350°C with varying pressures and part flow ratios. The trends are similar for the different firing temperatures studied. The stars represent the optimal part flow ratios chosen for use in the performance maps presented in Figs. 7 and 8.

It can be seen in Fig. 9 that at higher pressures (30–35 bar) an efficiency maximum exists, whereas a power maximum is found at lower pressures (20 bar). The characteristic of the part-flow curve is found to be dependent on two factors: the TOT and the temperature difference between the turbine and compressor outlets.

At a higher working pressure, the TOT encountered is low and colder than the compressor outlet temperature. The low TOT means large amounts of heat cannot be recovered by the high-pressure HRSG boiler and should be adsorbed by the H-ECO. As more air is passed through the humidification tower, the water outlet temperature is lowered and more heat is recovered from the flue gas, hence improving the efficiency and power output. However, as the turbine outlet is colder than the compressor outlet, the air sent to the humidifier will never recover its original temperature level, costing the cycle fuel and efficiency. The balance between these two factors will create an efficiency maximum, as seen for the 30- and 35-bar PEvGT cases in Fig. 9. While extra power may be gained at ψ values higher than the maximum, the gains become smaller while the heat exchanger area and thus costs increase linearly with ψ . A detailed economic study is required to find the optimal part-flow rate; however, in this article the maximum efficiency is chosen for further evaluation. Jonsson and Yan [28] carried out a detailed economic analysis of part-flows for three different core engines.

At low pressures, high TOTs and low COTs are found. In this case, the HRSG is well suited to the flue gas and little heat is left for the humidification tower. Therefore only a small part-flow percentage is needed to complete the heat recovery. Leading more air than this amount through the HC serves only to shift heat away from the HRSG to the H-SH, thus increasing sensible heat recovery and decreasing the humidity. As the power output is heavily dependent on the humidity, there is accordingly a power maximum at low to moderate part-flow ratios, illustrated by the 20-bar PEvGT case. Higher ψ values may deliver higher efficiencies, but again the heat exchange area and hence costs also increase. Hence the power maximum is chosen for evaluation in this study.

At moderate pressures (25 bar) both of the above effects are present. The turbine outlet temperature is low, but still slightly warmer than the compressor outlet. Hence sending more air through the humidification circuit in general, and the H-SH in particular, increases the efficiency weakly. Moreover, the HRSG also leaves significant amounts of heat available for the humidifier that is more effectively accessed with high ψ , due to a lower water temperature from the HT. Thus both the power output and the efficiency increase quickly with the part-flow ratio to an efficiency maximum at 30%, after which the gains are marginal.

Sensitivity Analysis. The parameters used in this study were chosen to conservatively model a feasible mid-sized gas turbine

cycle. Hence the pressure drops and pinch points were chosen such that the HGT cycles' performances are not overstated nor the heat exchange size and costs ignored. Table 5 presents a study of the potential of the HGT cycles when these two parameters are lowered. For the case of low approach temperature differences, "low Δt ", water–gas heat exchangers have an approach Δt of 5 K, the boiler drum pinch point is reduced to 5 K, the recuperator effectiveness is raised to 95%, and the effectiveness of the superheaters are raised to 90%. In the case "low HC Δp ," the pressure drop associated with the humidification circuit is halved. Similarly, the flue gas pressure drop in the heat exchangers is halved in the case "low flue gas Δp ."

Table 5 shows that the FEvGT benefits the most from all measures. This demonstrates that the FEvGT is the most sensitive HGT cycle to changes in approach temperatures and pressure drops. Therefore the FEvGT is more exposed to technology levels than the other cycles. A significant portion of the 0.75-point increase that occurs when improving the FEvGT's approach temperatures comes from the improved recuperator performance. Similarly, the recuperator contributes to most of the pressure drop penalties in the flue gas and humidification circuit. Therefore, the recuperator is essentially the determining factor of the competitiveness of the FEvGT.

It is important to stress that the potential of the HGT cycles cannot be found by adding the three end columns in Table 5. If the approach temperatures are reduced, then heat exchange area will increase and the pressure drop will also rise. Thus, in reality, any approach temperature changes will be partly counteracted by increased heat exchange pressure drop penalties.

Conclusions

In part I of this two-paper series, nonintercooled HGT cycles were examined for use in mid-sized power applications. The heat recovery characteristics of the STIG, FEvGT, and PEvGT cycles were analyzed using composite curves. Furthermore, the cycles' performances were mapped across a range of pressures and firing temperatures, with the PEvGT also examined with differing part flow ratios. The following points may be concluded.

- The full-flow EvGT (FEvGT) cycle is unsuitable for nonintercooled cycles. Much larger quantities of heat are transferred in the FEvGT cycle than the other HGT cycles, especially in gas–gas heat exchangers. This fact points to higher costs. Furthermore, the performance of the FEvGT cycle was found to be only moderate, with the part-flow EvGT cycle superior to the FEvGT for most relevant working pressure and firing temperature combinations.
- The STIG cycle shows good potential, with the lowest amount of heat transfer of the HGT cycles and very low amounts of gas–gas exchange; thus promising low heat exchange costs. The efficiency of the STIG cycle was not significantly lower than the other cycles, especially at high firing temperatures and working pressures.
- Steam cooling the turbine, rather than using air cooling, significantly benefits the STIG cycle by allowing more boiling and low-temperature heat recovery from the flue gas. The efficiency of the other cycles showed a lower dependency on the cooling media as the humidification tower already allows them to recover low-temperature heat.
- The part-flow EvGT (PEvGT) cycle is the most promising HGT cycle for nonintercooled core engines. Higher efficiencies than the other cycles are obtained, especially at moderate to high pressures, and good power densities. The total amount of heat transfer is kept 35% lower than the FEvGT, with gas–gas transfer 50% lower. The optimal part-flow ratio is dependent on the relationship between the compressor and turbine outlet temperatures, but was found to always be under 30%.
- HGT cycles are quite sensitive to how the heat exchange network is modeled, i.e., choices of approach temperatures and pressure drops. The FEvGT is especially sensitive and thus most dependent on component technology levels.

This article showed that the performances of the HGT cycles are quite similar, with at most a 2-percentage-point difference in the efficiency between the different optimized FEvGT, PEvGT, and STIG cycles. Furthermore, the power output at the optimal efficiencies also varied modestly. These facts point to the importance of an economic analysis to find the most attractive cycle.

In Part II of this series, intercooled HGT cycles examined and both intercooled and nonintercooled cycles are selected for economic analysis and comparison.

Acknowledgments

The authors would like to thank the financial and technical support of the EvGT Consortium members during this work: the Swedish Energy Agency, Vattenfall AB, Sydkraft AB, Energy E2, ALSTOM Power AB, and Elforsk.

Nomenclature

Cycle Abbreviations.

CC	= Combined cycle
EvGT	= Evaporative gas turbine
FEvGT	= Full-flow evaporative gas turbine
HAT	= Humid air turbine
HGT	= Humidified gas turbine
PEvGT	= Part-flow evaporative gas turbine
RWI	= Recuperated-water-injected gas turbine
STIG	= Steam-injected gas turbine

Heat Exchanger Abbreviations.

AC	= Aftercooler
BC	= Boiler circuit
B-ECO	= Boiler circuit economizer
B-SH	= Boiler circuit superheater
FGC	= Flue gas condenser
HC	= Humidification circuit
H-ECO	= Humidification circuit economizer
H-FWPH	= Humidification circuit feed water preheater
H-SH	= Humid air superheater
HT	= Humidification tower
IC	= Intercooler
REC	= Recuperator

Parameters.

CDP	= Compressor discharge pressure, bar
COT	= Compressor outlet temperature, °C
LHV	= Lower heating value
P_{el}	= Power output, MW _e (net)
t	= Temperature
TIT	= Turbine inlet temperature (combustor outlet temperature), °C
TOT	= Turbine outlet temperature, °C
η_{el}	= Cycle electrical efficiency, % LHV
ω	= Cycle humidification rate, kg _{H₂O} /kg _{intake air}
ψ	= Part-flow ratio, per kg compressor intake air

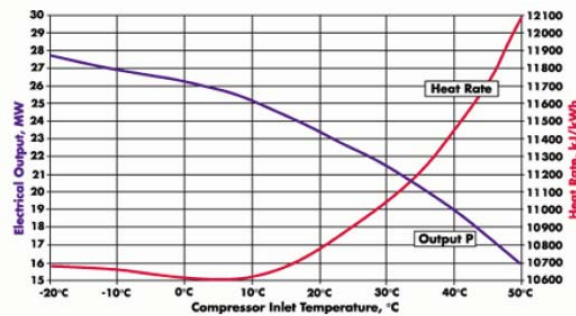
Subscripts.

ad	= adiabatic
i.a.	= intake air

References

- [1] Rao, A. D., and Joiner, J. R., 1990, "A Technical and Economic Evaluation of the Humid Air Turbine Cycle," Proc. 7th Annual International Pittsburgh Coal Conference, September 10–14.
- [2] Ågren, N. D., 2000, "Advanced Gas Turbine Cycles With Water-Air Mixtures as Working Fluid," Ph.D. thesis, Royal Institute of Technology, Dept. of Chemical Engineering/Energy Processes, Stockholm, Sweden, ISSN 1104-3266 ISRN KTH/KET/R—120—SE.
- [3] Lindquist, T., 2002, "Evaluation, Experience and Potential of Gas Turbine Based Cycles With Humidification," Ph.D. Thesis, Lund University, Dept. of Heat and Power Engineering, Lund, Sweden, ISBN 91-628-5330-9.
- [4] Rydstrand, M., Westermark, M., and Bartlett, M., 2002, "An Analysis of the Efficiency and Economy of Humidified Gas Turbines in District Heating Applications," Proc. ECOS 2002, Vol. II, pp. 695–703.
- [5] Poggio, A., and Strasser, A., 1996, "CHENG Cycle Cogeneration System Application and Experience of Exhaust Gas Condensing," Proc. POWERGEN '96, June 26–28, Budapest.
- [6] Nilsson, P. A., ed., 1996, "EvGT—evaporative Gas Turbine—Block 3," Technical report, Lund Institute of Technology, Dept. of Heat and Power Technology, Lund, Sweden.
- [7] Kellerer A., and Spangenberg C., 1998, "Operating Experience With a Cheng-Cycle Unit," VGB PowerTech, November 1998, pp. 16–22.
- [8] Larson, E. D., and Williams, R. H., 1987, "Steam-Injected Gas Turbines," ASME J. Eng. Gas Turbines Power, **109**, pp. 55–63.
- [9] Tuzson, J., 1992, "Status of Steam-Injected Gas Turbines," ASME J. Eng. Gas Turbines Power, **114**, pp. 682–686.
- [10] Cheng, D. Y., 1978, "Regenerative Compound Dual-Fluid Heat Engine," US Patent No. 4,128,994.
- [11] Macchi, E., and Poggio A., 1994, "Cogeneration Plant Based on Steam Injection Gas Turbine With Recovery of Water Injected: Design Criteria and Initial Operating Experience," ASME Paper No. 94-GT-17.
- [12] dePaape, M., and Dick, E., 1999, "Water Recovery in Steam-Injected Gas Turbines: A Technological and Economical Analysis," European J. Mech. Environ. Eng., **44**, pp. 195–204.
- [13] Gasparovic, N., and Stapersma, D., 1973, "Gas Turbine With Heat Exchanger and Water Injection in the Compressed Air," Combustion, **45**, pp. 6–16.
- [14] Mori, T. R., Nakamura, H., Takahashi, T., and Yamamoto, K., 1983, "A Highly Efficient Regenerative Gas Turbine System by New Method of Heat Recovery With Water Injection," Proc. 1983 Tokyo International Gas Turbine Congress, Vol. 1, pp. 297–303.
- [15] Fruttschi, H. U., and Plancherel, A., 1988, "Comparison of Combined Cycle With Steam Injection and Evaporation Cycles," Proc. 2nd Sym. on Turbomachinery, Combined-Cycle Technologies and Cogeneration, IGTI, Vol. 3, pp. 137–145.
- [16] Nakamura, H., Takahashi, T., Narazaki, N., Yamamoto, F., and Sayama, N., 1981, "Regenerative Gas Turbine Cycle With Water Addition and Method of Operation Therefore," U.S. Patent No. 0,053,045 B1.
- [17] Day, W. H., and Rao, A. D., 1992, "FT4000 HAT With Natural Gas Fuel," ASME COGEN-TURBO, American Society of Mechanical Engineers, International Gas Turbine Institute, Vol. 7, pp. 239–245.
- [18] Rao, A. D., 1989, "Process for Producing Power," U.S. Patent No. 4,829,763.
- [19] Chiesa, P., Lozza, G., Macchi, E., and Consonni, S., 1995, "An Assessment of the Thermodynamic Performance of Mixed Gas-Steam Cycles: Part B—Water-Injected and HAT Cycles," ASME J. Eng. Gas Turbines Power, **117**, pp. 499–508.
- [20] Eidensten, L., Svedberg, G., Yan, J., and Ågren, N., 1994, "New Heat and Power Production Processes (Nya el- och värme-produktionsprocesser)," Technical Report (in Swedish), Royal Institute of Technology, ISSN-1104-3466/TRITA-KET R19.
- [21] Stecco, S. S., Desideri, U., Frachini, B., and Bettagli, N., 1993, "The Humid Air Cycle: Some Thermodynamical Considerations," ASME Paper No. 93-GT-77.
- [22] Rosén, P., 1993, "Evaporative Gas Turbine Cycles—A Thermodynamic Evaluation of Their Potential," Licentiate Thesis, Department of Heat and Power Technology, Lund Institute of Technology, Lund, Sweden, ISRN LUTMDN/TMVK-7010-SE.
- [23] Yan, J., Eidensten, L., and Svedberg, G., 1995, "Investigation of the Heat Recovery System in Externally Fired Evaporative Gas Turbines," ASME Paper No. 95-GT-72.
- [24] Ågren, N. D., Westermark, M. O., Bartlett, M. A., and Lindquist, T., 2000, "First Experiments on an Evaporative Gas Turbine Pilot Plant—Water Circuit Chemistry and Humidification Evaluation," ASME Paper No. 2000-GT-168.
- [25] Bartlett, M., and Westermark, M., 2001, "Experimental Evaluation of Air Filters and Metal Ion Migration in Evaporative Gas Turbines," ASME Paper No. JPGC2001/PWR-19119.
- [26] Dalili, F., and Westermark, M., 2002, "Experimental Study on a Packed Bed Humidifier in an Evaporative Gas Turbine," ASME Paper No. JPGC2002-26106.
- [27] Thern, M., Lindquist, T., and Torrison, T., 2003, "Theoretical and Experimental Evaluation of a Plate Heat Exchanger Aftercooler in an Evaporative Gas Turbine Cycle," ASME Paper No. GT2003-38099.
- [28] Jonsson, M., and Yan, J., 2003, "Economic Assessment of Evaporative Gas Turbine Cycles With Optimized Part Flow Humidification," ASME Paper No. GT2003-38009.
- [29] Bartlett, M. A., Wikman, K., Holmgren, K., and Westermark, M., 2002, "Effective Waste Utilisation in Hybrid Cycles for CHP Applications—A Cycle and System Study," Proc. ECOS 2002, Vol. II, pp. 804–813.
- [30] Simonsson, N., Anheden, M., Eidensten L., and Tollin, J., 2002, "Evaporative Gas Turbines—Humidified Air Gives Flexible Power for the Future," Proc. POWERGEN 2002, Milan, Italy.
- [31] Westermark, M., 1996, "Method and Device for Generation of Mechanical Work and, if Desired, Heat in an Evaporative Gas Turbine Process," International Patent Application No. PCT/SE96/00936.
- [32] Utriainen, E., 2001, "Investigation of Some Heat Transfer Surfaces for Gas Turbine Recuperators," Ph.D. thesis, Lund University, Dept. of Heat and Power Engineering, Lund, Sweden, ISBN 91-7874-118-1.

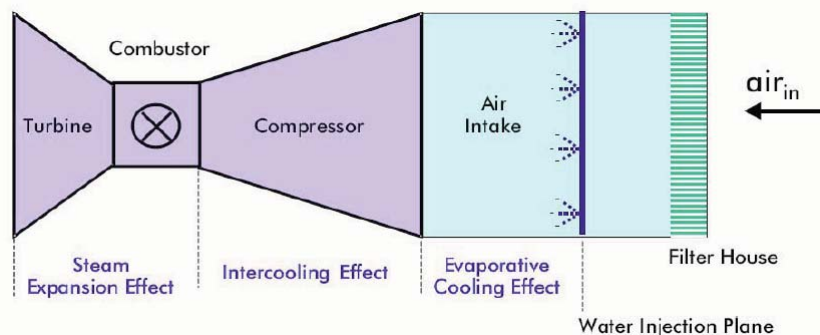
- Air temperature and altitude have a strong influence on the power produced and on efficiency (influence on density)
- Small effect also of humidity



a) Generator output and heat rate versus compressor inlet air temperature

Performance Data: SGT-600 Industrial Gas Turbine - 25 MW (Source: Siemens Westinghouse)

- Temperature decrease leads to a higher air mass flow swallowed. Relative humidity of the air increased to nearly saturation.
- Water evaporation inside compressor reduces compression work.
- Turbine power output is increased proportionally to the increased mass flow



Source: Soares, Gas Turbine Handbook, 2005

Gas Turbine Inlet Cooling

Scope, cost and performance for new and retrofit power plant projects

Turbine inlet cooling has always been prized for its ability to increase power output and improve the efficiency of simple cycle and combined cycle gas turbines in hot day operation.

Increasingly, operators have also come to see cooling as a low cost alternative for providing up to 25% more zero-emissions plant capacity without the environmental hassle, delay and cost of building a new plant. More specifically:

■ **Capacity.** Nominal increase in kW output on a 90F day can range from 5% to 25% of gas turbine nameplate rating depending on the inlet cooling technology, gas turbine design and ambient air conditions.

■ **CO₂ emissions.** The added capacity is accompanied by a decrease in site or regional CO₂ and other fuel-related emissions directly proportional to the increase in kW output, a

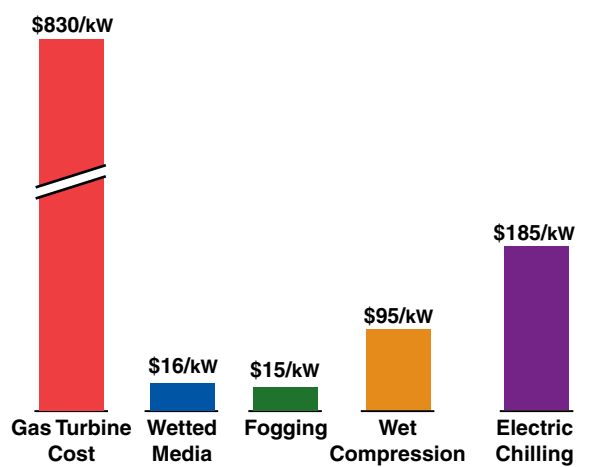
reduction in plant heat rate (Btu/kWh), and associated suppression of generating with less efficient machines in order to meet system demands.

■ **Capital cost.** Installed costs can range from \$15 per kW for evap/fog water spray inlet cooling to \$185 per kW for refrigerated chilling, as referenced to the gas turbine plant's standard ISO base load rating.

Aside from the considerable spread in capital cost of different cooling technologies (see Fig. 1) there is wide variation in their ability to enhance gas turbine performance during hot, cool or humid operating conditions.

Ultimately, the optimum choice of technologies is largely determined by site weather conditions, but it also depends on what you want to accomplish and how much you have to spend. Basic choices include:

Fig. 1. Ballpark estimates of TIC system costs for an F-Class combined cycle plant



Source: TICA White Paper, November 2009

Relative capital cost of turbine inlet cooling system installations referenced to the \$/kW cost of a new F-Class combined cycle power plant prior to the addition of gas turbine inlet cooling.

Wetted media. Turbine inlet air flowing through a continuously wetted honeycomb type fiber material (normally cellulose) evaporates water off surrounding surfaces of the wet medium thereby cooling itself. Wetted media can cool the inlet to within 85% to 95% of the difference between ambient dry bulb and wet bulb temperature. In low humidity areas, the evaporative cooling can boost power output by up to 15%, while in high humidity areas the increase is more likely to be under 10%, approaching zero at the point of saturation (100% relative humidity).

Fogging. Very fine droplets of water are sprayed into the warm inlet air stream where the droplets evaporate to cool the air (similar to wetted media systems). In this case, the fogging can be controlled to produce droplets of various sizes, depending on desired evaporation and inlet residence time under prevailing ambient air temperature and humidity conditions. Fogging can cool inlet air by 95% to 99% of the difference between ambient dry bulb and wet bulb temperatures which makes it a bit more effective than wetted media.

Wet compression. More finely atomized water than needed for inlet cooling alone is sprayed into the

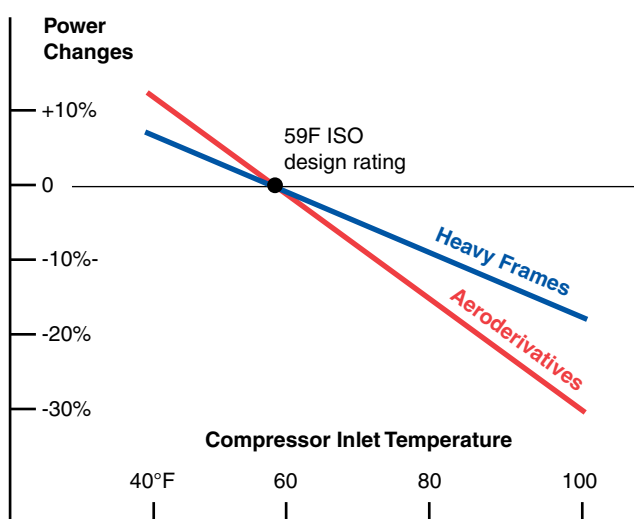
intake as micro-sized droplets. Typically 3x to 4x more fogging is added than can be evaporated in the inlet (sometimes referred to as high fogging or overspray). The air stream carries over the excess water fog into the compressor section of the gas turbine where it further evaporates for compressor inter-cooling and mass flow enhancement. Combination of inlet and compressor cooling can boost power output by upwards of 25% independent of ambient temperature conditions.

Chilling. Refrigeration based system where the ambient intake air is cooled by chilled heat transfer fluid circulating through cooling coils placed inside the inlet ductwork. Electrically driven mechanical chillers or absorption chillers (steam or hot water) may be used to cool the heat transfer fluid. Chilling is not limited by humidity so it is possible to cool ambient air below its wet bulb temperature, typically down to around 45F to 55F, for upwards of a 25% increase in power output.

Gas turbine sensitivity

The power output of any gas turbine is very sensitive to ambient temperature. Maximum power typically drops by about 0.3% to 0.5% for each degree Fahrenheit increase in ambient

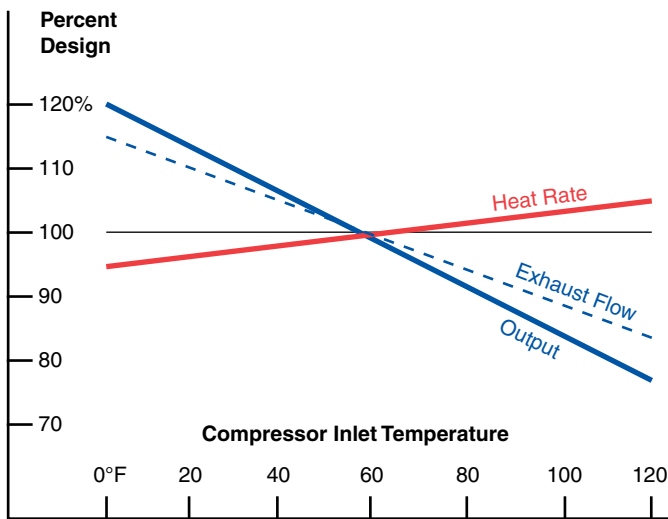
Fig. 2. Generic response of gas turbine power to changes in ambient air temperature



Source: GE Energy Oil & Gas

All gas turbines lose power as ambient air temperature increases, with higher pressure ratio aeroderivative designs losing almost twice as much per degree rise in temperature than do lower pressure ratio heavy frame units.

Fig. 3. Impact of temperature on MS7001 power output, exhaust flow and heat rate



Source: GE Energy Oil & Gas

Each gas turbine model has its own temperature-effect curve determined by cycle parameters (such as pressure ratio) and component efficiencies as well as air mass flow.

temperature (0.5% to 0.9% for each degree Celsius rise).

Heavy frame machines are less sensitive than aeroderivative units. Typically, they operate at lower pressure ratios than aero units but with much higher mass flow, so that temperature changes have proportionately less impact.

For example, on a 95F day, the power output of an old heavy frame unit operating at a pressure ratio of around 10 to 1 will decline by 7 or 8% (off its standard 59F nameplate rating) as compared to a 15% drop for a new aeroderivative gas turbine operating at a 30 to 1 pressure ratio (see Fig.2).

The chart shows the generic sensitivity of heavy frame and aero gas turbine output to changes in ambient temperature. In real life, each gas turbine model has a unique temperature-effect curve specific to its design parameters and component efficiencies with respect to change in power output, heat rate and exhaust flow (see Fig.3).

How inlet cooling helps

High ambient temperatures usually coincide with peak

demand periods and are especially detrimental during hot summer days when the reduction in power output is greatest.

Inlet cooling offers a low cost solution to offset power loss at high ambient temperatures. Cooling the inlet air below 59F allows gas turbines to exceed their rated output.

In addition, inlet cooling and particularly wet compression helps minimize the degradation in heat rate with increases in ambient temperature. Since gas turbine heat rate is inversely proportional to fuel efficiency, any increase in heat rate means higher fuel consumption – along with fuel related CO₂ emissions and other pollutants.

Inlet cooling also has a positive effect on steam production and power output of combined cycle plants. Increased gas turbine mass flow entering the heat recovery boiler produces more steam which, in turn, helps increase steam turbine kW output.

Retrofitting a high efficiency combined cycle plant with inlet cooling is also an effective way of increasing peak power output and reducing the cost of elec-

tricity (COE) compared to an advanced simple cycle peaker (see Fig. 4).

Annualized \$65/MWh cost of electricity for a 2x1 combined cycle 207F peaking plant with chilling added is over 40% less than the \$115/MWh COE for a simple cycle LM6000PC Sprint peaker with hot selective catalytic reduction and inlet cooling.

Combined cycle cost includes an annual fixed long term service fee of \$20 per ton (\$110,000) for the chiller plus an off-peak power cost of \$40 per MWh (amortized over peak hours) to recharge thermal energy storage tanks.

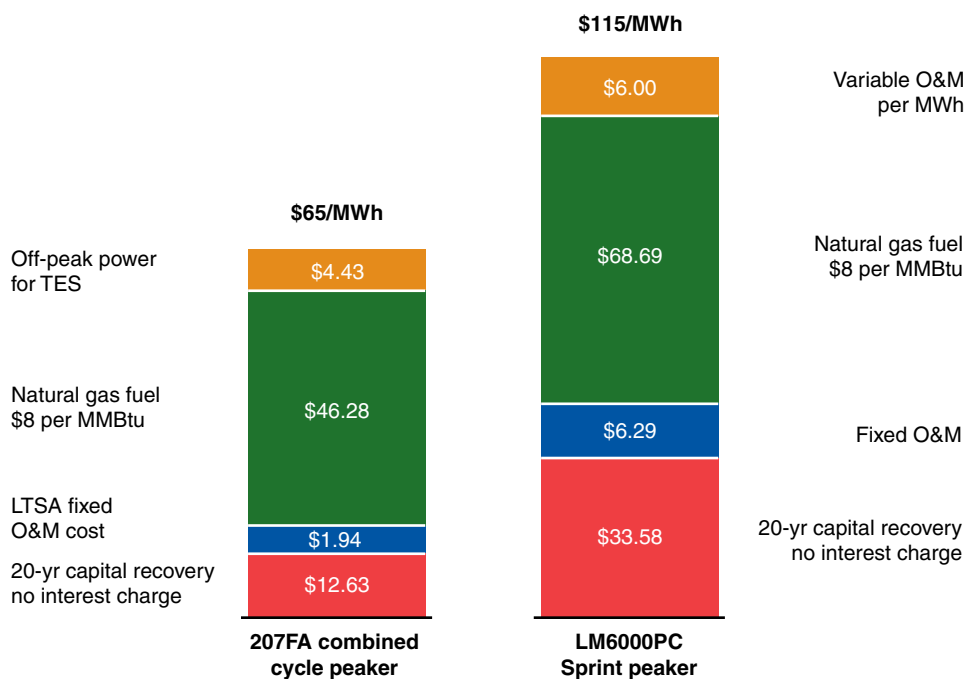
COE for simple cycle LM6000PC includes a fixed cost of \$250,000 per year for scheduled overhaul and maintenance, \$6 per MWh variable O&M cost, plus additional fuel cost.

Dispatch factors

The preferred order of dispatch for providing electric power from a combined cycle peaking plant incorporating turbine inlet cooling and duct firing is to bring the most efficient combination of technologies online first (see Fig. 5).

This chart is based on a 2x1 Fr 207FA combined

Fig. 4. Chilling improves comparative COE of combined cycles (\$65 vs. \$116/MWh)



Source: TICA White Paper, November 2009

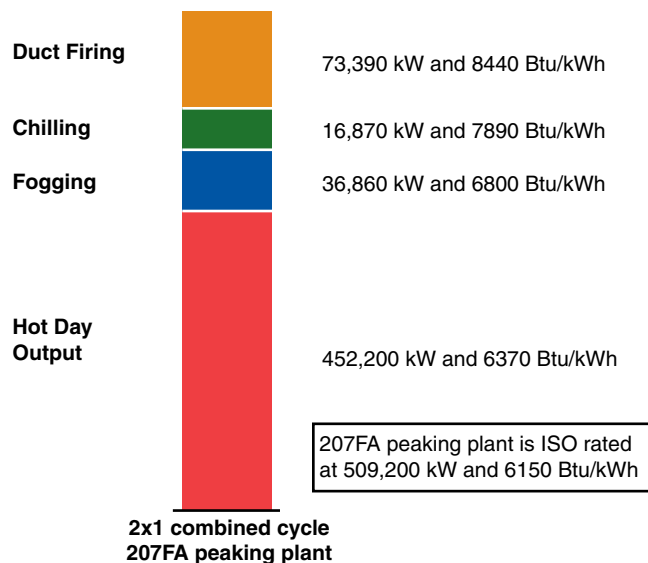
cycle peaking plant ISO rated at 509,200 kW and 6150 Btu/kWh heat rate (55.5% efficiency) equipped with evap/fogging and inlet chilling plus supplementary duct firing to increase HRSG steam output.

Calculations show that plant performance falls off to around 452,200 kW output and 6370 Btu/kWh heat rate (53.6% efficiency) at 95F dry bulb and 78F wet bulb inlet air temperature conditions.

Cooling the inlet air flow by fogging to its dew point will add 36,860 kW and increase net plant output to 489,060 kW at 6800

Cost of incremental energy (\$/MWh) for a chilled 207FA combined cycle peaking plant is significantly lower than for a simple cycle LM6000PC Sprint peaker with inlet cooling.

Fig. 5. Turbine inlet cooling has priority over duct firing for max dispatch efficiency



Source: TICA White Paper, November 2009

Power output of a 2x1 207FA combined cycle can be raised to almost 580 MW from 452 MW on a 95F DB and 78F WB day by fogging to dew point for a 36.9 MW gain, chilling to 50F for another 16.9 MW, and supplementary duct firing for a 73.4 MW boost in steam turbine output.

Btu/kWh heat rate (50.2% efficiency). Chilling to further cool the air to 50F will add another 16,870 kW for a net plant increase to 505,930 kW and 7895 Btu/kWh heat rate (43.2% efficiency).

Supplementary duct firing could boost steam turbine generation by 73,900 kW and increase total combined cycle plant output to 579,830 kW at 8440 Btu/kWh heat rate (40.4% efficiency).

CO₂ reduction

One major environmental benefit of inlet cooling technology is that it enables simple cycle and combined cycle gas turbine plants to operate at higher than rated power output and efficiency, despite hot and humid air conditions.

The increase in capacity helps defer (and sometimes eliminate) the need to bring older and less efficient power plants online to meet grid demand, particularly for peaking power. Higher efficiency reduces fuel consumption and production of collateral CO₂ emissions and other fuel-related pollutants.

Turbine inlet cooling for already efficient combined cycle plants allows them to operate at significantly lower CO₂ emissions per

kWh of generation in comparison to highly efficient simple cycle gas turbines equipped with inlet cooling (see Fig. 6).

The 1x1 F-Class combined cycle plant shown in the chart is rated at 260MW and 57% to 58% efficiency. Under 95F dry bulb and 78F wet bulb temperature conditions, with inlet air cooling, the combined cycle plant will generate about 700 lb of CO₂ per MWh of generation compared to 980 lb for the same plant without cooling.

That is less than the 1100 lb of CO₂ per MWh for a simple cycle LM6000 Sprint peaking plant equipped with inlet cooling – and significantly lower than the 1900 lb of CO₂ produced by a natural gas-fired steam plant.

Regulated criteria pollutants

Additional benefits of gas turbine inlet cooling include a decrease in emissions of all kinds that accompany improvements in heat rate.

The reduction in regulated criteria pollutants, notably hydrocarbons (HC), carbon monoxide (CO) and nitrogen oxide (NO_x), is similar to that of carbon dioxide emissions for inlet cooled simple cycle and combined cycle plants.

Compare a 2x1 207FA combined cycle plant with those of a simple cycle LM6000PC Sprint peaking plant, for example, both plants operating with selective catalytic reduction (SCR) to limit NOx emissions to 3 ppm and both equipped with turbine inlet cooling (see Fig. 7).

As shown in the bar chart, the combined cycle plant produces 0.19 lb of regulated criteria pollutants per MWh of generation versus 0.42 lb for the simple cycle plant – better than 50% lower in all categories.

TIC project benefits

Operational and economic benefits of turbine inlet cooling apply to new gas turbine projects, both simple cycle and combined cycle plants, and to existing plants on a retrofit basis.

For new projects, the economic benefit of inlet cooling is that the \$/kW cost for the increase in capacity is usually well below the \$/kW capital cost of the plant on its own.

When retrofitted to existing plant installations, especially combined cycles, the added capacity can be enough to eliminate the need for new generating capacity.

The relative potential of various cooling technologies to increase capacity (without burning more fuel) depends on ambient air conditions. Take for instance a 2x1 501FD combined cycle plant ISO rated at 500 MW (Fig. 8).

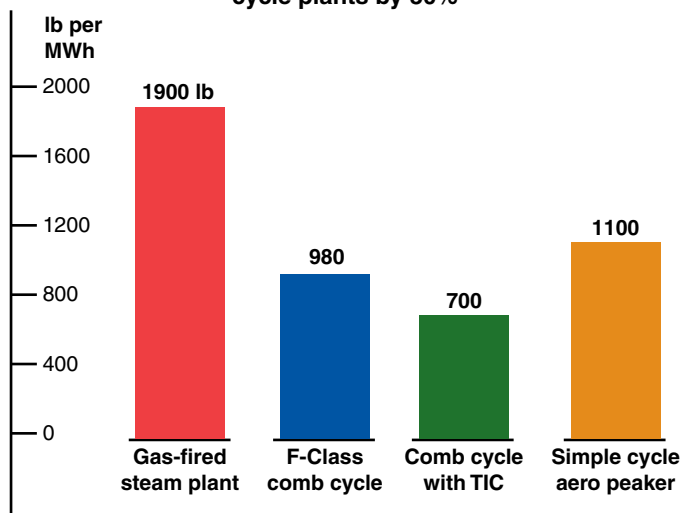
As shown, wetted media and fog cooling are more effective adding capacity when the relative humidity of the ambient air is lower; chilling and wet compression are both much less dependent on humidity.

It is worth noting that many comparative charts (including those in this reference section of the GTW Handbook) are based on reasonable assumptions for each technology based on experience and in-depth design study of equipment capabilities and performance.

They are intended to provide a generic grasp of commonly applied cooling technologies and should be treated accordingly rather than be accepted as gospel or case history.

For preliminary planning purposes or questions about performance, the major TIC system suppliers are always the best source for information directly related to your project interests.

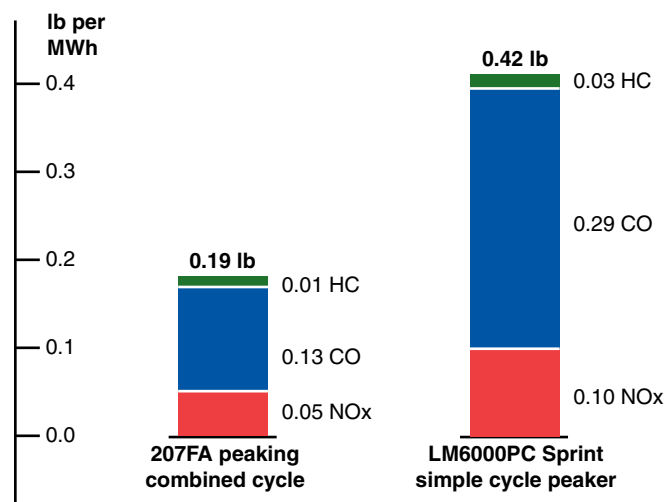
Fig. 6. Inlet cooling can also reduce CO₂ of combined cycle plants by 30%



Source: TICA White Paper, November 2009

Adding inlet cooling to a typical F-Class combined cycle plant can reduce CO₂ to 700 lb/MWh at 95F DB and 78 WB conditions, far less than the CO₂ emissions produced by simple cycle aero peaking and gas-fired steam plants.

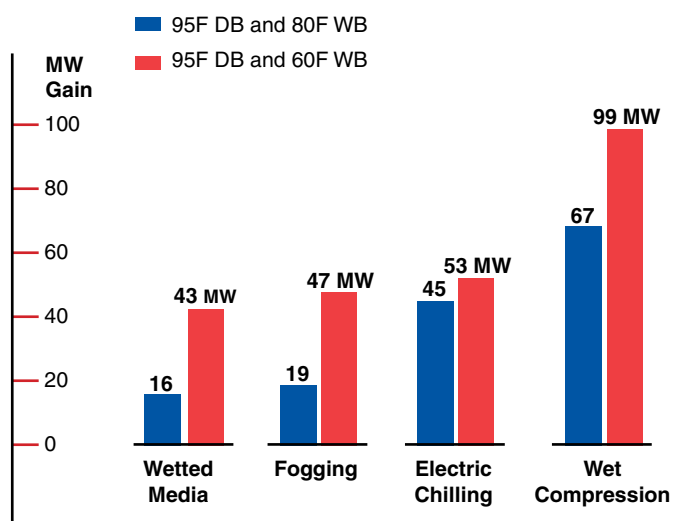
Fig. 7. Inlet cooling reduces total emissions of regulated criteria pollutants



Source: TICA White Paper, November 2009

Nominal 530 MW 207FA combined cycle peaking plant, with inlet cooling, will produce less than half the regulated criteria pollutants (0.19 lb/MWh) of an inlet cooled simple cycle LM6000PC Sprint peaking plant (0.42 lb/MWh).

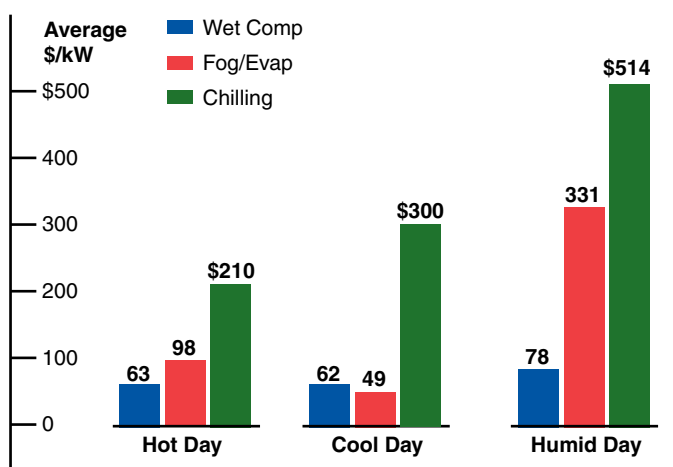
Fig. 8 Impact of humidity on hot day power gain of turbine inlet cooling technologies



Source: Caldwell Energy, January 2010

Chilling and wet compression are much more effective than evap/fogging at both high and low humidity levels, as shown here for a retrofitted 500 MW 2x1 W501FD1 combined cycle plant on a 95F day.

Fig. 9. Cost per kW of power augmentation for a 24-hour period



Source: Caldwell Energy, January 2010

Calculating the \$/kW cost of inlet cooling based on the kW gain under hot, cool and humid conditions is a better indicator of true costs than a plant's \$/kW capital cost.

Evaluation factors

The power capacity enhancement potential of different turbine inlet cooling technologies for a specific project application depend largely on geographic location of the plant (climate and weather) and gas turbine design performance characteristics.

The economic choice of technologies depends largely on the projected return on investment with respect to expected hours of operation during the year under comparable temperature and humidity conditions, amount and value of the incremental increase in power produced, and competitive cost of outside purchased power.

The same historical weather data that utility planners work with to analyze peak load demand during different seasons and hours of the day can also be used to evaluate and estimate the annual gas turbine inlet cooling load and frequency of hot, cool and humid days of operation (see Fig. 9).

For purposes of this chart, a hot day is defined as 90F dry bulb and 60F wet bulb temperatures at 15% relative humidity; cool day as 67F DB and 50F WB at 27% relative humidity; and humid day as 72F DB and 64F WB at 65% relative

humidity.

Hourly costs (\$/kW) are averaged over the entire day that a system is used to approximate the relative cost of cooling technology options operating at hot day, cool day and humid day ambient air conditions.

For hot day operation, as the chart shows, the wet compression average cost is \$63/kW; fog/evap cooling is \$98/kW; and chilling \$210/kW. The significant difference between these technologies, say cooling project engineers, is due to the varying spread between dry and wet bulb temperature throughout the day.

Similarly, energy gains (MWh) differ for each technology (see Fig. 10). For hot day operation, wet compression shows a gain of 854 MWh; fog/evap cooling 235 MWh; and chilling 301 MWh.

The cooling technology gains for hot day, cool day and humid day operation represent the increase in saleable energy over a 24-hour period.

Built-in cooling

Gas turbine builders also incorporate compressor intercooling to augment power output. GE Energy Aero, for one, has been in-

creasing the power output of its LM6000 series by at least 15% to 20% with its Sprint (spray intercooling) design upgrades.

The latest LM6000PF model is ISO rated at around 43 MW and 8220 Btu/kWh heat rate (41.5% simple cycle efficiency). The LM6000F Sprint version, with water intercooling, is rated at 48 MW.

Last year, Rolls-Royce introduced its new Trent 60 gas turbine design with an inlet spray intercooling (ISI) option that integrates inlet and compressor fogging to significantly enhance performance.

For instance, the Trent 60 DLE design is nominally rated at around 52 MW base load output and 8100 Btu/kWh heat rate (42% simple cycle efficiency) at 59F ISO conditions. The same machine can be uprated by inlet spray intercooling to around 58 MW

and 7965 Btu/kWh heat rate (42.8% efficiency).

Results are even more dramatic for hot day operation where the Trent 60 DLE design is rated at 42 MW and 8580 Btu/kWh heat rate (39.8% efficiency).

With ISI enhancement, the same machine can be uprated to 53 MW and 8200 Btu/kWh heat rate (41.6% efficiency) at an ambient air temperature of 90F (see Fig. 11).

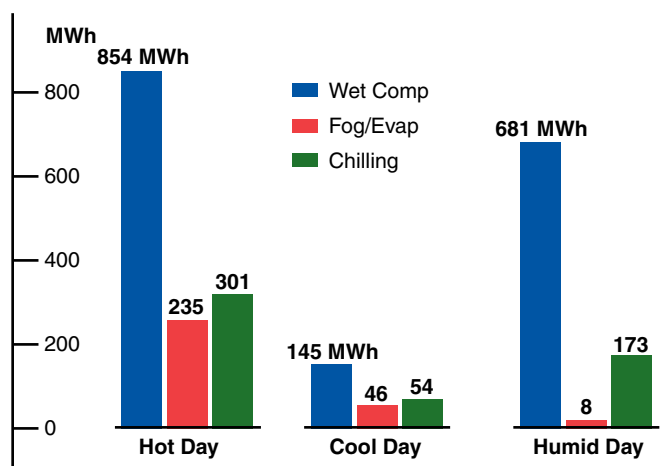
GE Energy's LMS100 gas turbine design incorporates off-engine intercooling (heat exchanger) to give it a nominal rating of 100 MW and 7580 Btu/kWh heat rate (45% simple cycle efficiency).

Several LMS100 power plant peaking and base load installations have been equipped with evaporative inlet cooling systems for hot day performance enhancement. ■

Reference material

We want to thank the industry suppliers and cooling system project engineers who contributed to this reference piece. For more information about the impact of power augmentation on reducing carbon footprint, we refer you to a White Paper published by the Turbine Inlet Cooling Association entitled *Turbine Inlet Cooling: An Energy Solution That's Better for the Environment, Ratepayers and Plant Owners*, dated November 24, 2009. You can reach the TIC Association online at www.turbineinletcooling.org.

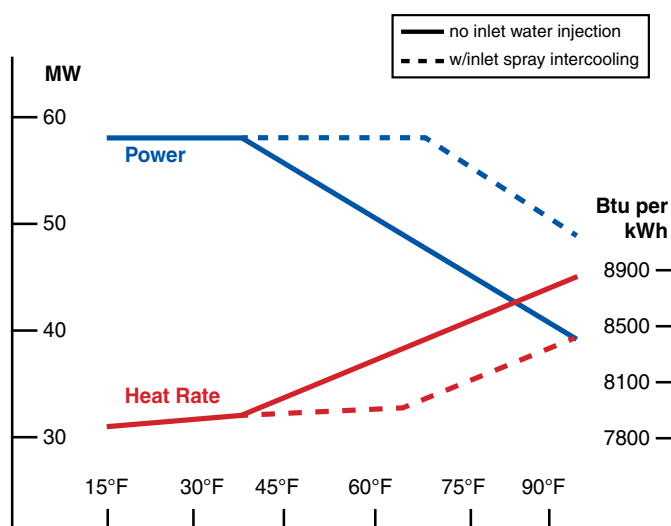
Fig.10. Increased daily energy from inlet cooling power augmentation



Source: Caldwell Energy, January 2010

Increased output of two 120 MW class gas turbines in combined cycle operation with turbine inlet cooling under hot, cool and humid day conditions represents the increase in saleable energy per MWh for a 24-hour period.

Fig. 11. Inlet water spray injection enhances Trent 60 DLE performance



Source: Gas Turbine World, Nov.-Dec. 2008

With water spray intercooling, power output can be increased from its 52 MW ISO design rating to a maximum 58 MW winter output from below zero to around 70F.



50/60 Hz market



- Large gas turbines have to run at frequency of electrical grid (no gears available)
- Europe, Africa, Asia: 50 Hz → 3000 rpm
America, Japan: 60 Hz → 3600 rpm
- In order to maintain the design of the flow channel and the velocities, the dimensions of 60 Hz variants are decreased by 5/6
- So mass flow and power are about 44 % larger in 50 Hz market

Table 4 Typical gas turbine scale factors

Machine	Frequency, Hz	Speed, rpm	Scale factors, linear area		Power, MW
GE Frame 7F	60	3600			159
GE Frame 9F	50	3000	1.2	1.44	226.5*
Siemens V64	90	5400			61.7†
Siemens V84	60	3600	1.5	2.25	139.5*
Siemens V94	50	3000	1.2	1.44	200.9

* scale factors are not exact where other cycle parameters also change

† excludes generator drive gearbox

Source: IEA Coal Research, 1995



Heavy Duty vs. Aeroderivative



Gas turbines are divided into **industrial gas turbines** („Heavy Duty“ or „Heavy Frame“) and in **aeroderivatives**

Aeroderivatives are re-designed jet engines and use jet engine technology with high specific power, good efficiency and high reliability (e.g. RR Olympus, GE CF6 → LM2500)

- mounted on light frames
- high performance leads to higher and thus increased maintenance efforts
- large number in operation
- often used in marine applications

Industrial gas turbines are robust, need less maintenance, but have - in general - lower efficiency

- Heavy and robust design



Fig. 13. The GE LM2500 (aeroderivative of the CF6-80C2). (Source: GE Power Systems)

Source: Soares, Gas Turbine Handbook, 2005



Heavy Duty vs. Aeroderivative

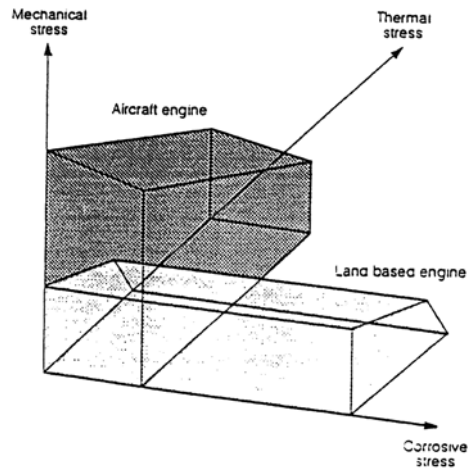


Figure 33 Schematic of the operational envelopes for aero and land-based turbines (Rickerby and Winstone, 1992)

Source: IEA Coal Research, 1995



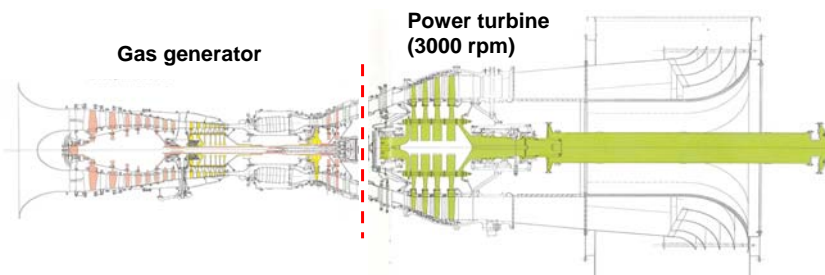
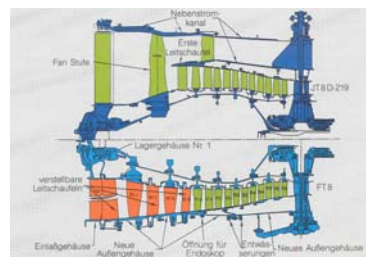
Aeroderivative FT8



JT8D by Pratt & Whitney (USA): 14 000 engines, 25 MW, high efficiency

Modifications to the gas generator:

- fan removed
- compressor casing
- one turbine stage removed



Source: MAN GHH

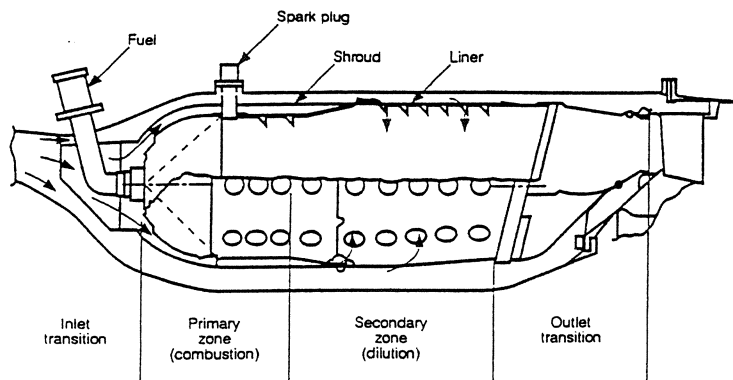


Figure 21 Combustion chamber flow diagram (Hazard, 1972)

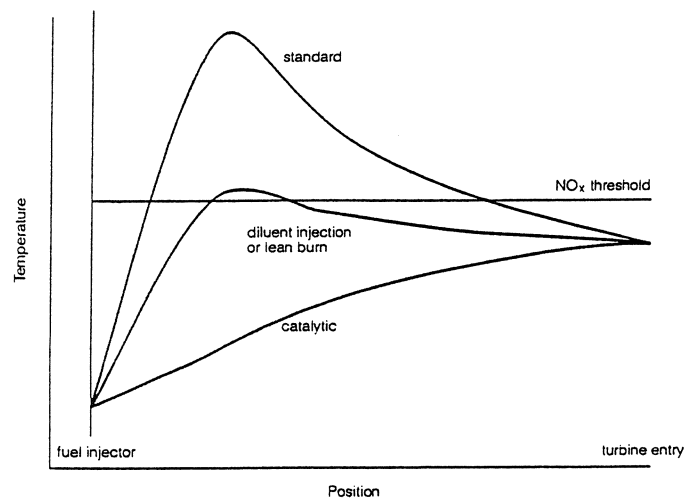
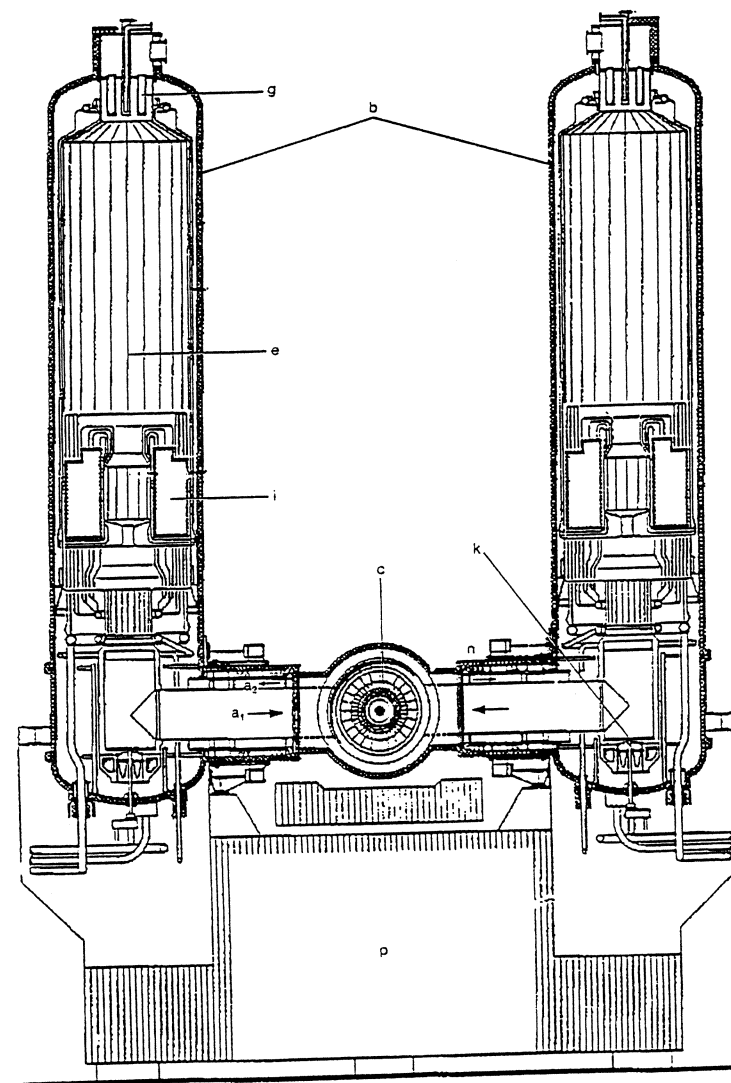


Figure 22 Combustion chamber temperature/distance profiles (Witton, 1993)



- | | |
|---|-----------------------|
| a ₁ - hot gas to turbine inlet | g - gas burner |
| a ₂ - compressor delivery air to combustor | i - superheater tubes |
| b - combustor with integral boiler | k - trim valve |
| c - gas turbine | n - expansion bellows |
| e - evaporator tubes | p - foundation |

Figure 25 Silo combustors with integral boiler surface (Dorstewitz, 1980)

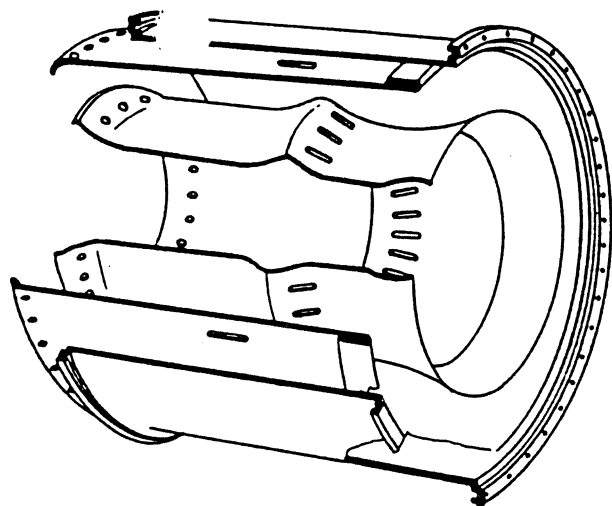


Bild 9.8 Einfache Ringbrennkammer

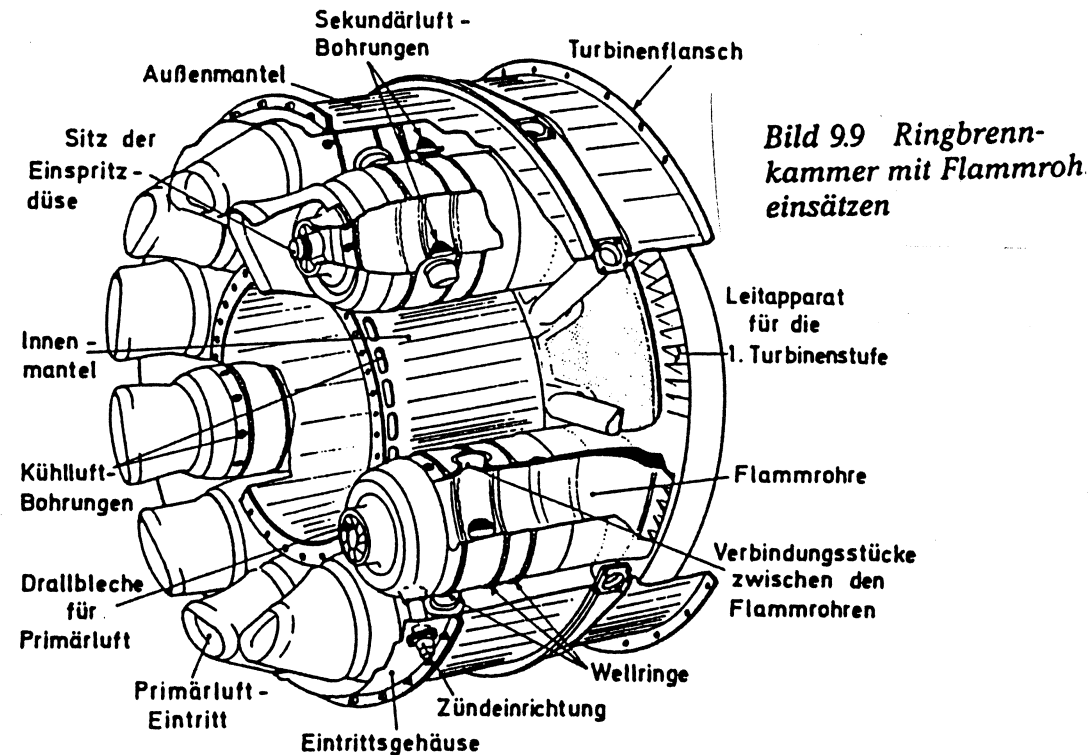


Bild 9.9 Ringbrennkammer mit Flammrohreinsätzen

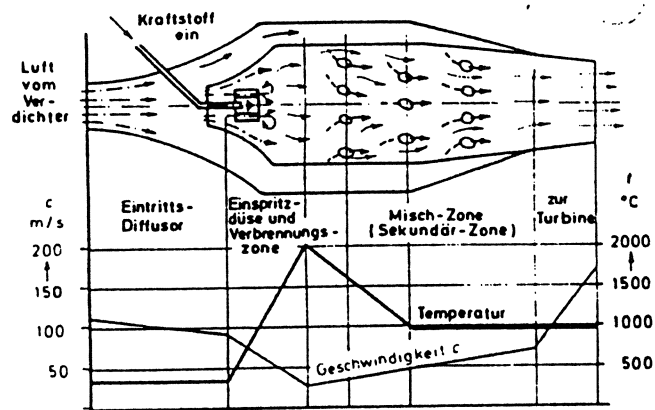


Bild 9.10 Geschwindigkeits- und Temperaturverlauf in einer Brennkammer

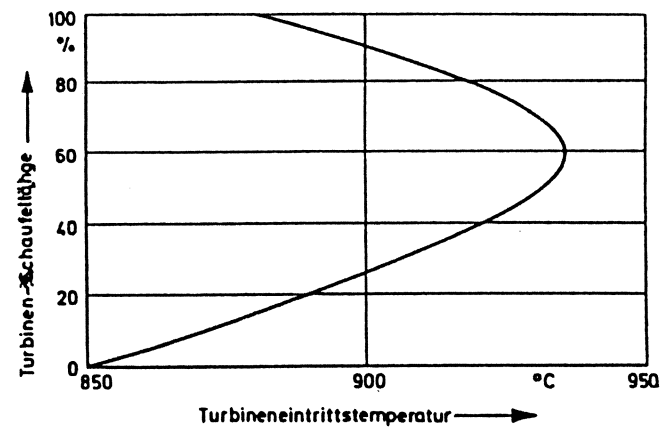


Bild 9.11 Temperaturverteilung am Turbineneintritt (nach Fa. AEG-KANIS)

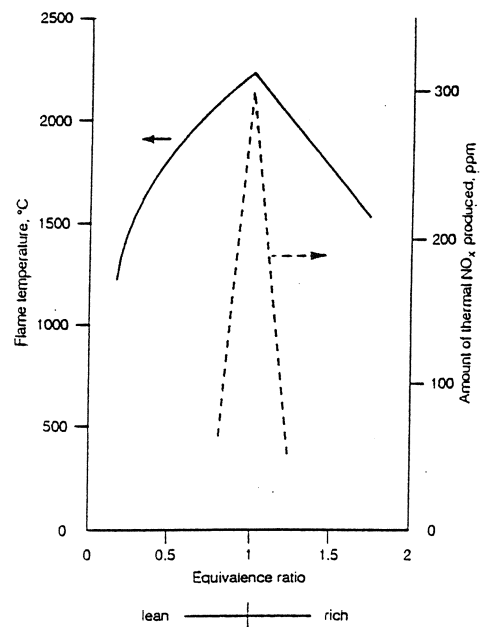


Figure 26 Variation of NO_x and temperature with equivalence ratio (Santos, 1993)

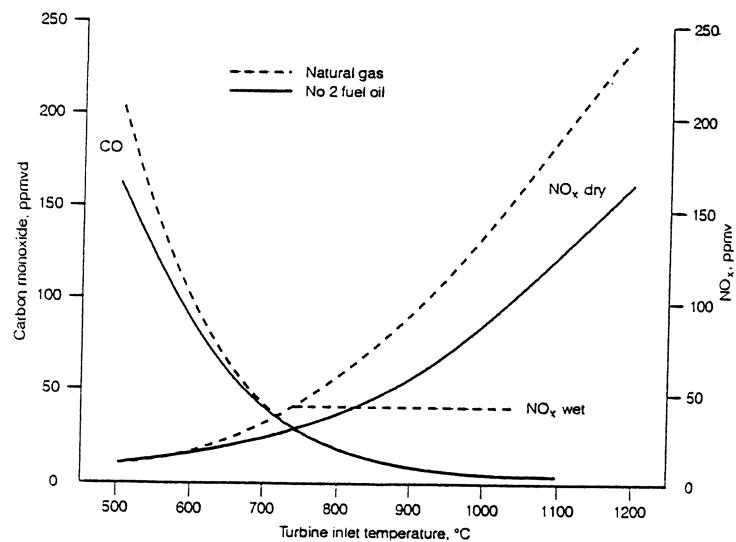


Figure 27 CO and NO_x variation with firing temperature (Schorr, 1992)

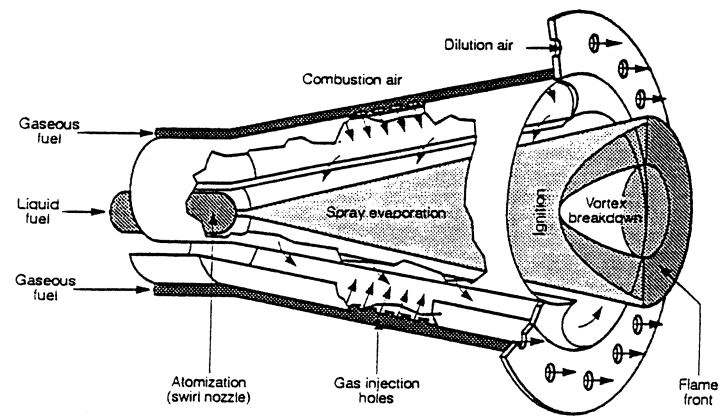


Figure 28 ABB environmental EV burner (Jeffs, 1989)

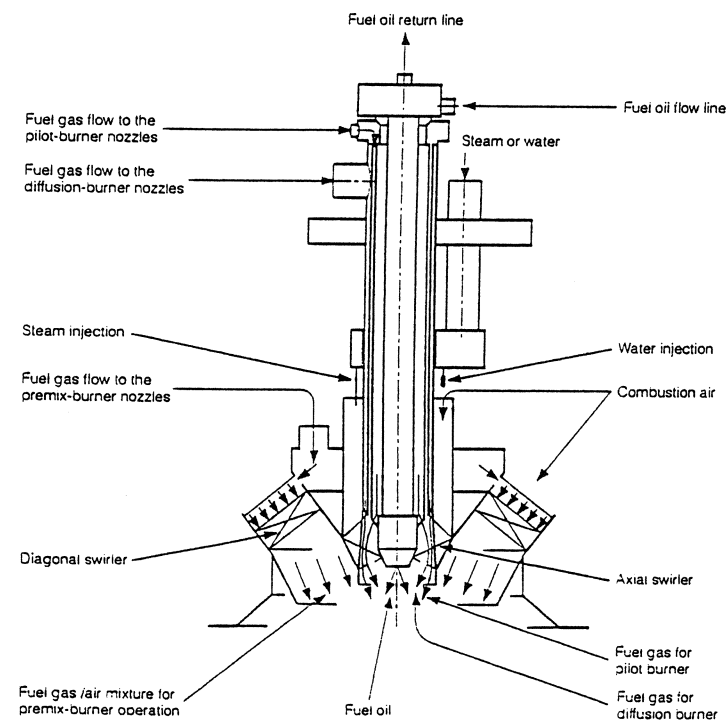


Figure 29 Siemens multi-fuel hybrid burner (Becker, 1988)

MARKET DRIVERS FOR ELECTRIC POWER GAS TURBINES: REASONS FOR THE REVOLUTION

by Lee Langston

INTRODUCTION

The record breaking thermal efficiencies of combined cycle gas turbine (CCGT) power plants and the clear advantages of simple cycle gas turbine (GT) power plants (quick start-up times, small size, lower manpower operating needs, small capital costs, and ready availability) have come together, making the gas turbine a revolutionizing force in electricity generating technology. Heavy frame industrial gas turbines (designed specifically for central and distributed power plants) and aeroderivative gas turbines (modified jet engines) are playing an increasingly important role in electric power generation. Figure 1 shows the orders placed (in megawatt capacities) for hydrocarbon-fueled electric power plants as a function of order year for the period 1970-1993. The plot¹

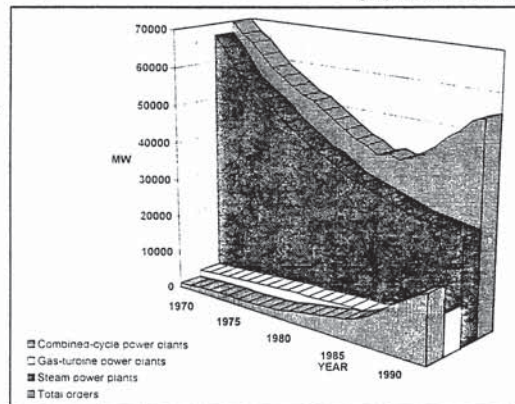


Figure 1. Development of orders placed (in megawatts, MW) worldwide for hydrocarbon-fueled power plants.

clearly shows the ascendancy of the gas turbine over "Big Steam". The worldwide orders for pure steam (Rankine cycle) power plants have decreased continuously, while those for CCGT and simple cycle GT (Brayton cycle) power plants have increased. These strong sales trends have carried over into the 1994-96 period, and show every sign of continuing into the next century.

Two years ago I wrote a *Global Gas Turbine News* "primer" on CCGT power plants², aimed at those (like myself) who have an aviation jet engine background and at others who may not be totally informed about the new dominant role being played by gas turbines in electrical power generation. In a CCGT power plant (Figure 2) the heavy frame or aeroderivative gas turbine is the key player, driving an electrical generator

and providing heat (the exhaust) to a heat recovery unit to make steam. Additional electricity is produced by the steam as it powers a steam turbine coupled to a generator. The combined thermal efficiency, η_{cc} , of these two cycles (Brayton, η_B ,

and Rankine, η_R) in today's operating plants is very close to an astonishing 60%. (As an undergraduate thermodynamics student some four decades ago, I remember the "gold standard" for prime mover thermal efficiency was about 40%.)

Continuing the primer theme for the information of those not directly aware of gas turbine electrical generation technology, I would like to briefly review some of the "market drivers" that influence the sale of gas turbines worldwide. By market drivers I mean those forces, conditions, or resources that cause or facilitate this new market dominated by gas turbine technology.

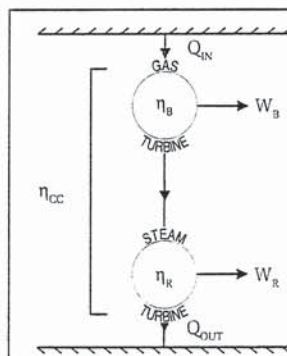


Figure 2. Combined cycle Brayton and Rankine engines, where $\eta_{cc} = \eta_B + \eta_R - \eta_B \eta_R$.

FUNDAMENTAL DRIVERS

The fundamental market drivers at those features of gas turbine power plants that are major determinants of the cost of producing electricity. The

cost is given by:

$$\begin{aligned} \text{Unit Cost of Electricity Produced} &= \text{Plant Operation and Maintenance Cost} \\ &+ \text{Capital and Finance Cost} \\ &+ \text{Fuel Cost.} \end{aligned}$$

This relationship is given by Horlock³ in a more quantitative form as:

$$(1) \quad Y = \frac{OM}{WH} + \frac{\beta C_p}{WH} + \frac{\zeta}{\eta}$$

Now let us look at the terms in (1) to better understand the fundamental market drivers:

Y - Unit Cost of Electricity Produced ... In the U.S. and the U.K. a typical value of Y could be \$0.03/kWh. Some more expensive power plants (e.g. nuclear) might be as high as \$0.05-0.07/kWh and some older hydroelectric power plants might have values of Y less than \$0.01/kWh. (In 1995 the price of electricity to consumers in industrial countries⁴ varied between \$0.04 and \$0.20/kWh.)

OM - Plant Operation and Maintenance Cost ... OM represents the cost of power plant operation and maintenance, expressed as \$/year. This term is generally much smaller for a GT power plant than for a nuclear power plant or a hydrocarbon-fueled steam plant, because of the GT's relatively long component life and low operating costs. For instance, a nuclear plant requires about 1 person/MW for efficient, safe operation. A GT power plant operates with about 0.1 person/MW, and some GT independent power producers (IPP's) claim less than 0.1 person/MW. Hydrocarbon-fueled steam power plant staffing needs fall somewhere between these GT and nuclear requirements.

W - Plant Output ... Plant output (W) is dependent upon the size of the unit and can range from 10 to 3000 MW. To get a good feel for what is a large and a small W, consider these approximate electrical loads:

- Entire State of Connecticut, or an "average" size U.S. electric utility: 5000 MW = 5,000,000 kW

- A "large" utility power plant: 1000 MW = 1,000,000 kW
- A smaller utility power plant, or a medium size independent power producer (IPP): 100 MW = 100,000 kW
- A large factory: 25 MW = 25,000 kW
- A 15,000 student university such as the University of Connecticut: 6 MW = 6,000 kW
- One kitchen toaster: 0.001 MW = 1 kW

H - Plant Utilization ... A base-load power plant, expected to operate continuously except for shutdown and maintenance, has a high value of H (hours/year), and operates more than about 6000 hours/year. Intermediate units generally run about 3000-4000 h/year and peaking units are brought on line for about 1000 h/year or less.

βC_p - Capital and Finance Cost ... βC_p (\$) represents the capital equipment and construction cost. C_p is the capital cost (\$) and β is the capital charge factor, which depends on the life of the plant, on the relative values of equity and debt financing, on whether the debt financing is less than the life of the plant, on tax rates and tax allowances (which vary from one country to another), and on inflation rates. (The interested reader can consult Horlock³ for an in depth discussion of β .)

The World Bank, export-import banks, independent power producer financiers and other money lenders have come to realize and appreciate the flexibility and lower risk offered by gas turbine power plants. This has kept β small in comparison to alternative power plants. In the words of one IPP entrepreneur, "Gas turbines are cheap, reliable and readily available ... practically off-the-shelf." Here are three β -reducing GT features the financial community has come to appreciate:

1. As one of the most compact of energy converters, gas turbines are very "portable". All but the largest frame machines can be moved as packaged units on flatbeds (truck

or train) or barges⁵. In the event of a loan default, a gas turbine is less likely than a nuclear or steam power plant to become a "stranded asset", and can be readily moved and resold.

2. Gas turbine power plants can be easily modularized, both physically and financially. If you are building a 300 MW plant using three 100 MW gas turbines, each unit can be financed as a standalone, producing power (revenue) as soon as construction is completed. Financial backers can count on financially sound project milestones and can easily adjust funding schedules if necessary.

3. Revenue production is maximized by short power plant construction times. Large gas turbine power plants can be constructed in as little as 1.5 to 2 years, while a steam power plant takes 3-5 years and a nuclear plant can take a decade.

The capital cost, C_p , of a power plant can vary widely depending on plant location, fuel utilized, government regulations, etc. Excluding the cost of land, C_p can be divided into three categories: rotating machinery (e.g. the gas and steam turbines), heat transfer and controls equipment, and construction/building costs. With a modern CCGT plant each cost category is about one-third of the total. Here are some current ranges of C_p , for large power plants, normalized by plant power output, W:

- Nuclear
\$1500 - 2000/kW
- Hydrocarbon-fueled Steam:
\$1200 - 1600/kW
- Combined cycle gas turbine:
about \$600/kW
- Simple cycle gas turbine:
about \$400/kW

Remember that these values for C_p must be multiplied by β in Equ. (1) to calculate the unit cost of electricity. However, they do show the clear

advantage of gas turbine electric power on a pure capital cost basis.

ζ/η - Fuel Costs ... The cost of fuel / plant efficiency, ζ/η (zeta / eta), is of paramount importance in determining the unit cost of electricity produced. Increasing thermal efficiency, η, yields lower fuel costs to the producer, and sixty-five years of gas turbine engineering have succeeded in bringing this about. The first electric power gas turbine ran in 1939 with η = 18% (Neuchatel, Switzerland). Now, simple cycle gas turbines are operating with thermal efficiencies exceeding 40% and CCGT power plants are operating in the 55-58% range. New "H" series frame machines are slated to reach or exceed CCGT efficiencies of 60%.

A key factor in the success of gas turbine electrical power generation has been low values of ζ, the unit cost of fuel (\$/kWh of input, or the fuel cost divided by the lower heating value of the fuel) brought about by burning natural gas. These low zeta values, coupled with high gas turbine efficiencies, η, tend to minimize Y in Equ. (1), creating the single most significant market driver for gas turbine sales. At present about 15% of the world's power plants* (based on rated output) are fueled by natural gas. Many of those powered by gas turbines are dual-fueled, with the capability of switching over (under load in many cases) to a stored distillate fuel.

Natural gas, composed mostly of methane, CH₄, has been called the "prince" of hydrocarbon fuels. It has the highest heating value per unit mass (21,520 Btu/lbm = 50.1 MJ/kg, LHV) of any of the hydrocarbon fuels (e.g. butane, diesel fuel, gasoline, etc.). It is the most environmentally benign of fuels, with impurities such as sulfur (hydrogen sulfide) removed before it enters the pipeline. (Just as an aside, the cost of transporting natural gas in pipelines is cheaper overall than transporting coal, but is more expensive than shipping oil long distances in ocean tankers.)

Since it has the lowest carbon content per unit mass, combusted methane produces about 30% less carbon dioxide per unit mass than does oil and about 43% less than coal. Combusting it does produce amounts of NO_x, with higher combustion temperatures producing greater amounts, something that can be controlled to a certain extent by the GT combustor designer.

A critical question is just how much natural gas is there? First of all, natural gas is not just a by-product of oil. It also occurs on its own in moderately sized fields and distribution in the world is more widespread than oil itself. I have replotted data given by Haamso et al¹ on the proven reserves and on production of both oil and natural gas in Fig. 3, for the years 1970-1992, normalized as tonnes of oil equivalent:

$$10^9 \text{ t.o.e.} = 0.04463 \times 10^{15} \text{ MJ} \\ = 4.227 \times 10^{16} \text{ Btu.}$$

One can see that the reserves of both oil and natural gas are quite large, compared to the production (consumption) of both. Also, Fig. 3 shows reserves and production of oil have been greater than those of natural gas. But, using the data in Fig. 3, Haamso points out that the average annual increase in reserves for natural gas is about 5.9% and that for oil is 2.8%, for the 1970-92 period. (See the curve slopes for each.) Based on these rates of reserve increase, the global gas reserves now (1996) exceed those of oil. However, the production of natural gas is still lower than that of oil, based on

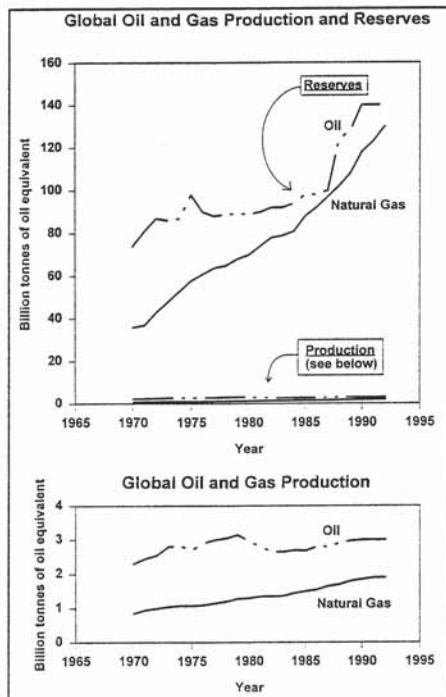


Figure 3. Global Oil and Gas Production and Reserves. (Bottom graph indicates production only, but on an expanded scale.)

extrapolation of the corresponding production curves.

Thus one can conclude that one of the most important gas turbine market drivers - cheap, abundant "environmentally clean" natural gas - should remain in place well into the next century. As a matter of fact, costs of finding more oil and gas are going down because of technical advances in seismology and much improved well drilling technology (so called "designer drilling"). These reduced costs and a new emphasis by drillers on finding gas fields (rather than just oil) should increase the natural gas reserve levels even more.

FUTURE DRIVERS

Now let us take a brief look at some of the trends and conditions not described by the terms in Equ. (1), that are gas turbine electric power market drivers now and will continue to be in the future.

UTILITY DEREGULATION AND PRIVATIZATION

Historically, electric utilities around the world, whether investor- or state-owned, have been regulated monopolies, generating electrical power, transmitting it over major transmission lines and distributing it to individual customers. This arrangement evolved from the confusion of the early days of electric service when competing companies in the late 1800s competed for customers, with power lines running haphazardly everywhere.

Now, following the trend of deregulation and privatization in other sectors (airlines, natural gas and communications), electric utilities are being broken up into generating companies (GENCO), transmission companies (TRANSCO) and distribution companies (DISCO) (called unbundling in the U.S.), eventually allowing the customers to choose GENCO based on a free market. This allows anyone to generate electric power, making it a market commodity similar to copper, corn and pork bellies. In the U.K., where public-sector utilities have been privatized since 1990, the price of marginal (non base-load) electric power is set by the "Pool" through daily spot market auctions, open to any power producer. In such a deregulated and unbundled market, significant price competition, as well as all of the fundamental gas turbine market drivers discussed earlier, will come into full play.

DISTRIBUTED POWER

This is a case of generating power where the people are located. From the discussion of fundamental

market drivers one can see that gas turbine power plants can be operated more efficiently and less expensively in smaller sizes than can steam or nuclear facilities. Smaller dispersed gas turbine units (below 200 MW), fueled by natural gas, can easily be used in place of a large single generating plant. In some locations the cost of bringing in a gas line for home heating and local industry can be justified by the installation of a gas turbine power plant producing revenue-earning electricity. Also, there is an argument that distributed power would make the electrical grid more robust, with the failure of any one smaller power plant of little consequence to the whole.

In developing countries (e.g. those in Southeast Asia) that have natural gas resources and that have either a "weak" electrical power grid or no grid, the financing of distributed power using gas turbines is much less expensive than installing a central power plant with an extensive and costly transmission system. (The grid can be put in place later when the economy is on a firmer, more advanced footing.)

REPOWERING

There are more than 200 investor-owned utilities in the U.S. supplying more than three-quarters of the electrical power consumed. Many of these utilities have delayed upgrading generation facilities because of the uncertainty of deregulation. Many of their existing plants can be "repowered" using gas turbines, making use of the existing power plant site. For instance, a relatively economical way is to replace worn-out boilers in a hydrocarbon-fueled steam plant with gas turbines and heat recovery units, converting the plant into a CCGT with higher efficiency and increased power output. Pollution levels also should drop with the removal of old inefficient boilers and their replacement with clean-burning gas turbines.

CONCLUSION

It was not possible in this short article to cover all aspects of electric power gas turbine market drivers. (For instance no mention was made of the important field of cogeneration and environmental issues weren't addressed in any great detail.) I hope that the reader has gained some insight into the reasons for the strong gas turbine sales shown in Fig. 1. If these sales trends continue, the annual sales value of electric power gas turbines soon will exceed that of aviation applications.

A strong argument can be made that the "market" discussed here has been brought about by the gas turbine itself. I quote the words of Robert Post, technology historian and author of *High Performance: The Culture and Technology of Drag Racing*:

"Often invention is the mother of necessity. No one foresaw the impact or the utility of telephones, cars, or television when they were first invented. But once people began to use them, they came to believe the products were invented for important reasons."

Frank Whittle, Hans von Ohain, the champions behind the 1939 Neuchatel gas turbine and thousands of other engineers have made the gas turbine the superbly efficient energy converter that it is today. We salute them and their collective efforts, for they are the real market drivers. *

REFERENCES

- ¹ Hansen, Teresa, "Gas-Turbine Industry Prepares to Become Base-Load Supplier", *Electric Light and Power*, PennWell, April, 1996, pp. 23-24. (Based on data from Siemens AG, RWV, Sept. 1995).
- ² Langston, Lee, "Combined Cycle Power Plants" *Global Gas Turbine News*, IGTI, Feb. 1994, pp. 24-25.
- ³ Horlock, J.H., *Combined Power Plants*, Pergamon, 1992, pp. 222-242.
- ⁴ The Economist, "Short Circuit", April 13, 1996, pp. 47-49.
- ⁵ Valenti, Michael, "Power Plants to Go", *Mechanical Engineering*, May, 1996, pp. 62-66.
- ⁶ UDI Datagram, Vol. 8, No. 1, McGraw-Hill, Spring, 1996.
- ⁷ Haamso, B., Mashayekhi, A., and Razavi, H., "International Gas Trade: Potential Major Projects", *Annual Rev. Energy Environ.*, Vol. 19, 1994, 37-73.

2017 Simple Cycle Genset Prices

Estimated equipment-only budget price for standard OEM bare bones design

How much does a simple cycle gas turbine packaged plant cost? All depends on the unit size and scope of equipment supply.

GTW's database covers a wide range of unit size and technology, and shows that price (\$) and unit price (\$ per kW), depend strongly on unit size and type of gas turbine (aero vs frame).

GTW's simple cycle plant prices are based on standard bare bones single-fuel (gas only) packaged units. A myriad of add-on options and customized design features are provided by the OEMs at additional cost.

The prices are quoted in US dollars, FOB factory, for single-unit purchases. They are for equipment only, and do not cover transportation, plant

engineering, construction, project-specific options or owner's project costs.

Except for some individual cases, where new information from the marketplace has indicated otherwise, this year's estimated gas turbine equipment prices reflect a slight downward trend compared to prior years.

This follows the general movement of the appropriate industrial price indices over the past two years (see <https://www.ihs.com/info/cera/ihsindexes/>).

The impact of the stronger US dollar relative to other major international currencies this past year has also put downward pressure on price levels (in US\$) for equipment manufactured in Europe and Asia.

Equipment scope. Limited to minimum scope of supply for an operational plant package built around a gas turbine engine, generator, associated mechanical and electrical auxiliary systems. Scope includes:

- **Gas turbine.** Skid-mounted gas turbine engine, starting motor, reduction gearbox (if any), lube oil and hydraulic fluid systems, compressor water wash, fuel forwarding and control, external turbine cooling (if any), interconnecting piping.

- **Generator.** Standard air-cooled generator package; hydrogen or enclosed water-air cooling (TEWAC) usually offered as options for larger units. Generator exciter is typically included in the standard package.

- **Balance of plant.** Standard auxiliaries such as air intake filter, inlet ducting and silencer, exhaust ducting and stack (short) with silencer, vibration monitoring, digital control.

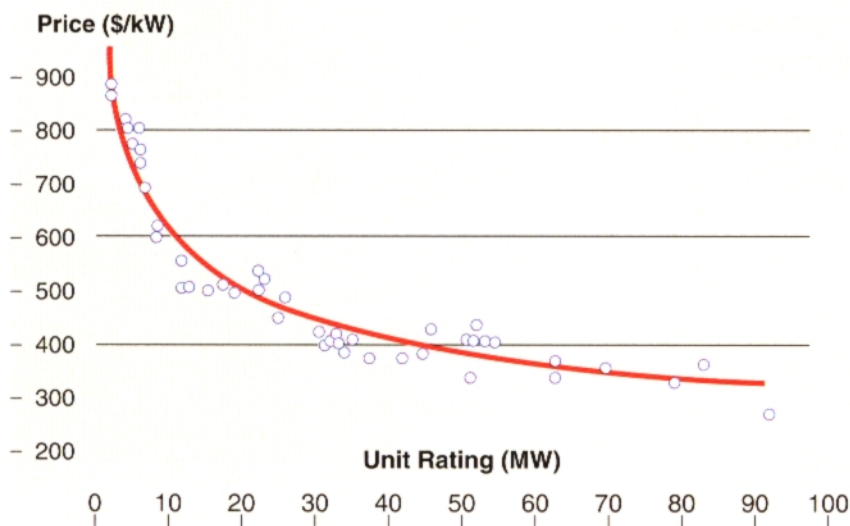
Packaged gensets typically include standard acoustic enclosures with ventilation and fire protection systems. Electrical auxiliaries include batteries, motor control center, voltage regulator and surge protection.

Mechanical and electrical auxiliaries for gas turbine operation are often pre-packaged and supplied as separate enclosed auxiliary skids.

Auxiliary transformers needed to condition power supply for plant motors (starting, lube oil pump and cool-

2017 Smaller Simple Cycle Gensets

Pricing data for simple cycle gensets rated below 100MW. "Best Fit" curve plotted as $\$/kW = 6815 \times (kW)^{-0.265}$.



ing fans) are usually optional, as is main power step-up transformer.

Other OEM options include liquid or dual-fuel (gas and liquid) combustion, inlet air chilling (or deicing), isolated phase bus, fuel gas compression, etc.

Performance. Gas turbine model power output and efficiency ratings in GTW's simple cycle pricing tables are OEM specified design ratings for base load operation at ISO standard (59°F ambient and sea level) conditions on natural gas fuel.

Estimated (\$ per kW) pricing, based on base load ratings, makes it possible to review and evaluate differences in unit pricing of equipment cost of competitively sized gas turbine plants.

The \$ per kW data also can estimate the likely ballpark price of gas turbine models not listed in the pricing table close enough in power output and efficiency to be competitive.

A best-fit relationship between kW rating vs \$-per-kW is provided for the data presented to assist in this calculation.

Other factors that influence GT package price are gas turbine type (i.e., frame vs. aero) and design parameters such as firing temperature, pressure ratio, mass flow, approximate weight and size.

Actual real-world OEM bid prices are quoted for customer-specified scope and with guarantees on net power and heat rate (efficiency) at site-specific conditions (i.e. ambient temperature, elevation and relative humidity) and specified fuel composition.

Bid quotes. OEMs strategically hedge project bidding with some performance margin, i.e. slightly lower power output and higher heat rate, to allow for normal variations in manufacturing tolerances and test uncertainties.

They will always bid on the basis of "factory new and clean" performance without allowance for degradation in performance with usage. Contract language usually specifies a limit in operating time before performance testing must be conducted.

Typically there is a margin of 0.5 to 1% on power and heat rate ratings. This explains why slightly better performance than expected may initially be realized.

Marketing factors that enter a project price quote include number of units ordered (there are usually quantity discounts), scope of equipment supply, site specifics, duty cycle, geographic location and local market share position.

Variation in currency valuations also play a significant role depending on which countries (i.e. currencies) are involved in the gas turbine's manufacture, purchase, and installation.

Gas turbine gensets designed for onshore oil and gas pipeline operation typically are priced around 10% higher



CLEAN AIR SOLUTIONS FOR TURBOMACHINERY

For more than 50 years, Camfil Power Systems has been developing and supplying clean air solutions that protect turbomachinery and maintain the highest efficiency. We offer you the optimum solution from the air inlet to the top of the stack.

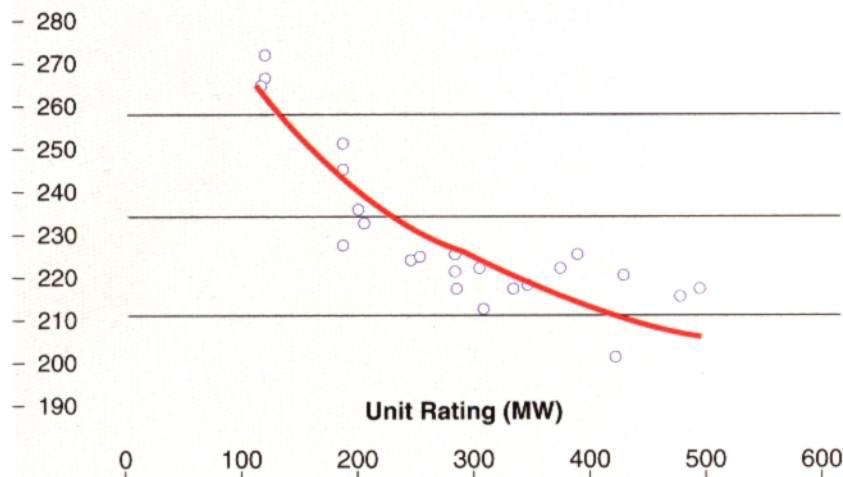
- Air Inlet systems
- Acoustic packages
- Enclosures
- Silencers
- Dampers & slides
- Service & retrofits
- Static & pulse filters
- Exhaust systems



2017 Larger Simple Cycle Gensets

Pricing data for large simple cycle genset units rated at over 100MW. "Best Fit" curve plotted as $\$/kW = 2165 \times (kW)^{-0.182}$.

Price (\$/kW)



than industrial or utility power plants. That is due to the cost of compliance with special packaging and safety requirements such as found in API specifications.

Offshore platform gas turbine packages command an additional price premium to cover costs such as specialized mountings and housing, marine-resistant coatings or ultra-efficient intake filter systems designed to handle salt-water laden air.

Scoping studies. This reference section of the GTW Handbook serves as

a benchmarking tool for assessing the equipment cost of different size and type plants.

To allow for uncertainties and changes in standard scope of supply offerings, these estimated budget prices should be treated as having a plus or minus 10% range of accuracy.

The data plot and best-fit curve shows the strong relationship of cost to plant size, especially with smaller units.

Small gas turbine plants rated in the 2 to 3MW range cost considerably more (\$/kW) than larger plants. A

2MW plant may be priced at around \$750 per kW compared to \$500 per kW for a 10MW plant.

From around 20MW on up to 100MW the \$ per kW price still falls off rather steeply (from more than \$500/kW to \$300/kW) with increasing output. This is due primarily to economies of scale which allow OEMs to reduce manufacturing costs (per kW) as unit size and power rating grow.

That holds true up to around 100MW beyond which the \$ per kW curve flattens and decreases more slowly, down to just over \$200/kW for the largest F, G, H and J class units.

The flat nature of the \$/kW vs kW curve for these advanced units reflect the high cost of more exotic materials, coatings, cooling techniques and more complex manufacturing required to operate at higher (2700°F to 2900°F) firing temperatures. All of which negate economies of scale that might otherwise be expected.

Regardless of gas turbine design and rating, however, remember that the cost of engineering and construction services can add from 60% to 100% and more to the cost of the equipment alone. For rough estimates, a rule of thumb could be to double the equipment price to estimate the cost of an installed unit. ■

2017 Simple Cycle Genset Prices

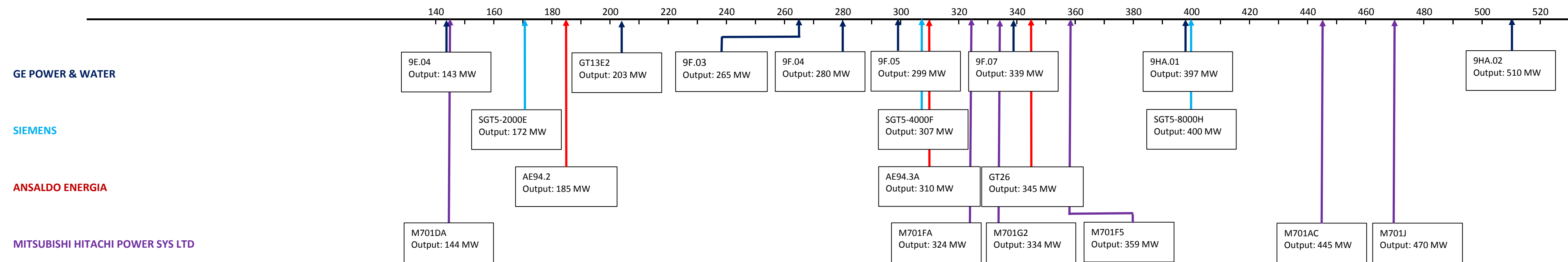
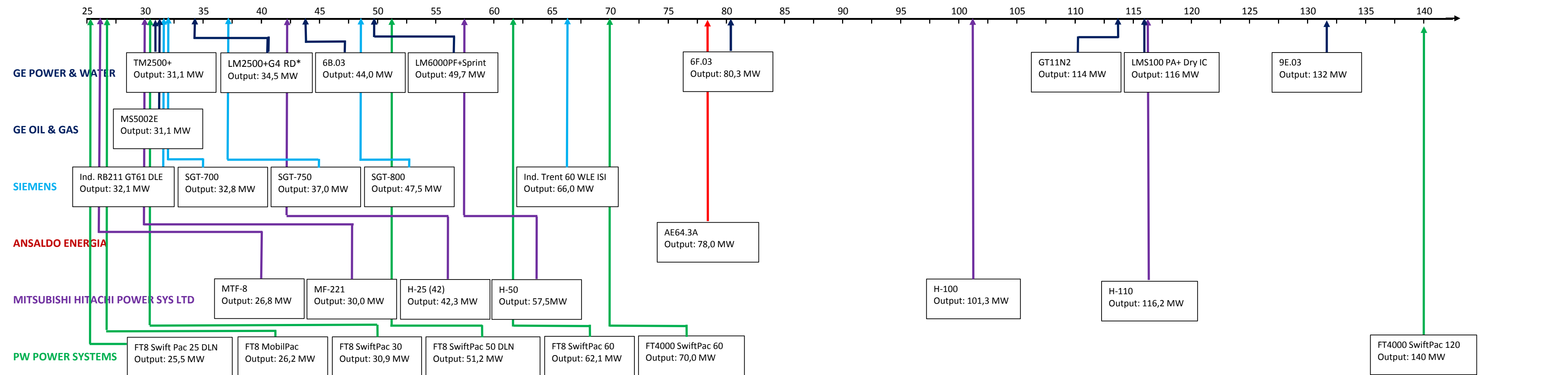
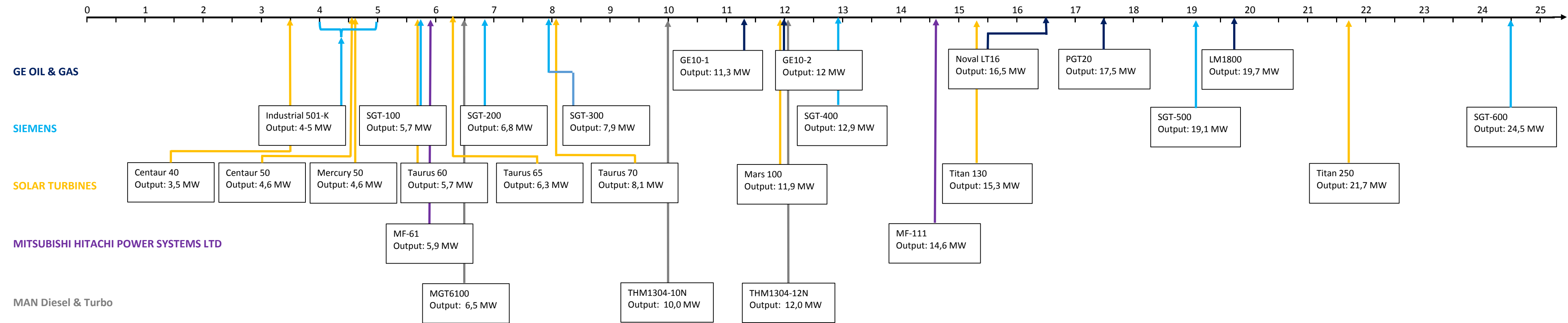
**Equipment-only budget price in fixed 2017 dollars
for standard OEM bare bones design**

Gas Turbine Model	Freq	Base Load Rating	Heat Rate Btu/ kWh	Efficiency	Budget Price	\$/kW
C200	50/60	200 kW	10,300 Btu	33.1%	\$210,000	\$1,050
M1A-17D	50/60	1,700 kW	12,701 Btu	26.9%	\$1,500,000	\$882
OP16-3C	50/60	1,850 kW	13,800 Btu	24.7%	\$1,600,000	\$865
Centaur 40	50/60	3,515 kW	12,240 Btu	27.9%	\$2,880,000	\$819
501-KB5S	50/60	3,980 kW	11,504 Btu	29.7%	\$3,200,000	\$804
Centaur 50	50/60	4,600 kW	11,630 Btu	29.3%	\$3,550,000	\$772
501-KB7S	50/60	5,380 kW	10,570 Btu	32.3%	\$4,300,000	\$799
SGT-100	50/60	5,400 kW	11,008 Btu	31.0%	\$4,120,000	\$763
Taurus 60	50/60	5,670 kW	10,830 Btu	31.5%	\$4,190,000	\$739
Taurus 65	50/60	6,300 kW	10,375 Btu	32.9%	\$4,350,000	\$690
SGT-300	50/60	7,901 kW	11,158 Btu	30.6%	\$4,750,000	\$601
Taurus 70	50/60	7,965 kW	9,955 Btu	34.3%	\$4,940,000	\$620
GE10-1	50/60	11,250 kW	10,867 Btu	31.4%	\$5,775,000	\$513
Mars 100	50/60	11,350 kW	10,365 Btu	32.9%	\$6,350,000	\$559
GTU-12PG-2	50/60	12,300 kW	10,469 Btu	32.6%	\$6,270,000	\$510
SGT-400	50/60	14,326 kW	9,647 Btu	35.4%	\$7,250,000	\$506
Titan 130	50/60	16,450 kW	9,605 Btu	35.5%	\$8,500,000	\$517
SGT-500	60	19,064 kW	10,132 Btu	33.7%	\$9,600,000	\$504
Titan 250	50/60	21,745 kW	8,775 Btu	38.9%	\$11,000,000	\$506
LM2500DLE	50	22,417 kW	9,636 Btu	35.4%	\$12,000,000	\$535
LM2500DLE	60	23,200 kW	9,317 Btu	36.6%	\$12,300,000	\$530
SGT-600	50/60	24,480 kW	10,161 Btu	33.6%	\$11,100,000	\$453
1x FT8 SP25 DLN	50/60	25,455 kW	8,960 Btu	38.1%	\$12,500,000	\$491
RB211-GT62 DLE	50/60	29,845 kW	9,089 Btu	37.5%	\$12,750,000	\$427
1 x FT8 SP30	50/60	30,892 kW	9,327 Btu	36.6%	\$12,500,000	\$405
LM2500+ DLE	60	31,900 kW	8,785 Btu	38.8%	\$13,250,000	\$415
RB211-GT61 DLE	50/60	32,130 kW	8,681 Btu	39.3%	\$13,750,000	\$428
SGT-700	50/60	32,820 kW	9,170 Btu	37.2%	\$13,250,000	\$404
MS5002E	50/60	33,310 kW	9,517 Btu	35.9%	\$13,000,000	\$390
LM2500+ G4 DLE	60	34,500 kW	8,709 Btu	39.2%	\$14,500,000	\$420

Gas Turbine Model	Freq	Base Load Rating	Heat Rate Btu/ kWh	Efficiency	Budget Price	\$/kW
SGT-750	50/60	37,031 kW	8,456 Btu	40.4%	\$14,100,000	\$381
H-25	50/60	41,030 kW	9,432 Btu	36.2%	\$15,600,000	\$380
6B.03	50/60	44,000 kW	10,180 Btu	33.5%	\$17,150,000	\$390
LM6000PF	60	45,000 kW	8,097 Btu	42.1%	\$19,400,000	\$431
LM6000PF Sprint	60	50,000 kW	8,109 Btu	42.1%	\$20,500,000	\$410
SGT-800	50/60	50,500 kW	8,899 Btu	38.3%	\$17,300,000	\$343
LM6000PG	50/60	51,204 kW	8,142 Btu	41.9%	\$21,000,000	\$410
2xFT8 SP50 DLN	50/60	51,235 kW	8,905 Btu	38.3%	\$22,500,000	\$439
LM6000PF+	60	53,000 kW	8,175 Btu	41.7%	\$21,600,000	\$408
Trent 60 DLE	60	54,020 kW	8,023 Btu	42.5%	\$22,000,000	\$407
2xFT8 SP60	50/60	62,086 kW	9,281 Btu	36.8%	\$21,450,000	\$345
Trent 60 DLE iSI	60	61,842 kW	7,867 Btu	43.4%	\$22,750,000	\$368
1xFT4000 SP60	50/60	68,747 kW	8,305 Btu	41.1%	\$24,500,000	\$356
AE64.3A	50/60	78,000 kW	9,400 Btu	36.3%	\$26,500,000	\$340
6F.03	50/60	82,000 kW	9,470 Btu	36.0%	\$30,200,000	\$368
7E.03	60	91,000 kW	10,060 Btu	33.9%	\$25,000,000	\$275
LMS 100 DLE	50/60	98,196 kW	7,580 Btu	45.0%	\$40,000,000	\$407
LMS100PB+ Wet	60	109,000 kW	7,746 Btu	44.0%	\$40,500,000	\$372
M501DA	60	113,950 kW	9,780 Btu	34.9%	\$30,000,000	\$263
LMS100PA+ Wet	60	117,000 kW	7,763 Btu	44.0%	\$40,500,000	\$346
SGT6-2000E	60	117,000 kW	9,705 Btu	35.2%	\$31,000,000	\$265
H-100	50	118,080 kW	8,919 Btu	38.3%	\$32,000,000	\$271
M701DA	50	144,090 kW	9,810 Btu	34.8%	\$38,600,000	\$268
AE94.2	50	185,000 kW	9,426 Btu	36.2%	\$46,000,000	\$249
M501F	60	185,400 kW	9,230 Btu	37.0%	\$45,000,000	\$243
SGT5-2000E	50	187,000 kW	9,426 Btu	36.2%	\$44,400,000	\$224
7F.04	60	198,000 kW	8,840 Btu	38.6%	\$46,000,000	\$232
GT13E2	50	203,000 kW	8,980 Btu	38.0%	\$46,500,000	\$229
7F.05	60	241,000 kW	8,580 Btu	39.8%	\$53,000,000	\$220
SGT6-5000F	60	250,000 kW	8,682 Btu	39.3%	\$55,100,000	\$220
7HA.01	60	280,000 kW	8,180 Btu	41.7%	\$62,000,000	\$221
9F.04	50	281,000 kW	8,830 Btu	38.6%	\$60,700,000	\$216
M501GAC	60	283,000 kW	8,531 Btu	40.0%	\$60,000,000	\$212
SGT6-8000H	60	305,000 kW	8,530 Btu	40.0%	\$66,300,000	\$217
SGT5-4000F	50	307,000 kW	8,532 Btu	40.0%	\$63,700,000	\$207
M501J	60	330,000 kW	8,105 Btu	42.1%	\$70,000,000	\$212
9F.06	50	342,000 kW	8,310 Btu	41.1%	\$73,000,000	\$213
GT26	50	345,000 kW	8,322 Btu	41.0%	\$74,000,000	\$214
M501JAC	60	370,000 kW	8,010 Btu	42.6%	\$80,000,000	\$216

Gas Turbine Model	Freq	Base Load Rating	Heat Rate Btu/ kWh	Efficiency	Budget Price	\$/kW
M701F	50	385,000 kW	8,144 Btu	41.9%	\$84,700,000	\$220
SGT5-8000H	50	420,000 kW	8,530 Btu	40.0%	\$82,000,000	\$195
9HA.01	50	429,000 kW	8,040 Btu	42.4%	\$92,300,000	\$215
M701J	50	478,000 kW	8,067 Btu	42.3%	\$100,400,000	\$210
M701JAC	50	493,000 kW	7,954 Btu	42.9%	\$104,500,000	\$212

GAS TURBINE Genset Overview 50 Hz



2016-17 GTW Simple Cycle Specs

Model	Intro Year	ISO Base Load (kW)	Heat Rate (Btu/kWh)	Efficiency	Press Ratio	Mass Flow (lb/sec)	Turbine Speed	Exhaust Temp	Approx Weight	Approx L x W x H	Comments
Ansaldo Energia											
AE-T100	2000	100 kW	11 362 Btu	30.0%	4.5	2.0 lb	70000 rpm	518 F	6 106 lb	12 x 3 x 6 ft	
AE64.3A	1996	78 000 kW	9 400 Btu	36.3%	18.3	474.0 lb	3000/3600	1063 F	134 000 lb	18 x 9 x 9 ft	includes gearbox
AE94.2	1981	185 000 kW	9 426 Btu	36.2%	12.0	1223.6 lb	3000 rpm	1006 F	524 000 lb	31 x 12 x 11 ft	low LHV fuel
AE94.2K	1981	170 000 kW	9 348 Btu	36.5%	12.0	1190.0 lb	3000 rpm	1013 F	539 000 lb	31 x 12 x 11 ft	
AE94.3A	1995	310 000 kW	8 573 Btu	39.8%	19.5	1653.0 lb	3000 rpm	1069 F	698 000 lb	33 x 15 x 15 ft	
GT26	2011	345 000 kW	8 322 Btu	41.0%	35.0	1576.0 lb	3000 rpm	1141 F	895 000 lb	39 x 16 x 18 ft	
GT36-S6	2016	340 000 kW	8 322 Btu	41.0%	24.0	1543.0 lb	3600 rpm	1166 F	807 000 lb	37 x 19 x 16 ft	
GT36-S5	2016	500 000 kW	8 222 Btu	41.5%	25.0	2227.0 lb	3000 rpm	1155 F	1 356 000 lb	44 x 21 x 19 ft	
Note: GT36-S weight without fuel distribution system and without cans											
Aviadvigatel											
GTU-2.5P	1994	2 560 kW	16 160 Btu	21.1%	5.9	56.4 lb	5500 rpm	682 F	100 530 lb	43 x 10 x 9 ft	w/ gearbox and gen losses
GTU-4P	2000	4 130 kW	14 220 Btu	24.0%	7.3	65.7 lb	5500 rpm	777 F	150 930 lb	45 x 10 x 9 ft	w/ gearbox and gen losses
GTU-6P	2004	6 140 kW	13 032 Btu	26.2%	8.7	74.7 lb	6925 rpm	885 F	161 820 lb	45 x 10 x 9 ft	w/ gearbox and gen losses
GTU-12PG-2	2004	12 300 kW	10 469 Btu	32.6%	15.9	101.2 lb	6500 rpm	925 F	296 970 lb	59 x 10 x 14 ft	w/ gearbox and gen losses
GTE-16PA	2007	16 300 kW	9 614 Btu	35.5%	19.9	124.0 lb	3000 rpm	898 F	389 400 lb	61 x 10 x 9 ft	w/ gen losses
GTE-25P	2008	23 000 kW	9 312 Btu	36.7%	27.3	169.1 lb	5000 rpm	883 F	467 710 lb	79 x 10 x 9 ft	w/ gearbox and gen losses
GTE-25PA	2013	25 500 kW	9 174 Btu	37.2%	28.5	172.6 lb	5000 rpm	935 F	369 495 lb	74 x 25 x 14 ft	w/ gearbox and gen losses
Bharat Heavy Electricals											
PG5371(PA)	1988	26 300 kW	11 990 Btu	28.5%	10.5	270.0 lb	5094 rpm	905 F	185 220 lb	38 x 11 x 12 ft	with standard combustor
PG6581(B)	2000	43 000 kW	10 303 Btu	33.1%	12.4	312.0 lb	5163 rpm	1008 F	200 655 lb	49 x 11 x 12 ft	with standard combustor
PG6111(FA)	2003	77 100 kW	9 611 Btu	35.5%	15.6	451.0 lb	5231 rpm	1109 F	231 525 lb	32 x 16 x 15 ft	with DLN combustor
PG9171(E)	1994	128 700 kW	9 952 Btu	34.3%	12.8	899.0 lb	3000 rpm	1012 F	617 400 lb	66 x 15 x 16 ft	with standard combustor
PG9171(E) - AGP	2012	130 400 kW	9 900 Btu	34.4%	12.9	912.0 lb	3000 rpm	1016 F	617 400 lb	67 x 15 x 16 ft	with standard combustor
V94.2	1997	157 000 kW	9 920 Btu	34.4%	11.1	1132.0 lb	3000 rpm	1004 F	650 475 lb	46 x 41 x 28 ft	
PG9351(FA)	1996	260 100 kW	9 099 Btu	37.5%	16.7	1430.0 lb	3000 rpm	1108 F	694 400 lb	74 x 16 x 18 ft	with DLN combustor
PG9371(FB)	2004	297 000 kW	8 782 Btu	38.9%	18.3	1420.0 lb	3000 rpm	1184 F	716 800 lb	74 x 16 x 18 ft	with DLN combustor

Model	Intro Year	ISO Base Load (kW)	Heat Rate (Btu/kWh)	Efficiency	Press Ratio	Mass Flow (lb/sec)	Turbine Speed	Exhaust Temp	Approx Weight	Approx L x W x H	Comments
Capstone Turbine											
C30	1998	30 kW	13 100 Btu	26.0%	3.6	0.7 lb	96000 rpm	530 F	891 lb	5 x 3 x 6 ft	grid parallel only
C65	2000	65 kW	11 800 Btu	29.0%	4.0	1.1 lb	96000 rpm	588 F	1 671 lb	6 x 3 x 6 ft	grid parallel only
C200	2008	200 kW	10 300 Btu	33.0%	4.0	2.9 lb	61000 rpm	535 F	6 120 lb	13 x 6 x 8 ft	grid parallel only
C600S	2015	600 kW	10 300 Btu	33.0%	4.0	8.8 lb	61000 rpm	535 F	31 300 lb	30 x 10 x 10 ft	grid parallel, 3xC200
C800S	2015	800 kW	10 300 Btu	33.0%	4.0	11.7 lb	61000 rpm	535 F	34 400 lb	30 x 10 x 10 ft	grid parallel, 4xC200
C1000S	2015	1 000 kW	10 300 Btu	33.0%	4.0	14.7 lb	61000 rpm	535 F	37 400 lb	30 x 10 x 10 ft	grid parallel, 5xC200
Centrax Gas Turbine											
CX501-KB5	1992	3 947 kW	11 747 Btu	29.1%	10.3	34.8 lb	14571 rpm	1031 F	85 980 lb	30 x 9 x 10 ft	Siemens 501-KB5
CX501-KB7	1993	5 335 kW	10 631 Btu	32.1%	13.9	46.6 lb	14571 rpm	923 F	85 980 lb	30 x 9 x 10 ft	Siemens 501-KB7
CX300-1S	2011	7 900 kW	11 158 Btu	31.0%	13.7	66.6 lb	14010 rpm	1008 F	126 000 lb	40 x 8 x 12 ft	Siemens SGT-300-1S
CX300-2S	2015	8 500 kW	9 855 Btu	34.6%	14.1	66.0 lb	11500 rpm	952 F	165 000 lb	61 x 9 x 13 ft	Siemens SGT-300-2S
CX400	2011	12 900 kW	9 817 Btu	34.8%	16.9	87.0 lb	9500 rpm	1031 F	165 000 lb	61 x 9 x 13 ft	Siemens SGT-400
CX400	2012	14 400 kW	9 647 Btu	35.4%	18.9	98.0 lb	9500 rpm	1004 F	165 000 lb	61 x 9 x 13 ft	Siemens SGT-400
Trent 60 DLE	2011	53 049 kW	8 055 Btu	42.6%	33.0	342.0 lb	3000 rpm	811 F	420 000 lb	67 x 15 x 17 ft	Siemens Trent 60
Trent 60 WLE ISI	2011	66 000 kW	8 226 Btu	41.5%	36.0	396.0 lb	3000 rpm	780 F	420 000 lb	67 x 15 x 17 ft	Siemens Trent 60
Dresser-Rand, a Siemens Business (50/60 Hz)											
KG2-3E	1989	1 895 kW	21 543 Btu	16.7%	4.7	33.0 lb	18800 rpm	1020 F	38 580 lb	22 x 7 x 9 ft	
KG2-3G	2014	2 000 kW	13 381 Btu	25.5%	7.0	20.9 lb	25500 rpm	1081 F	35 300 lb	22 x 7 x 9 ft	
Vectra 30G	2007	22 767 kW	9 428 Btu	36.2%	17.9	149.7 lb	6200 rpm	1017 F	88 200 lb	30 x 14 x 15 ft	LM2500 gas generator
Vectra 40G	1998	30 460 kW	8 780 Btu	38.9%	22.4	190.2 lb	6200 rpm	979 F	88 200 lb	30 x 14 x 15 ft	LM2500+ gas generator
Vectra 40G4	2007	33 209 kW	8 737 Btu	39.1%	23.6	198.4 lb	6200 rpm	1006 F	88 200 lb	30 x 14 x 15 ft	LM2500+G4 gas generator
Dresser-Rand, a Siemens Business (60 Hz)											
DR-61G	1981	23 394 kW	9 280 Btu	36.8%	18.2	153.1 lb	3600 rpm	992 F	88 200 lb	30 x 14 x 15 ft	LM2500 gas turbine
DR-61GP	1995	30 742 kW	8 821 Btu	38.7%	22.5	192.2 lb	3600 rpm	959 F	88 200 lb	30 x 14 x 15 ft	LM2500+ gas turbine
DR-61G4	2005	33 175 kW	8 811 Btu	38.7%	23.0	201.8 lb	3600 rpm	978 F	88 200 lb	30 x 14 x 15 ft	LM2500+G4 gas turbine
DR-63G PC	1994	43 738 kW	8 166 Btu	41.8%	27.8	279.1 lb	3600 rpm	848 F	83 800 lb	27 x 14 x 19 ft	LM6000PC gas turbine
DR-63G PG	2008	50 447 kW	8 213 Btu	41.6%	30.8	308.0 lb	3930 rpm	880 F	83 800 lb	27 x 14 x 19 ft	LM6000PG gas turbine
Note: All D-R models with standard annular combustor except KG2-3E											
EthosEnergy											
TG20B7/8UG	2014	45 400 kW	10 843 Btu	31.5%	11.5	369.0 lb	4918 rpm	989 F	176 320 lb	22 x 10 x 10 ft	50/60 Hz
TG50D5U	2007	144 500 kW	9 850 Btu	34.6%	14.8	1063.0 lb	3000 rpm	951 F	433 429 lb	36 x 13 x 13 ft	50 Hz

Model	Intro Year	ISO Base Load (kW)	Heat Rate (Btu/kWh)	Efficiency	Press Ratio	Mass Flow (lb/sec)	Turbine Speed	Exhaust Temp	Approx Weight	Approx L x W x H	Comments
GE Energy Oil & Gas (50/60 Hz)											
NovaLT5-1	2015	5 600 Kw	11 127 Btu	30.7%	14.8	43.2 lb	16630 rpm	1065 F	63 900 lb	20 x 8 x 10 ft	DLE <25ppm Nox
GE10-1	2000	11 250 kW	10 867 Btu	31.4%	15.5	104.7 lb	11000 rpm	900 F	74 960 lb	30 x 8 x 20 ft	
NovaLT16	2014	16 000 kW	9 478 Btu	36.0%	19.0	119.0 lb	7800 rpm	914 F	110 230 lb	33 x 12 x 13 ft	DLN 25ppm Nox
PGT20	2002	17 464 kW	9 704 Btu	35.2%	15.7	137.9 lb	6500 rpm	887 F	83 005 lb	30 x 11 x 11 ft	
PGT25	1981	22 417 kW	9 401 Btu	36.3%	17.9	151.9 lb	6500 rpm	976 F	83 005 lb	30 x 11 x 11 ft	
PGT25+	1996	30 226 kW	8 610 Btu	39.6%	21.5	185.8 lb	6100 rpm	932 F	67 790 lb	21 x 12 x 13 ft	
PGT25+G4	2005	33 057 kW	8 530 Btu	40.0%	23.2	197.7 lb	6100 rpm	950 F	68 010 lb	21 x 12 x 13 ft	
LM6000PD	1997	43 069 kW	8 173 Btu	41.7%	28.0	275.0 lb	3600 rpm	851 F	68 345 lb	31 x 14 x 14 ft	DLE 25 ppm Nox
LM6000PF	2006	43 069 kW	8 173 Btu	41.7%	28.0	275.0 lb	3600 rpm	851 F	68 345 lb	31 x 14 x 14 ft	DLE 15 ppm Nox
LM6000PG	2008	51 204 kW	8 142 Btu	41.9%	30.0	317.3 lb	3600 rpm	878 F	65 645 lb	32 x 15 x 15 ft	
LMS100	2005	98 196 kW	7 580 Btu	45.0%	40.0	456.0 lb	3600 rpm	782 F	201 000 lb	59 x 15 x 15 ft	DLE
GE Energy Oil & Gas (Frame units)											
MS5001	1987	26 830 kW	12 025 Btu	28.4%	10.5	276.1 lb	5094 rpm	901 F	192 750 lb	38 x 11 x 12 ft	MS heavy frame series DLN-2
MS5002E	2003	33 310 kW	6 884 Btu	37.0%	17.4	226.0 lb	5714 rpm	954 F	257 940 lb	56 x 11 x 13 ft	
MS6001B	1978	42 100 kW	10 644 Btu	32.1%	12.2	311.0 lb	5163 rpm	1016 F	211 645 lb	52 x 11 x 12 ft	
MS7001EA	1984	85 400 kW	10 417 Btu	32.7%	12.7	652.5 lb	3600 rpm	995 F	266 760 lb	38 x 11 x 12 ft	60 Hz
MS9001E	1976	126 100 kW	10 094 Btu	33.8%	12.7	921.0 lb	3000 rpm	1004 F	479 505 lb	73 x 15 x 21 ft	50 Hz
Note: All GE Oil & Gas units with standard combustor; weights and sizes without enclosure											
GE Power & Water Aeroderivative (50 Hz)											
TM2500	****	34 300 kW	9 665 Btu	35.3%	24.5	203.9 lb	3000 rpm	963 F	247 520 lb	105 x 11 x 13 ft	
LM2500	1981	23 786 kW	10 053 Btu	33.9%	19.0	157.2 lb	3000 rpm	986 F	250 000 lb	57 x 9 x 10 ft	water injection DLE
LM2500 DLE	1981	22 417 kW	9 636 Btu	35.4%	18.1	150.9 lb	3000 rpm	1017 F	250 000 lb	57 x 9 x 10 ft	
LM2500+	1995	30 031 kW	9 624 Btu	35.5%	23.1	197.3 lb	3000 rpm	920 F	250 000 lb	57 x 9 x 10 ft	water injection DLE
LM2500+ DLE	1995	31 059 kW	9 169 Btu	37.2%	23.6	195.8 lb	3000 rpm	1003 F	250 000 lb	57 x 10 x 10 ft	
LM2500+ G4	2005	34 500 kW	9 676 Btu	35.3%	24.6	212.9 lb	3000 rpm	966 F	250 000 lb	65 x 10 x 23 ft	water injection, gearbox DLE, gearbox
LM2500+ G4 DLE	2005	33 400 kW	9 166 Btu	37.2%	24.0	205.1 lb	3000 rpm	1026 F	250 000 lb	65 x 10 x 23 ft	
LM6000PC	1997	45 424 kW	8 505 Btu	40.1%	29.7	286.0 lb	3627 rpm	817 F	673 370 lb	65 x 14 x 15 ft	water injection, gearbox water injection, gearbox
LM6000PC Sprint	1998	51 057 kW	8 456 Btu	40.4%	31.5	298.2 lb	3627 rpm	841 F	673 370 lb	65 x 14 x 15 ft	
LM6000PF	1997	45 000 kW	8 126 Btu	42.0%	30.1	280.6 lb	3627 rpm	855 F	673 370 lb	65 x 14 x 15 ft	DLE, gearbox DLE, gearbox
LM6000PF Sprint	2006	50 000 kW	8 132 Btu	42.0%	31.6	292.6 lb	3627 rpm	858 F	673 370 lb	65 x 14 x 15 ft	

Model	Intro Year	ISO Base Load (kW)	Heat Rate (Btu/kWh)	Efficiency	Press Ratio	Mass Flow (lb/sec)	Turbine Speed	Exhaust Temp	Approx Weight	Approx L x W x H	Comments
GE Power & Water Aeroderivative (50 Hz)											
LM6000PG	2009	56 000 kW	8 506 Btu	40.1%	33.5	316.1 lb	3911 rpm	878 F	673 370 lb	65 x 14 x 15 ft	water injection, gearbox
LM6000PG Sprint	2009	59 000 kW	8 564 Btu	39.8%	34.0	318.3 lb	3911 rpm	896 F	673 370 lb	65 x 14 x 15 ft	water injection, gearbox
LM6000PF+	2016	53 000 kW	8 154 Btu	41.8%	32.1	298.2 lb	3911 rpm	932 F	673 370 lb	65 x 14 x 15 ft	DLE, gearbox
LM6000PF+ Sprint	2016	57 000 kW	8 239 Btu	41.4%	34.0	315.7 lb	3911 rpm	914 F	673 370 lb	65 x 14 x 15 ft	DLE, gearbox
LMS100PA+	2015	114 000 kW	7 885 Btu	43.3%	42.5	509.8 lb	3000 rpm	792 F	1 976 589 lb	111 x 78 x 50 ft	water injection
LMS100PB+	2016	108 000 kW	7 776 Btu	43.9%	42.2	500.5 lb	3000 rpm	790 F	1 976 589 lb	111 x 78 x 50 ft	water injection
GE Power & Water Aeroderivative (60 Hz)											
TM2500	****	37 100 kW	9 171 Btu	37.2%	24.7	208.6 lb	3600 rpm	950 F	247 520 lb	105 x 11 x 13 ft	water injection
LM2500	1981	24 800 kW	9 729 Btu	35.1%	19.0	156.9 lb	3600 rpm	977 F	250 000 lb	57 x 9 x 10 ft	water injection
LM2500 DLE	1981	23 200 kW	9 317 Btu	36.6%	18.0	150.3 lb	3600 rpm	1002 F	250 000 lb	57 x 9 x 10 ft	DLE
LM2500+	1995	31 800 kW	9 252 Btu	36.9%	23.1	196.9 lb	3600 rpm	914 F	250 000 lb	57 x 9 x 10 ft	water injection
LM2500+ DLE	1995	31 900 kW	8 785 Btu	38.8%	23.1	191.7 lb	3600 rpm	978 F	250 000 lb	57 x 10 x 10 ft	DLE
LM2500+ G4	2005	37 100 kW	9 171 Btu	37.2%	24.7	212.8 lb	3600 rpm	950 F	250 000 lb	65 x 10 x 10 ft	water injection
LM2500+ G4 DLE	2005	34 500 kW	8 709 Btu	39.2%	23.6	201.7 lb	3600 rpm	995 F	250 000 lb	65 x 10 x 10 ft	DLE
LM6000PC	1997	46 000 kW	8 458 Btu	40.3%	29.6	284.4 lb	3600 rpm	824 F	673 370 lb	56 x 14 x 15 ft	water injection
LM6000PC Sprint	1998	52 000 kW	8 444 Btu	40.4%	31.3	295.1 lb	3600 rpm	851 F	673 370 lb	56 x 14 x 15 ft	water injection
LM6000PF	1997	45 000 kW	8 097 Btu	42.1%	29.8	277.0 lb	3600 rpm	861 F	673 370 lb	56 x 14 x 15 ft	DLE
LM6000PF Sprint	2006	50 000 kW	8 109 Btu	42.1%	31.4	289.7 lb	3600 rpm	865 F	673 370 lb	56 x 14 x 15 ft	DLE
LM6000PG	2009	56 000 kW	8 524 Btu	40.0%	33.5	315.9 lb	3905 rpm	879 F	673 370 lb	56 x 14 x 15 ft	water injection, gearbox
LM6000PG Sprint	2009	59 000 kW	8 581 Btu	39.8%	34.0	318.0 lb	3905 rpm	897 F	673 370 lb	56 x 14 x 15 ft	water injection, gearbox
LM6000PF+	2016	53 000 kW	8 175 Btu	41.7%	32.1	297.9 lb	3905 rpm	932 F	673 370 lb	56 x 14 x 15 ft	DLE, gearbox
LM6000PF+ Sprint	2016	57 000 kW	8 256 Btu	41.3%	34.0	315.4 lb	3905 rpm	914 F	673 370 lb	56 x 14 x 15 ft	DLE, gearbox
LMS100PA+	2015	117 000 kW	7 763 Btu	44.0%	42.5	508.6 lb	3600 rpm	781 F	1 976 589 lb	111 x 78 x 50 ft	water injection
LMS100PB+	2016	109 000 kW	7 746 Btu	44.1%	42.1	500.0 lb	3600 rpm	784 F	1 976 589 lb	111 x 78 x 50 ft	water injection
GE Power & Water Heavy Duty (50/60 Hz)											
6B.03	1978	44 000 kW	10 180 Btu	33.5%	12.7	320.0 lb	5163 rpm	1019 F	220 450 lb	41 x 13 x 13 ft	available in 50 & 60 Hz
6F.01	2003	52 000 kW	8 880 Btu	38.4%	21.0	278.0 lb	7266 rpm	1117 F	154 350 lb	21 x 14 x 14 ft	available in 50 & 60 Hz
6F.03	2003	82 000 kW	9 470 Btu	36.0%	16.4	470.0 lb	5231 rpm	1135 F	220 500 lb	33 x 12 x 15 ft	available in 50 & 60 Hz

Model	Intro Year	ISO Base Load (kW)	Heat Rate (Btu/kWh)	Efficiency	Press Ratio	Mass Flow (lb/sec)	Turbine Speed	Exhaust Temp	Approx Weight	Approx L x W x H	Comments	
GE Power & Water Heavy Duty (50 Hz)												
9E.03	1992	132 000 kW	9 860 Btu	34.6%	13.1	924.0 lb	3000 rpm	1012 F	471 800 lb	37 x 17 x 17 ft	9HA ratings are net	
9E.04	2014	145 000 kW	9 210 Btu	37.0%	12.3	916.0 lb	3000 rpm	1007 F	482 896 lb	37 x 17 x 17 ft		
GT13E2 2005	2005	185 000 kW	9 027 Btu	37.8%	16.9	1250.9 lb	3000 rpm	941 F	756 200 lb	37 x 18 x 17 ft		
GT13E2 2012	2012	203 000 kW	8 980 Btu	38.0%	18.2	1376.0 lb	3000 rpm	934 F	772 000 lb	36 x 18 x 18 ft		
9F.03	1996	265 000 kW	9 020 Btu	37.8%	16.7	1466.0 lb	3000 rpm	1104 F	679 850 lb	35 x 15 x 16 ft		
9F.04	2015	281 000 kW	8 830 Btu	38.6%	16.9	1471.0 lb	3000 rpm	1127 F	679 850 lb	35 x 15 x 16 ft		
9F.05	2003	299 000 kW	8 810 Btu	38.7%	18.3	1470.0 lb	3000 rpm	1187 F	709 100 lb	35 x 16 x 16 ft		
9F.06	2016	342 000 kW	8 310 Btu	41.1%	20.0	1612.0 lb	3000 rpm	1144 F	851 550 lb	35 x 16 x 16 ft		
9HA.01	2011	446 000 kW	7 910 Btu	43.1%	23.5	****	3000 rpm	1164 F	851 550 lb	35 x 16 x 16 ft		
9HA.02	2014	544 000 kW	7 766 Btu	43.9%	23.8	****	3000 rpm	1177 F	951 800 lb	35 x 16 x 16 ft		
GE Power & Water Heavy Duty (60 Hz)												
7E.03	1984	91 000 kW	10 060 Btu	33.9%	13.0	650.0 lb	3600 rpm	1026 F	293 000 lb	38 x 12 x 12 ft	7HA ratings are net	
7F.04	2009	198 000 kW	8 840 Btu	38.6%	16.7	1013.0 lb	3600 rpm	1151 F	392 000 lb	28 x 13 x 13 ft		
7F.05	2009	241 000 kW	8 580 Btu	39.8%	18.4	1188.0 lb	3600 rpm	1171 F	443 400 lb	28 x 13 x 13 ft		
7F.06	2016	270 000 kW	8 250 Btu	41.4%	22.1	1311.0 lb	3600 rpm	1100 F	547 000 lb	30 x 13 x 14 ft		
7HA.01	2012	289 000 kW	8 150 Btu	41.9%	21.6	****	3600 rpm	1161 F	547 000 lb	30 x 13 x 14 ft		
7HA.02	2014	372 000 kW	8 020 Btu	42.5%	23.1	****	3600 rpm	1181 F	602 000 lb	32 x 13 x 14 ft		
Note: All GE Heavy Duty models with inlet loss, exhaust loss and shaft driven auxiliaries losses												
Hitachi Zosen												
GT10	2006	4 130 kW	11 582 Btu	29.5%	10.4	34.3 lb	14200 rpm	1050 F	1 270 lb	7 x 3 x 3 ft		501-KB5S, steam injection
GT13	2006	5 600 kW	10 646 Btu	32.1%	14.3	47.0 lb	14600 rpm	940 F	1 691 lb	9 x 4 x 3 ft	501-KB7S, steam injection	
VHP6	2006	6 260 kW	8 847 Btu	38.6%	12.5	40.0 lb	14600 rpm	991 F	1 270 lb	8 x 3 x 3 ft	501-KH5, gas fuel	
IHI Power Systems (50/60 Hz)												
IM270	1996	2 000 kW	13 880 Btu	24.6%	12.2	21.3 lb	20300 rpm	1013 F	4 409 lb	8 x 3 x 3 ft	dry low NOx	
LM2500RB	2006	31 970 kW	8 720 Btu	39.2%	23.0	193.9 lb	6100 rpm	958 F	31 228 lb	19 x 8 x 9 ft		
LM6000PH	2010	49 009 kW	8 323 Btu	41.0%	35.0	305.5 lb	3930 rpm	884 F	****	****		
LM6000PH Sprint	2010	51 342 kW	8 316 Btu	41.0%	35.0	308.5 lb	3930 rpm	878 F	****	****		
LM6000PG	2009	54 621 kW	8 365 Btu	40.8%	35.0	315.9 lb	3930 rpm	871 F	16 240 lb	16 x 7 x 7 ft		
LM6000PG Sprint	2009	55 985 kW	8 490 Btu	40.2%	35.0	321.8 lb	3930 rpm	876 F	16 240 lb	16 x 7 x 7 ft		
LM6000PF+	2016	51 430 kW	8 182 Btu	41.7%	32.9	300.0 lb	3930 rpm	917 F	****	****		
LM6000PF+ Sprint	2016	55 240 kW	8 241 Btu	41.4%	32.9	318.7 lb	3930 rpm	892 F	****	****		

Model	Intro Year	ISO Base Load (kW)	Heat Rate (Btu/kWh)	Efficiency	Press Ratio	Mass Flow (lb/sec)	Turbine Speed	Exhaust Temp	Approx Weight	Approx L x W x H	Comments
IHI Power Systems (50 Hz)											
LM2500PE	1976	21 900 kW	10 290 Btu	33.2%	20.0	154.3 lb	3000 rpm	986 F	7 815 lb	15 x 6 x 6 ft	
LM2500PK	1998	28 440 kW	9 150 Btu	37.3%	23.0	181.2 lb	3000 rpm	952 F	8 485 lb	16 x 6 x 6 ft	
LM2500PR	1981	29 642 kW	9 281 Btu	36.8%	23.0	195.1 lb	3000 rpm	982 F	****	****	
LM2500RD	2005	32 612 kW	8 916 Btu	38.3%	23.0	203.7 lb	3000 rpm	1009 F	****	****	
LM2500RC	2005	35 788 kW	9 203 Btu	37.1%	23.0	212.2 lb	3000 rpm	981 F	****	****	
LM6000PC	1997	43 367 kW	8 516 Btu	40.1%	30.0	282.0 lb	3000 rpm	821 F	15 498 lb	16 x 7 x 7 ft	
LM6000PC Sprint	1997	48 718 kW	8 477 Btu	40.3%	30.0	293.4 lb	3000 rpm	839 F	15 498 lb	16 x 7 x 7 ft	
LM6000PD	1997	42 547 kW	8 273 Btu	41.2%	31.0	274.8 lb	3000 rpm	851 F	19 158 lb	16 x 7 x 7 ft	DLE
LM6000PD Sprint	1997	47 482 kW	8 256 Btu	41.3%	31.0	290.8 lb	3000 rpm	846 F	19 158 lb	16 x 7 x 7 ft	DLE
LM6000PF	2006	42 547 kW	8 273 Btu	41.2%	31.0	274.8 lb	3000 rpm	851 F	19 158 lb	16 x 7 x 7 ft	DLE
LM6000PF Sprint	2006	47 482 kW	8 256 Btu	41.3%	31.0	290.8 lb	3000 rpm	846 F	19 158 lb	16 x 7 x 7 ft	DLE
IHI Power Systems (60 Hz)											
LM2500PE	1976	22 800 kW	9 960 Btu	34.3%	20.0	154.3 lb	3600 rpm	968 F	7 815 lb	15 x 6 x 6 ft	
LM2500PK	1998	28 500 kW	8 660 Btu	39.4%	23.0	176.1 lb	3600 rpm	937 F	8 485 lb	16 x 6 x 6 ft	
LM2500PR	1981	30 530 kW	8 835 Btu	38.6%	23.0	191.3 lb	3600 rpm	960 F	****	****	
LM2500RD	2005	32 941 kW	8 826 Btu	38.7%	23.0	200.9 lb	3600 rpm	981 F	****	****	
LM6000RC	2005	36 150 kW	9 111 Btu	37.4%	23.0	211.8 lb	3600 rpm	966 F	****	****	
LM6000PC	1997	43 805 kW	8 431 Btu	40.5%	30.0	282.0 lb	3600 rpm	821 F	15 498 lb	16 x 7 x 7 ft	
LM6000PC Sprint	1997	49 210 kW	8 392 Btu	40.7%	30.0	293.4 lb	3600 rpm	839 F	15 498 lb	16 x 7 x 7 ft	
LM6000PD	1997	42 977 kW	8 190 Btu	41.7%	31.0	274.8 lb	3600 rpm	851 F	19 158 lb	16 x 7 x 7 ft	DLE
LM6000PD Sprint	1997	47 961 kW	8 174 Btu	41.7%	31.0	290.8 lb	3600 rpm	846 F	19 158 lb	16 x 7 x 7 ft	DLE
LM6000PF	2006	42 977 kW	8 190 Btu	41.7%	31.0	274.8 lb	3600 rpm	851 F	19 158 lb	16 x 7 x 7 ft	DLE
LM6000PF Sprint	2006	47 961 kW	8 174 Btu	41.7%	31.0	290.8 lb	3600 rpm	846 F	19 158 lb	16 x 7 x 7 ft	DLE
Kawasaki Heavy Industries											
M1A-13A	1989	1 490 kW	14 104 Btu	24.2%	9.4	17.8 lb	1500/1800	970 F	7 209 lb	8 x 5 x 7 ft	
M1A-13D	1995	1 490 kW	14 246 Btu	24.0%	9.6	17.6 lb	1500/1800	988 F	7 518 lb	8 x 4 x 7 ft	DLE
M1A-17D	2010	1 700 kW	12 701 Btu	26.9%	10.5	17.8 lb	1500/1800	970 F	7 826 lb	10 x 5 x 7 ft	DLE
M1T-13A	1989	2 930 kW	14 312 Btu	23.8%	9.4	35.6 lb	1500/1800	970 F	13 668 lb	8 x 7 x 6 ft	
M1T-13D	1995	2 930 kW	14 445 Btu	23.6%	9.6	35.3 lb	1500/1800	988 F	13 801 lb	8 x 7 x 7 ft	DLE
M7A-01	1993	5 530 kW	11 510 Btu	29.6%	13.1	47.9 lb	1500/1800	1013 F	9 921 lb	12 x 5 x 6 ft	
M7A-02	1997	6 800 kW	11 250 Btu	30.3%	15.9	59.5 lb	1500/1800	960 F	11 023 lb	12 x 5 x 6 ft	

Model	Intro Year	ISO Base Load (kW)	Heat Rate (Btu/kWh)	Efficiency	Press Ratio	Mass Flow (lb/sec)	Turbine Speed	Exhaust Temp	Approx Weight	Approx L x W x H	Comments
Kawasaki Heavy Industries (cont'd)											
M7A-01D	1993	5 470 kW	11 550 Btu	29.5%	13.1	47.8 lb	1500/1800	1007 F	10 340 lb	12 x 5 x 6 ft	DLE
M7A-02D	1997	6 740 kW	11 270 Btu	30.3%	15.9	59.5 lb	1500/1800	955 F	11 470 lb	12 x 5 x 6 ft	DLE
M7A-03D	2006	7 800 kW	10 190 Btu	33.6%	15.6	59.9 lb	1500/1800	973 F	12 700 lb	14 x 5 x 6 ft	DLE
L20A	2001	18 522 kW	9 948 Btu	34.3%	18.6	131.8 lb	1500/1800	1006 F	36 377 lb	22 x 7 x 9 ft	DLE
L30A	2012	30 120 kW	8 502 Btu	40.1%	24.9	195.6 lb	1500/1800	878 F	68 343 lb	24 x 11 x 12 ft	DLE
MAN Diesel & Turbo											
MGT6100	2012	6 630 kW	10 610 Btu	32.2%	15.0	57.5 lb	1500/1800	941 F	****	****	
THM1304-10N	1980	10 080 kW	11 690 Btu	29.2%	10.0	102.5 lb	1500/1800	914 F	169 785 lb	52 x 9 x 17 ft	
THM1304-12N	2004	12 000 kW	11 170 Btu	30.5%	11.0	108.0 lb	1500/1800	959 F	169 785 lb	52 x 12 x 21 ft	
MAPNA Group											
MGT-30	2014	25 700 kW	9 586 Btu	35.6%	22.0	197.6 lb	3000 rpm	898 F	33 000 lb	21 x 8 x 8 ft	UGT25000 design
MGT-70(3)	2016	183 000 kW	9 478 Btu	36.0%	12.0	1223.1 lb	3000 rpm	1010 F	650 400 lb	46 x 41 x 28 ft	
Mitsubishi Hitachi Power Systems (50/60 Hz)											
H-25	2008	41 030 kW	9 432 Btu	36.2%	17.9	253.0 lb	7280 rpm	1056 F	121 000 lb	26 x 13 x 13 ft	without inlet and exhaust losses
H-50	2015	57 450 kW	9 013 Btu	37.8%	19.5	333.0 lb	5040 rpm	1047 F	165 000 lb	28 x 13 x 13 ft	without inlet and exhaust losses
Mitsubishi Hitachi Power Systems (50 Hz)											
H-100	2013	118 080 kW	8 919 Btu	38.3%	20.1	695.0 lb	3000 rpm	1025 F	476 000 lb	46 x 16 x 20 ft	without inlet and exhaust losses
M701DA	1981	144 090 kW	9 810 Btu	34.8%	14	999.0 lb	3000 rpm	1008 F	440 917 lb	41 x 17 x 17 ft	
M701G	1997	334 000 kW	8 630 Btu	39.5%	21	1664.0 lb	3000 rpm	1089 F	925 926 lb	60 x 20 x 20 ft	
M701F	1992	385 000 kW	8 144 Btu	41.9%	21	1650.0 lb	3000 rpm	1167 F	1 058 220 lb	57 x 19 x 19 ft	
M701J	2014	478 000 kW	8 067 Btu	42.3%	23	1977.0 lb	3000 rpm	1166 F	1 234 590 lb	60 x 23 x 23 ft	
M701JAC	2015	493 000 kW	7 954 Btu	42.9%	23	1977.0 lb	3000 rpm	1187 F	1 234 590 lb	60 x 23 x 23 ft	
Mitsubishi Hitachi Power Systems (60 Hz)											
H-100	2010	105 780 kW	8 930 Btu	38.2%	18.4	646.0 lb	3600 rpm	993 F	386 000 lb	40 x 15 x 18 ft	without inlet and exhaust losses
M501DA	1980	113 950 kW	9 780 Btu	34.9%	14	780.0 lb	3600 rpm	1009 F	319 665 lb	38 x 19 x 14 ft	
M501F	1989	185 400 kW	9 230 Btu	37.0%	16	1032.0 lb	3600 rpm	1136 F	429 894 lb	46 x 15 x 15 ft	
M501G	1997	267 500 kW	8 730 Btu	39.1%	20	1349.0 lb	3600 rpm	1113 F	734 140 lb	50 x 18 x 18 ft	
M501GAC	2011	283 000 kW	8 531 Btu	40.0%	20	1364.0 lb	3600 rpm	1143 F	595 250 lb	50 x 18 x 18 ft	
M501J	2011	330 000 kW	8 105 Btu	42.1%	23	1367.0 lb	3600 rpm	1176 F	698 870 lb	50 x 18 x 18 ft	
M501JAC	2015	370 000 kW	8 010 Btu	42.6%	23	1479.0 lb	3600 rpm	1211 F	698 870 lb	50 x 18 x 18 ft	
Note: All MHPS ratings on natural gas, LHV at generator terminals with inlet and exhaust losses											

Model	Intro Year	ISO Base Load (kW)	Heat Rate (Btu/kWh)	Efficiency	Press Ratio	Mass Flow (lb/sec)	Turbine Speed	Exhaust Temp	Approx Weight	Approx L x W x H	Comments
OPRA Turbine											
OP16-3A	2004	1 850 kW	13 800 Btu	24.7%	6.7	19.8 lb	26000 rpm	1063 F	3 594 lb	8 x 4 x 5 ft	DLE for low Btu fuels
OP16-3B DLE	2004	1 850 kW	13 800 Btu	24.7%	6.7	19.8 lb	26000 rpm	1063 F	3 594 lb	8 x 4 x 5 ft	
OP16-3C	2014	1 850 kW	13 800 Btu	24.7%	6.7	19.8 lb	26000 rpm	1063 F	4 325 lb	8 x 4 x 5 ft	
Orenda Aerospace											
OGT2500	1994	2 670 kW	12 780 Btu	26.7%	12.0	33.1 lb	1500/1800	860 F	5 512 lb	10 x 4 x 7 ft	
OGT6000	1993	6 200 kW	11 299 Btu	30.2%	14.0	68.3 lb	3000/3600	797 F	9 921 lb	15 x 6 x 6 ft	
OGT8000	2002	8 300 kW	10 597 Btu	32.2%	17.0	74.3 lb	3000/3600	891 F	11 023 lb	15 x 6 x 6 ft	
OGT16000	1991	15 500 kW	11 115 Btu	30.7%	13.0	211.6 lb	3000/3600	662 F	35 274 lb	19 x 9 x 10 ft	
OGT15000	1996	16 500 kW	9 977 Btu	34.2%	20.0	156.5 lb	3000/3600	788 F	28 219 lb	20 x 7 x 8 ft	
OGT25000	1996	25 600 kW	9 612 Btu	35.5%	21.0	194.0 lb	3000/3600	905 F	35 274 lb	21 x 8 x 9 ft	
Note: all Orenda models weights and size, engine only											
PW Power Systems (50/60 Hz)											
FT8 MOBILPAC	2005	28 528 kW	9 834 Btu	34.7%	21.2	203.0 lb	3000 rpm	924 F	****	****	comb, water inj, transportable
FT8 MOBILPAC	2005	30 941 kW	9 312 Btu	36.7%	21.3	202.0 lb	3600 rpm	916 F	****	****	comb, water inj, transportable
FT8 SWIFTPAC 25 DLN	2003	25 455 kW	8 960 Btu	38.1%	19.5	187.0 lb	3000/3600	856 F	****	****	
FT8 SWIFTPAC 50 DLN	2003	51 235 kW	8 905 Btu	38.3%	19.5	374.0 lb	3000/3600	856 F	****	****	
FT8 SWIFTPAC 30	1990	30 892 kW	9 327 Btu	36.6%	21.3	202.0 lb	3000/3600	916 F	****	****	combustor water injection
FT8 SWIFTPAC 60	1990	62 086 kW	9 281 Btu	36.8%	21.3	404.0 lb	3000/3600	916 F	****	****	combustor water injection
FT4000 SWIFTPAC 60	2012	68 747 kW	8 305 Btu	41.1%	36.7	388.0 lb	3000/3600	799 F	****	****	comb inj, wet comp, inlet fog
FT4000 SWIFTPAC 120	2012	137 802 kW	8 286 Btu	41.2%	36.7	776.0 lb	3000/3600	799 F	****	****	comb inj, wet comp, inlet fog
PW Power Systems (50 Hz)											
FT8 MOBILPAC	2005	28 528 kW	9 834 Btu	34.7%	21.2	203.0 lb	3000 rpm	924 F	****	****	comb water inj, transportable
PW Power Systems (60 Hz)											
FT8 MOBILPAC	2005	30 941 kW	9 312 Btu	36.7%	21.3	202.0 lb	3600 rpm	916 F	****	****	comb water inj, transportable
Siemens Energy (50/60 Hz)											
Industrial 501-KB5S	1993	3 980 kW	11 504 Btu	29.7%	10.3	33.9 lb	14200 rpm	1040 F	1 270 lb	8 x 3 x 3 ft	engine dimensions only
Industrial 501-KB7S	1999	5 380 kW	10 570 Btu	32.3%	13.9	47.0 lb	14600 rpm	921 F	1 690 lb	9 x 4 x 4 ft	engine dimensions only
Industrial 501-KH5	1985	6 620 kW	8 285 Btu	41.2%	10.3	40.6 lb	14600 rpm	986 F	1 270 lb	8 x 3 x 3 ft	engine dim. only, case steam inj.

Model	Intro Year	ISO Base Load (kW)	Heat Rate (Btu/kWh)	Efficiency	Press Ratio	Mass Flow (lb/sec)	Turbine Speed	Exhaust Temp	Approx Weight	Approx L x W x H	Comments
Siemens Energy (50/60 Hz) (cont'd)											
SGT-100	1997	5 050 kW	11 292 Btu	30.2%	14.0	43.1 lb	17384 rpm	1013 F	77 000 lb	36 x 9 x 13 ft	
SGT-100	2010	5 400 kW	11 007 Btu	31.0%	15.6	45.4 lb	17384 rpm	988 F	77 000 lb	36 x 9 x 13 ft	
SGT-200	1981	6 750 kW	10 892 Btu	31.5%	12.2	64.5 lb	11053 rpm	871 F	124 000 lb	41 x 8 x 11 ft	
SGT-300	1995	7 901 kW	11 158 Btu	30.6%	13.7	66.6 lb	14010 rpm	1008 F	129 800 lb	39 x 9 x 13 ft	
SGT-400	1997	12 900 kW	9 815 Btu	34.8%	16.8	86.8 lb	9500 rpm	1031 F	184 800 lb	46 x 10 x 14 ft	
SGT-400	2010	14 326 kW	9 647 Btu	35.4%	18.9	97.7 lb	9500 rpm	1004 F	184 800 lb	46 x 10 x 14 ft	
SGT-500	1968	19 064 kW	10 132 Btu	33.8%	13.0	215.9 lb	3600 rpm	696 F	331 000 lb	70 x 13 x 12 ft	
SGT-600	1981	24 480 kW	10 161 Btu	33.6%	14.0	179.2 lb	7700 rpm	1009 F	330 000 lb	62 x 15 x 13 ft	WLE in DLE combustors
SGT-700	1999	32 820 kW	9 170 Btu	37.2%	18.7	209.0 lb	6500 rpm	991 F	373 000 lb	62 x 15 x 13 ft	
SGT-750	2012	39 810 kW	8 456 Btu	40.3%	24.3	253.5 lb	6100 rpm	875 F	385 809 lb	67 x 16 x 14 ft	
SGT-800	1998	47 500 kW	9 048 Btu	37.7%	20.1	292.8 lb	6608 rpm	1007 F	705 500 lb	64 x 15 x 50 ft	
SGT-800	2010	50 500 kW	8 899 Btu	38.3%	21.0	295.8 lb	6608 rpm	1027 F	705 500 lb	64 x 15 x 50 ft	
SGT-800	2016	54 000 kW	8 725 Btu	39.1%	21.4	298.7 lb	6608 rpm	1045 F	705 500 lb	64 x 15 x 50 ft	
Industrial RB211-G62 DLE	1993	27 216 kW	9 387 Btu	36.4%	20.6	200.6 lb	4800 rpm	934 F	****	61 x 13 x 16 ft	
Industrial RB211-GT62 DLE	1999	29 845 kW	9 089 Btu	37.6%	21.7	209.4 lb	4800 rpm	937 F	****	61 x 13 x 16 ft	
Industrial RB211-GT61 DLE	2000	32 130 kW	8 681 Btu	39.3%	21.6	207.2 lb	4850 rpm	950 F	****	61 x 13 x 16 ft	
Siemens Energy (50 Hz)											
Industrial RB211-GT30 DLE	2015	31 917 kW	9 141 Btu	37.3%	22.6	218.7 lb	3000 rpm	939 F	****	****	
Industrial RB211-GT30 non-DLE	2015	32 172 kW	9 110 Btu	37.5%	22.9	220.0 lb	3000 rpm	937 F	****	****	
Industrial Trent 60 DLE	1996	53 119 kW	8 045 Btu	42.0%	34.5	342.1 lb	3000 rpm	812 F	420 000 lb	87 x 15 x 17 ft	
Industrial Trent 60 DLE ISI	1996	63 512 kW	7 888 Btu	43.2%	37.9	389.0 lb	3000 rpm	782 F	420 000 lb	97 x 15 x 17 ft	
Industrial Trent 60 WLE	2004	66 000 kW	8 240 Btu	41.4%	39.1	392.5 lb	3000 rpm	797 F	420 000 lb	87 x 15 x 17 ft	water injection
Industrial Trent 60 WLE ISI	2011	66 000 kW	8 217 Btu	41.5%	39.0	393.5 lb	3000 rpm	792 F	420 000 lb	97 x 15 x 17 ft	water injection
SGT5-2000E	1981	187 000 kW	9 426 Btu	36.2%	12.8	1230.0 lb	3000 rpm	997 F	417 000 lb	34 x 13 x 13 ft	
SGT5-4000F	1995	329 000 kW	8 385 Btu	40.7%	20.0	1598.0 lb	3000 rpm	1114 F	688 000 lb	35 x 17 x 16 ft	
SGT5-8000H	2008	420 000 kW	8 530 Btu	40.0%	19.2	1918.0 lb	3000 rpm	1193 F	981 000 lb	41 x 18 x 18 ft	
Siemens Energy (60 Hz)											
Industrial RB211-GT30 DLE	2015	32 537 kW	8 907 Btu	38.3%	22.3	215.8 lb	3600 rpm	932 F	****	****	
Industrial RB211-GT30 non-DLE	2015	33 158 kW	8 873 Btu	38.5%	22.7	218.0 lb	3600 rpm	933 F	****	****	
Industrial Trent 60 DLE	1996	54 020 kW	8 023 Btu	42.5%	33.6	347.4 lb	3600 rpm	808 F	420 000	87 x 15 x 17 ft	
Industrial Trent 60 DLE ISI	1997	61 842 kW	7 867 Btu	43.4%	36.2	370.6 lb	3600 rpm	789 F	420 000	97 x 15 x 17 ft	
Industrial Trent 60 WLE	2004	62 920 kW	8 268 Btu	41.3%	37.4	373.6 lb	3600 rpm	804 F	420 000	87 x 15 x 17 ft	water injection
Industrial Trent 60 WLE ISI	2011	65 660 kW	8 303 Btu	41.1%	38.0	379.3 lb	3600 rpm	798 F	420 000	97 x 15 x 17 ft	water injection

Model	Intro Year	ISO Base Load (kW)	Heat Rate (Btu/kWh)	Efficiency	Press Ratio	Mass Flow (lb/sec)	Turbine Speed	Exhaust Temp	Approx Weight	Approx L x W x H	Comments
Siemens Energy (60 Hz) (cont'd)											
SGT6-2000E	1989	117 000 kW	9 705 Btu	35.2%	12.0	811.0 lb	3600 rpm	990 F	238 353 lb	30 x 11 x 11 ft	9 ppm NOx
SGT6-5000F	1989	250 000 kW	8 682 Btu	39.3%	18.9	1296.0 lb	3600 rpm	1108 F	483 000 lb	33 x 13 x 15 ft	
SGT6-8000H	2010	305 000 kW	8 530 Btu	40.0%	19.5	1411.0 lb	3600 rpm	1202 F	637 000 lb	34 x 14 x 14 ft	
Solar Turbines											
Saturn 20	1960	1 210 kW	14 040 Btu	24.3%	6.7	14.4 lb	22300 rpm	945 F	22 500 lb	22 x 8 x 9 ft	recuperated gas turbine
Centaur 40	1992	3 515 kW	12 240 Btu	27.9%	10.1	41.9 lb	15000 rpm	830 F	73 820 lb	32 x 9 x 11 ft	
Centaur 50	1993	4 600 kW	11 630 Btu	29.3%	10.6	42.1 lb	16500 rpm	950 F	83 300 lb	32 x 9 x 10 ft	
Mercury 50	1997	4 600 kW	8 865 Btu	38.5%	9.9	39.3 lb	15000 rpm	690 F	100 700 lb	37 x 10 x 12 ft	
Taurus 60	1993	5 670 kW	10 830 Btu	31.5%	12.4	48.1 lb	13950 rpm	950 F	83 600 lb	32 x 9 x 10 ft	
Taurus 65	2005	6 300 kW	10 375 Btu	32.9%	15.0	46.5 lb	15000 rpm	1020 F	87 300 lb	36 x 9 x 12 ft	
Taurus 70	1994	7 965 kW	9 955 Btu	34.3%	17.6	59.3 lb	11000 rpm	945 F	136 215 lb	36 x 9 x 12 ft	
Mars 100	1994	11 350 kW	10 365 Btu	32.9%	17.7	93.8 lb	9500 rpm	905 F	181 000 lb	47 x 9 x 13 ft	
Titan 130	1998	16 450 kW	9 605 Btu	35.2%	17.1	109.8 lb	8500 rpm	915 F	208 100 lb	47 x 11 x 11 ft	
Titan 250	2008	21 745 kW	8 775 Btu	38.9%	24.1	150.4 lb	7000 rpm	865 F	311 100 lb	60 x 11 x 13 ft	
UEC-Gas Turbines JSC											
GTES-2.5	1990	2 500 kW	12 544 Btu	27.2%	12.0	33.0 lb	14000 rpm	797 F	78 265 lb	45 x 10 x 9 ft	dual fuel burner available
GTA-6RM	2001	6 000 kW	13 648 Btu	25.0%	8.6	102.0 lb	3000 rpm	781 F	99 209 lb	38 x 12 x 12 ft	dual fuel burner available
GTA-8RM	2003	8 000 kW	13 225 Btu	25.8%	9.8	112.0 lb	3000 rpm	932 F	90 390 lb	38 x 12 x 12 ft	dual fuel burner available
GTA-10GT	2014	9 650 kW	10 012 Btu	34.1%	17.7	72.0 lb	4500 rpm	968 F	94 799 lb	49 x 12 x 12 ft	
GTA-16	2014	16 300 kW	9 611 Btu	35.5%	19.5	123.0 lb	5300 rpm	936 F	132 278 lb	49 x 15 x 13 ft	
GTA-25	2017	25 530 kW	9 162 Btu	37.4%	28.2	171.0 lb	5000 rpm	941 F	141 097 lb	49 x 15 x 13 ft	
Vericor											
VPS3	1978	3 152 kW	12 560 Btu	27.2%	8.8	28.3 lb	16000 rpm	1110 F	70 000 lb	27 x 8 x 23 ft	
VPS4	1999	3 522 kW	11 906 Btu	28.7%	10.1	30.4 lb	16000 rpm	1076 F	70 000 lb	27 x 8 x 23 ft	
Zorya-Mashproekt											
UGT 2500	1992	2 670 kW	12 780 Btu	26.7%	12.8	36.4 lb	1800/3000	860 F	77 100 lb	39 x 10 x 11 ft	with gearbox
UGT 5000	2011	5 100 kW	11 010 Btu	31.0%	14.0	47.4 lb	1800/3000	896 F	22 400 lb	26 x 8 x 8 ft	
UGT 6000	1978	6 200 kW	11 300 Btu	30.2%	13.8	68.0 lb	3000/1500	802 F	121 600 lb	62 x 23 x 18 ft	
UGT 16000	1980	15 520 kW	11 150 Btu	30.6%	12.5	211.6 lb	3000 rpm	662 F	295 000 lb	80 x 24 x 19 ft	
UGT 15000	1988	16 500 kW	9 980 Btu	34.2%	19.5	156.5 lb	3000 rpm	788 F	300 700 lb	80 x 24 x 19 ft	
UGT 25000	1993	25 680 kW	9 590 Btu	35.6%	21.5	192.9 lb	3000 rpm	905 F	332 600 lb	80 x 24 x 19 ft	
UGT 45000	2015	46 000 kW	9 780 Btu	34.9%	14.0	305.3 lb	3000 rpm	1022 F	****	****	with gearbox
UGT 60000	2015	61 300 kW	9 100 Btu	37.5%	18.0	384.8 lb	3000 rpm	968 F	****	****	with gearbox

GAS TURBINES

PORTFOLIO AND OVERVIEW

Efficient, Flexible, Reliable Power

GE’s portfolio of heavy duty and aeroderivative gas turbines helps provide a sense of certainty in an uncertain world, delivering operational flexibility and performance needed to adapt to a rapidly evolving power generation environment. With gas turbine products ranging in individual output from 22 MW to 519 MW, GE has a solution to reliably and efficiently deliver the power needed by utility power generators, industrial operators, and communities. Even in remote locations and harsh conditions, you can count on GE to deliver a gas turbine that will meet your needs.

All of our gas turbines share the common heritage of jet engine technology pioneered by GE in the first half of the 20th century. They are typically categorized as either heavy duty (sometimes also called “frame”) or aeroderivative gas turbines, although some turbines recently have adopted features of both design types. In general, the differences between the aeroderivative and heavy duty gas turbines are weight, size, combustor type, and turbine design. Heavy duty gas turbines are usually field constructed and maintained in place, whereas aeroderivative gas turbines are designed to allow for quick replacement of the entire engine when maintenance is required.

High-Efficiency H-Class

- Most cost-effective conversion of natural gas to electricity in the H-class industry
- Includes the world’s largest high efficiency turbine: 519 MW
- First H-class gas turbine fleet to reach 240,000 operating hours

Industry-Leading F-Class

- Introduced F-class technology nearly 30 years ago
- World’s largest fleet, with more than 1,100 installed units and 50 million operating hours of experience
- Industry’s best reliability at 99.4 percent

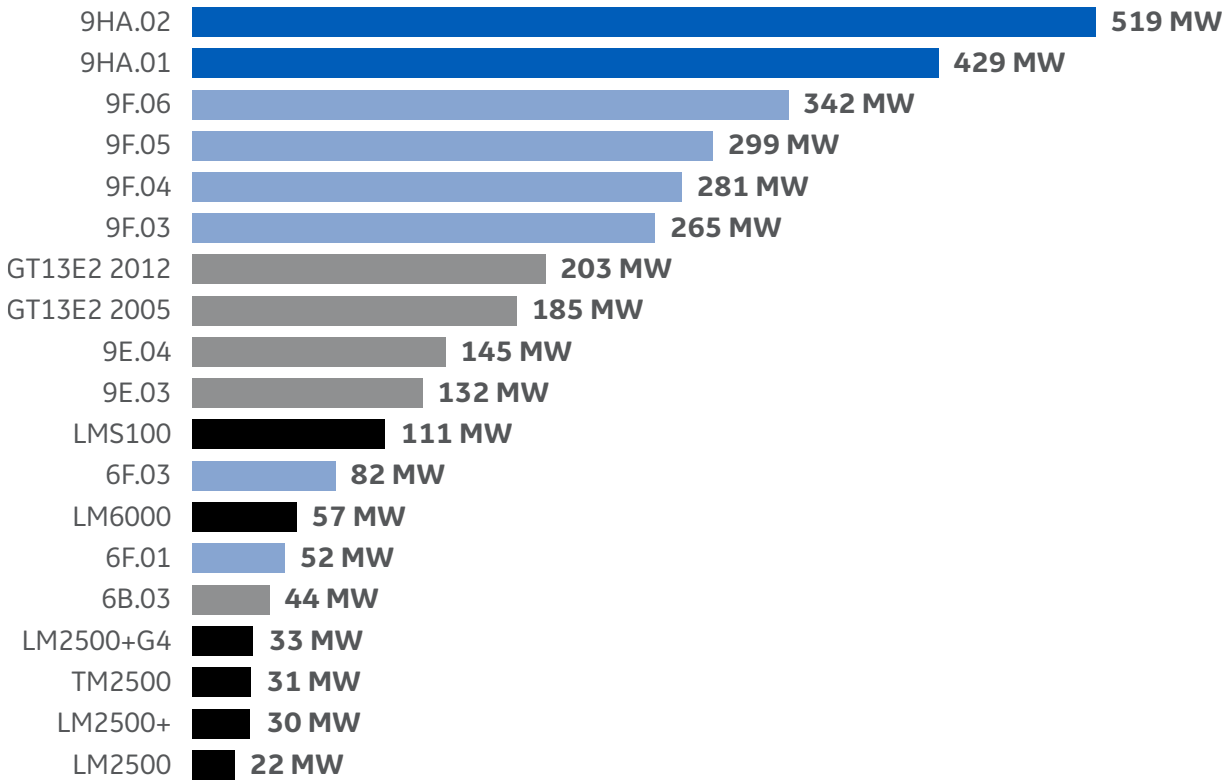
Reliable E-Class

- Rugged and available, even in harsh climates
- Industry-leading fuel flexibility, burning more than 50 gases and liquids
- Quick installation for fast-track projects
- More than 3,000 units installed
- More than 143 million operating hours of experience

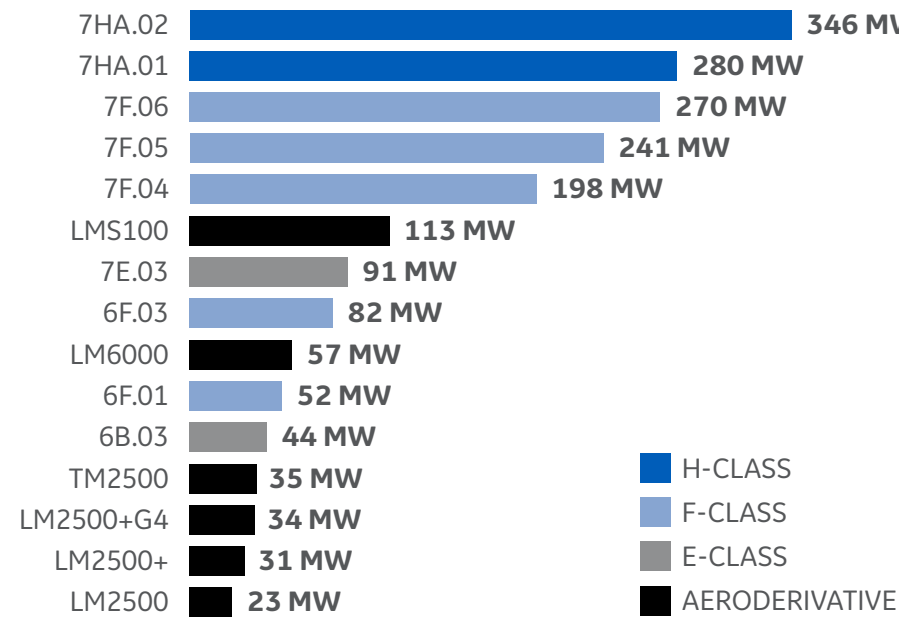
Compact and Proven Aeroderivatives

- Flexible and reliable power generation packages with aviation derived engines
- Over 100 million operating hours of experience
- Up to 56 percent combined cycle efficiency and over 80 percent efficiency in cogeneration applications

50 Hz Portfolio by Rating



60 Hz Portfolio by Rating

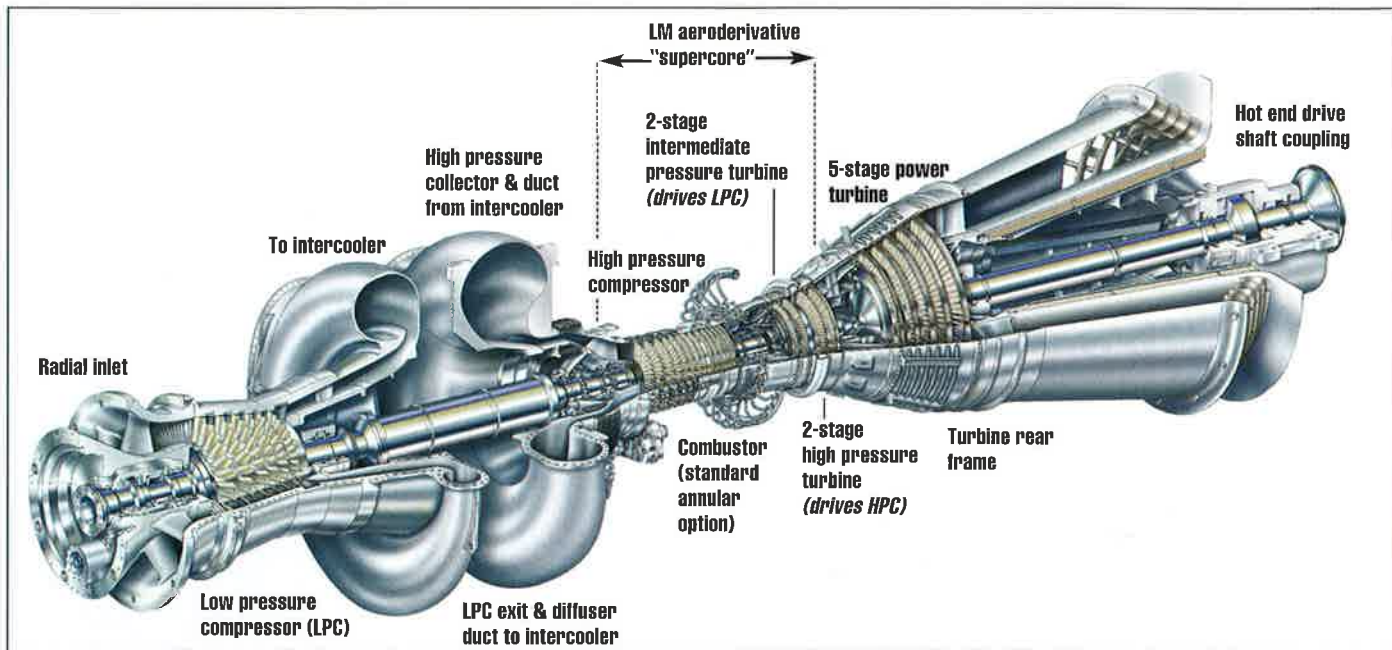


- H-CLASS
- F-CLASS
- E-CLASS
- AERODERIVATIVE



LMS100: 46% in simple cycle

An off engine intercooler in the compression section is the key to the extraordinary efficiency claimed for GE's latest gas turbine. It is the first modern production power generation gas turbine to use this technology.



When asked to describe their requirements for future power generation facilities, GE says its customers put the following high on their priority list: 100 MW blocks of power; high efficiency at full and part power; cycling capability; fast start; peaking capability; sustained hot-day power; fuel flexibility; and, of course, low emissions. The new LMS100 gas turbine aims to respond to these needs, "changing the game in the power generating industry", claims GE.

The new LMS100 design is the first GE gas turbine to combine actual components from the company's heavy duty frame gas turbines with those from its aeroderivative machines.

The LMS100 features an inlet and low pres-

sure compressor (LPC) comprised of the first six stages of an MS6001FA (heavy duty gas turbine) compressor. These stages are followed by an aerodynamically designed volute which ducts the low pressure compressed air into the off-engine intercooler. Cooled air from the intercooler is ducted back through another volute into the high efficiency aeroderivative "supercore". The latter is a term coined by GE for the LMS100.

The supercore module is described as "rotatable", which means that when an existing module has to go away for depot maintenance, a lease or spare unit can be installed in 24 hours. The supercore consists of:

- A high pressure compressor (HPC), based on the CF6-80C2 aircraft engine compressor, strengthened for the high (42:1) pressure ratio of the LMS100.
- The combustor, which can be either a standard annular combustor (SAC) or an advanced dry low emissions (DLE2) combustor.
- A high pressure turbine (HPT), derived from the CF6-80E1 aircraft engine. This drives the HPC.
- A 2-stage intermediate pressure turbine (IPT), which drives the LPC through a mid-shaft and flexible coupling.

The intercooler, which can be either air-to-

air or air-to-water, is the key contributor to the remarkably high efficiency claimed for the LMS100: 46% in simple cycle. The cooled flow from the intercooler means less work for the high pressure compressor, which increases overall efficiency and power output.

Furthermore, the HPC exit air is in turn cooler. This HPC exit air is used for turbine cooling, so its reduced temperature allows increased gas turbine firing temperature, also enhancing efficiency and raising power output.

Following the IPT, on a separate shaft, is a five-stage aerodynamically coupled power turbine. This has been designed specifically for the LMS100, but the exhaust frame and aft drive shaft are based on heavy-duty gas turbine exhaust design.

Where water is scarce or very expensive, an air-to-air intercooler will be used of the A-frame tube and fin type, as commonly found in the oil and gas industry.

In high ambient temperature climates, an evaporative cooling system can be added for power augmentation. This system would use a small amount of water for short periods as required.

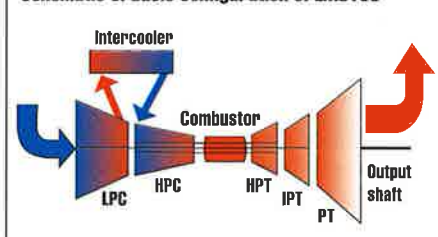
Where water is readily abundant or less expensive the intercooler can be of the air-to-water type, with a tube and shell configuration, also used in many industrial applications.

Both intercooler types would be connected through a system of piping and expansion bellows.

The LMS100 SAC will be equipped with dual fuel capability so that it can burn either natural gas or distillate fuels. The LMS100 DLE will operate on gas fuel.

As well as the high efficiency of the LMS100 at its rated output (about 10% better than the LM6000) also remarkable is the new machine's high efficiency at part load. At 50%

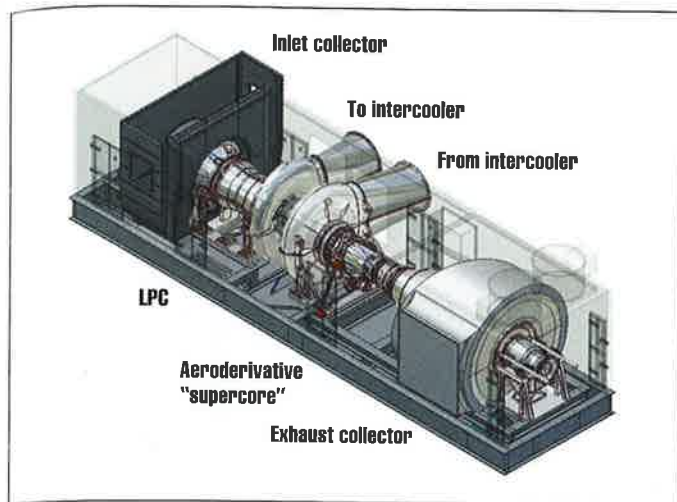
Schematic of basic configuration of LMS100



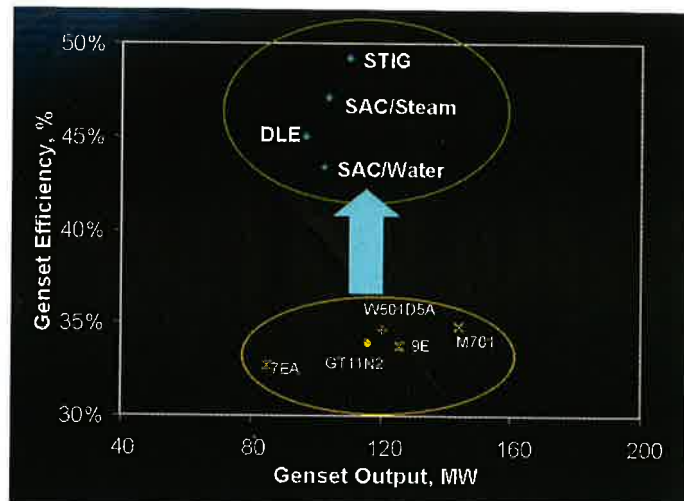
LMS100 expected performance data, simple cycle (60Hz/50Hz)

TYPE	MWe	HEAT RATE (Btu/kWh)	EFFICIENCY (%)
DLE	98.7/99	7509/7821	48/45
SAC (with water diluent for NO _x control)	102.8/102.5	7813/8247	44/44
SAC (with steam diluent for NO _x control)	102.1/102.2	7187/7603	48/47
STIG (with steam injection for power augmentation)	112.2/110.8	6845/7263	50/50

(Conditions: performance at generator terminals; NO_x = 25 ppm; 15°C, 80% RH; losses 0mm/0mm inlet/exhaust; fuel LHV = 44.2MJ/kg)



LMS100 gas turbine package



Efficiency of LMS100 (STIG, SAC/steam, SAC/water and DLE versions) compared with other machines in the 80-160 MWe range (source GE and Gas Turbine World)

turndown, the efficiency is 40%, which "is greater than most gas turbines at full power in the market today", notes GE.

Other attractive features mentioned by GE include cycling capability without increased maintenance cost, low lapse rate for hot day power (without the need for inlet conditioning), and the ability to achieve full power in ten minutes.

The key markets envisaged for the LMS100 are peaking and mid-range dispatch power generation.

In CHP applications the high power-to-steam ratio allows the LMS100 to meet the steam demand served by 40-50MW gas turbines while delivering more than twice the power. Using both exhaust and air-to-water intercooler energy, an LMS100 CHP plant could reach over 85% thermal efficiency.

Another possible application mentioned by GE is the rather novel one of using the LMS100 in coal plants as a boiler feedwater heat source to boost efficiency.

The new machine is not particularly targeted to the combined cycle market, and indeed its envisaged combined cycle efficiency, 54%, with a CCGT plant output of about 120 MWe, is not that high compared the latest CCGT designs based on larger heavy duty frame gas turbines. But GE believes that, even in CCGT mode, the new machine has some advantages, in particular stemming from the low exhaust temperature, which results in lower cost exhaust system materials, smaller steam turbines, condensers and generators, leading to a lower steam plant installed cost.

Another benefit claimed from the lower exhaust temperature is more power from duct firing (up to 30MW, taking potential CCGT power to 150 MWe).

The LMS100 gas turbine with the SAC combustor (using water or steam for NO_x control) and the advanced DLE combustor (DLE2) is designed to achieve 25 ppm NO_x. This represents a 7 to 18% reduction in mass emissions rate (lb/kWh) compared with GE's LM6000 gas turbine.

In places where less than 25 ppm NO_x is required, a low temperature SCR can be used. The high efficiency of the LMS100 results in exhaust temperatures below 800°F (427°C), which permits the use of low temperature SCR without tempering air.

The LMS100 can operate at 50Hz and 60Hz

without a gearbox. This is because the power turbine, on its own separate shaft, can be made to operate efficiently in either regime by changing its first stage nozzle.

The absence of a gearbox reduces system complexity, plot size and cost, while increasing reliability.

The LMS100 will also operate with very little power variation for up to 5% reduction in grid frequency, allowing grid support in times of high demand and load fluctuations.

The generator is dual rated for 50 or 60 Hz applications. Either an air-cooled or TWAC configuration can be provided, GE says.

Features contributing to good maintainability include: modular construction, allowing replacement of the aero components without total disassembly; multiple borescope ports; split casing construction of the LPC and aeroderivative compressor, which allows detailed on-site inspection, and blade replacement; and a hot-section design that only needs a few days for field maintenance, GE says.

The company has established a target availability of 97.5% for a mature LMS100 power plant, with a target reliability of 98.5%. The expected service intervals for the new machine, based on normal operation include:

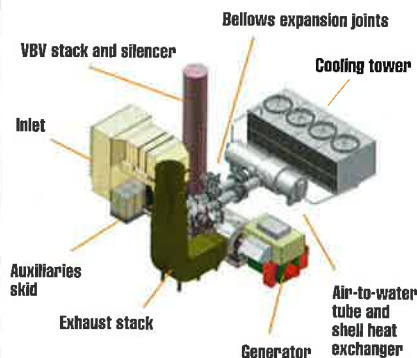
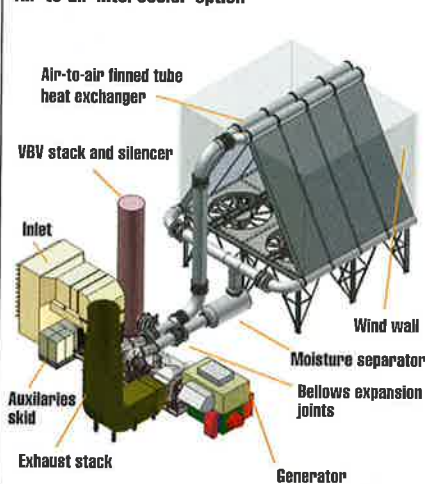
On-site hot-section replacement	25 000 fired hours
Depot maintenance; overhaul of hot section and inspection of all systems, power turbine overhaul	50 000 fired hours
Next on-site hot section replacement	75 000 fired hours
Depot maintenance	100 000 fired hours

GE notes that these are actual fired hours, with no multipliers needed for cycling.

Significant emphasis has been placed on controls design for increased reliability of the entire power plant. The LMS100 will use the new GE Mark VIe control system, which has dual channel architecture with a cross-channel data link providing redundancy which will allow multiple failures without engine shutdown.

A fibreoptic distributed I/O system located outside the module will be unaffected by electromagnetic or radio frequency interference, which will eliminate noisy wiring. Site interconnects are reduced by 90% compared to the typical gas turbine control systems, says GE.

Air-to-air intercooler option



Air-to-water intercooler option

As regards noise, the LMS100 gas turbine-generator will be rated at 85 dBA average at 3 ft (1 m). An option for 80 dBA at 3 ft will be available.

As well as many GE businesses, also involved with the LMS100 project are Avio of Italy, Volvo of Sweden and Sumitomo of Japan.

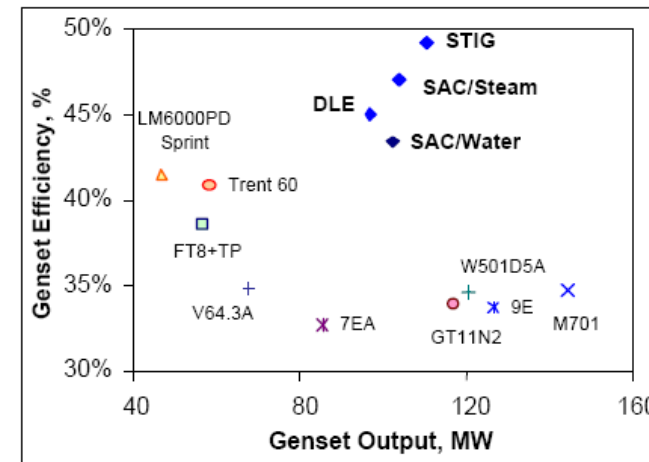
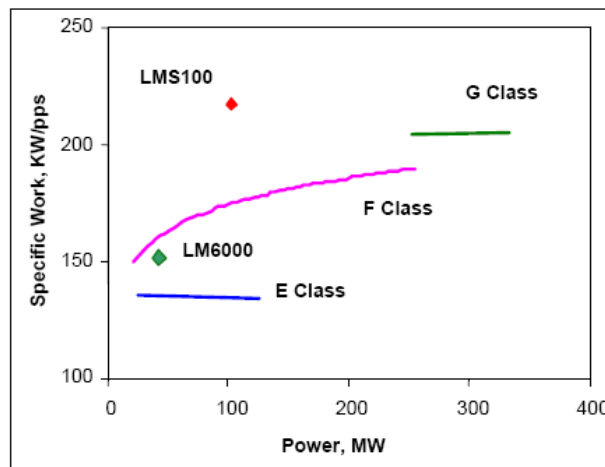
Development testing is due to start in May 2004. First production units with the standard annular combustor are due to be available in the second half of 2005. The STIG version is scheduled to be available in early 2006, followed by the DLE in the second half of 2006.



GE LMS 100

LMS100 ISO Performance Data

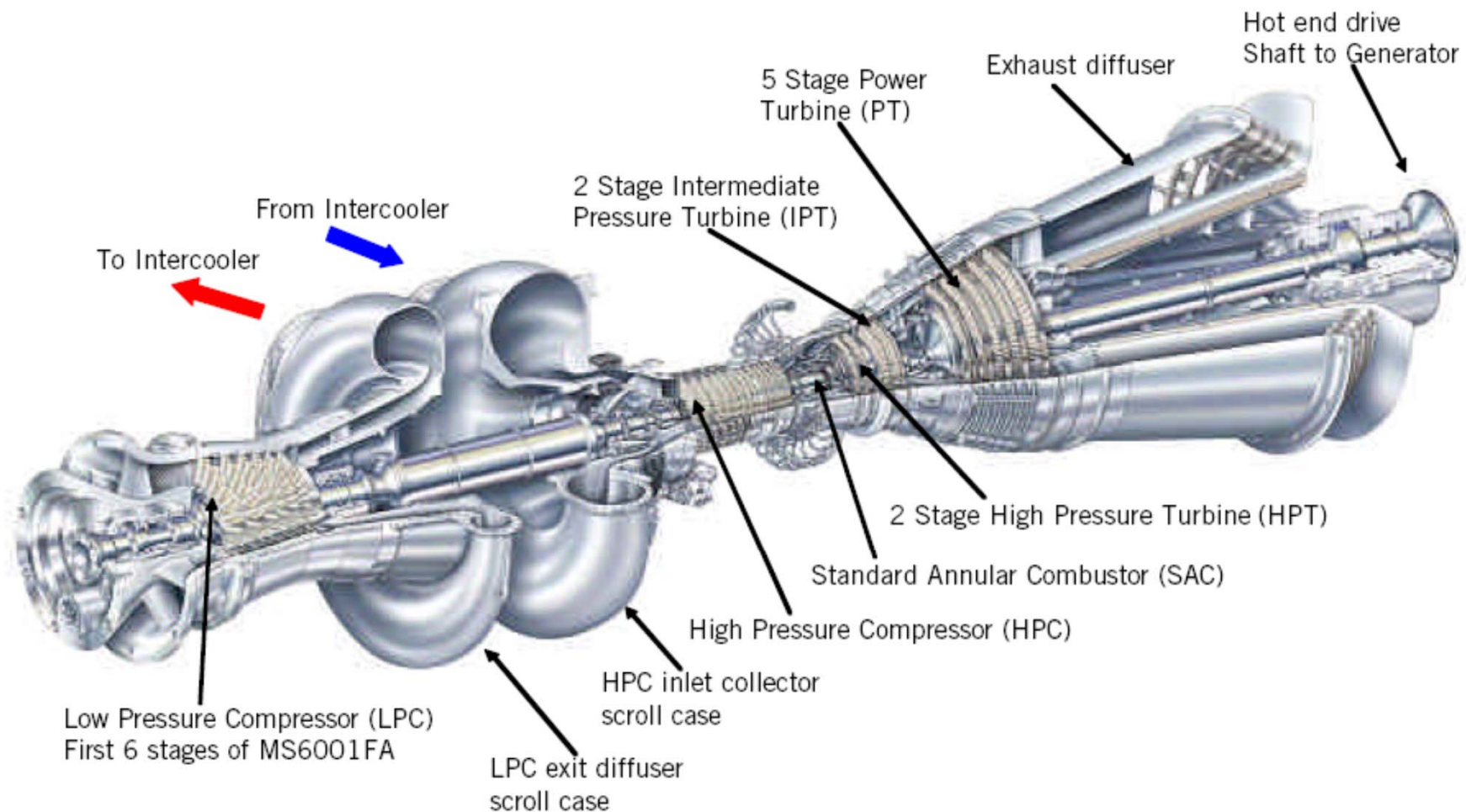
Model	ISO Base Rating (kW)	Heat Rate (Btu/kWh)	Efficiency%	Mass Flow (lb/sec)	Turbine Speed (RPM)	Exhaust Temp (F)	Comments
LMS100PB	97,718	7,592	45.0%	453	3,600	783	DLE, 25 ppm NO _x
LMS100PB	97,878	7,579	45.0%	453	3,000	784	DLE, 25 ppm NO _x
LMS100PA	103,112	7773	43.9%	469	3,600	770	water injected to 25 ppm NO _x
LMS100PA	103,162	7769	43.9%	469	3,000	767	water injected to 25 ppm NO _x



- Attractive for peaking and mid-range dispatch applications, where cyclic operation is required and efficiency becomes more important
- Limited applicability for combined cycle operation due to low exhaust temperature: 120 MW at 53.8 % efficiency



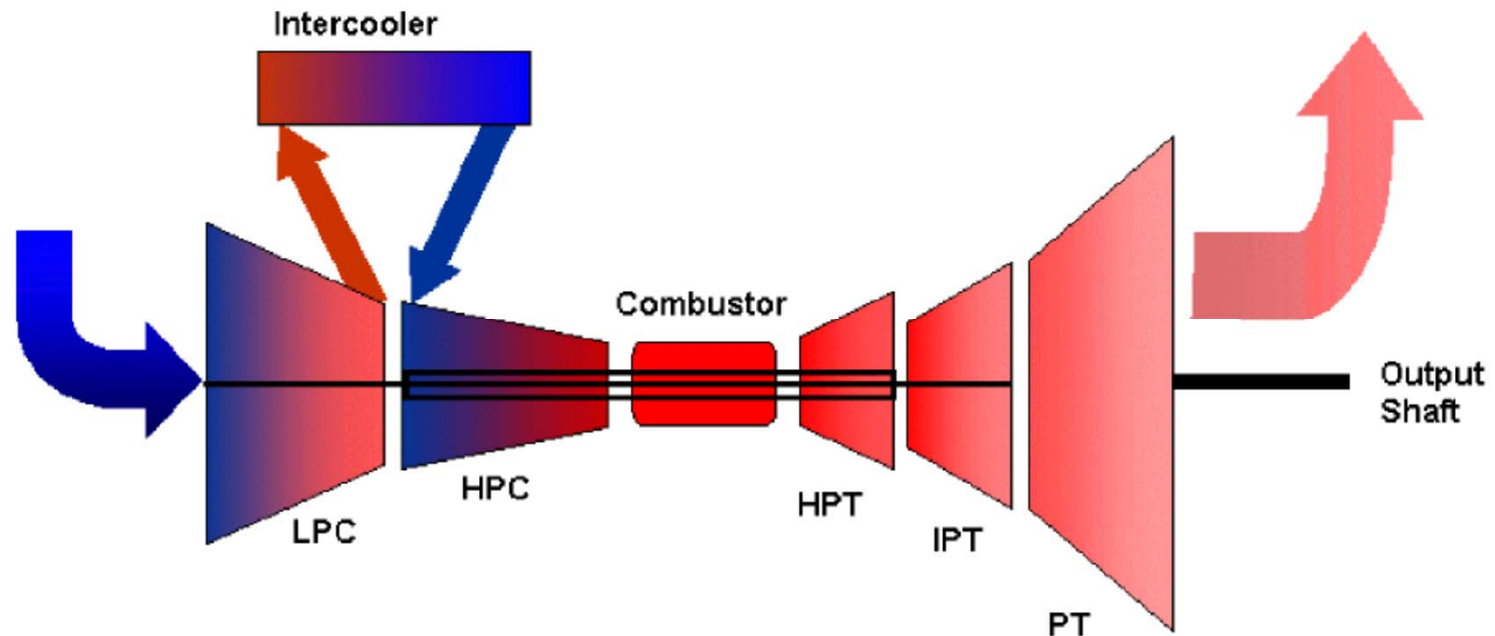
GE LMS 100



- **LPC uses stationary FA gas turbine technology**
- **CF6 aeroengine technology for supercore (HPC, Combustor, HPT, IPT)**



- Output 100 MW
- Highest simple cycle efficiency of 45 %
- Cycle pressure ratio 42:1
- Off-engine intercooling reduces compression work and supplies colder cooling air
- Three-spool design
- 1380°C firing temperature class



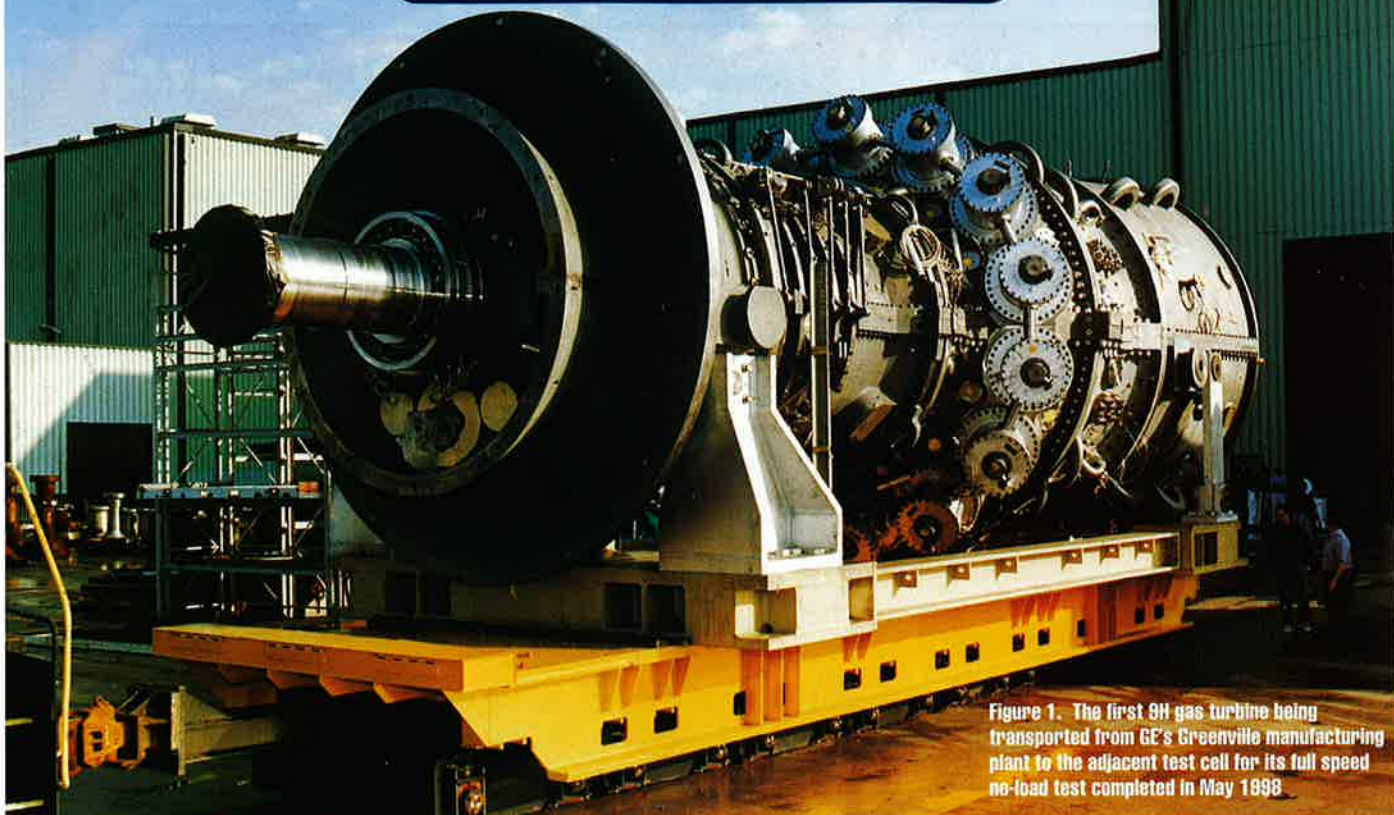


Figure 1. The first 9H gas turbine being transported from GE's Greenville manufacturing plant to the adjacent test cell for its full speed no-load test completed in May 1998

First H System gas turbine planned for Baglan

The first GE H System 50 Hz steam cooled gas turbine, fully integrated into a single 500 MWe 9H combined cycle chp plant unit is now planned for the old BP Chemicals site at Baglan Bay near Neath in South Wales, UK.

David Smith

The GE H System 50 Hz steam-cooled gas turbine combined cycle power plant to be built in South Wales is the most advanced of next generation gas turbines (Figure 1). It incorporates all the US DOE advanced turbine system (ATS) programme elements on which the 60 Hz 7H machine will be based. It will have a nominal combined cycle output of 480 MWe and a thermal efficiency of over 60 per cent. For further details on this and future DOE programmes, see p45 of this issue.

The steam cooling permits a radical increase in firing temperature while reducing the operating temperature of turbine blading as well as eliminating loss of cooling air flow for traditional turbine blade cooling. Figure 2 shows a cross section of the new turbine and Figure 3 shows the steam cooling schematic.

The original site was the 1000 MWe 9H Fleetwood Power project in Lancashire, England, which was abandoned due to the UK government's *de facto* moratorium on new gas-fired power plants, as also was the Partington project near Manchester which was to have the first 9FA++ gas turbines.

A single 500 MWe 9H combined cycle chp power plant unit is now planned for the old BP Chemicals site at Baglan Bay near Neath. The project will replace a more ambitious

1200 MWe project on the same site - with three 9FA gas turbines plus a single 550 MWe steam turbine - for which Section 36 application was made in December 1996.

Project development

Following the submission of a significantly revised application for the construction of the new 500 MWe power station at the Baglan Energy Park, South Wales, UK Secretary of State for Trade and Industry Stephen Byers confirmed his approval of the application under Section 14 of the Energy Act.

The proposal will now be submitted to the local planning process to secure final consent to trigger development of Baglan Energy Park - a joint initiative by the Welsh Development Agency, Neath Port Talbot County Borough Council and BP Chemicals. Although the proposal flies in the face of issues cited in the UK government's White Paper supporting the 'moratorium' on new gas-fired power plants, it unlikely that further permit applications will be refused.

The notification to Baglan Cogeneration Company Project Manager Ken Allison pointed out that "... certain types of generating stations may, however, have benefits that outweigh the government's concerns about new gas-fired power stations (paragraph

10.41 of the white paper)."

The government's determination to promote chp technology is well known, but the notification stresses the desperate lack of employment in the area which started with the closure of coal mines in the area.

"The Secretary of State has noted that the Neath/Port Talbot area is in a proposed European Union Objective 1 area for the purpose of eligibility for EU Structural Funds grants. It suffers a relatively high unemployment rate and the area has been historically dependent on ageing industries which are fast disappearing." Employment in manufacturing in the region has fallen by 59 per cent since 1980 compared with 27 per cent in Wales as a whole.

Some 2800 jobs will be lost this year. The Pembroke 2000 MWe oil-fired power station, which was closed down after it was denied a licence to burn orimulsion, was a major employer, and the loss of this facility has resulted in a power supply deficit in the area.

Also, the BP Chemicals plant producing styrene and isopropanol, a major employer in the area in the 1970's, is now running down and moving production to its east coast and Grangemouth complexes using natural gas feedstock from the North Sea instead of Welsh coal. It is increasingly becoming a brown field site on which Baglan Energy Park is to be built.

"We believe that by locating this new turbine in South Wales, the Baglan Energy Park can become the core for a new centre of technological excellence in Wales which will set global standards for performance, efficiency and emissions control well into the 21st century" said Bob Nardelli, President and CEO of GE Power Systems, which will invest \$450 million in constructing the new power plant.

BP Chemicals already has a 100 MWe oil-fired chp plant on the site. The new 500 MWe plant will supply bulk steam, water, nitrogen and oxygen to local industrial users. The station will also have a black-start facility to re-energise the grid in event of system failure, as well as providing security of supply to the chemicals plant.

After five years of the most intensive component, system and materials testing ever applied to a heavy industrial gas turbine, the first complete machine will be installed with its integrated steam bottoming cycle for commercial field operation in a merchant chp plant.

9H combined cycle

Recently demonstrated to invited potential utility customers, the GE 9H will only be introduced to the market as a single shaft combined cycle power unit with a purpose-built exhaust heat recovery boiler and the new specially designed GE Mark 6 control system.

This new control system is perhaps the most recently developed and advanced constituent of the technology. It not only incorporates the digital algorithms necessary to optimise supply of blade cooling steam to gas turbine, it must also integrate control algorithms to optimise chemical process plant dynamics for every operating scenario of the BP Chemicals complex it will supply, as well as the project district heating loads in local government buildings and new factories to be established in and around the Energy Park.

The major advances in turbine output and efficiency mainly derive from the use, for the first time, of closed-cycle steam cooling of turbine stationary and rotating blades and incorporation of GE's advanced aircraft engine

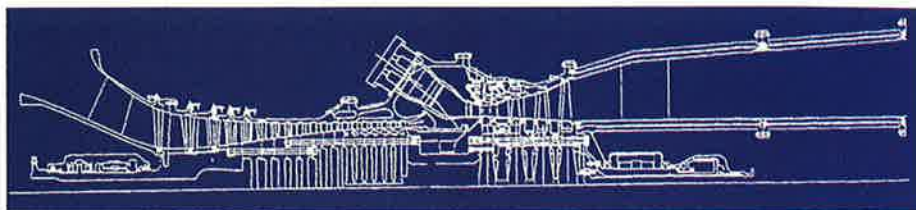


Figure 2. Cross section through the H System gas turbine

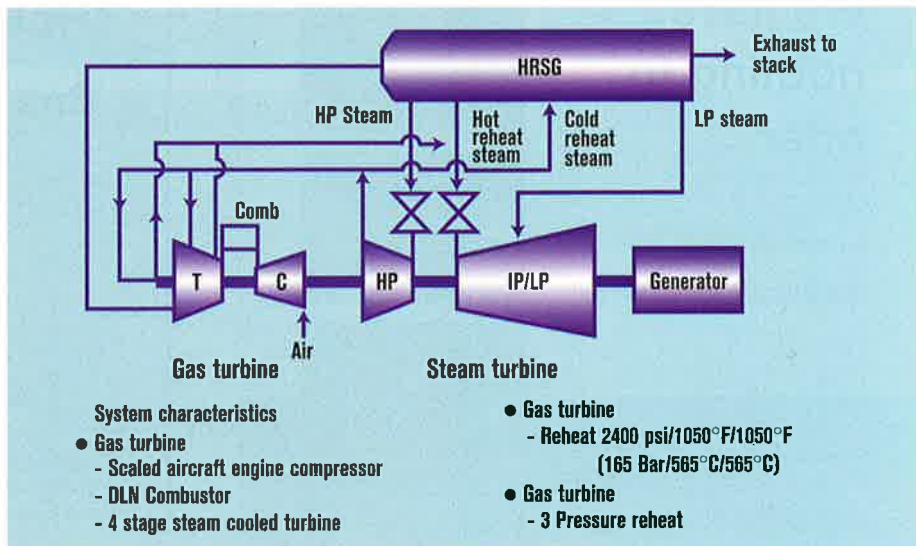


Figure 3. The H System combined cycle cooling system

technology, including optimised compressor aerodynamics, single crystal turbine blades and advanced thermal barrier coating. The rotor for the first 9H is shown in Figure 4.

The exhaust heat recovery steam generator will not be very different from a typical three pressure level combined-cycle boiler, except that a substantial proportion of the cold reheat steam from the HP exhaust system will be diverted into the gas turbine steam cooling system to be returned into the IP section of the condensing steam turbine. At an output level of 395 MWe, some 25 per cent of the cold reheat steam is used for gas turbine cooling.

The gas turbine

GE's MS9001H and MS7001H turbines contain an 18-stage compressor, a can-annular dry low NO_x (DLN) combustion system, and a four-stage turbine. A 2600°F/1427°C firing temperature and closed-circuit steam-cooling are used in the gas turbine. The rotor is similar to prior GE gas turbines, being supported by two bearings and the first rotor bending critical above the operating range. Through-bolt rotor construction is used in both compressor and turbine rotors. The rotor thrust bearing is at the inlet end of the gas turbine (Figures 2 and 4).

The MS9001H and MS7001H compressors provide a 23:1 pressure ratio with 685 kg/s and 558 kg/s airflow for the MS9001H and MS7001H turbines respectively. This is a higher pressure ratio and airflow than GE's FA gas turbine compressors (Table 1). The higher airflow provides increased output and economic scale efficiencies, while the higher pressure ratio is necessary to keep exhaust temperatures at an acceptable level. Without the higher pressure ratio, elevated exhaust temperatures driven by gas turbine firing temperature and closed steam cooling in the turbine would have an undesirable cost and life impact on the exhaust system and HRSG.

The H System compressors are derived from GE's high-pressure compressor used in the CF6-80C2 aircraft engine and the LM6000 aeroderivative gas turbine. This compressor has recorded many million hours of experience providing reliable operation. For use in the H gas turbines, the CF6-80C2 compressor is scaled up (2.6: 1 for the MS7001H and 3.1:1 for the MS9001H) with four stages added to achieve the desired combination of airflow and pressure ratio. On the MS9001H, the four additional stages are on the back of the CF6-80C2 compressor. On the MS7001H, the last stage from the MS9001H compressor is elimi-

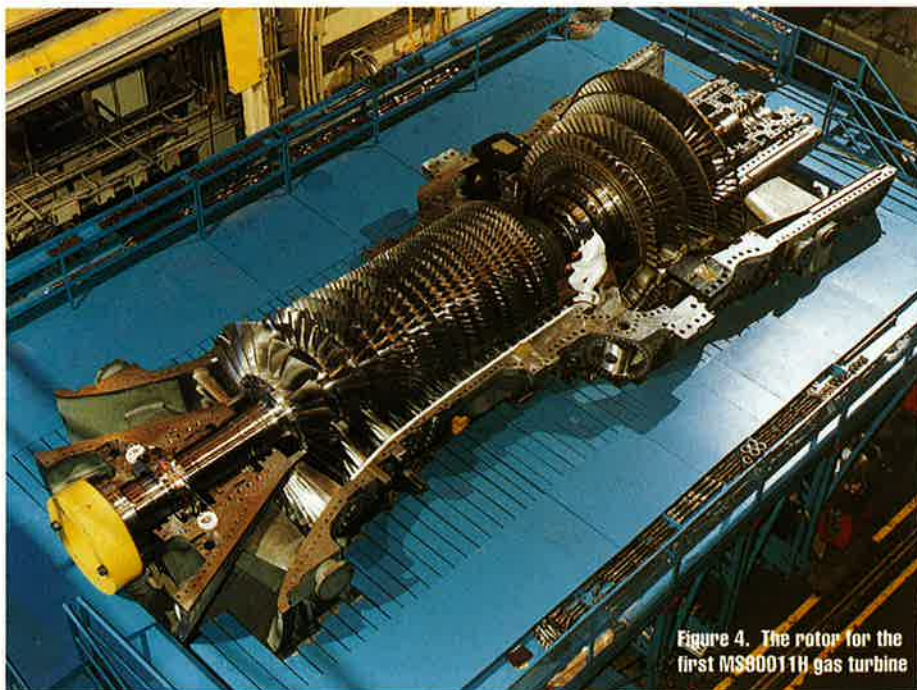


Figure 4. The rotor for the first MS9001H gas turbine

nated and a zero stage added at the front.

The H compressors have four stages of variable stator vanes (VSV) at the front of the compressor. They are used, in conjunction with the IGV, to control compressor airflow during turn-down as well as optimise operation for variations in ambient temperature.

The H can-annular combustor is a lean pre-mix DLN system similar to current GE systems. Fourteen cans are used on the MS9001H and 12 cans on the MS7001H. The combustion system is a reverse-flow type, with double wall construction with impingement sleeves surrounding the transition ducts and combustion liners. These sleeves provide impingement and convective cooling of the liners and transition pieces, using compressor discharge air. The DLN technology was developed for and proven on the F class machines.

A four-stage turbine is used for compatibility with the compressor 23:1 pressure ratio. Previous GE gas turbines have operated successfully with three turbine stages. However, with the increase in pressure ratio, three turbine stages would have increased the loading on each stage causing reduced stage efficiency. By using four stages, the H turbine is able to achieve optimum work loading on each stage and high turbine efficiency.

The turbine uses closed-loop steam cooling of Stage 1 and 2 nozzles and buckets plus Stage 1 shroud (see Figure 5). Steam from the combined-cycle steam system is introduced into the turbine components, provides cooling, and is returned to the steam bottoming cycle for work extraction in the steam turbine. Air cooling is used for the Stage 3 nozzle and bucket with the fourth stage being uncooled.

In operation, the turbine will be taken up to approximately 10 per cent load on air-cooled blades, and then switched over from air cooling to steam cooling.

A single crystal material with thermal barrier coating (TBC) is used for both the Stage 1 nozzle and bucket. The single crystal alloy is a nickel-based cast superalloy possessing excellent high temperature properties which was developed and patented by GE. It has been used by GE Aircraft in full scale production since 1988. Stages 2 to 4 rotating blades utilise a directionally solidified material used in GE's F gas turbines today. Stage 2 is also thermal barrier coated. Stages 2 through 4 stationary blade materials are also used in GE's gas turbines and aircraft engines. Stages 2 and 3 are also thermal barrier coated.

No steam or water injection is used for NO_x

Table 1.

H System combined cycle plant performance characteristics

	7FA	7G	7H	9H
Firing temperature (°C)	1300	1430	1430	1430
Air flow (kg/s)	442	558	558	685
Compressor pressure ratio	15	23	23	23
Specific work (MW/kg/s)	0.57	0.63	0.72	0.70
Combined cycle net output (MWe)	253	350	400	480
Net thermal efficiency (%)	55	58	60	60
NO _x (ppmvd at 15% O ₂)	9	25	9	9

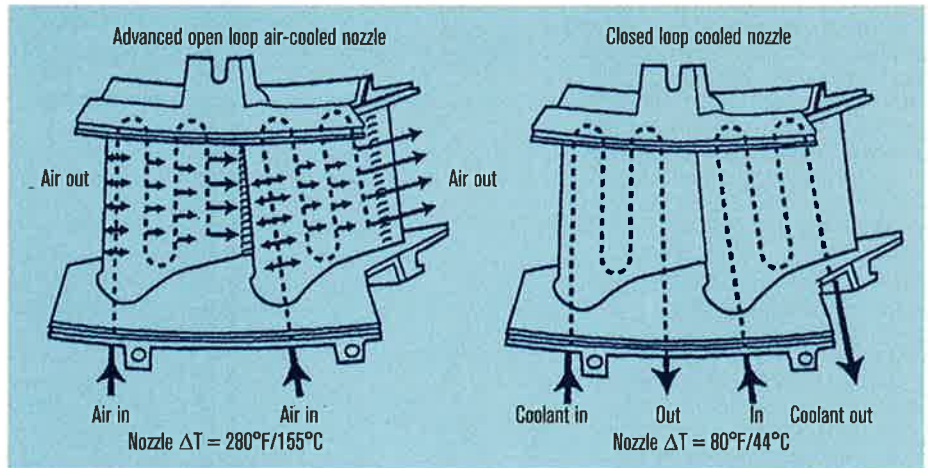


Figure 5. The impact of Stage 2 nozzle cooling

reduction, since single figure NO_x - 9 ppm, has already been demonstrated with the GE DLN combustors in the F and FA marque.

Nominal output for the 50 Hz 9H is 480 MWe, compared to 400 MWe of the 60 Hz 7H, which will be the first of the US Department of Energy's ATS specification machines. All enabling technology for the ATS has been built into the Baglan Bay 9H, but the ATS designation applies exclusively to the 60 Hz version. Favourable site ambient conditions are cited as the reason for increased output of 50 MWe at Baglan Bay. Detailed characteristics of the H System machines were first published in the June 1995 issue of *Modern Power Systems*.

Test programme

It is, of course, not possible to test a new turbine of some 500 MWe output on a factory test-bed using a dynamometer, the first test operation of any GE H System turbine will be the Baglan Bay combined cycle chp unit.

The first running up and operation of the Baglan Bay machine took place during no-load testing at GE's Greenville facility from April to June 1998. Currently the machine is being stripped down for extensive inspection and analysis before rebuilding for delivery to the site. The machine will be very highly instrumented and the first year of test operation on power will be critical to both H System development and the ATS programme.

Baseline compressor test results

A baseline compressor rig was used to validate the fundamental design approach of using the CF6-80C2 derived compressor in heavy duty gas turbine operation during 1995. Test objectives included validation of performance, power turndown operability, stall margin and aeromechanics. The rig was tested for over 200 hours. Nearly 600 data points were recorded verifying the design approach by meeting all test objectives.

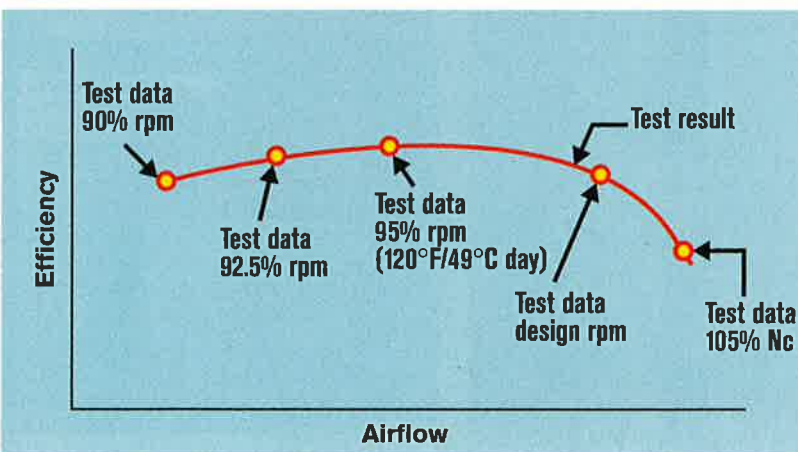


Figure 6. Baseline compressor efficiency confirms pre-test prediction

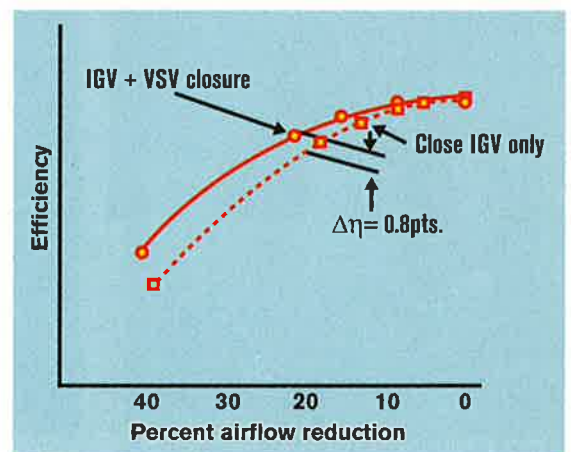


Figure 7. Baseline compressor turndown efficiency vs flow

The baseline compressor had excellent efficiency confirming the design value of product efficiency. Figure 6 shows a plot of compressor adiabatic efficiency as a function of airflow.

Power turndown performance and operability testing was successfully conducted to validate the baseline compressor at conditions which are not encountered in aircraft operation. During power turndown, airflow is reduced at constant speed which compares to the CF6-80C2 aircraft engine where airflow reduction is accompanied by a speed reduction. The baseline compressor, at constant speed, achieved 50 per cent airflow reduction, exceeding the design objective of 40 per cent. During power turndown testing, the added flexibility of having VSVs was explored.

A plot of compressor efficiency at ISO conditions as a function of flow turndown is shown in Figure 7. Testing revealed that up to 0.8 points of compressor efficiency improvement are achieved by using the IGV plus VSVs for airflow reduction compared to the IGV only. This testing also validated that using the IGV plus VSVs at maximum flow turndown avoids pressure or temperature drop through the first compressor stage. This eliminated the need for inlet heating on the H gas turbines.

An important part of the baseline test was establishment of the high speed compressor map, shown in Figure 8. Testing was used to validate the no load operating line, full load operating line and stall margin. There is an ample stall margin at ISO full load conditions. The minimum stall margin occurs at cold day, maximum flow turndown but still exceeds GE's design practice value for minimum stall margin.

All the compressor blades were instrumented with strain gages to obtain aero-mechanical data over the entire compressor operating range to validate airfoil operation. Data from the tests have since been used to complete mechanical, aerodynamic and aero-mechanical design modification necessary to convert from the baseline compressor to the commercial MS9001H compressor design.

Turbine test programme

An extensive test programme has been conducted on the H turbine to confirm that successful operation has been fully defined and validated for operation with steam cooling.

The Stage 1 nozzle ring comprises single

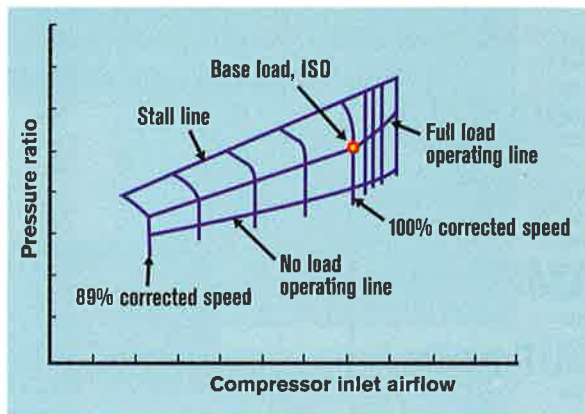


Figure 8. Baseline compressor high speed compressor map

vane castings with 42 vanes in the MS9001H and 36 vanes in the MS7001H.

The airfoil and sidewall band areas are steam cooled with heat transfer enhancement by a similar impingement process to that used in the FA Stage 1 nozzle. The difference is that rather than the spent impingement air being exhausted to the flow path as film cooling in air-cooled designs, in the H System the spent impingement steam is collected and returned to the steam bottoming cycle.

Stage 1 nozzle material

The Stage 1 nozzle single crystal material is a high nickel and chromium containing alloy which possesses superior pitting resistance which is also very stable at the steam cooling conditions to which it will be exposed. It is not expected to exhibit a loss of chromium at the grain boundaries, loss of alloy to precipitates or other destabilising effects. The testing programme to validate its use in a steam environment included:

Oxidation testing - Isothermal oxidation testing was conducted to study the long term isothermal oxidation, corrosion and stress corrosion cracking (SCC) susceptibility. Specimens were loaded into steam autoclaves for aging. The samples included coated specimens and potential braze and weld materials. Samples were removed at set intervals for evaluation and quantification of oxidation, corrosion and SCC susceptibility, the majority of which showed no detrimental effects of steam on the properties of the single crystal alloy.

Cyclic oxidation tests - were also conducted to determine if thermal cycling conditions in steam changed the oxidation behaviour of the materials. At H conditions, test results reported no effects of thermal cycling on the oxidation behaviour as compared to the isothermal results.

Mechanical property testing - Mechanical property testing on both bulk properties and structure-sensitive properties was initiated at H temperature and stress conditions. Tests include creep testing, low cycle fatigue (LCF) testing, slow strain rate tensile testing and fatigue crack propagation.

TBC coating

Thermal barrier coating previously used on the flow path surfaces of the Stage 1 nozzle operate at different conditions than those in steam-cooled components. Multi-path development of TBCs to perform at H conditions have been tested under a validation programme including laboratory durability tests

and field trials.

A high thermal gradient electron beam facility was constructed for testing of TBC specimens duplicating the thermal-mechanical conditions which will be experienced in the H Stage 1 nozzle and other airfoils. The electron beam is the energy source providing flux to the hot side of the specimens, with the backside of the metal substrate cooled to maintain the thermal flux, thereby generating the desired temperature gradient through the TBC and/or metal.

Nozzle heat transfer

Internal and external heat transfer tests fully characterised the thermal environment of the Stage 1 nozzle. A test

programme was performed to obtain design data on the effects of surface roughness levels, inlet free-stream turbulence intensity and vane Reynolds number on H Stage 1 nozzle external heat transfer. This facility used a half-scale, linear airfoil model representative of the pitch line section of the Stage 1 nozzle, operating at an overall pressure ratio of 1:86.

Airfoil heat transfer distributions were measured using a thin-walled stainless steel airfoil having imbedded thermocouples. A thin-foil surface heater was used to provide a known heat flux condition, with room temperature mainstream air at approximately 5 atm pressure.

Airfoil surface roughness was varied from smooth to very rough, with either uniform or distributed roughness features. Inlet turbulence intensity could also be varied. In addition to acquiring design data for the H Stage 1 nozzle, the results are used for the verification and improvement of the predictive methods used in designing turbine airfoils.

Nozzle cascade tests

Heat transfer, steam purity and steam compatibility test results have been incorporated into three dimensional aerodynamic, thermal and stress models to confirm that the Stage 1 nozzle will meet operating life requirements.

Further validation has been acquired from cascade tests on actual full size prototype, steam cooled Stage 1 nozzle segments under H System thermal conditions. This involves mounting two nozzle segments were mounted in a test stand behind a DLN combustion system and transition piece as shown in Figure 9. Figure 10 shows the good correlation between aerodynamic test results and pretest analysis.

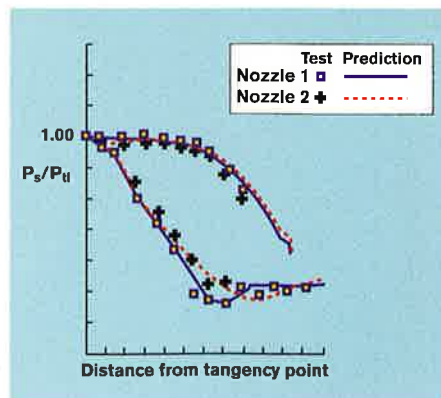
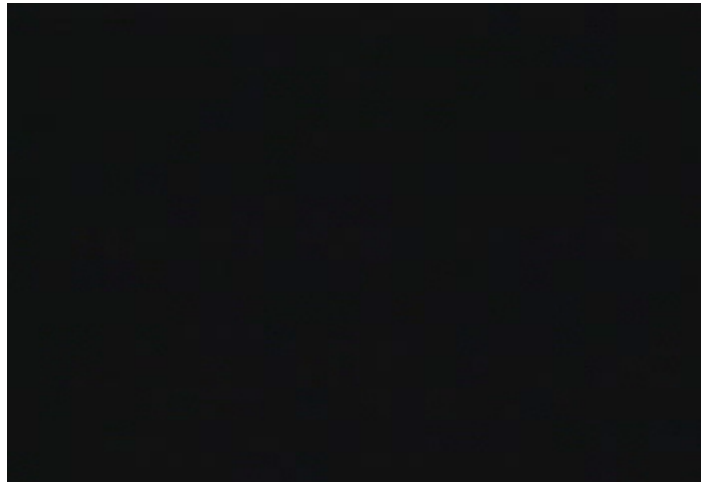


Figure 10. Nozzle cascade aerodynamic test results validate pretest analysis



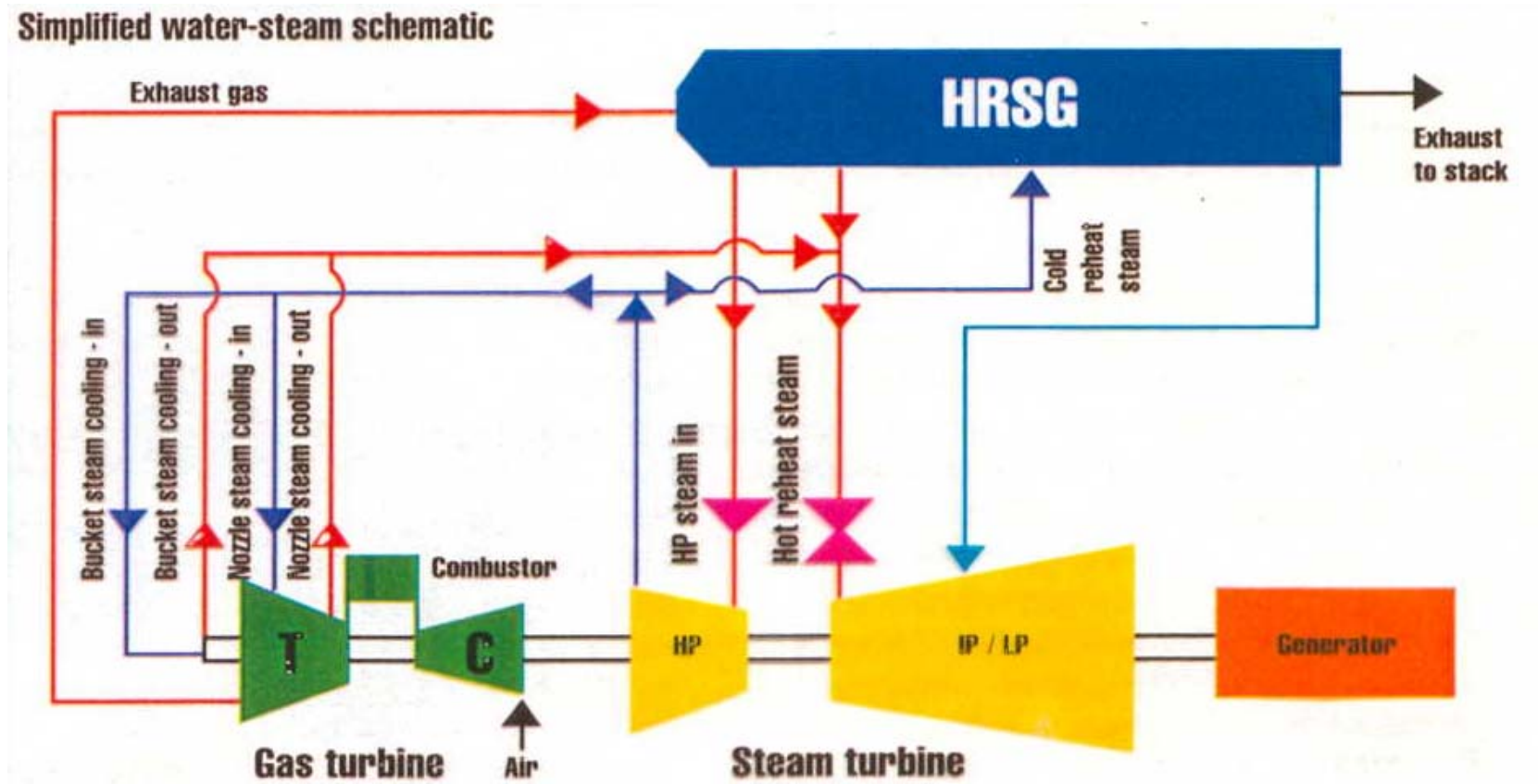


GE 9001H in Baglan Bay, UK



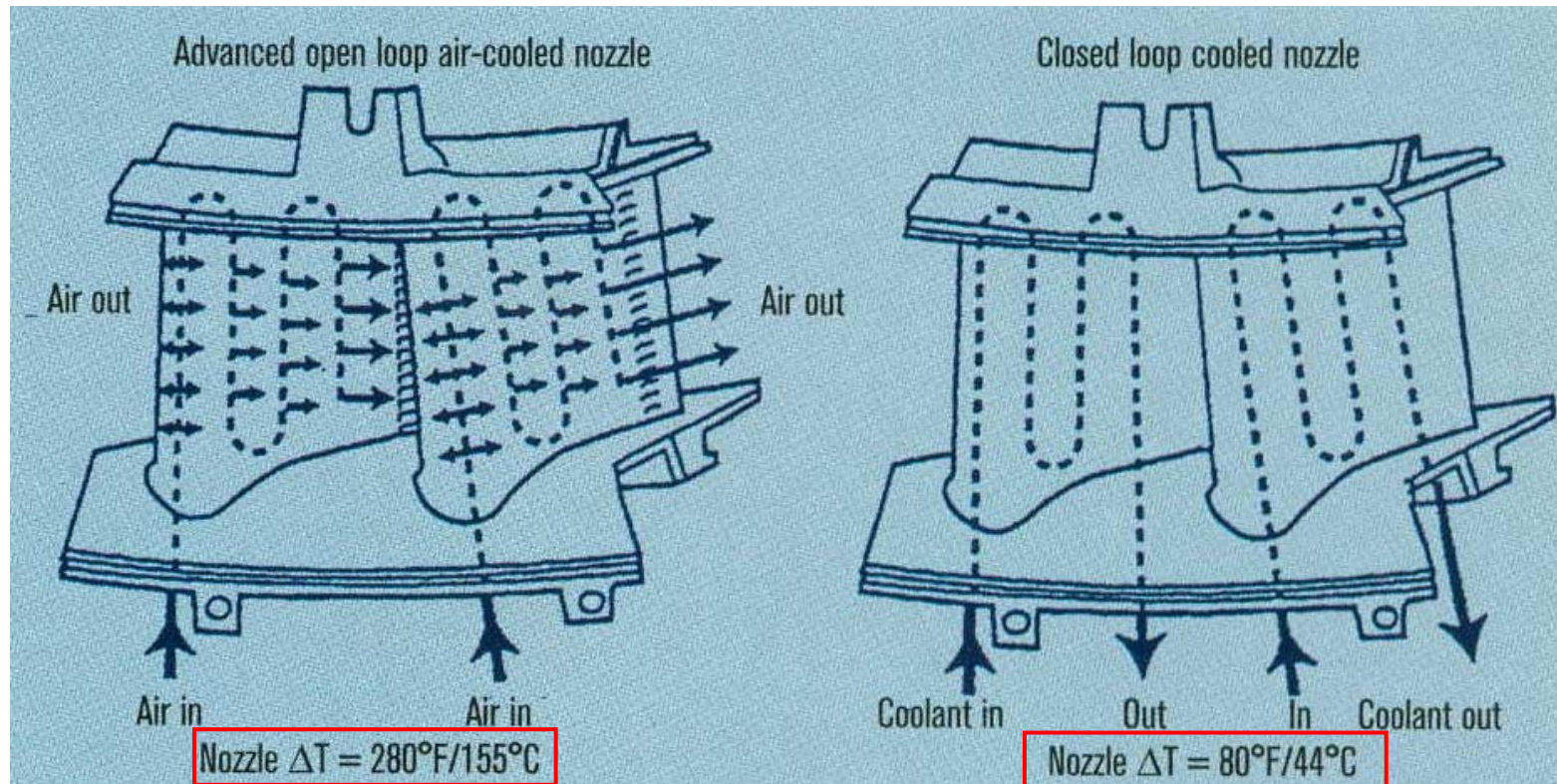


Reheat steam from steam cycle is used for cooling the turbine rotor and first and second stage blades





H technology by GE (and Mitsubishi)



H technology demands convective cooling of blades

Higher heat capacity of steam compared to air gives better cooling effectiveness



H technology by GE (and Mitsubishi)

H System combined cycle plant performance characteristics				
	7FA	7G	7H	9H
Firing temperature (°C)	1300	1430	1430	1430
Air flow (kg/s)	442	558	558	685
Compressor pressure ratio	15	23	23	23
Specific work (MW/kg/s)	0.57	0.63	0.72	0.70
Combined cycle net output (MWe)	253	350	400	480
Net thermal efficiency (%)	55	58	60	60
NOx (ppmvd at 15% O ₂)	9	25	9	9

**First plant at Baglan Energy
Park, UK, in September 2003**

**March 2005: 8000 hrs of
commercial service**



Fig. 15. GE-9H gas turbine is prepared for testing (Source: GE Power Systems)



H technology by GE (and Mitsubishi)

MHI also has a long experience in steam cooling technology, mainly for the combustor liner, but also for turbine blades

As of March 2004, MHI had 150,000 operating hours of steam cooling experience with their G units.

Both their G and H models have steam cooled combustion liners.

The H model also has blades and vanes in the first two rows of its turbine rotor and the blade rings steam cooled.

Table 5. Categories of gas turbines for the Mitsubishi Gas Turbine product line ⁵

GT type	TIT	Cooling Type		Performance (ISO: LHV)				NOx
	deg C	Turbine Combustor		Gas turbine		Combined Cycle		ppm
M501DA	1250	Air	Air	114MW	34.9%	167MW	51.4%	9
M501F	1350	Air	Air	153MW	35.3%	229MW	52.8%	25
M501F3	1400	Air	Air	185MW	37.0%	285MW	57.1%	9
M501G	1500	Air	Steam	254MW	38.7%	371MW	58.0%	25
M501G1	1500	Air	Steam	267MW	39.1%	399MW	58.4%	15
M501H	1500	Steam	Steam	-	-	403MW	60.0%	15

GE introduced the first high-efficiency H-class gas turbines to the power generation industry in 2002. The steam-cooled units have logged 200 000 hours of operation and counting and have proven themselves to be stalwarts within GE's gas turbine lineup. Now, thanks to advances in technology and shared knowledge from its myriad business units, GE is introducing the 7HA and 9HA air-cooled gas turbines.

"We are offering our air-cooled H-class gas turbines in two versions for the 50 Hz market — the 9HA.01 and 9HA.02 — and two versions for the 60 Hz market — the 7HA.01 and 7HA.02," said Vic Abate, President and CEO, Power Generation Products, for GE Power & Water. "The air-cooled H-class gas turbines are designed for cyclic and base-load operation in a simple-cycle and combined-cycle applications."

In a simple-cycle configuration, the 9HA.01 is rated 397 MW and the 9HA.02 is rated 470 MW, each at 3000 r/min, offering greater than 41% efficiency. In a 1x1 combined-cycle configuration, the 9HA.01 is rated 592 MW and the 9HA.02 is rated 701 MW, each at 3000 r/min, offering greater than 61% efficiency.

In a simple-cycle configuration, the 7HA.01 is rated 275 MW and the 7HA.02 is rated 330 MW, each

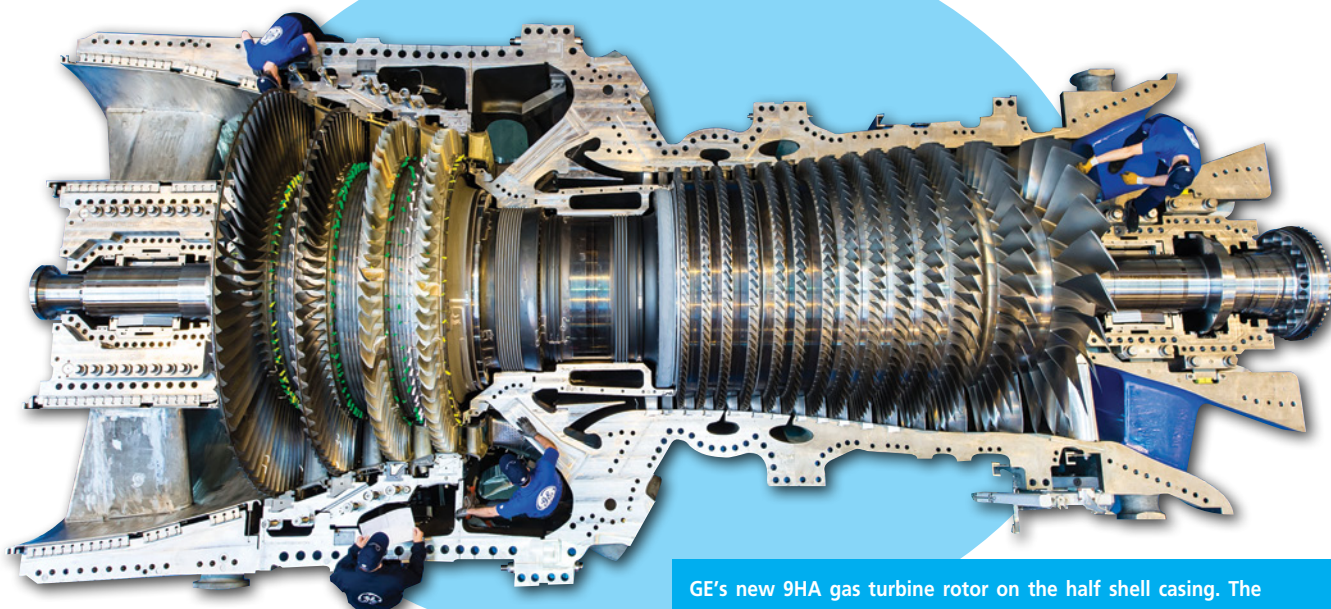
New Air-Cooled H-Class

GE adds air-cooled H-class to its gas turbine lineup

BY BRENT HAIGHT

The first 9HA gas turbine was manufactured in Belfort, France, and will be delivered to GE's Greenville, South Carolina, U.S.A., test facility during the second quarter of 2014, where it will undergo full-scale, full-load testing.





GE's new 9HA gas turbine rotor on the half shell casing. The air-cooled H-class gas turbines are designed for cyclic and base-load operation in simple-cycle and combined-cycle applications.

at 3600 r/min, offering greater than 41% efficiency. In a 1x1 combined-cycle configuration, the 7HA.01 is rated 405 MW and the 7HA.02 is rated 486 MW, each at 3600 r/min, offering greater than 61% efficiency.

"The high-efficiency segment accounts for more than 30% of the power generation market," Abate said. "That is where the air-cooled H-class comes in. The 7HA.01 is 275 MW. The 7HA.02 is 330 MW. Those two machines, in the 60 Hz market, give you a 400 MW combined-cycle power plant, a 500 MW combined-cycle power plant and then you can bulk into 800 and 1000 MW, or 1200 and 1500. Those sizes fit extremely well with the retirement of coal that we see and some of the natural markets for fixed gears.

"Then in the 50 Hz they are a scale version, the 9HA.01 and 9HA.02, at 397 MW and 470 MW. So those then reach 600 MW and 700 MW in combined-cycle, and can bulk into 1200 and 1400 MW, or 1800 and 2100 MW.

"We define H-class as over 2600°F firing temperature. The entire industry has probably 250 000 hours. GE has been in the H-class for more

than a decade. We have a tremendous amount of experience and are confident in where we are going with this next step."

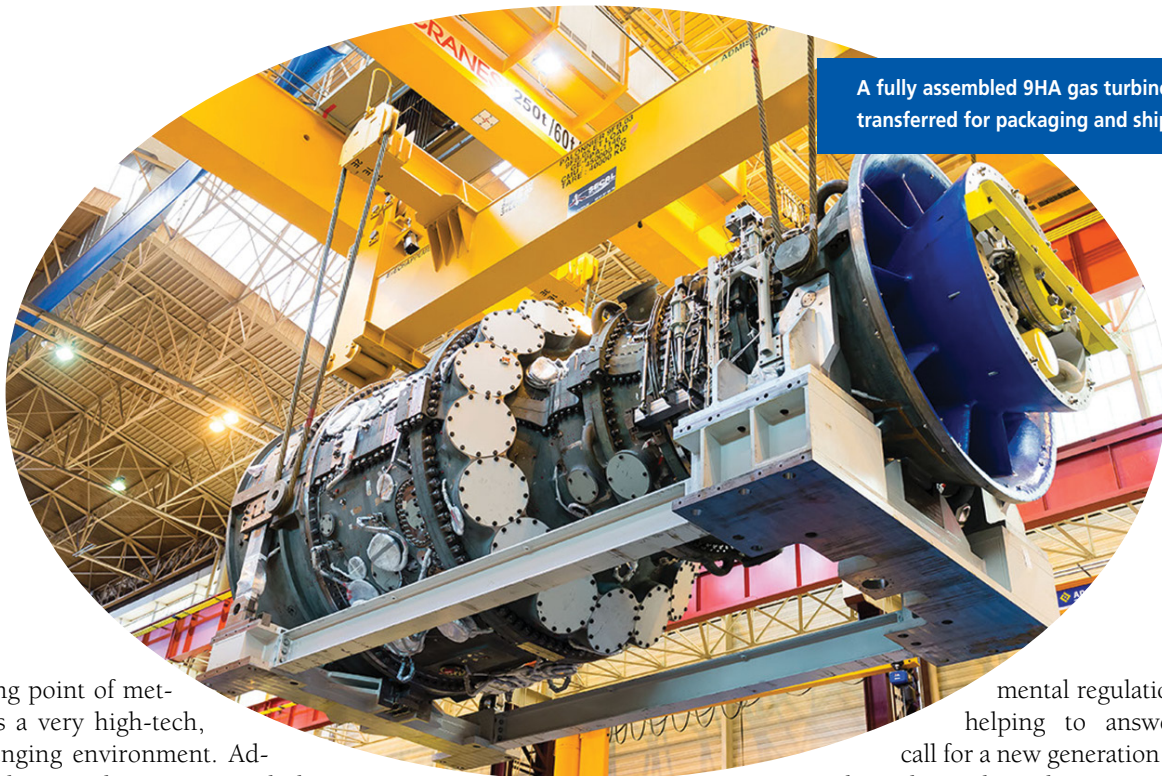
According to Abate, air-cooled H-class gas turbines offer the reliability, flexibility and availability of GE's popular F-class fleet and leverage technology from GE's aviation business as well as its extensive experience within the power generation marketplace.

The air-cooled H-class gas turbine incorporates an aerodynamic 14-stage compressor, leveraged from GE's proven aircraft engine technology, and includes an advanced radial diffuser. Combined with the Dry Low NO_x (DLN) 2.6+AFS (Axial Fuel Staged) combustion system, this allows improved operation of the combustion liner and transition piece cooling, according to GE. The DLN 2.6+AFS combustion system provides advanced fuel staging for enhanced steady state and transient performance. To modulate airflow, a variable inlet guide vane (IGV) and three stages of variable stator vanes (VSVs) manage compressor operability during start-up, control compressor airflow during turndown, and

facilitate variations in ambient temperature and load.

"We've taken the engine compressor design from our aircraft engine division and implemented it into our air-cooled H-class gas turbine," Abate said. "What that does, the compressor has to compress twice the amount of air that you need because half of it goes to produce power and half of it goes to driving the compressor. If you can get the compressor to be more efficient, that is a huge opportunity.

"With regard to combustion, as you fire hotter you trade emissions. Holding emissions at world class levels is paramount for GE as we have always been an emissions leader. We've continued to develop our DLN emissions technology, which enables us to hold emissions with our air-cooled H-class gas turbines. The enhanced DLN 2.6+AFS combustion system supports improved fuel distribution and operability while reducing thermal loading on the cap, liner, and transition piece. When you think about the power turbine section, we release about 1 million horsepower in 3 feet. These engines are operating 400°F-plus above the



A fully assembled 9HA gas turbine being transferred for packaging and shipping.

melting point of metal. It's a very high-tech, challenging environment. Advanced materials coatings, including thermal barrier coatings on the airfoil and single-crystal super alloys on the airfoil wall, promote durability and extend parts life by 1.5% versus comparable technology."

The first 9HA gas turbine was manufactured in Belfort, France, and will be delivered to GE's Greenville, South Carolina, U.S.A., test facility during the second quarter of 2014, where it will undergo full-scale, full-load testing.

The Greenville test facility replicates real-world plant conditions with the required accessories to run a fully loaded gas turbine on natural gas and liquid fuel. To eliminate limitations of the grid, testing is performed without a generator and grid connection. The facility is capable of testing 50 and 60 Hz products. (See "Beyond Real-World Testing," *Diesel & Gas Turbine Worldwide*, September 2012, p. 54.)

"What is interesting about this test facility, is that by being independent of the grid, we have the ability to modify speed, we can get off-design conditions and monitor the responses of air foils, structural components, etc.," Abate said. "We can see all of ranges of the unit's performance. With that we can un-

leash more value through application engineering and also mitigate risk with application.

"Natural gas is becoming the fuel of choice globally and for customers who operate larger blocks of power. The desire for increased operating efficiency and flexibility has never been greater. Technological advancements and increasingly stringent environ-

mental regulations are helping to answer the call for a new generation of machines by pushing the power generation industry to achieve new performance standards.

"The whole strategy surrounding GE is technology leadership. The beauty of a high-tech natural gas plant is that you don't sell them on style, you sell them because they have the best economics, they have the best technical capability and they provide our customers the best return." 🗣️

A 9HA gas turbine traveling through Belfort, France, from the GE manufacturing facility to the Port of Strasbourg. More than 3000 people turned out to see the 9HA make its way through Belfort.





THE NEXT EVOLUTION OF THE HA GAS TURBINE

GE's 7HA.03 gas turbine is the next evolution of the HA. It is the world's largest, most efficient and flexible gas turbine with the lowest cost conversion of gas to electricity for 60 Hz customers.

POWERFUL

Offering power producers the highest capacity 60 Hz gas turbine, 430 MW simple cycle output and the largest combined cycle block of power: 640 MW (1x1) and 1,282 MW (2x1).

EFFICIENT

Unmatched at >64% in combined cycle configuration and offering customers the lowest \$/kwh conversion of gas to electricity.

FLEXIBLE

Full GT load in 10 minutes, full CC plant load in <30 minutes, 75 MW/min ramp rate and double the fuel flexibility of 7HA.02. An ideal complement to intermittent renewable sources.

BENEFITS

- The 14-stage compressor increases airflow enabling greater nominal and hot day output
- The combustion system's advanced premixer and axial fuel staging offer a step change in fuel flexibility
- A 15% park mode enables customers to minimize fuel burn and plant shutdown/startup costs during periods of low demand while providing a faster ramp to full load

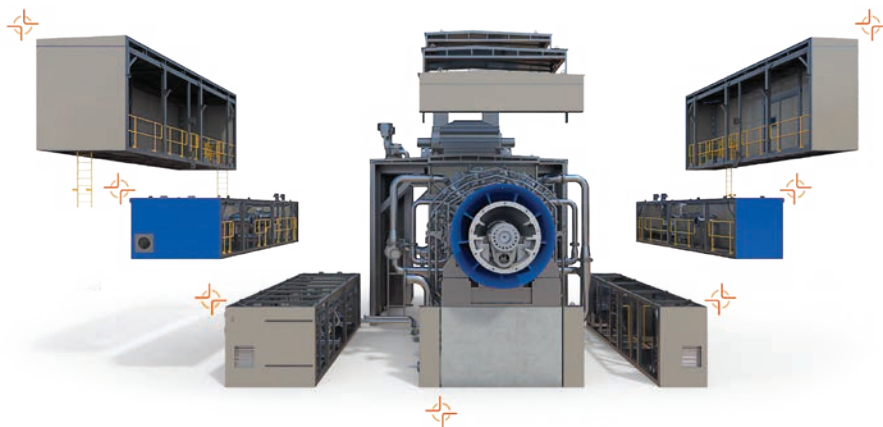


READY TODAY. REINVENTING TOMORROW.

www.ge.com/power/7HA03

7HA.03

THE NEXT EVOLUTION OF THE HA GAS TURBINE



The 7HA.03 gas turbine modular packaging configuration shortens the critical path installation cycle by eight weeks.

98%
REDUCTION
IN FIELD-INSTALLED VALVES

64%
REDUCTION
IN ELECTRICAL
TERMINATION POINTS

63%
REDUCTION
IN FIELD CONNECTIONS

55%
REDUCTION
IN TURBINE FIELD WELDS

GE'S HA TECHNOLOGY WORLD RECORDS:

- 63.08% gross CC efficiency at Chubu Electric's Nishi Nagoya power plant in Japan (7HA.01, 60 Hz)
- 62.22% net CC efficiency at EDF's Bouchain power plant in France (9HA.01, 50 Hz)

		7HA.01	7HA.02	7HA.03
SC Plant Performance	SC Net Output (MW)	290	384	430
	SC Net Heat Rate (Btu/kWh, LHV)	8,120	8,009	7,897
	SC Net Heat Rate (kJ/kWh, LHV)	8,567	8,450	8,332
	SC Net Efficiency (% LHV)	42.0%	42.6%	43.2%
1x CC Plant Performance	CC Net Output (MW)	438	573	640
	CC Net Heat Rate (Btu/kWh, LHV)	5,481	5,381	5,342
	CC Net Heat Rate (kJ/kWh, LHV)	5,783	5,677	5,636
	CC Net Efficiency (% LHV)	62.3%	63.4%	63.9%
	Plant Turndown - Minimum Load (%)	33.0%	33.0%	33.0%
	Ramp Rate (MW/min)	55	60	75
	Startup Time (RR Hot, Minutes)	<30	<30	<30
2x CC Plant Performance	CC Net Output (MW)	880	1,148	1,282
	CC Net Heat Rate (Btu/kWh, LHV)	5,453	5,365	5,331
	CC Net Heat Rate (kJ/kWh, LHV)	5,753	5,660	5,624
	CC Net Efficiency (% LHV)	62.6%	63.6%	64.0%
	Plant Turndown - Minimum Load (%)	15.0%	15.0%	15.0%
	Ramp Rate (MW/min)	110	120	150
	Startup Time (RR Hot, Minutes)	<30	<30	<30

NOTE: All ratings are net plant, based on ISO conditions and natural gas fuel. Actual performance will vary with project-specific conditions and fuel.



READY TODAY. REINVENTING TOMORROW.
www.ge.com/power/7HA03

© 2019 General Electric Company. All rights reserved.



Mercury 50 introduces high efficiency recuperation to stationary gas turbines

A 4.2 MWe gas turbine generator set with a thermal efficiency of 40.5 per cent, over 30 per cent higher than current gas turbines in this size class, has been introduced to the stationary generating set market by Solar Turbines in San Diego, California. Using an advanced but well proven recuperator design packaged for optimal performance and simple servicing, the Mercury 50 was developed under the US DOE ATS programme. The first unit is to be installed by Rochelle Municipal Utilities near Chicago for use in economic dispatch mode.

Staff report

The Mercury 50 gas turbine is the result of a \$164.8 million, five year co-operative effort with the US Department of Energy (DOE) as one of four main streams in the ATS (advanced turbine systems) programme. The key component – the primary surface recuperator – has been under development by Solar Turbines and Caterpillar Inc., its parent company, since the early 1970s.

The resulting product has now been launched into the market at two recent venues – the Power Gen International '97 conference in Dallas, Texas, and the US DOE ATS Annual Program Review meeting in Morgantown, West Virginia.

Recuperated cycles have been used with gas turbines in the past with dubious success – mainly in the petrochemical industry. In general, bulky shell and tube or plate-fin heat exchangers were added to standard machine designs using elaborate and cumbersome piping with little effort to optimise the thermal cycle.

Limited performance improvement was gained at the cost of poor thermal transient response, thermal cracking and other mechanical performance problems. The Mercury 50 is the first attempt to design a gas turbine arrangement specifically to work with an advanced recuperator, starting from a clean sheet. The turbine, and particularly the innovative compressor, is a remarkable demonstration of state of the art turbine technology development.

The result is an electrical efficiency of 40.2 per cent, single figure NO_x emissions, and an extraordinarily compact but readily serviceable power plant. Its power output rating is 4.2 MWe continuous duty at ISO conditions.

Configuration

The single shaft gas turbine, running at 14 179 r/min, drives either 60 Hz or 50 Hz generators via an epicyclic gearbox driven from the compressor end of the turbine. The layout of the turbine/recuperator arrangement has been effectively adapted for optimum simplification of the gas flow paths between the compressor, recuperator, combustor and turbine. The flow path has been organised to naturally follow the flow of the recuperator.

Compressor discharge is at the end of the machine in the same plane as the inlet header to the recuperator. The inlet to the combustor is also situated at the end of the machine in the same plane as the recuperator discharge header.

The turbine exhausts upwards through the recuperator at the centre of the engine. This has necessitated the reversal of the normal layout of the compressor and turbine to provide a greatly simplified and streamlined flow path.

This configuration requires the design of a centre frame structure to interconnect the turbine and compressor housings in place of the hot strut design used in most gas turbine assemblies. The load carrying members of the centre frame are located in a cool environment out of the turbine hot gas flow

path, thus minimizing axial extension of the turbine case due to thermal growth and allowing tight blade tip clearances to be maintained.

A high degree of modularity allows each of the major sub-system including the combustor system, the turbine, recuperator, gearbox or generator to be changed independently in the field in a single shift without the need to replace the entire engine.

Great efforts have been made to reduce ancillary equipment power consumption, which typically takes as much as eight per cent of the power output. By using a double-helical epicyclic gearbox for the generator drive and variable frequency AC motors for lubricating oil pumps and fans instead of mechanical drive from the turbine, an additional one per cent increase in efficiency is obtained.

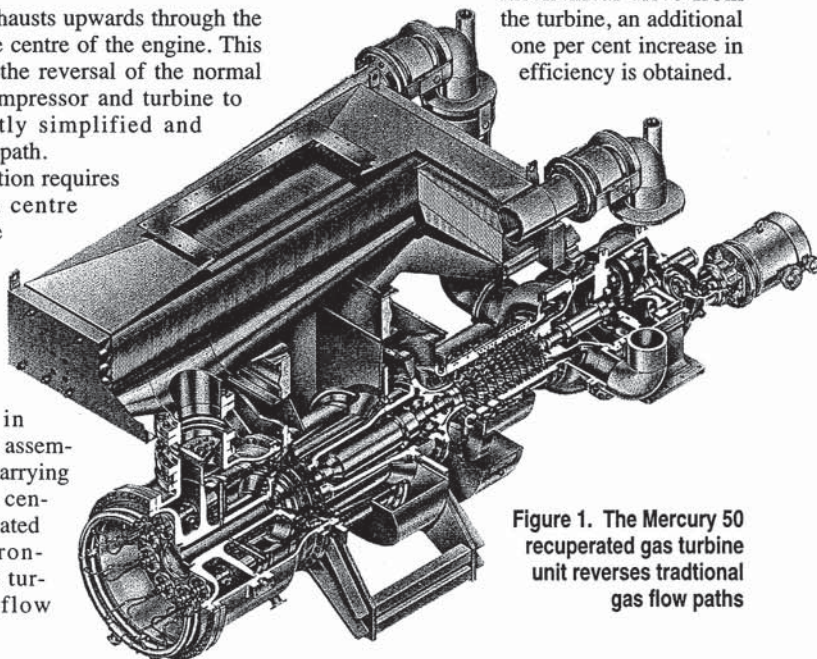


Figure 1. The Mercury 50 recuperated gas turbine unit reverses traditional gas flow paths

MPS REVIEW

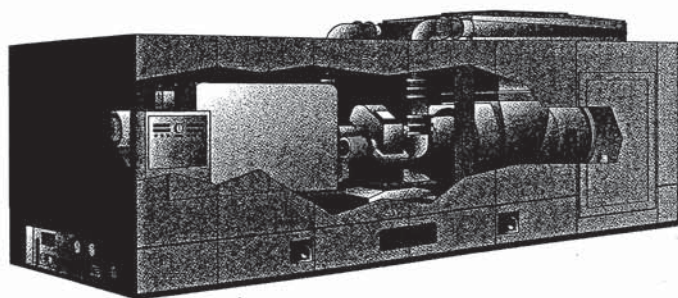
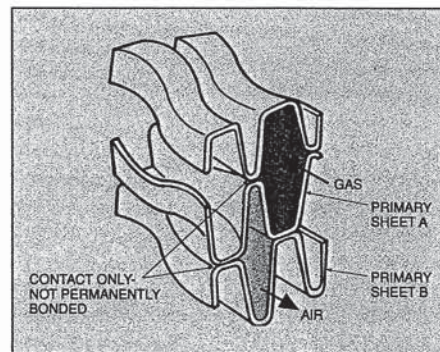


Figure 2. The packaged Mercury 50 makes a compact 4.2 MW generating set

Figure 3. Primary surface recuperator air cell structure



With an exhaust temperature of 368°C and a mass flow of 61 200 kg/h, there is substantial scope for combined heat and power operation, and supplementary firing would increase performance in this kind of service.

ACE compressor

Working in concert with Dr John Adamczyk of the NASA Lewis research centre in Cleveland, Ohio, Solar have developed the ACE (advanced component efficiency) compressor using the latest three dimensional flow blading design codes and modelling techniques. The techniques used in the Mercury 50 design were first used for the redesign of the Mars T15000 compressor in 1993.

The ACE design, it is claimed, benefits from 3-dimensional wide chord airfoils that are lightly loaded, resulting in a 40 per cent reduction in the number of airfoils for a given pressure rise.

The Mercury 50 compressor has a pressure ratio of 9.1:1 from a ten-stage compressor which makes for increased flexibility of fuel supply – the minimum pressure requirement is only 12 bar.

A variable inlet guide vane in the first stage is followed by stages of variable guide vanes that are ganged together and controlled as a unit for optimum compressor control across the operating load range.

The compressor design was validated at the Compressor Research Facility of the Wright Patterson Air Force Base in Dayton, Ohio. During the testing, which was completed in July 1997, the performance was fully mapped and compared to Mercury 50 design goals as well as the current compressors. The results were reported to validate the design goals and showed an efficiency gain of over two points over Solar's current compressors.

Recuperator design

Solar PSRs have now accumulated well in excess of 1.5 million operating hours without encountering much of the

incipient problems reported by other recuperator technologies. The design is inherently resistant to low cycle fatigue failure because the clamped air cell structure allows the assembly to flex freely to relieve stresses rather than concentrating stresses at the weld locations.

The air cells are constructed from 0.1 mm thick 347 stainless steel formed into an undulating corrugated pattern which maximizes the primary surface area in contact with the hot exhaust gases on one side and the compressor discharge air on the other. Pairs of these sheets are welded together

around the circumference to form air cells as shown in Figure 3.

There are no internal welds or joints within the air cell. Layers of these cells are clamped together with clamping bars and the assembly is welded to the intake and discharge headers.

As well as being inherently resistant to low cycle fatigue failure, high cycle fatigue is also minimized due to the damping characteristics of the clamped design. The stacking of the cells presents multiple friction interfaces for energy absorption. This latter characteristic also provides sufficient sound attenuation to eliminate the need for an additional silencing device and avoids the resulting pressure drop.

The modules, which are claimed to give over 90 per cent effectiveness with only moderate pressure drop, are manufactured in Solar's newly automated production facility located in Channel view, Texas.

Two-stage design

The two-stage design of the Mercury 50 turbine was selected because of its inherent cost advantages. The extra cost of the additional cooling required for a third stage would have negated the resulting performance advantage. Another consideration is that it becomes increasingly important to minimize the use of cooling air since the trend towards lean, premixed combustion to minimize NO_x emission has made the availability of cooling air a critical commodity.

The turbine rotor inlet temperature (TRIT) is fairly high at 1163°C, and the fully cooled first stage turbine is highly loaded. The second stage incorporates cooled vanes and uncooled, shrouded blades.

A novel leading edge cooling scheme known as vortex cooling has been used in the first stage blades. This involves the use of swirled cooling flow to the leading edge cooling circuit as shown in Figure 5. This technique is seen as having

Table 1. General specifications of the Mercury 50 gas turbine

Type	Industrial, single-shaft PST recuperated
Output rating - continuous (MWe)	4.2
Output rating - Intermediate duty (MWe)	4.6
Output rating - peaking and standby (MWe)	4.8
Thermal efficiency (%)	40.5
Shaft speed (r/min)	14 170
Compressor:	
Type	Axial flow, Variable inlet guide vanes
Inlet air flow (kg/s)	16.1
No. of stages	10
Compression ratio	9.1:1
Recuperator:	
Type	Primary surface type (PST)
Material	347 stainless steel
Combustion chamber:	
Type	Annular
Pollution control	Dry, ultra-lean premix
Geometry	Variable
Ignitor system	Torch
No. of fuel injectors	8
Turbine:	
Type	Axial flow, reaction
No. of stages	2
Inlet temperature - TIT (°C)	1093
Bearings - radial:	
Number	2
Type	Viscous damped rolling element
Bearings - thrust:	
Number	1
Type	Viscous damped rolling element
Reduction gearbox:	
Type	Double helical epicyclic
Output speed for 50 Hz (r/min)	1500
Output speed for 60 Hz (r/min)	1800
Generator:	
Type	Salient pole, 3 phase 6 wire Wye connected Synchronous Brushless PMG(3) voltage regulator NEMA Class F with Class F rise (standard) NEMA Class F with Class B rise (optional)
Exciter type	
Regulation	
Insulation	

Table 2. Typical heat recovery performance

Electrical output - continuous (kWe)	4072
Exhaust temperature (°C)	351
Turbine fuel input (GJ/h)	37.5
Air mass flow (kg/h)	60 600
Process steam - unfired (t/h)	4.6
Net system efficiency - unfired (%)	69.0
Process steam - supplemental firing to 926°C	22.5
Supplementary fired - Additional fuel (GJ/h)	40.8
Supplementary fired - Net system efficiency (%)	88.8
Process steam - supplemental firing to 1593°C	44.1
Supplementary fired - Additional fuel (GJ/h)	91.3
Supplementary fired - Net system efficiency (%)	94.7

considerable improvement potential without incurring the performance penalties associated with showerhead cooling which would otherwise be required.

Of particular interest in the Mercury 50 are the new alloys and materials that have been introduced into the turbine. The film-cooled first stage nozzles are made from MAR-M-247, while the uncooled second stage vanes are constructed from equiaxed forms of the same material.

For the unshrouded first stage blades, a third generation single crystal alloy, Cannon - Muskegon's CMSX-10, has been selected. The blades will be mounted on a Waspaloy disk using fir tree root fixing modified to take improved disk-post cooling.

The second stage blades are Solar's first shrouded design. These are also made from equiaxed MAR-M-247. Dispensing with cooling in the second stage blades resulted in requirement for the disk beyond the properties of currently used materials. A powdered metal forging of Udimet 720 was selected. The fine grain structure of the rim makes it suitable for the higher rim operating temperatures while still maintaining sufficient low-cycle fatigue strength at the hub.

Combustion alternatives

The combustion system of the Mercury 50 is designed to accommodate ultra-lean premix (ULP) or catalytic-type combustors. ULP annular burner design developed from Solar's existing SoLoNox combustion system, with the new feature of a diverter

valve, will direct air flow either through the combustor, or through a bypass circuit to a point downstream of the combustor. This will provide the necessary function of regulating flow through the combustor at part load.

The metallic combustor liner will be protected by a plasma sprayed thermal barrier coating in the first machines.

The company is now working on the development of ceramic combustor linings which should be adopted during the product's market life.

A catalytic combustion system using a catalyst bed developed by Catalytica is being worked on as an alternative when this approach attains operational status. Since in the recuperated turbine cycle the combustor

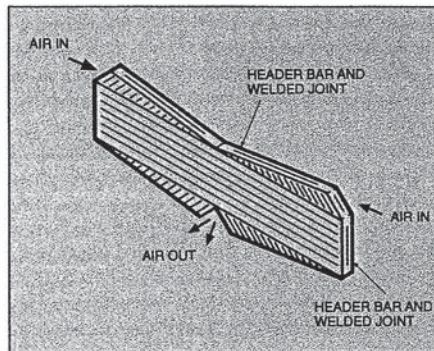


Figure 4. Primary surface recuperator air cell assembly

temperature is generally higher than the catalyst bed auto-ignition temperature, the need for a preburner to bring the catalyst up to operating temperature is precluded.

Single figure NO_x levels are expected from both combustion systems, however, the initial Mercury 50 field units will have an introductory emission level of 25 ppmv on natural gas.

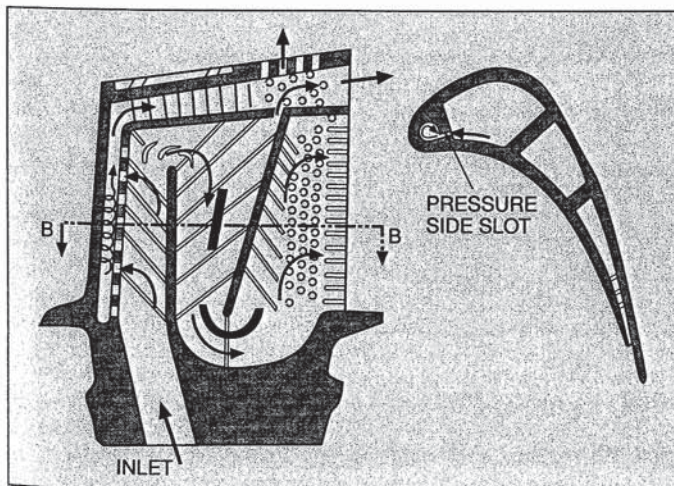


Figure 5. Turbine first row blade vortex cooling

Rochelle field test

The site for the first field test of the Mercury 50, now approved by the US DOE, is a municipal utility group with a service area of some 100 square miles in North Central Illinois, 120 km from Chicago, entirely surrounded by Commonwealth Edison country. The area has one radial transmission connection to the Com-Ed grid.

The host operator will be Rochelle Municipal Utilities. Rochelle currently purchases 95 to 98 per cent of its power and operates a number of reciprocating engines as peak shavers. The utility will utilise the Mercury 50 gas turbine generator set in economic dispatch mode to reduce its cost of power and to improve system reliability.

The new Mercury 50 gas turbine unit will be located proximate to the Rochelle Food Processing and Distribution Centre, which accommodates Hormel, Kraft Foods and Erie Foods International in the food processing business, Del Monte Corp. in the canned food distribution business, and also Americold and Total Logistics Control in the frozen food distribution business.

Other industries in the location include office supplies dealer Avery Dennison, electrical parts supplier Eaton Corp. in addition to can manufacturing company Silgon Container Corp.

General manager Ray Schwartz describes the utility's power supply policy as:

- purchase 95 to 98 per cent of power
- several rate schedules of firm power purchased
- load following with general purpose (GP) power
- generation assets used for economic dispatch
- generate when GP power cost exceeds in-house asset costs
- total output in 1996 = 179 284 000 kWh.

The new Mercury 50 is expected to see between 4000 to 6000 hours per year under normal operating conditions. Mercury 50 design features which minimize efficiency degradation when running at part load or when ambient conditions change are likely to play an important role in the economic dispatch of the prototype unit. □

Heat Rate

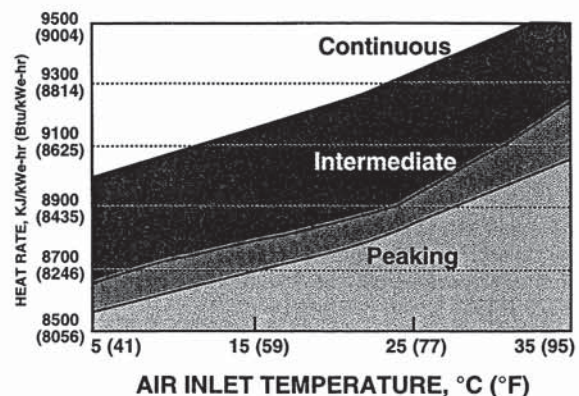


Figure 6. Heat rate dependence on ambient temperature

Technical performance

Gas turbine range

The ideal solution for all applications

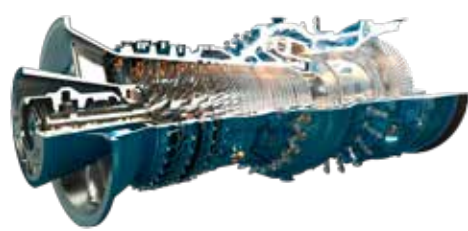
Alstom's gas turbines offer **outstanding performance, operational and fuel flexibility as well as availability and reliability**. Alstom's gas turbines are the ideal solution for all applications (simple-cycle, combined-cycle, co-generation etc.) and operating profiles.

- Lower cost of electricity from proven technology
- Today's products already feature tomorrows requirements
- Evolutionary product development for highly reliable products

GT26



GT24



KEY BENEFITS

Advanced-class gas turbine technology with superior part-load efficiency and operational flexibility. Superior fuel flexibility for operating over the widest range of natural gas compositions.

GT26

Advanced-class gas turbine

Fuel	Natural Gas
Frequency	50 Hz
Turbine speed	3,000 rpm
Gross electrical output	345.0 MW
Gross electrical efficiency	41.0%
Gross heat rate	8,780 kJ/kWh 8,322 Btu/kWh
Exhaust gas flow	715 kg/s 1,576 lb/s
Exhaust gas temperature	616 °C 1,141 °F
Weight	406 t 895,000 lb
Dimensions (L × W × H)	12.0 × 4.9 × 5.5 m 39 × 16 × 18 ft

GT24

Advanced-class gas turbine

Fuel	Natural Gas
Frequency	60 Hz
Turbine speed	3,600 rpm
Gross electrical output	235.0 MW
Gross electrical efficiency	40.0%
Gross heat rate	9,000 kJ/kWh 8,531 Btu/kWh
Exhaust gas flow	505 kg/s 1,113 lb/s
Exhaust gas temperature	608 °C 1,126 °F
Weight	230 t 507,000 lb
Dimensions (L × W × H)	10.7 × 4.0 × 4.6 m 35 × 13 × 15 ft

General notes: Gas turbine gross electrical output and heat rate at the generator terminals, including gear box, where applicable and generator losses but excluding duct and auxiliary losses. Performance calculated with 100% methane, ISO conditions. GT24/GT26 performance includes contribution of Once-Through Cooler (OTC) to water/steam cycle. Dual fuel burner option available

GT13E2

Conventional-class gas turbine

CONFIGURATION	2005	MXL2	2012
Fuel	Natural Gas	Natural Gas	Natural Gas
Frequency	50 Hz	50 Hz	50 Hz
Turbine speed	3,000 rpm	3,000 rpm	3,000 rpm
Gear	No	No	No
Gross electrical output	185.0 MW	188.0 MW	202.7 MW
Gross electrical efficiency	37.8%	38.6%	38.0%
Gross heat rate	9,524 kJ/kWh 9,027 Btu/kWh	9,326 kJ/kWh 8,840 Btu/kWh	9,474 kJ/kWh 8,980 Btu/kWh
Exhaust gas flow	565 kg/s 1,245 lb/s	548 kg/s 1,208 lb/s	624 kg/s 1,376 lb/s
Exhaust gas temperature	505 °C 941 °F	512 °C 954 °F	501 °C 934 °F
Weight	343 t 756,185 lb	343 t 756,185 lb	350 t 772,000 lb
Dimensions (L×W×H)	11.2×5.4×5.2 m 36.7×17.7×17.0 ft	11.2×5.4×5.2 m 36.7×17.7×17.0 ft	11.0×5.4×5.5 m 36×18×18 ft

GT11N2

Conventional-class gas turbine

Fuel	Natural Gas	Natural Gas
Frequency	50 Hz	60 Hz
Turbine speed	3,610 rpm	3,600 rpm
Gear	Yes	No
Gross electrical output	113.6 MW	115.4 MW
Gross electrical efficiency	33.3%	33.9%
Gross heat rate	10,811 kJ/kWh 10,247 Btu/kWh	10,619 kJ/kWh 10,066 Btu/kWh
Exhaust gas flow	400 kg/s 882 lb/s	400 kg/s 882 lb/s
Exhaust gas temperature	526 °C 979 °F	526 °C 979 °F
Weight	190 t 419,000 lb	190 t 419,000 lb
Dimensions (L×W×H)*	13.1×5.5×10.1 m 43×18×33 ft	9.4×5.5×10.1 m 31×18×33 ft

* Length includes the gear box

General note: Dual burner option available, as well as combustor for low calorific gases (LBtu) such as blast furnace gases without need for enrichment.

GT13E2



KEY BENEFITS

Conventional-class gas turbine technology with superior performance and Alstom's unique flexible operation concept. Superior fuel flexibility for operating over the widest range of natural gas compositions.

GT11N2



KEY BENEFITS

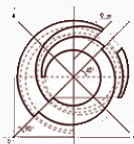
Proven technology designed for operation under harshest conditions. Ideal for power production in steel plants, where Blast Furnace Gas (BFG) can be burnt unblended, without need for enrichment.

For more information
please contact Alstom Power:

Alstom Power
Brown Boveri Strasse 7
5401 Baden
Switzerland

Phone: +41 58 505 7733

Visit us online: www.alstom.com

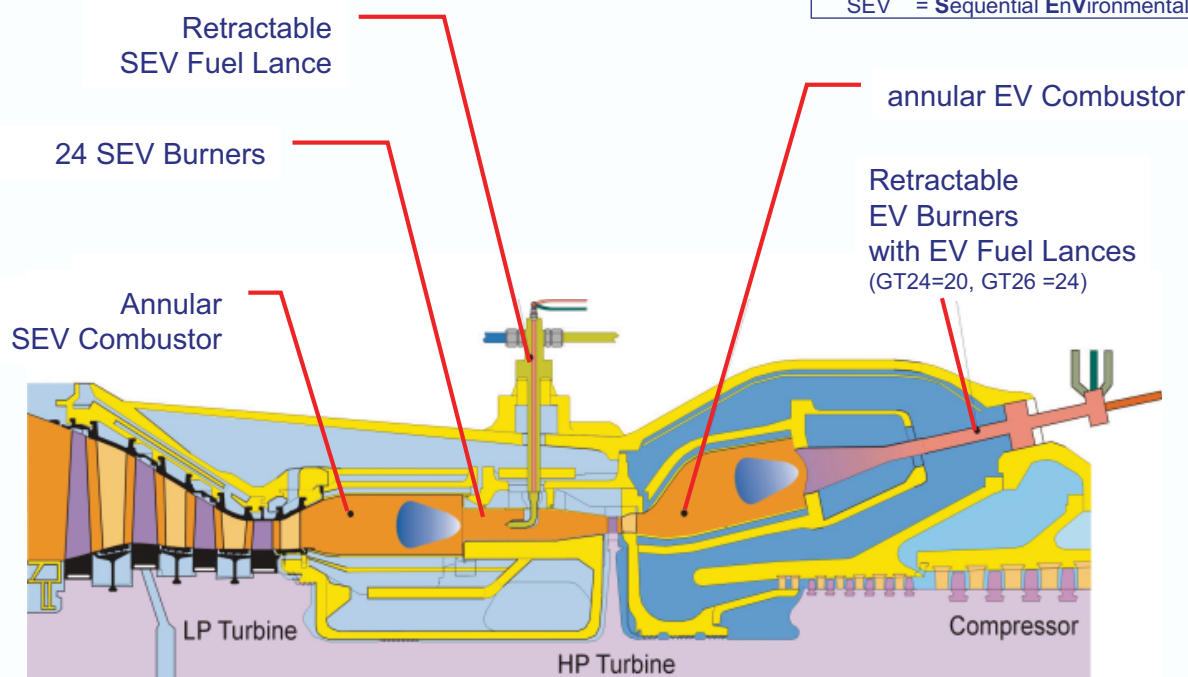


GT24/GT26 Technology

Single Shaft Sequential Combustion

ALSTOM

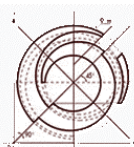
EV = EnVironmental
SEV = Sequential EnVironmental



Jornada Tecnológica
26 Oct 06/jw
R 4.38(26)

© ALSTOM 2006. All rights reserved. Information contained in this document is provided without liability for information purposes only and is subject to change without notice. No representation or warranty is given or to be implied as to the completeness of information or fitness for any particular purpose. Reproduction, use or disclosure to third parties, without express written authority, is strictly prohibited.

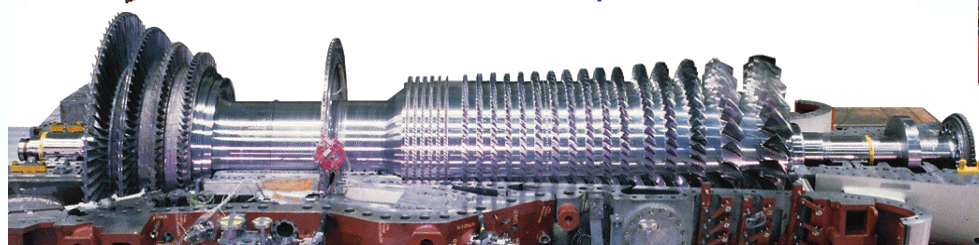
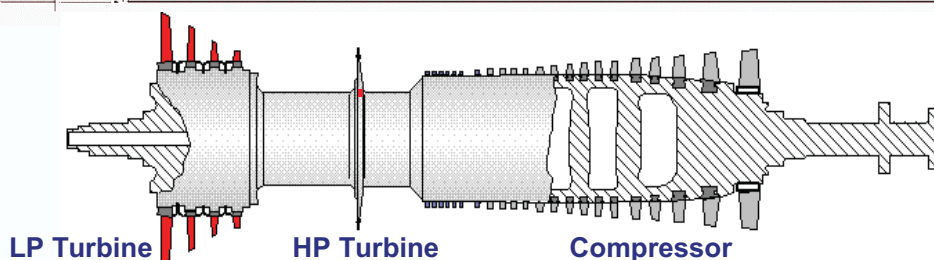
7



GT24/GT26 Technology

Welded Rotor

ALSTOM



- One piece design with forged discs welded together
- Applied since 1929 to all GT and ST rotors
- Maintenance free - no restacking required – no major overhaul

**No major overhauls:
Increased availability and reduced maintenance**

Jornada Tecnológica
26 Oct 06/jw
R 4.38(26)

© ALSTOM 2006. All rights reserved. Information contained in this document is provided without liability for information purposes only and is subject to change without notice. No representation or warranty is given or to be implied as to the completeness of information or fitness for any particular purpose. Reproduction, use or disclosure to third parties, without express written authority, is strictly prohibited.

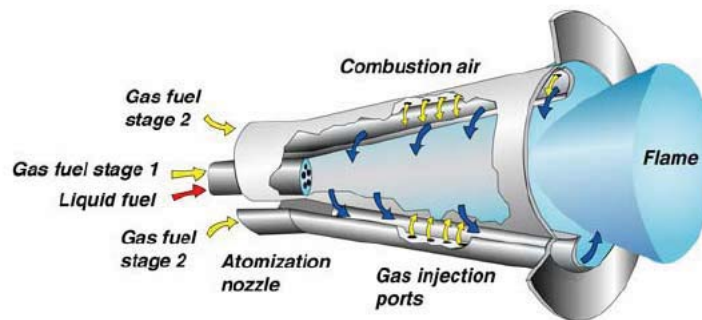
6



Siemens DLE/ Alstom EV Burner



- Burner consists of a cone split in two halves, slightly offset to form two slots for the combustion air
- Main gas supply also enters through these slots via tubes
- Primary fuel is injected at the tip of the cone.
- Richer fuel mixture stabilizing the flame over a range of load conditions
- Burner lowers NO_x by reducing the flame temperature (< 25 ppmv)
- When burning liquid fuel water injection is required to reduce NO_x.



Source: Siemens Industrial Turbomachinery AB, 2006

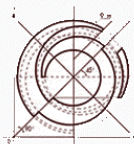


Siemens DLE/ Alstom EV Burner



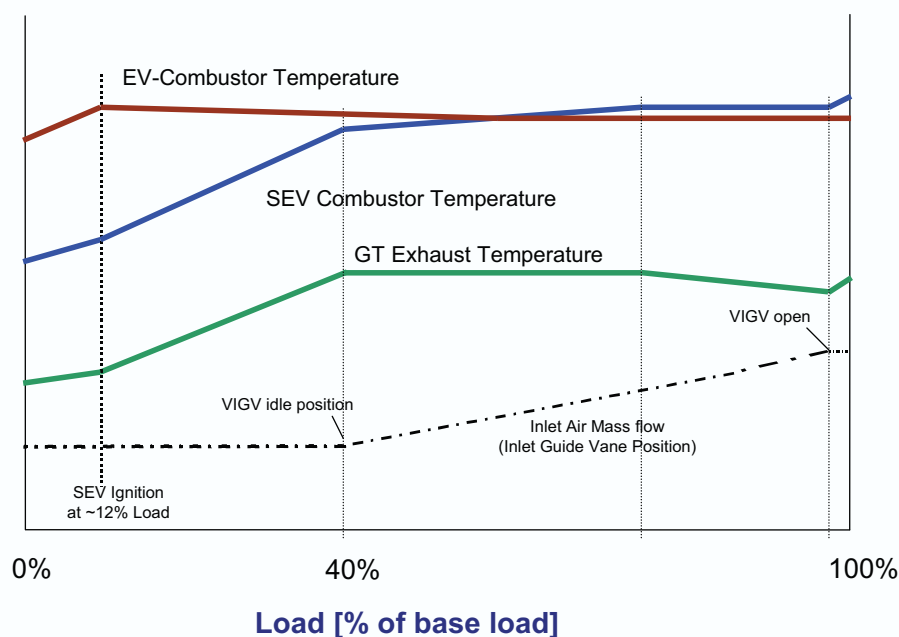
Fig. 32. The SGT-600 dry, low-emission (DLE) combustion system
Source: Siemens Westinghouse

Source: Soares, Gas Turbine Handbook, 2005

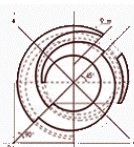


GT24/GT26 Operation Operation Concept

ALSTOM

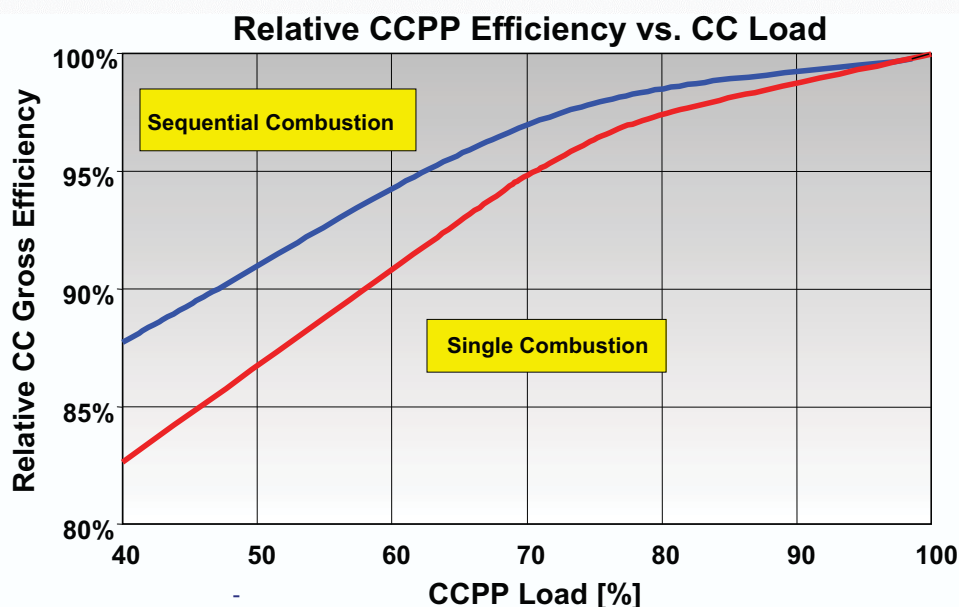


- EV temperature maintained from about 30%-100% load **for low emissions**
- High exhaust temperature maintained from 40%-100% load **for high CC part load efficiency**

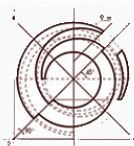


GT24/GT26 Gas Turbine Part Load Efficiency

ALSTOM



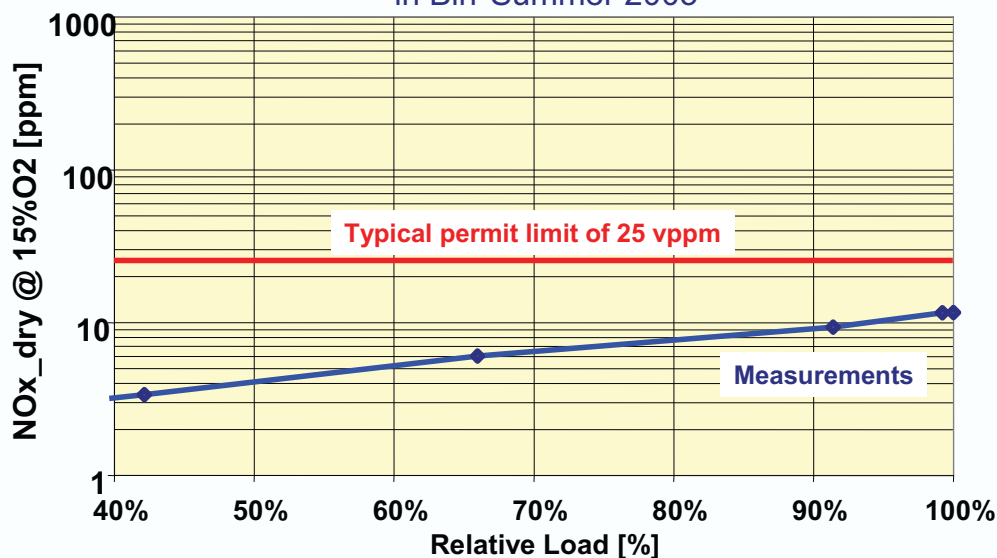
- GT exhaust temperature maintained from 40% to 100% GT load
- High exhaust energy - optimal for high steam parameters under full and part load conditions



GT26 Technology NO_x Emissions

ALSTOM

Measurements at the GT26 Test Power Plant
in Birr Summer 2005



**Lowest NO_x Emissions from 40% - 100% Load
with the GT26 Sequential Combustion System**

Jornada Tecnológica
26 Oct 06/jw
R 4.38(26)

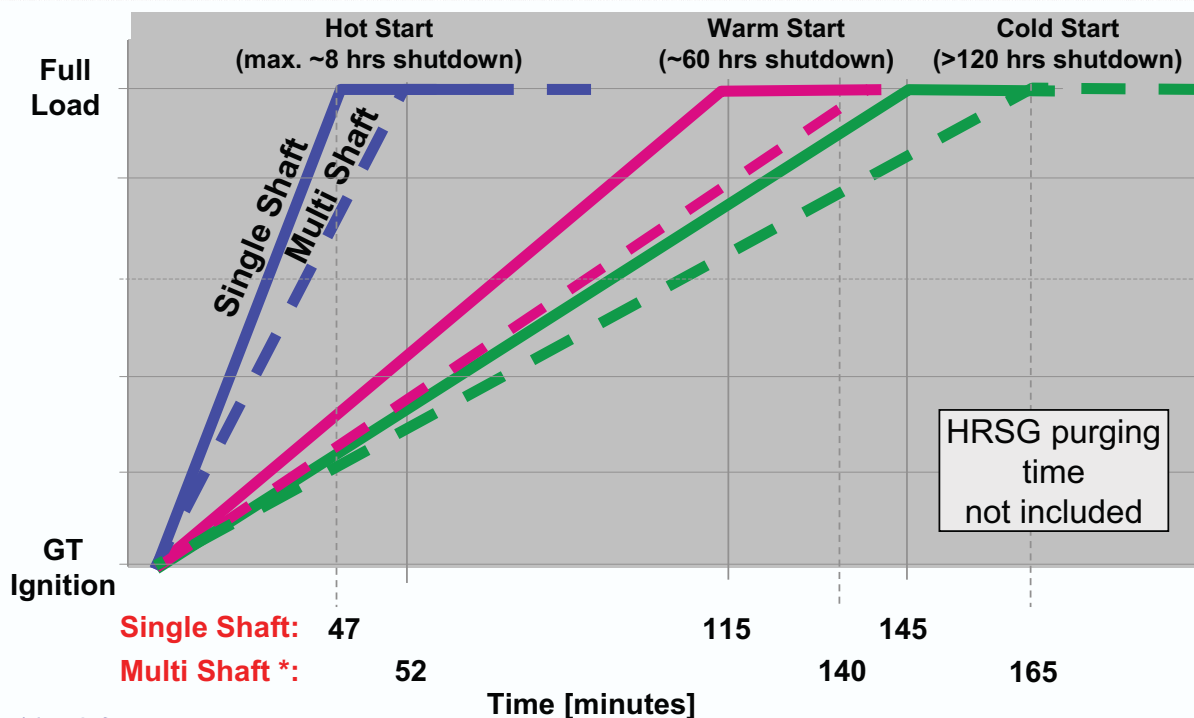
© ALSTOM 2006. All rights reserved. Information contained in this document is provided without liability for information purposes only and is subject to change without notice. No representation or warranty is given or to be implied as to the completeness of information or fitness for any particular purpose. Reproduction, use or disclosure to third parties, without express written authority, is strictly prohibited.

12



GT24/GT26 Gas Turbine Combined Cycle Start-up Curves

ALSTOM



* 1 static frequency converter
-> sequential start-up of GT's

Jornada Tecnológica
26 Oct 06/jw
R 4.38(26)

© ALSTOM 2006. All rights reserved. Information contained in this document is provided without liability for information purposes only and is subject to change without notice. No representation or warranty is given or to be implied as to the completeness of information or fitness for any particular purpose. Reproduction, use or disclosure to third parties, without express written authority, is strictly prohibited.

13

Ansaldo to acquire GT26/GT36 as condition of GE/Alstom deal

11 September 2015

Ansaldo's position in the heavy duty gas turbine market will be greatly strengthened thanks to conditions being imposed by the European Commission on the proposed acquisition of Alstom's energy businesses by GE.

Following an in-depth review, the Commission on 8 September announced it had approved the acquisition subject to divestment of key parts of Alstom's heavy duty gas turbines business to Ansaldo Energia of Italy, which currently principally offers machines derived from former Siemens models in this sector of the market (V64.3A, V94.2, V94.2K, V94.3A).

The Commission had worries that the GE/Alstom transaction as initially proposed would have eliminated one of the main global competitors of GE in the heavy duty gas turbines market, where GE is the world's largest manufacturer and Alstom is the number three or four player globally. This would have led to less innovation and higher prices in a market for a technology vital to meeting climate change goals. The commitments offered by GE address these concerns, the Commission said.

Concerning the other businesses that are part of the transaction, namely the thermal power generation businesses (other than gas), grid and renewables, the Commission did not identify any competition concerns essentially because the activities of the two companies are complementary and do not overlap.

Commissioner Margrethe Vestager, in charge of competition policy, said: "I am glad that we can approve this transaction, which shows that Europe is open for business and that Europe-based technology can thrive and attract foreign investment. We have had a very close and successful co-operation with the Antitrust Division of the US Department of Justice both as regards the investigation and the analysis of suitable remedies. Divestment of Alstom's key technology to produce heavy duty gas turbines to Ansaldo will ensure that European business and consumers continue to benefit from this innovation and know how.

Furthermore, advanced heavy duty gas turbine technology is crucial to face the challenges of climate change and modernising our energy supply. It is the most efficient, cleanest and flexible fossil fuel power generation technology and an important complement to more unpredictable generation from renewables - when the wind stops blowing it is mostly flexible gas-fired plants that can step in."

The Commission's concerns

The Commission's in-depth investigation focused on the markets for the sale and servicing of heavy duty gas turbines operating at 50 Hz, where Alstom competes directly with GE in Europe.

The market for heavy duty gas turbines is concentrated, observes the Commission, with only four globally active full technology competitors: market leader GE, number two Siemens, Alstom and Mitsubishi Hitachi Power Systems (MHPS). This is due to the large upfront investments in R&D, testing and manufacturing required, setting very high technological and financial barriers to enter the market. The fifth player, Ansaldo, has more limited R&D capabilities, a narrower product range and a more limited geographic reach, the Commission noted.

The GE/Alstom merged entity, as originally notified to the Commission, would have accounted for more than 50% of the European market for heavy duty gas turbines and also very high market shares in the

worldwide market for 50 Hz heavy duty gas turbines. In fact, in Europe, the transaction as initially notified would have brought together two of the three main competitors, the Commission observed.

Alstom, with its GT26 and new GT36 turbine under development, which could be described as H class, is active in both large and very large heavy duty gas turbines segments, which are the technologically most advanced, said the Commission.

This makes it a significant and close competitor of GE and Siemens both from a technological and commercial point of view, especially in Europe, where operational flexibility provided by such turbines is very important to customers. MHPS on the other hand is a more distant competitor because of its different technological focus and because it is less active in Europe. An economic analysis of bids for heavy duty gas turbine tenders over the last five years confirmed significant competitive interaction between the bids by GE and Alstom and indicated a risk of price rises, the Commission said.

The deal as originally proposed would also have risked eliminating an important innovator, the Commission concluded. Alstom's heavy duty gas turbine technology is one of the most advanced, flexible and cleanest available, particularly well-suited to meet European customers' requirements for operational flexibility, the Commission said. The transaction as notified would have reduced customer choice, R&D and innovation, with serious risks that certain Alstom heavy duty gas turbine models would be discontinued and that the newly developed and most advanced model (the GT36) would not be commercialised. This was of concern for many market participants, including major European power utilities.

Another issue was that the transaction as originally proposed would have eliminated competition from Alstom's servicing subsidiary Power Systems Manufacturing (PSM) - purchased by Alstom from Calpine in 2012 - in the service market for GE's mature technology heavy duty gas turbines (in particular the 9FA model). As GE is the dominant player in this market and PSM its most significant potential competitor, said the Commission, this would have created a risk of higher prices and less innovation.

The commitments

In order to address the Commission's concerns, the parties to the GE/Alstom transaction offered to divest the main, technologically most advanced, parts of Alstom's heavy duty gas turbine business and the key personnel that would be involved with its future development. In particular:

- ¥ Alstom's heavy duty gas turbine technology for the GT26 and GT36 turbines, existing upgrades and pipeline technology for future upgrades, excluding essentially only the technology for Alstom's older GT13 model for which the Commission had no competition concerns. The GT36 is currently a technology development programme, which "upon completion would result in an H-class gas turbine product", says GE.

- ¥ A large number of Alstom R&D engineers involved with developing Alstom heavy duty gas turbine technology.

- ¥ Two test facilities, for the GT26 and GT36 turbine models, in Birr, Switzerland.

- ¥ Long term service agreements for 34 GT26 turbines sold in recent years by Alstom (with the service business for the remainder of Alstom's gas turbine installed base (approximately 720 units) transferring to GE, as envisaged in the original acquisition proposal). And

- ¥ Alstom's Florida-based PSM service business (although GE will receive a licence to the PSM intellectual property used to offer after-market services for non-GE gas turbines).

GE proposed Ansaldo of Italy as a potential purchaser for these assets. Ansaldo is an existing competitor in the heavy duty gas turbine market. It already has know-how, experience and an efficient factory for gas turbines and other power plant components (such as steam turbines and generators) that are often sold together with heavy duty gas turbines, the

Commission noted.

The commitments offered by GE will allow the purchaser (ie, Ansaldo) to replicate Alstom's previous role in the market thereby maintaining effective competition. Moreover, the divestment guarantees the continuation of Alstom's distinctive sequential (two stage) combustion heavy duty gas turbine technology, which is particularly well suited to the flexibility needs of European customers, while at the same time offering the purchaser advanced R&D capabilities and incentives to continue pushing innovation in this important market for Europe.

Subject to these conditions, the Commission was able to approve the transaction under the EU Merger Regulation.

By way of background information on the heavy duty gas turbine market, the Commission cites International Energy Agency (IEA) forecasts that gas is expected to continue to be a significant source of electricity generation in Europe in the medium term and to grow further in the long term. The Commission also notes that modern heavy duty gas turbine technology is very research and capital intensive, while flexible and efficient heavy duty gas turbine technology will continue to be essential for creating a more climate friendly electricity generation system in Europe because it is complementary to renewables and also the most environmentally-friendly form of fossil fuel generation, which is "why EU funds under the Research and Technological Development Framework Programme are dedicated to heavy duty gas turbine research."

International co-operation

Given the complexity of the case and the global reach of the parties' activities, the Commission says it co-operated with the competition authorities of a significant number of countries. This involved in particular close and successful co-operation with the Antitrust Division of the Department of Justice (DoJ) in the US. While the scope of the DoJ's concerns was different due to different conditions in the US markets for heavy duty gas turbines (operating at 60 Hz), the co-operation involved regular exchanges of views and evidence and a joint approach to remedy discussions leading to satisfactory and mutually aligned remedy solutions for both EU and US concerns.

The Commission has co-operated throughout the procedure also with agencies in Brazil, Canada, China, Israel and South Africa.

GE says the European Commission and DoJ clearances pave the way for it to complete the transaction as early as possible in the fourth quarter of 2015.

GE also says it is close to finalising a deal to divest the above assets to Ansaldo and that this transaction would be expected to close after the closing of the GE/Alstom transaction, subject to required regulatory approvals.

Reduced purchase price

GE reached an agreement with Alstom in April of 2014 to purchase its power and grid businesses for €12.35 billion. Adjusting for the joint ventures announced in June 2014 (renewables, grid, and nuclear), changes in the deal structure, price adjustments for remedies listed above, and net cash at close, the purchase price is now expected to drop to approximately €8.5 billion.

Follow Us:  [LinkedIn](#)

Modern Power Systems is a product of Global Trade Media, a trading division of Progressive Media Group Limited. © 2017, All Rights Reserved.

[Privacy Policy](#)



PRESS RELEASE

Genoa, February 26, 2016

Ansaldo Energia, with the acquisition of key Alstom technology and assets from General Electric, extends its global footprint in Europe, the Middle East and the United States and broadens its portfolio of products and services

The operation consolidates Ansaldo Energia's international leadership of the gas turbine sector, making it possible for the company to double its turnover in the next five years

Following the signing of the agreement on November 2, 2015, Ansaldo Energia, in which Fondo Strategico Italiano and Shanghai Electric hold stakes of 44.8% and 40% respectively, announces the closing of its acquisition from General Electric of Alstom's advanced heavy duty gas turbine business and subsidiary company Power System Manufacturing.

The deal includes the following assets:

- All intellectual property rights held by Alstom for the latest ratings of the GT26 and GT36 heavy duty gas turbines, existing upgrades and pipeline technology for future upgrades.
- Servicing agreements for 34 GT26 turbines already sold and installed by Alstom in recent years.
- More than 400 Alstom employees in Baden, Switzerland, who will continue to develop the heavy duty gas turbine technology acquired and support the service and equipment business.
- Power System Manufacturing, LLC ("PSM"), the Alstom subsidiary based in Florida, United States, and a leading F-class technology provider in the General Electric, Siemens and Mitsubishi aftermarket service business.
- Ansaldo Energia will own the assets used to manufacture the GT36 and the latest versions of the GT26, as well as having access to the existing supply chain.

Following the acquisition, Ansaldo Energia will license the following assets to General Electric for after-market services:

- The intellectual property held by PSM relating to Siemens-Mitsubishi gas turbines.
- Intellectual property held by Alstom for the portions of the company's heavy duty gas turbine business that are retained by General Electric.

In addition, General Electric will provide in the short term transitional services to support the continuity and viability of the business.



Siemens SGT5 – 8000H



- Largest gas turbine with 340 MW output
- Weight: 440 t (Airbus 380: 361 t), Length: 13.2 m, Height: 5 m, Width: 5m
- Pressure ratio: 19.2 : 1
- Exhaust temperature: 620°C
- 60 % efficiency in combined cycle operation (530 MW)



Source: Siemens Power Generation

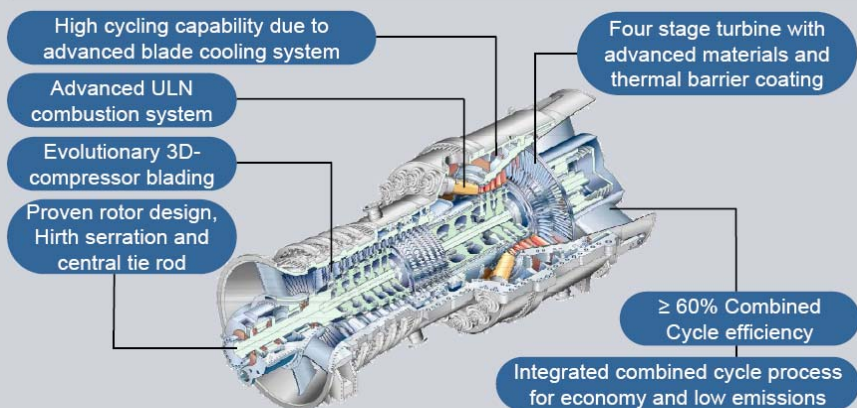


Siemens SGT5 – 8000H



SIEMENS

SGT5-8000H – World Largest Gas Turbine



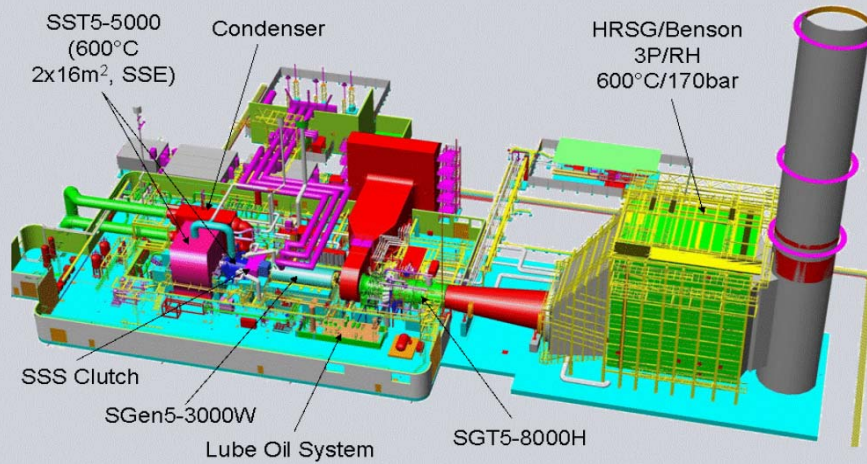
Harmonization of 'V' and 'W' frames uses best features from both and introduces new technologies on low risk.

Source: Siemens Power Generation



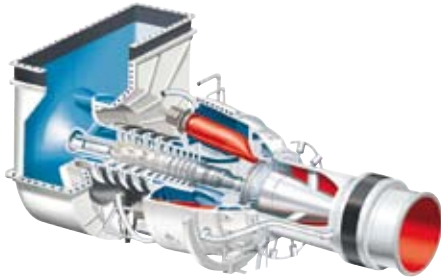
Irsching 4 CC plant SCC5-8000H Overview Main Components

SIEMENS



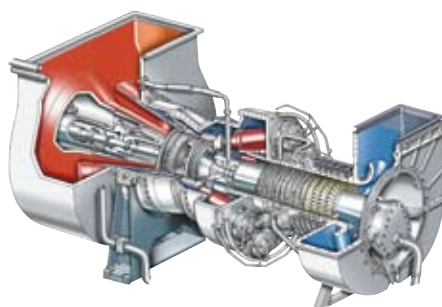
Industrial gas turbines

The comprehensive Siemens product range from 4 to 47 megawatts



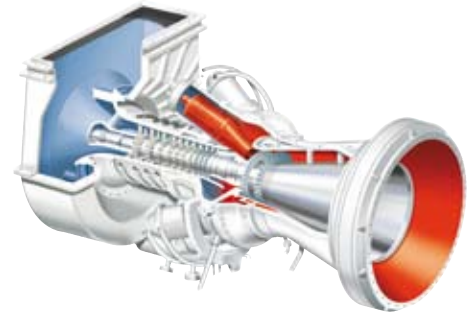
SGT-100

Power generation	5.4MW(e)
• Fuel:	Natural gas*
• Frequency:	50/60Hz
• Electrical efficiency:	31 %
• Heat rate:	11,613kJ/kWh (11008Btu/kWh)
• Turbine speed:	17,384 rpm
• Compressor pressure ratio:	15.6:1
• Exhaust gas flow:	20.6kg/s (45.4lb/s)
• Exhaust temperature:	531° C (988° F)
• NO _x emissions (with DLE, corrected to 15 % O ₂ dry):	≤ 25ppmV



SGT-200

Power generation	6.75MW(e)
• Fuel:	Natural gas*
• Frequency:	50/60Hz
• Electrical efficiency:	31.5 %
• Heat rate:	11,418kJ/kWh (10,823Btu/kWh)
• Turbine speed:	11,053 rpm
• Compressor pressure ratio:	12.2:1
• Exhaust gas flow:	29.3kg/s (64.5lb/s)
• Exhaust temperature:	466° C (871° F)
• NO _x emissions (with DLE, corrected to 15 % O ₂ dry):	≤ 25ppmV



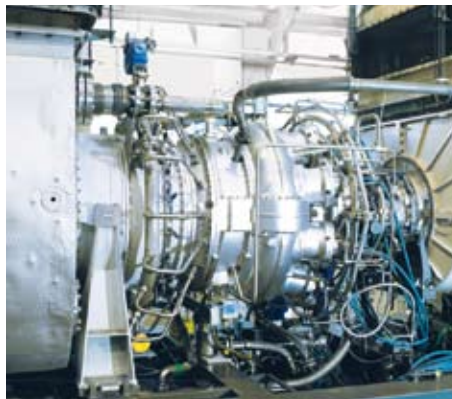
SGT-300

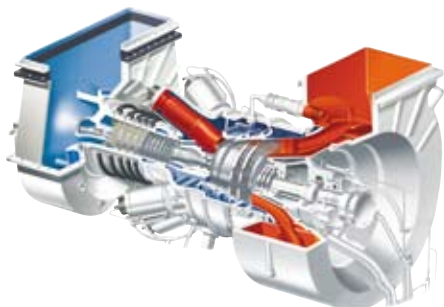
Power generation	7.90MW(e)
• Fuel:	Natural gas*
• Frequency:	50/60Hz
• Electrical efficiency:	30.6 %
• Heat rate:	11,773kJ/kWh (11,158Btu/kWh)
• Turbine speed:	14,010 rpm
• Compressor pressure ratio:	13.7:1
• Exhaust gas flow:	30.2kg/s (66.6lb/s)
• Exhaust temperature:	542° C (1008° F)
• NO _x emissions (with DLE, corrected to 15 % O ₂ dry):	≤ 15ppmV

Mechanical drive	5.7MW (7,640bhp)
• Fuel:	Natural gas*
• Efficiency:	32.9 %
• Heat rate:	10,948kJ/kWh (7,738Btu/bhph)
• Turbine speed:	13,000 rpm
• Compressor pressure ratio:	14.9:1
• Exhaust gas flow:	19.7kg/s (43.4lb/s)
• Exhaust temperature:	543° C (1009° F)
• NO _x emissions (with DLE, corrected to 15 % O ₂ dry):	≤ 25ppmV

Mechanical drive	7.68MW (10,300bhp)
• Fuel:	Natural gas*
• Efficiency:	33 %
• Heat rate:	10,906kJ/kWh (7,708Btu/bhph)
• Turbine speed:	10,950 rpm
• Compressor pressure ratio:	12.3:1
• Exhaust gas flow:	29.5kg/s (65.0lb/s)
• Exhaust temperature:	489° C (912° F)
• NO _x emissions (with DLE, corrected to 15 % O ₂ dry):	≤ 15ppmV

Mechanical drive	8.2MW (11,000bhp)
• Fuel:	Natural Gas*
• Efficiency:	34.6 %
• Heat rate:	10,400 kJ/kWh (7,350 Btu/bhph)
• Turbine speed:	11,500 rpm
• Compressor pressure ratio:	13.3:1
• Exhaust gas flow:	29.0 kg/s (63.9 lb/s)
• Exhaust temperature:	498° C (928° F)
• NO _x emissions (with DLE, corrected to 15 % O ₂ dry):	≤ 15ppmV





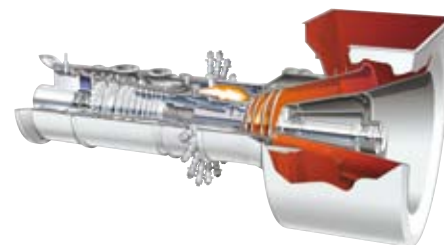
SGT-400

Power generation	12.90MW(e)
• Fuel:	Natural gas *
• Frequency:	50/60Hz
• Electrical efficiency:	34.8 %
• Heat rate:	10,355kJ/kWh (9,815Btu/kWh)
• Turbine speed:	9,500 rpm
• Compressor pressure ratio:	16.8:1
• Exhaust gas flow:	39.4kg/s (86.8lb/s)
• Exhaust temperature:	555°C (1,031°F)
• NO _x emissions (with DLE, corrected to 15 % O ₂ dry):	≤ 15ppmV



SGT-500

Power generation	19.10MW(e)
• Fuel:	Natural gas
• Frequency:	50/60Hz *
• Electrical efficiency:	33.8 %
• Heat rate:	10,664 kJ/kWh (10,107 Btu/kWh)
• Turbine speed:	3,600 rpm
• Compressor pressure ratio:	13:1
• Exhaust gas flow:	97.9 kg/s (215.9 lb/s)
• Exhaust temperature:	369°C (697°F)
• NO _x emissions (with DLE, corrected to 15 % O ₂ dry):	≤ 42ppmV



SGT-600

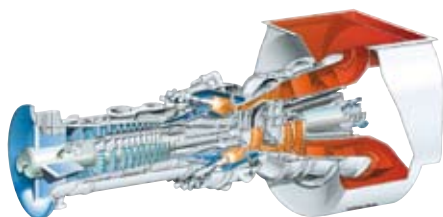
Power generation	24.77MW(e)
• Fuel:	Natural gas *
• Frequency:	50/60Hz
• Electrical efficiency:	34.2 %
• Heat rate:	10,533kJ/kWh (9,983Btu/kWh)
• Turbine speed:	7,700 rpm
• Compressor pressure ratio:	14:1
• Exhaust gas flow:	80.4kg/s (177.3lb/s)
• Exhaust temperature:	543°C (1,009°F)
• NO _x emissions (with DLE, corrected to 15 % O ₂ dry):	≤ 25ppmV

Mechanical drive	13.40MW (18,000bhp)
• Fuel:	Natural gas *
• Efficiency:	36.2 %
• Heat rate:	9,943kJ/kWh (7,028Btu/bhph)
• Turbine speed:	9,500 rpm
• Compressor pressure ratio:	16.8:1
• Exhaust gas flow:	39.4kg/s (86.8lb/s)
• Exhaust temperature:	555°C (1,031°F)
• NO _x emissions (with DLE, corrected to 15 % O ₂ dry):	≤ 15ppmV

Mechanical drive	19.52 MW (26,177bhp)
• Fuel:	Natural gas *
• Efficiency:	34.5 %
• Heat rate:	10,432kJ/kWh (7,373Btu/bhph)
• Turbine speed:	3,450 rpm
• Compressor pressure ratio:	13:1
• Exhaust gas flow:	97.9 kg/s (215.9 lb/s)
• Exhaust temperature:	369°C (697°F)
• NO _x emissions (with DLE, corrected to 15 % O ₂ dry):	≤ 42ppmV

Mechanical drive	25.40MW (34,100bhp)
• Fuel:	Natural gas *
• Efficiency:	35.1 %
• Heat rate:	10,258kJ/kWh (7,250Btu/bhph)
• Turbine speed:	7,700 rpm
• Compressor pressure ratio:	14:1
• Exhaust gas flow:	80.4kg/s (177.3lb/s)
• Exhaust temperature:	543°C (1,009°F)
• NO _x emissions (with DLE, corrected to 15 % O ₂ dry):	≤ 25ppmV

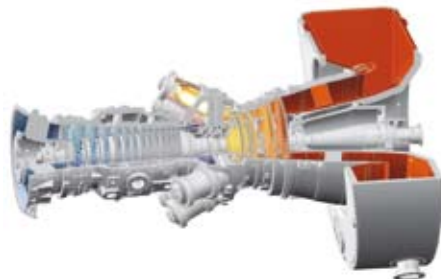




SGT-700

Power generation	31.21MW(e)
• Fuel:	Natural gas *
• Frequency:	50/60Hz
• Electrical efficiency:	36.4 %
• Heat rate:	9,882kJ/kWh (9,367Btu/kWh)
• Turbine speed:	6,500 rpm
• Compressor pressure ratio:	18.6:1
• Exhaust gas flow:	94kg/s (208lb/s)
• Exhaust temperature:	528°C (983°F)
• NO _x emissions (with DLE, corrected to 15 % O ₂ dry):	≤ 15ppmV

Mechanical drive	32.04MW (42,966bhp)
• Fuel:	Natural gas *
• Efficiency:	37.4 %
• Heat rate:	9,629kJ/kWh (6,806Btu/bhph)
• Turbine speed:	6,500 rpm
• Compressor pressure ratio:	18.6:1
• Exhaust gas flow:	94kg/s (207lb/s)
• Exhaust temperature:	528°C (983°F)
• NO _x emissions (with DLE, corrected to 15 % O ₂ dry):	≤ 15ppmV



SGT-750

Power generation	35.93MW(e)
• Fuel:	Natural gas *
• Frequency:	50/60Hz
• Electrical efficiency:	38.7 %
• Heat rate:	9,296kJ/kWh (8,811 Btu/kWh)
• Turbine speed:	6,100 rpm
• Compressor pressure ratio:	23.8:1
• Exhaust gas flow:	113.3 kg/s (249.8 lb/s)
• Exhaust temperature:	462°C (864°F)
• NO _x emissions (with DLE, corrected to 15 % O ₂ dry):	≤ 15ppmV

Mechanical drive	37.11MW (49,765bhp)
• Fuel:	Natural gas *
• Efficiency:	40.0 %
• Heat rate:	9,002 kJ/kWh (6,362Btu/bhph)
• Turbine speed:	3,050–6,405 rpm
• Compressor pressure ratio:	23.8:1
• Exhaust gas flow:	113.3 kg/s (249.8 lb/s)
• Exhaust temperature:	462°C (864°F)
• NO _x emissions (with DLE, corrected to 15 % O ₂ dry):	≤ 15ppmV



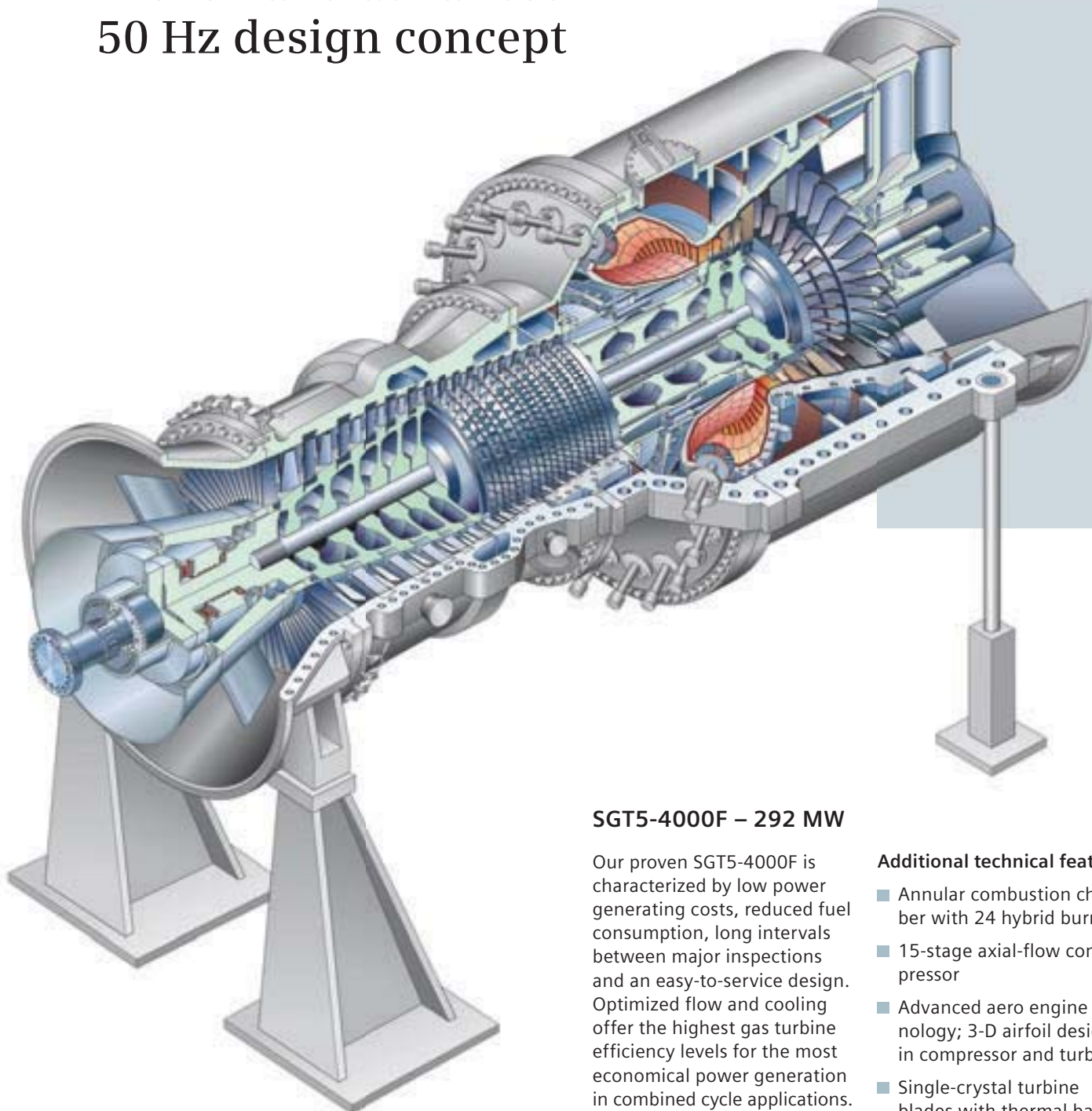
SGT-800

Power generation	47.00MW(e)
• Fuel:	Natural gas *
• Frequency:	50/60Hz
• Electrical efficiency:	37.5 %
• Heat rate:	9,597kJ/kWh (9,096Btu/kWh)
• Turbine speed:	6,608 rpm
• Compressor pressure ratio:	19:1
• Exhaust gas flow:	131.5kg/s (289.9lb/s)
• Exhaust temperature:	544°C (1,011°F)
• NO _x emissions (with DLE, corrected to 15 % O ₂ dry):	≤ 15ppmV



*No intake or exhaust loss; other gaseous, liquid and/or dual fuel options available

Proven and advanced 50 Hz design concept



SGT5-4000F – 292 MW

Our proven SGT5-4000F is characterized by low power generating costs, reduced fuel consumption, long intervals between major inspections and an easy-to-service design. Optimized flow and cooling offer the highest gas turbine efficiency levels for the most economical power generation in combined cycle applications. Its advanced technology is based on proven design features, resulting in a fleet reliability of over 99% and a combined experience of nearly 4,500,000 operating hours for all family members.

Additional technical features:

- Annular combustion chamber with 24 hybrid burners
- 15-stage axial-flow compressor
- Advanced aero engine technology; 3-D airfoil design in compressor and turbine
- Single-crystal turbine blades with thermal barrier coating and film cooling
- Advanced cooling technology
- Multiple fuels capability
- Hydraulic turbine blade tip clearance control

Siemens Gas Turbines and Siemens Combined Cycle Plants for 50 Hz Grids (Standard design, ISO ambient conditions)

	SGT5-4000F	SGT5-2000E
Siemens Gas Turbines		
Gross power output (MW)	292	168
Gross efficiency (%)	39.8	34.7
Gross heat rate (kJ/kWh)	9,038	10,366
Gross heat rate (Btu/kWh)	8,567	9,825
Pressure ratio	18.2	11.7
Siemens Gas Turbine Packages*		
	SGT5-PAC 4000F	SGT5-PAC 2000E
Net power output (MW)	288	165
Net efficiency (%)	39.5	34.5
Net heat rate (kJ/kWh)	9,114	10,471
Net heat rate (Btu/kWh)	8,638	9,925
Exhaust temperature (°C/°F)	580/1,075	539/1,002
Exhaust mass flow (kg/s)	688	526
Exhaust mass flow (lb/s)	1,516	1,161
Generator type	Air-cooled	Air-cooled
Siemens Combined Cycle Plants*		
	SCC5-4000F 1S	SCC5-2000E 1x1
Single-Shaft		
Net power output (MW)	423	251
Net efficiency (%)	58.4	52.2
Net heat rate (kJ/kWh)	6,164	6,895
Net heat rate (Btu/kWh)	5,842	6,535
	SCC5-4000F 2x1	SCC5-2000E 2x1
Multi-Shaft		
Net power output (MW)	848	505
Net efficiency (%)	58.5	52.5
Net heat rate (kJ/kWh)	6,158	6,860
Net heat rate (Btu/kWh)	5,836	6,502

* incl. pressure losses



SGT5-4000F



SGT5-2000E

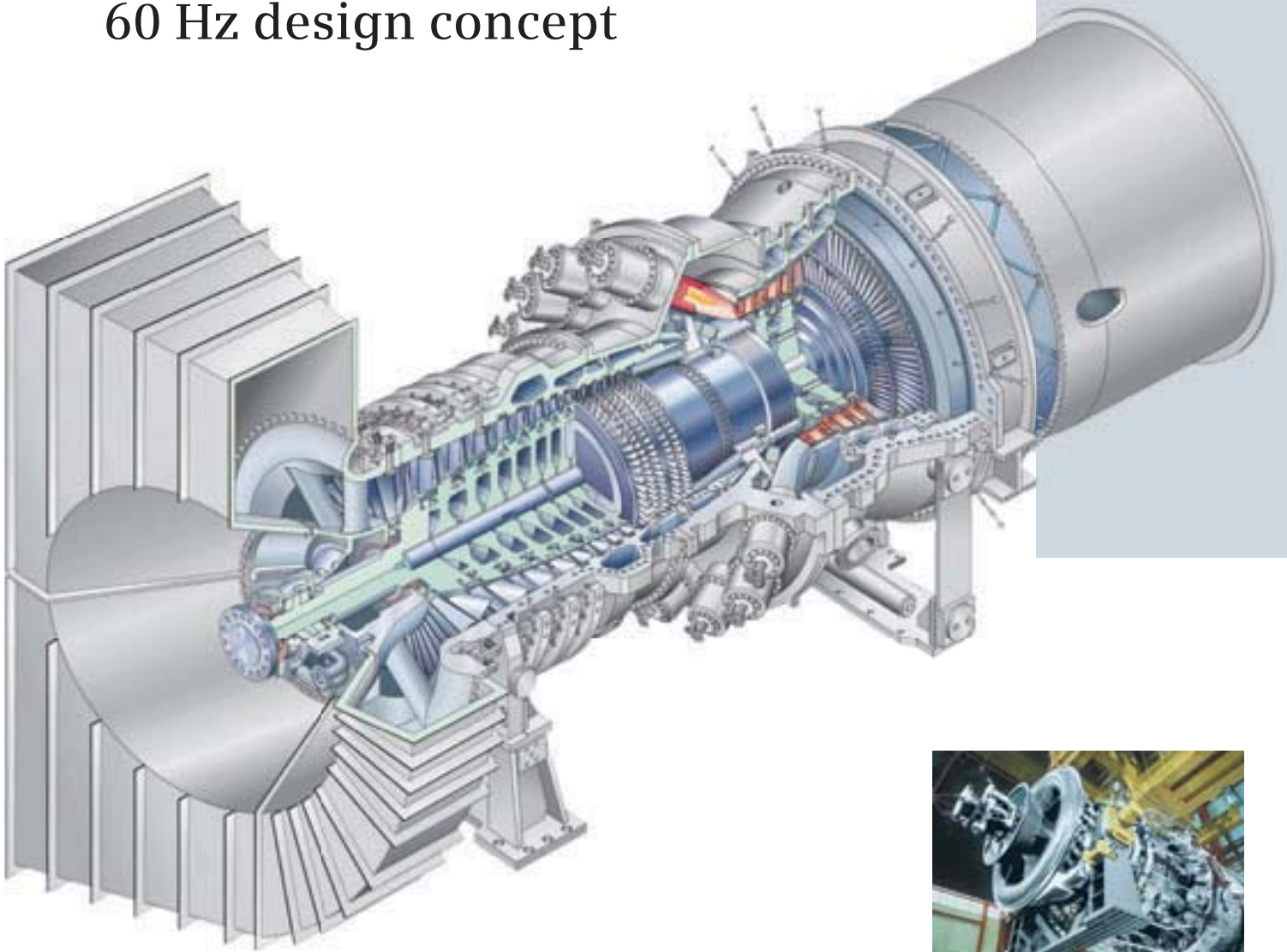
SGT5-2000E – 168 MW

The SGT5-2000E is a long-proven machine for simple or combined cycle applications, with or without combined heat and power, and for all load ranges – particularly peak-load operation. The machine is capable of burning a variety of fuels – from low to high caloric gaseous and/or liquid fuels to treated heavy oil at lowest emission levels. For IGCC applications, we offer the SGT5-2000E (LCG) machine with a modified compressor. The SGT5-2000E has a record of durability with more than 300 units accounting for over 6,400,000 operating hours. This gas turbine is also available for 60 Hz markets named SGT6-2000E.

Additional technical features:

- Two walk-in combustion chambers for hot-gas-path inspection without cover lift
- Combustion chambers lined with individually replaceable ceramic tiles
- 16-stage axial-flow compressor
- Hybrid burners for premix and diffusion mode operation with natural gas, fuel oil and special fuels, such as heavy oil and refinery residues
- Fast inlet guide vanes for peak-load operation and frequency stabilization (optional)
- Wet compression (optional)

Proven and advanced 60 Hz design concept



SGT6-5000F – 200 MW



SGT6-2000E

Siemens Gas Turbines and Siemens Combined Cycle Plants for 60 Hz Grids

(Standard design, ISO ambient conditions)

	SGT6-5000F	SGT6-2000E
Siemens Gas Turbines		
Gross power output (MW)	208	113
Gross efficiency (%)	38.1	34.0
Gross heat rate (kJ/kWh)	9,446	10,606
Gross heat rate (Btu/kWh)	8,953	10,052
Pressure ratio	17.2	11.8
Siemens Gas Turbine Packages*		
	SGT6-PAC 5000F	SGT6-PAC 2000E
Net power output (MW)	206	111
Net efficiency (%)	37.6	34.0
Net heat rate (kJ/kWh)	9,580	10,717
Net heat rate (Btu/kWh)	9,081	10,158
Exhaust temperature (°C/°F)	600/1,113	545/1,014
Exhaust mass flow (kg/s)	504	365
Exhaust mass flow (lb/s)	1,110	805
Generator type	Air-cooled	Air-cooled
Siemens Combined Cycle Plants*		
	SCC6-5000F 1x1	SCC6-2000E 1x1
Net power output (MW)	314	171
Net efficiency (%)	57.0	51.3
Net heat rate (kJ/kWh)	6,320	7,007
Net heat rate (Btu/kWh)	5,990	6,642
	SCC6-5000F 2x1	SCC6-2000E 2x1
Net power output (MW)	623	342
Net efficiency (%)	57.2	51.6
Net heat rate (kJ/kWh)	6,290	6,971
Net heat rate (Btu/kWh)	5,960	6,608

* incl. pressure losses



SGT6-5000F – 208 MW

The SGT6-5000F gas turbine continues to break reliability and continuous operation records.

With more than 4,600,000 hours of fleet operation, the SGT6-5000F is ideally suited for either simple cycle or heat recovery applications including cogeneration, combined cycle and repowering.

Our SGT6-PAC 5000F provides economical, rapid on-line generation that is ideal for peaking duty, intermediate operation or continuous service.

Additional technical features:

- 16 can-type combustors in a circular array
- 13-stage axial-flow compressor with advanced 3-D design technology
- Multiple power augmentation options
- Best 60 Hz simple cycle efficiency in its class
- Fuel flexibility for diverse applications
- Low emissions technologies including 9 ppm NO_x combustion system
- Robust and proven rotor design

SGT6-2000E - 113 MW

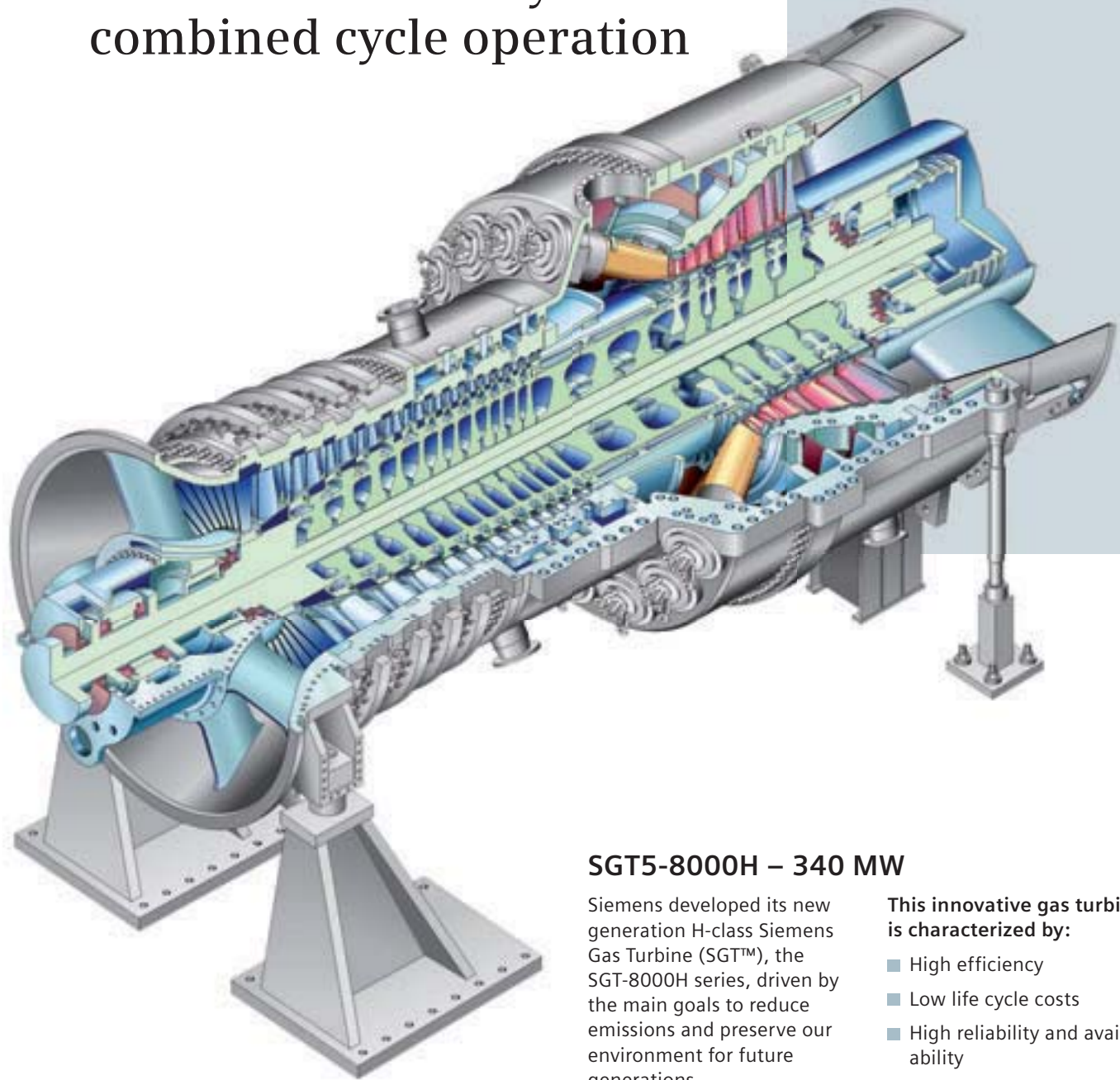
The SGT6-2000E gas turbine is designed for reliable, efficient and flexible power generation. With more than 3 million hours of fleet operation, the SGT6-2000E is a proven machine for simple cycle and combined cycle applications for all load ranges.

Additional technical features:

- Two walk-in combustion chamber for hot gas path inspection without cover lift
- Combustion chambers lined with individually replaceable ceramic tiles
- Multiple fuel capability



Designed to achieve more than 60 % efficiency in combined cycle operation



SGT5-8000H – 340 MW

Siemens developed its new generation H-class Siemens Gas Turbine (SGT™), the SGT-8000H series, driven by the main goals to reduce emissions and preserve our environment for future generations.

The new, advanced SGT-8000H series gas turbines and the SCC-8000H series combined cycle power plants feature the best-in-class technology captured from our long line of large direct-drive Siemens 50 Hz and 60 Hz heavy-duty gas turbines and power plants.

This innovative gas turbine is characterized by:

- High efficiency
- Low life cycle costs
- High reliability and availability
- Operational flexibility
- Low emissions

Siemens Gas Turbine SGT5-8000H and Siemens Combined Cycle Plant SCC5-8000H

(Standard design, rated data at ISO ambient conditions)

Siemens Gas Turbine		SGT5-8000H
Grid frequency (Hz)		50
Gross power output (MW)		340
Pressure ratio		19,2
Exhaust temperature (°C/°F)		625/1,157
Exhaust mass flow (kg/s)		820
Exhaust mass flow (lb/s)		1,808
Gas Turbine Emissions		
NO _x (ppm)		25
CO (ppm)		10
Gas Turbine Physical Dimensions		
Weight (t)		440
Length (m)		13.2
Height (m)		5.0
Width (m)		5.0
Siemens Combined Cycle Power Plant		
Single-Shaft		SCC5-8000H
Net power output (MW)		530
Net efficiency (%)		60
Net heat rate (kJ/kWh)		6,000
Net heat rate (Btu/kWh)		5,687



Features for high efficiency include:

- New compressor with advanced blade design
- Advanced materials to increase the firing and exhaust-gas temperature
- Advanced sealing system for low-leakage cooling air
- Advanced high-efficiency, high-pressure, high-temperature combined cycle process with BENSON® boiler, based on the high mass flow and exhaust-gas temperature of the new engine

Features for lowest life cycle cost include:

- H-class – designed for more than 60 % efficiency in combined cycle mode and reduced emissions at part load
- Less complexity in engine and parts which can lead to lower maintenance and operating costs
- Straightforward operational concept



Features for advanced operating flexibility include:

- Air-cooled engine for a cooling method that is always present at speed
- Fast start-up and cycling capability to support intermediate load requirements
- Less complexity in engine and plant design leading to more flexibility in operation and reduced start-up time
- Improved turndown capability for high efficiency and low-emissions part-load operation

Performance Benefits Using Siemens Advanced Compressor Cleaning System

Christoph Pels Leusden

Siemens AG Power Generation,
Service Development,
Mülheim a.d.R., Germany

Christoph Sorgenfrey

Siemens AG Power Generation,
Marketing Modernisation and Upgrades Gas
Turbine Power Plants,
Berlin, Germany

Lutz Dümmel

Kraftwerk Oberburg GmbH,
Oberburg, Germany

Extensive operational performance data from the Siemens Power Generation V64.3 unit in Obernburg, Germany (operated by Kraftwerk Obernburg GmbH) is evaluated. The unit was commissioned in 1996 and has been running continuously in base load operation with fuel gas to supply heat and power to a nearby chemical plant. In rare cases, fuel oil is used as a backup fuel. During the first major outage after approximately 25,000 equivalent operating hours (EOH), the Siemens PG Advanced Compressor Cleaning System (ACCS) was implemented at Obernburg. ACCS features separate nozzle systems for on-line and offline compressor cleaning accounting for different operating conditions. For online cleaning, the droplet size is optimized for the droplets to remain in the main air flow in order to minimize erosion effects while providing a homogeneous field over the whole air intake. With reduced rotational speed during offline compressor cleaning, erosion is less critical. Offline nozzles therefore provide higher mass flow and larger droplets in order to maximize cleaning performance for all compressor stages. ACCS, in its maximum automated version, features operation from the control room, online-washing at low ambient temperatures (officially released down to -15°C without GT anti-icing) and minimum use of manpower. The ACCS system in Obernburg was operated according to the recommended online washing procedure. By June 2002, the V64.3 unit in Obernburg reached 50,000 EOH and the second major inspection was carried out. For this paper, operational data from the second inspection intervals (24,350–49,658 EOH) and from three performance tests with calibrated equipment are compared in order to evaluate the effectiveness of the advanced compressor cleaning system. Statistical evaluation of single-wash performance recovery and the evolution of long-term performance are presented. The effects of degradation and fouling are differentiated. It is shown that ACCS has a significant benefit for long-term engine performance. [DOI: 10.1115/1.1787512]

Introduction

With the growing interest in life cycle costs for heavy-duty gas turbines, equipment operators are investigating the tradeoff between performance improvements and associated maintenance costs. One of the key factors leading to performance losses during the plant operation is compressor fouling. This is the adherence of particles and small droplets to the blading surface. Also, the flow capacity and thereby, the pressure ratio of the unit are reduced. This leads to an overall loss in power output and efficiency of a gas turbine. Fouling causes increased surface roughness of compressor blading, thereby reducing its efficiency. In the literature, there have been estimates that fouling causes up to 85% of the accumulated performance loss during operation [1]. A cost estimate is given by Diakunchak [2]. In extreme cases, fouling may also result in surge problems. Despite the use of advanced filtering methods and filter maintenance, the ingestion of substances that can cause fouling cannot be completely suppressed. The fouling rate depends largely on the site location, surrounding environment, the layout of the air intake system, atmospheric parameters, and plant maintenance. While the first four factors cannot be influenced during the operation, the plant maintenance is the critical one for preventing extra costs resulting from degraded plant performance.

Various methods have been used in the past to clean fouled compressors. At times when heavy duty gas turbines did not yet

possess highly sophisticated cooling schemes and coated compressor blades, cleaning was achieved by abrasion with the injection of solid compounds such as nutshells or rice husks. This had to be replaced by wet cleaning methods (water or solvent based) to protect modern coatings and to keep state of the art cooling systems from blockages. The most effective wet cleaning process is the crank soak or offline wash. For this, the unit has to be shut down and cooled off in order to assure that the cleaning agent is reaching all compressor stages and does not evaporate. The cleaning agent is injected into the compressor with the turbine turning at low speed. After a soaking time, the compressor is rinsed with water, which must be drained from the engine. Before the unit can be operated again commercially, it has to be dried. Thus offline washing reduces the availability of a unit.

With a growing number of gas turbines being used in combined cycle or combined heat and power applications, there was the need for the development of online washing systems with performance benefits comparable to offline systems but without required shut down times of the turbine. These systems are now state-of-the-art in modern heavy-duty gas turbines.

In this work, we analyze performance benefits of the Siemens Advanced Compressor Cleaning System (ACCS), which can be integrated as an upgrade product into all Siemens and Siemens Westinghouse gas turbine frames. For this, we have evaluated detailed operational performance data from one Siemens Power Generation V64.3 turbine where ACCS was implemented during the first major outage after 24,350 equivalent operating hours. In the following, we first describe special site conditions and features of ACCS and explain the data evaluation process. Presenting the results, we discuss the positive effects of ACCS taking into account other processes leading to performance degradation.

In literature, there has been comparable work describing the

Contributed by the International Gas Turbine Institute (IGTI) of THE AMERICAN SOCIETY OF MECHANICAL ENGINEERS for publication in the ASME JOURNAL OF ENGINEERING FOR GAS TURBINES AND POWER. Paper presented at the International Gas Turbine and Aeroengine Congress and Exhibition, Atlanta, GA, June 16–19, 2003, Paper No. 2003-GT-38184. Manuscript received by IGTI October 2002; final revision March 2003. Associate Editor: H. R. Simmons.

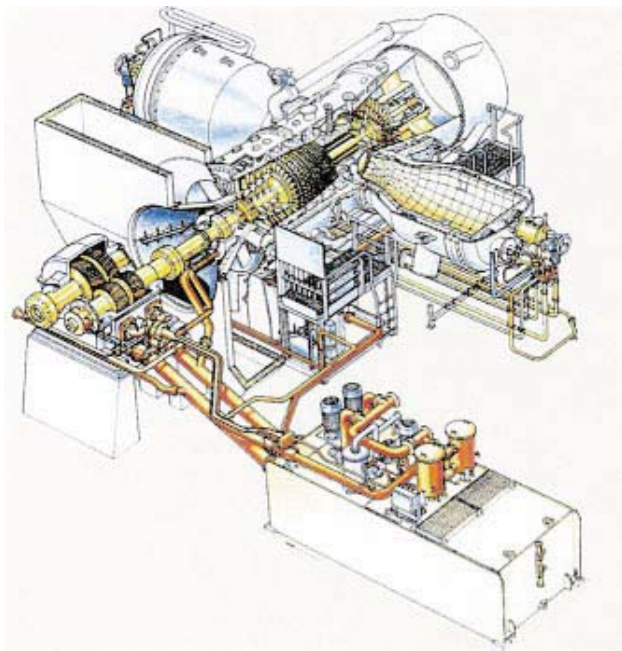


Fig. 1 Siemens AG Power Generation V64.3 unit

benefits of other cleaning systems [3–7]. It has to be underlined that fouling and, consequently, the compressor cleaning benefits are closely coupled to site specific conditions and cleaning intervals (especially of offline-cleaning). Therefore a direct comparison with measured benefits at other sites is not done in this work.

Site Conditions

For this work, performance data from the Siemens Power Generation V64.3 unit (see Fig. 1) that is operated in Obernburg, Germany, by Kraftwerk Obernburg GmbH is evaluated. The power plant is located within a chemical plant, which produces fibers for industrial and textile applications. Therefore it can be concluded that the site conditions are not particularly favorable for low fouling conditions. The nominal power output and efficiency of the unit are contained in Table 1 where these parameters are listed for three performance tests that were carried out in Obernburg with calibrated high-precision instrumentation. All data is from tests at stable base load operation with fuel gas in combined cycle mode and was corrected to ISO conditions (see Table 2). Generally, there is a strong interaction between ISO turbine inlet temperature (calculated according to Ref. [8]) and power output. In order to allow appropriate comparison of performance, power output is computed for constant turbine inlet temperature. The reference value of 1130 °C is the design value for V64.3 units.

V64.3-type turbines rotate at 90 Hz and use a gear box to shift the speed to the grid frequency. Other features and an extensive summary of operational experiences can be found in Ref. [9].

Table 1 Power output and efficiency measured with calibrated instrumentation and corrected to ISO reference conditions

Parameter	Unit	Test 1	Test 2	Test 3	Test 3 (corrected)
Date		Sept. 1996	Aug. 1999	June 2002	June 2002
EOH	H	2586	24,350	49,200	49,200
Gross power output	MW	62.5	63.4	60.9	61.6
Gross efficiency	%	35.3	35.7	35.2	35.4

Table 2 ISO conditions for the correction of measured performance data

Parameter	Unit	ISO conditions
Ambient temperature	°C	15
Ambient pressure	bars	1.013
Relative humidity	%	60
Fuel		methane
Pressure loss inlet/outlet	mbar	0/0
Power factor	1	0.8

Since its commissioning in 1996 the gas turbine has been running with fuel gas and in rare cases with fuel oil as a backup fuel. Because the plant has to provide constant heat and power to a nearby chemical factory, it is of great economical importance that the unit runs at baseload continuously. It is only shut down for forced and planned maintenance activities. Thus offline cleaning can only be carried out during those shut down periods which may occur only at large intervals (e.g., up to 12 months). Therefore the performance of online compressor cleaning is critical for this site. Until the outage for the first major inspection at 24,350 EOH in July 1999, the V64.3 unit at Obernburg was equipped with the Standard Siemens washing equipment.

During the 1999 major inspection, the entire compressor was hand washed and new turbine blading with new engine surface quality was implemented for the first three of the four-stage turbine. The success of the work carried out during the outage is reflected by the data in Table 1: the performance following the outage (test 2) clearly exceeded that of the acceptance test in 1996 (test 1).

Furthermore, the unit was equipped with the Advanced Compressor Cleaning System (ACCS). With the implementation of ACCS, the performance of the unit was monitored continuously until the second major outage in June 2002. With ACCS, the compressor was washed according to Siemens recommendations. This was one online wash per day. For one out of three (later changed to one out of two) washing sequences, the solvent-based detergent SIWASH was used. The remaining online washing sequences were done with demineralized water. Offline compressor cleaning was only performed when the plant was shut down for other imperative maintenance reasons.

In June 2002 the V64.3 at Obernburg reached the second major inspection with 49,658 equivalent operating hours (EOH). Before this inspection, a third performance test with high-precision equipment was carried out at 49,200 EOH. The results are also shown in Table 1 (test 3). It should be noted that the compressor could not be offline washed directly before that test due to operational reasons. The last offline wash took place approximately 1200 equivalent operating hours prior to test 3. In order to compare the performance to the other tests where the unit was offline cleaned directly before the test, we have corrected the parameters. This was done by multiplying the mean gradients for power and efficiency losses during operation without offline cleaning (derived in “Results and Discussion” section) with the number of operating hours between the last offline wash and the performance test 3. These corrected values are listed in the column which is denoted 3 (corrected) in Table 1.

Features of the Advanced Compressor Cleaning System

In order to support operators in reducing maintenance costs associated with regular compressor cleaning, ACCS offers a high level of automation. Semi-automatic or jet-pump skids enable automated online washing processes. Only the starting point for the cleaning has to be set manually. All operation parameters are software controlled by the PLC of the skid. In the fully automated version, parameters are calculated taking into account GT operation signals and outside temperature. Only a minimum use of

manpower is necessary, for example, to close drain valves on the GT during offline cleaning. Also, one ACCS supply package may serve up to five gas turbines.

A solvent based cleaner (SIWASH S) was developed for use against organic pollution, especially hydrocarbon particles (e.g., emissions from traffic, combustion particles) which were identified as contributing significantly to the fouling process. SIWASH S is specially designed for good online cleaning results where water based products fail. Even in areas with low industrial pollution, hydrocarbons create sticky layers on the blade surfaces, which also speeds up fouling with inorganic particles. For offline cleaning a water based cleaning agent (SIWASH W) is available in order to reduce costs of waste disposal.

ACCS has different nozzles for offline and online compressor cleaning. This is due to the difference in flow characteristics of a gas turbine intake during these operational modes.

For online cleaning special shaft nozzles with length depending on the intake housing depth are used to keep the droplets in the main air flow (prevent the droplets from recirculating in dead water regions). The nozzles are designed to provide a narrow spectrum of droplets with an optimum size for best cleaning properties. They are big enough not to evaporate before they reach the blades and to provide a mechanical cleaning effect on the blade surface. On the other hand, they are small enough to follow the streamlines into the compressor and not to damage the blades excessively by droplet erosion. A homogenous field of droplets during online operation is guaranteed by a high number of shaft nozzles in the GT intake and their optimised distribution. In contrast, offline nozzles provide a high mass flow of bigger droplets.

Conventional cleaning systems may not be operated at compressor inlet temperatures below +6 °C due to icing in the compressor. ACCS, with the semiautomatic supply skid tied to the gas turbine PLC, is released for online cleaning down to -15 °C (5 F) and offline cleaning down to -10 °C (14 F) without use of the gas turbine anti-icing system. Operation at such low temperatures is possible with the use of an antifreezing agent.

Other features of the system are:

- Washing parameters may be computed, displayed and optimized using a state of the art monitoring and diagnostic system (WIN-TS).
- The closed-loop supply system prevents operator staff from getting into contact with cleaning solution.
- ACCS lowers the costs associated with waste disposal of offline cleaning residuals.
- Implementation during a minor inspection is possible.

Currently, ACCS is in operation or commissioning in a total of 16 Siemens Power Generation V units of all major types (including V94.2, V64.3, V84.3A, and V94.3A). Cumulative operating experience reached, at the end of 2002, more than 200,000 GT operating hours without any major defect. There has been very positive customer feedback regarding the reliability and the performance of the system (efficiency improvement of up to 150 kJ/kWh_{el}).

Data Processing

For this analysis, one set of operational data for each 8-h work shift was recorded from the gas turbine diagnostic system in Obernburg. For each data set, the following performance parameters were computed:

- power output,
- efficiency,
- ISO turbine inlet temperature according to ISO standard 2314 [8],
- compressor air mass flow.

In order to compare the performance parameters recorded at different operating times, all values were corrected to the equivalent conditions. This included corrections to constant ISO turbine inlet temperature as well as constant ambient reference conditions, which are listed in Table 2. This was done with curves that were

derived from a thermodynamic model for V64.3 units [10]. This model was developed using data from acceptance tests of several V64.3 units using high-precision measurement instrumentation.

In order to compute all of the above-mentioned parameters and to carry out the correction, each data set contains the following quantities:

- power output at generator terminals, speed and power factor,
- temperatures at compressor inlet, outlet and turbine exhaust,
- static pressure loss in the intake and exhaust ducts,
- pressure ratio,
- fuel volume flow, temperature, and pressure,
- ambient pressure and humidity.

Constant standard values were used for the gear box efficiency, cooling air consumption, and inlet and outlet parameters of the cooling air cooler.

The computation of most of the above-mentioned performance parameters is very sensitive to the total heat flux of the fuel mass flow. Uncertainty of this parameter results in errors that exceed those coming from other measured quantities. The heat flux is the product of fuel volume flow, its density, and lower heat value. While the fuel volume flow is a measured quantity, the lower heat value and the density can only be derived from the gas composition. Due to the absence of an online gas chromatograph in Obernburg, the composition could not be recorded in the diagnostic system. Therefore a constant average gas composition was used for a preliminary calculation of all performance parameters. Due to the sensitivity, the evaluation of the performance parameters contains a significant error if the real composition deviates from the assumed one. In order to avoid this error, the following adjustment method for the results of the preliminary computation was implemented:

The method is based upon the application of Stodola's law [11]:

$$\dot{m}_T \propto \frac{p_T}{\sqrt{T_T}} \quad (1)$$

Therein, \dot{m}_T denotes the mass flow through the turbine section, p_T and T_T the pressure and temperature at the turbine inlet. As mentioned above, the correction is done to equivalent reference conditions and constant turbine inlet temperature. Thereby, the mass flow is proportional to the pressure level at turbine inlet or, for further simplification, to the pressure ratio of the engine. With this reasoning, the measured pressure ratio was used to control the turbine air mass flow in the preliminary computation. If that air mass flow leaves a tolerance band of +/- 5% of the expected air flow (derived from the pressure ratio applying Eq. (1), the heat flux (being the most sensitive input parameter) is adjusted. This process can be justified by the fact that the heat flux in the preliminary computation is partially an assumed quantity because the fuel gas composition is not known in detail.

If the air mass flow is within the above-mentioned tolerance band, no adjustment is made. No other measured parameters were modified. Following the final calculation, it is verified that the air mass flow is now within the tolerance band derived from the pressure ratio. All data presented in this work are results from the final calculation.

In the next section, we will base our analysis on the following performance parameters, the computation of which is explained below.

Mean Monthly Performance (P_m and η_m). The monthly mean for power output (P_m) and efficiency (η_m) was computed by averaging the measured values after correction to ISO conditions. When comparing results of different months, we used the performance level recorded in the first month of operation after the major outage at 24,350 EOH as a reference value for normalization. When an offline compressor cleaning took place during a month, the evaluation of P_m and η_m was split for the time before and after the offline wash.

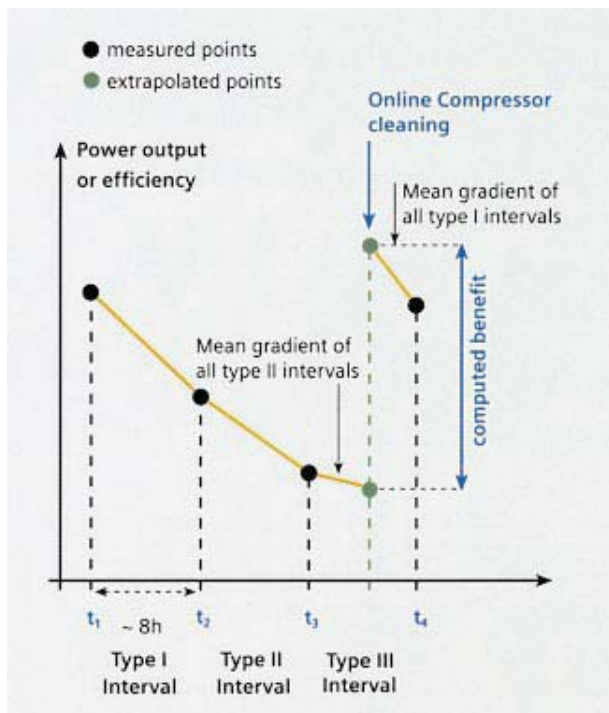


Fig. 2 Typical results for performance parameters for 24 h of operation. Evaluation of benefits for online-compressor cleaning.

Performance Gradient During Operation Without Compressor Wash (dP_{OP}/dt and $d\eta_{OP}/dt$). Figure 2 displays typical results for measured power output or efficiency after correction to ISO conditions (see Table 2) for four consecutive data recordings. Times between data recording were approximately 8 h and one online wash per day was performed. Therefore the operational interval containing a compressor wash was preceded by two intervals without wash, which are denoted type I and II intervals in Fig. 2. The performance gradient for operation without compressor wash can therefore be computed for those two intervals.

Performance Benefit of Online-Compressor Cleaning (ΔP_{ON} and $\Delta \eta_{ON}$). For the computation of these parameters, the mean values of dP_{OP}/dt and $d\eta_{OP}/dt$ for type I and II intervals were computed. As it is shown in Fig. 2, the mean gradients were used to extrapolate from the measured points before and after online compressor cleaning to the point in time when the cleaning took place. The benefit then results from the difference in performance at the time of cleaning. Because the individual data points that were derived from operational data possess a measurement error, the benefit computed with this method will also show a statistical distribution. We used the mean gradient here for the extrapolation instead of the measured gradient because the measured one is more sensitive to individual measurement errors. Therefore the procedure chosen here resulted in a lower uncertainty for the benefit of compressor cleaning.

When analysing performance data over long periods of operation, other mechanisms of degradation have to be taken into account. Potential main sources for degradation are corrosion and erosion effects in the compressor and turbine parts, turbine fouling, foreign object damage, and thermal distortion [12,13]. Generally, these effects are not influenced by fouling and therefore remain constant when compressor washing is carried out. Thus the total degradation of a performance parameter is the sum of four types of losses as is shown schematically in Fig. 3:

- losses that can be recovered by an online wash (A),

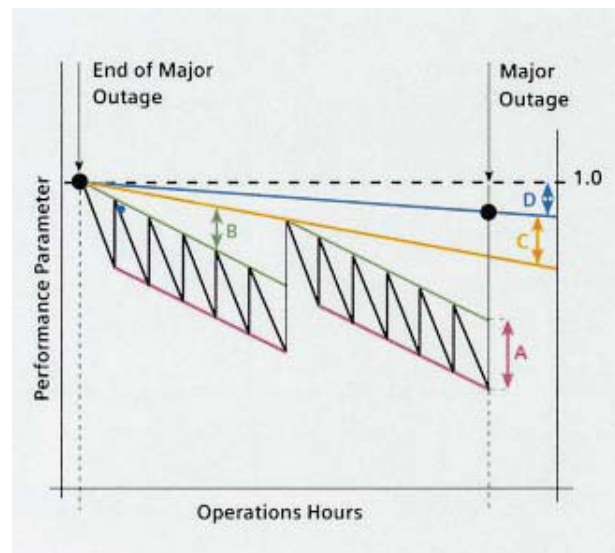


Fig. 3 Types of losses leading to overall performance degradation

- losses that can be recovered by an offline wash (B),
- losses that can be recovered during major inspection (C),
- and losses that cannot be recovered at all (D).

From that reasoning, one can easily see that all degradation mechanisms other than fouling lead to losses of type C and D. There may also be contributions of fouling to type C and D losses if fouling cannot be completely removed even with offline compressor cleaning. In this study, we concentrate on data that have been acquired within the second inspection interval of approximately 25,000 equivalent operating hours (EOH) for the V64.3 unit at Oernburg. Therefore the losses of type C and D are treated together for the most part.

Results and Discussion

Figure 4 shows the evolution of the monthly mean of power output P_m and efficiency η_m relative to their initial values, after the major inspection, as a function of equivalent operating hours. Both parameters show similar behavior with a distinct performance recovery due to offline compressor cleaning. In each of the seven intervals between offline washes, the performance decreases with a similar gradient. Some phenomena are of particular interest:

None of the offline washes leads to the initial performance level. However, even towards the end of the 25,000 EOH-inspection interval, offline compressor cleaning leads to a performance level that is comparable with the level reached with the first offline cleaning. This finding can be interpreted as follows. During the inspection, the entire compressor was hand cleaned leading to an optimal condition. This condition cannot be taken as representative for long-term operation of heavy-duty gas turbines. During the first weeks of operation, it can be assumed that there is onset of fouling in all compressor stages which causes the deterioration of the performance level. All of this initial fouling cannot be removed even with offline cleaning, because this cleaning method is not as effective as hand cleaning of all compressor stages. Therefore there are some contributions of fouling to losses of type C and D. This reasoning may also explain why performance test data from test 2 (recorded within the first 24 h after the inspection) was clearly better than test 1 (recorded 2586 EOH after first fire).

In order to distinguish the types of losses described in the previous section (compare Fig. 3), we used the performance levels directly following each offline wash in order to fit a line using

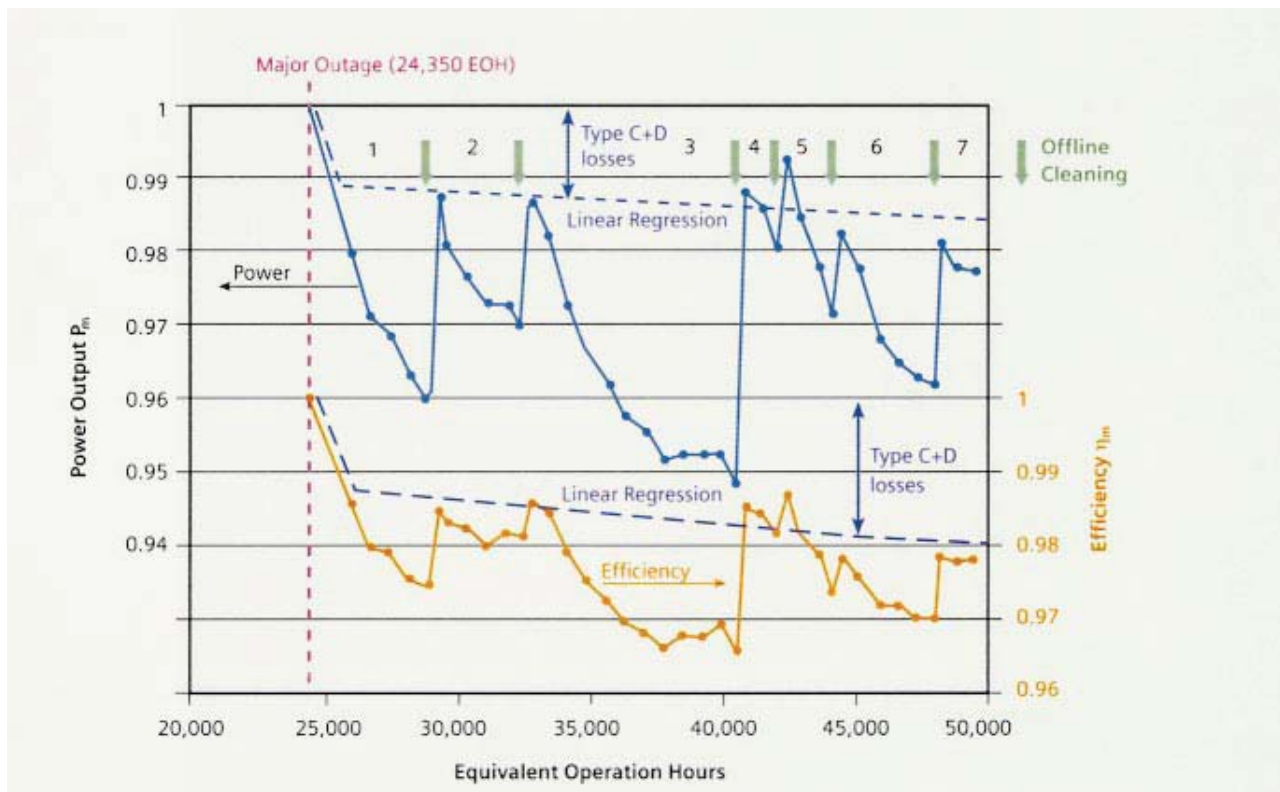


Fig. 4 Evaluation of mean monthly performance relative to initial performance after the first major outage

linear regression. These lines for power output and efficiency are also displayed in Fig. 4. The slopes of the regression lines are comparable for power output and efficiency (0.02%/1000 EOH and 0.03%/1000 EOH).

The third interval between offline washes is particularly long (7782 EOH). With increasing operating time after the last offline cleaning, the gradient both for power and efficiency decreases, indicating a saturation in the losses caused by fouling.

In order to characterize type-B losses, we have computed the average performance evolution of the seven intervals as a function of operating time after offline compressor cleaning. The values were calculated relative to the performance directly following the offline wash. Because the interval lengths are different, the mean values were computed for a varying amount of individual data points. The results for type-B losses are displayed in Fig. 5 for power output and Fig. 6 for efficiency. Within the first 3500 EOH after offline washing the slope remains relatively constant with 1% per 1000 EOH for power output and 0.5% per 1000 EOH for efficiency. Beyond 3500 EOH, the slope decreases significantly. Still, type-B losses exceed those of type C and D.

For the evaluation of performance benefits resulting from on-line compressor cleaning, we show the statistical results in the form of the probability density function for power output and efficiency in Figs. 7 and 8. The measured recovery by online cleaning was approximated by a normal distribution for both parameters with the mean value of 0.33% for power output and 0.27% for efficiency. These can be interpreted as mean values for type-A losses. Therefore they can be transferred into a parallel line in Figs. 5 and 6. It might be surprising that type-B losses largely exceed type-A losses. However, it has to be noted that regular online cleaning will lead to a smaller gradient for type-B losses.

This can be seen in Fig. 9 where we show performance gradients for intervals in which online compressor cleaning was not carried out. In the 25,000 EOH analyzed here, five of those intervals, lasting up to 11 days, were identified. The gradients of all

intervals clearly exceed the average gradients for type-B losses. Therefore it can be concluded that regular online washing cannot prevent type-B performance losses but does minimize them.

It was explained above that the compressor could not be offline washed directly before performance test 3 (see Table 1) due to operational reasons. The last offline wash took place 1200 equiva-

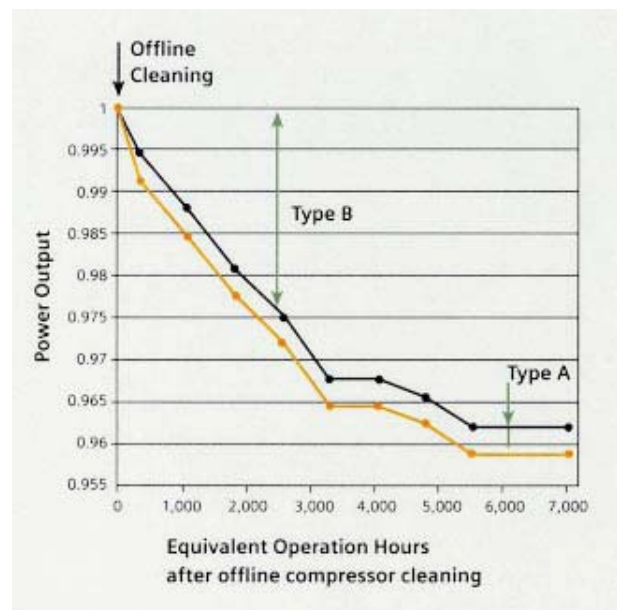


Fig. 5 Measured evolution of power output following offline compressor cleaning

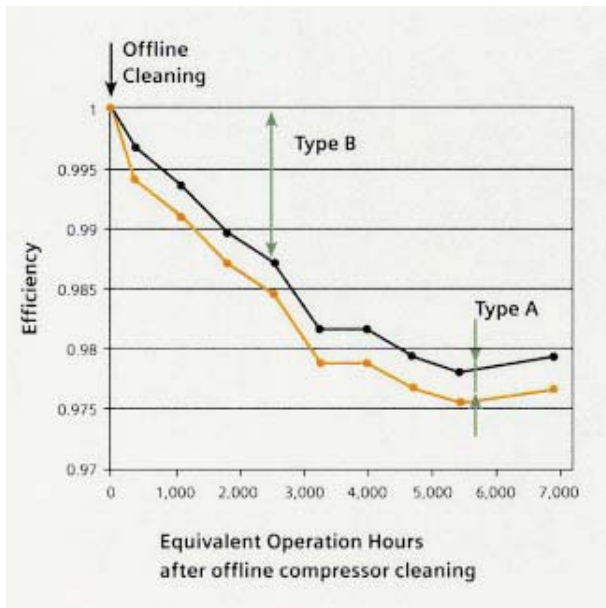


Fig. 6 Measured evolution of efficiency following offline-compressor cleaning

lent operating hours prior to that test. If the initial gradients for power and efficiency (compare Figs. 5 and 6) are taken into account, the values of test 3 can be corrected for an offline cleaned condition. The corrected values are listed in the column which is denoted test 3 (corrected) in Table 1. With this correction, there is a total loss in power output of 900 kW (1.4%) compared to the acceptance test (test 1). For efficiency, there are no losses after almost 50,000 EOH of operation. These values are remarkably low, underlining the positive impact of this state of the art cleaning system.

When tests 2 and 3 (corrected) are compared, the losses between major outages are 1800 kW (2.8%) for power output and 0.3% ($\Delta \eta / \eta = 0.8\%$) for efficiency. Again, it should be mentioned that test 2 values were above the acceptance test performance and were recorded with a fully hand cleaned compressor. This level cannot be considered as fully representative for long term commercial operation.

The test 2 and 3 values in Table 1 do not fully correspond to the curves in Fig. 4. This is due to the higher measurement errors of the plant instrumentation and the associated correction procedure.

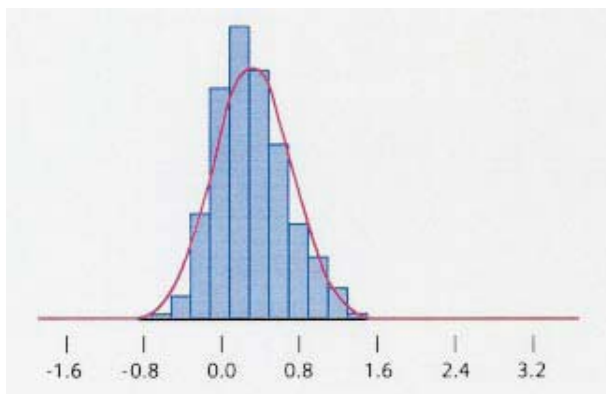


Fig. 7 Probability density function for power output benefits resulting from online-compressor cleaning

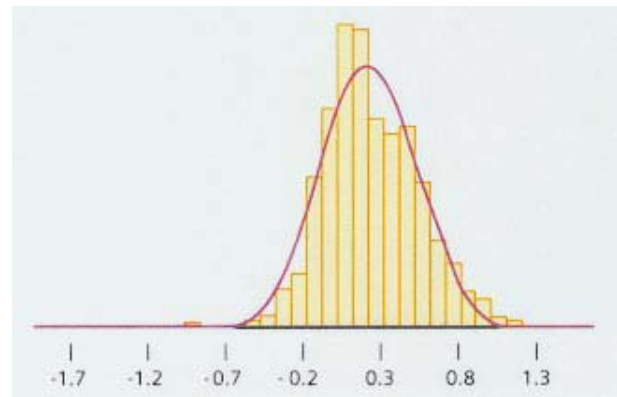


Fig. 8 Probability density function for efficiency benefits resulting from online-compressor cleaning

However, the results obtained from the plant instrumentation clearly show the characteristic behavior of the benefit resulting from on- and offline compressor cleaning.

Conclusion

In this work, we have analyzed operational performance data of a Siemens Power Generation V64.3 unit equipped with an Advanced Compressor Cleaning System (ACCS). With its high level of automation and optimized online cleaning characteristics, this system is designed to lower maintenance cost and to increase long-term performance and availability for heavy-duty gas turbines. Although online compressor cleaning cannot be as effective as offline cleaning because of the evaporation of the cleaning agent in the compressor, we have shown that online cleaning leads to a lower gradient of performance losses in the intervals between offline washes. Furthermore, the performance level that was reached after almost 50,000 EOH was remarkably high, underlining the positive impact of ACCS for the prevention of long-term performance degradation.

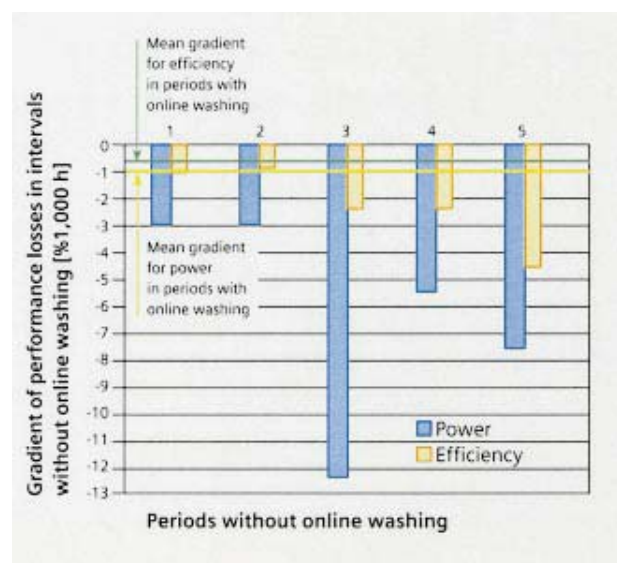


Fig. 9 Gradients of performance losses for intervals where online-washing was not carried out

Acknowledgment

We gratefully acknowledge the support of Jan-Dirk Beiler for the careful preparation and evaluation of the data and the diagrams.

Nomenclature

\dot{m} = massflow
 p = pressure
 T = temperature
 P = power output
 η = efficiency

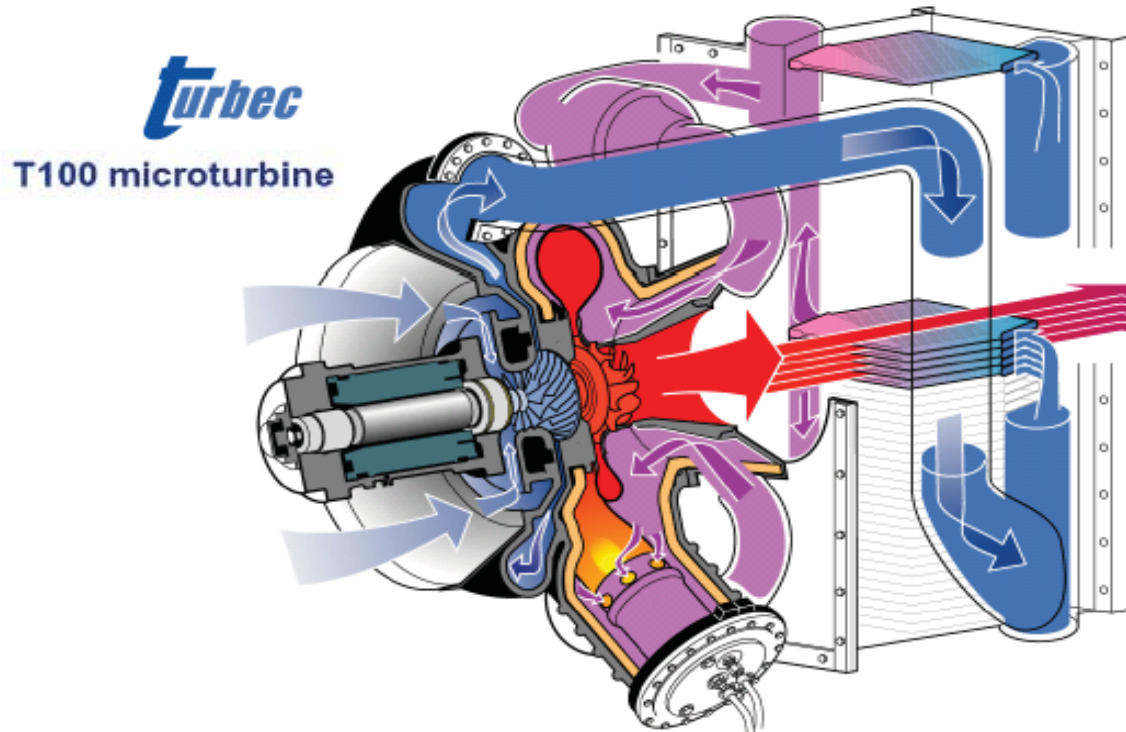
Indices:

T = turbine
 m = monthly mean
ON = online cleaning
OP = operation

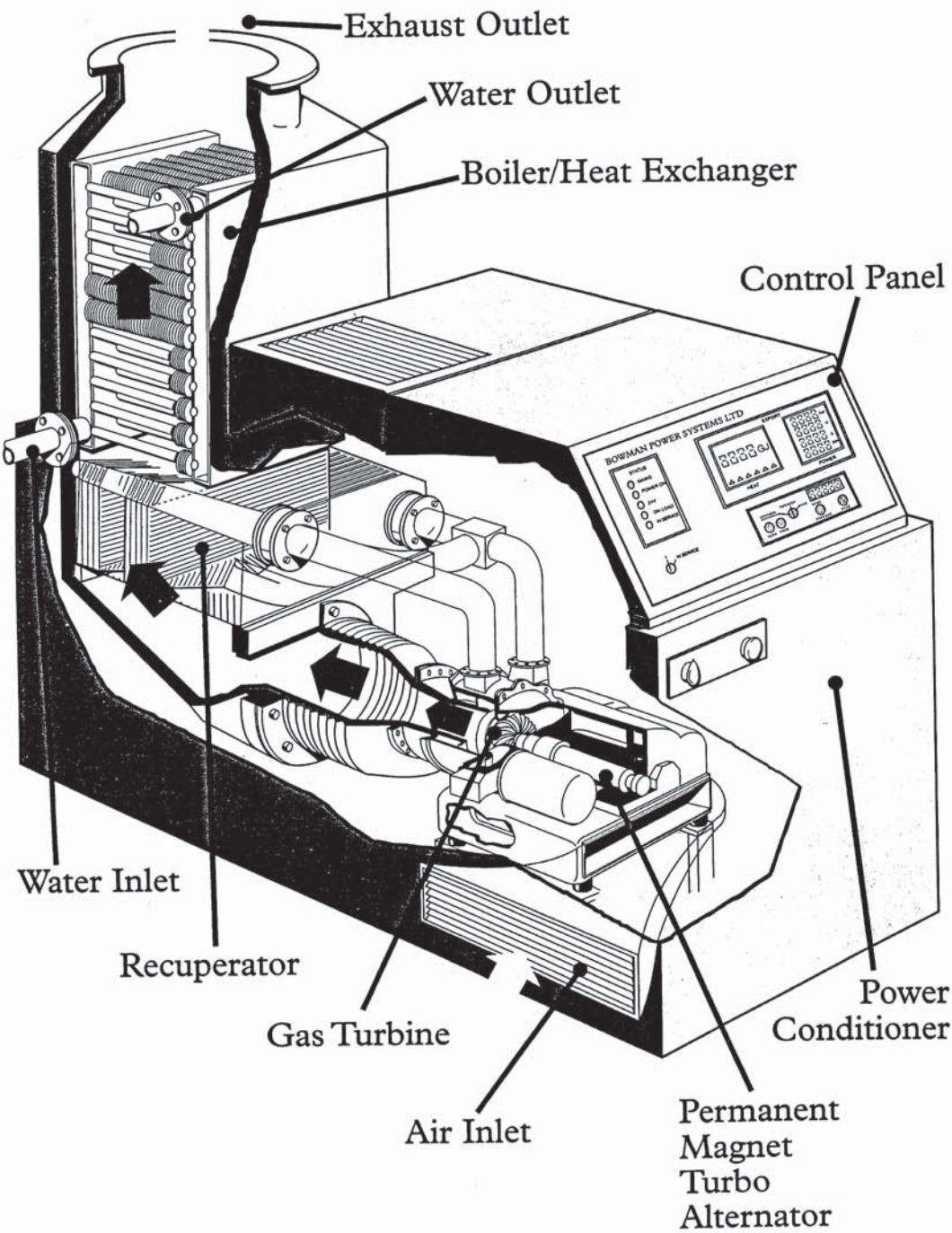
References

- [1] Meher-Homji, C. B., 2000, "Compressor Fouling . . . Causes and Solutions," Global Gas Turbine News, IGTI, **40**(3).
- [2] Diakunchak, I. S., 1991, "Performance Deterioration in Industrial Gas Turbines," ASME Paper 91-GT-228.
- [3] Adams, J., and Schmitt-Wittrock, P., 1981, "Optimierung der Reinigungsintervalle von Gasturbinenverdichtern," Brennst.-Warme-Kraft, **33**(1).
- [4] Haub, G. L., and Hauhe, W. E., 1990, "Field Evaluation of Online-Compressor Cleaning in Heavy Duty Industrial Gas Turbines," ASME-paper 1990-GT-107.
- [5] de Jong, M. P., Laagland, G. H. M., and Zeijseink, A. G. L., 2000, "Optimizing Compressor Cleaning," Power Gen.
- [6] Stalder, J.-P., 1994, "Compressor Washing Maintains Plant Performance and Reduces Cost of Energy Production," ASME Paper 1994-GT-436.
- [7] Stalder, J.-P., 1998, "Gas Turbine Compressor Washing State of the Art—Field Experiences," ASME Paper 1998-GT-420.
- [8] ISO 2314, International Standard, "Gas turbines—Acceptance Tests," 2nd edition, 1989.
- [9] Umlauf, R., and Lipiak, G., 2000, "Operating Experience and Potential After 10 Years of Siemens VX4.3 Gas Turbines," Power Gen.
- [10] KREISPR, Siemens Internal Computer-Tool for Gas Turbine Thermodynamic Cycle Calculations, current version, 2002.
- [11] Traupel, W., 1988, *Thermische Turbomaschinen*, 3rd edition, Springer-Verlag, Berlin.
- [12] Kurz, R., and Brun, K., 2000, "Degradation of Gas Turbine Systems," ASME Paper 2000-GT-345.
- [13] Zwebek, A. I., and Pilidis, P., 2001, "Degradation Effects on Combined Cycle Power Plants Performance, Part 1: Gas Turbine Cycle Component Degradation Effects," ASME paper 2001-GT-388.

- Microturbines are small fast-running gas turbines
- Power range: 20 – 500 kW
- Pressure ratio: $\sim 4 : 1$ High shaft speed $> 40\,000$ rpm
- Recuperator to increase electrical efficiency (25 – 30 %)
- Direct drive high-frequency alternator
- Attractive for distributed power generation and cogeneration application
- Recuperator bypass control for variable heat production for cogeneration



System Arrangement



TG80 Cogeneration System Performance
85% Effective Recuperator

Recuperator By-Pass Ratio	%	0	20	40	60	80	100
Recuperator In Gas Temp (EGT)	°C	615	615	615	615	615	615
Heat Exchanger Inlet Temperature	°C	278	352	426	484	547	615
Flue Temp	°C	95	95	95	95	95	95
Air Mass Flow	kg/s	0.835	0.835	0.835	0.835	0.835	0.835
Exhaust Mass Flow	kg/s	0.843	0.844	0.845	0.845	0.845	0.845
Thermal Output Power *	kW(th)	155	216	277	323	372	425
Water In Temp	°C	70	70	70	70	70	70
Water Out Temp	°C	90	90	90	90	90	90
Water Flow	kg/s	1.85	2.58	3.31	3.85	4.44	5.07
Engine Speed	RPM	68000	68000	68000	68000	68000	68000
Electrical Output Power	kW(e)	80	80	80	80	80	80
Generating Set Efficiency	%	26.00	23.00	20.00	17.60	15.80	14.10
Gas Fuel LHV	mJ/m ³	34.88	34.88	34.88	34.88	34.88	34.88
Gas Fuel Consumption	m ³ /hr	34.00	38.25	42.04	46.91	52.26	58.56
System Efficiency (not including GBC)	%	76	85	89	89	89	89
GBC Power Consumption	kW(e)	4.10	4.61	5.07	5.65	6.30	7.06
Net System Electrical Efficiency (Including GBC Loss)	%	24.67	21.67	18.73	16.36	14.56	12.86
Net System Power Output (Including GBC Loss)	kW(e)	75.90	75.39	74.93	74.35	73.70	72.94
Overall System Efficiency (Including GBC loss)	%	75	84	88	87	88	88

All values at uninstalled ISO conditions (sea level and 15°C)
* Includes heat recovered from oil

Output Available: 208-480 V, 3 phase, 50/60 Hz

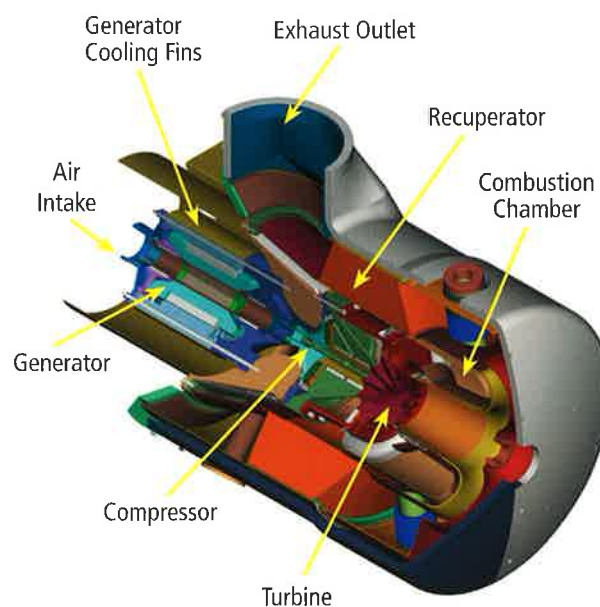
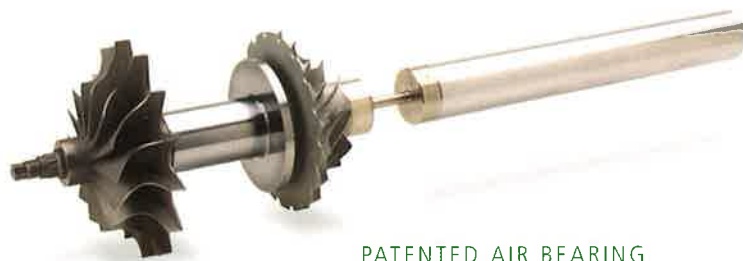
Engine Derating: As per curves ref TN/00028, Issue 2

Capstone Microturbines

Capstone microturbines are used in distributed power generation applications including cogeneration, resource recovery, secure power, and hybrid electric vehicles (HEV).

Low-emission, clean-and-green Capstone microturbines are scalable from 30kW to 10MW. The C1000 Power Package, the world's first megawatt microturbine power system, can be configured into smaller 800kW and 600kW solutions – all within a single ISO-type container. Models are available that operate on: Natural Gas, Propane, Landfill Gas, Digester Gas, Diesel, Aviation, and Kerosene fuels.

- Ultra-low emissions
- One moving part – minimal maintenance and downtime
- Patented air bearing – no lubricating oil or coolant required
- 5 and 9 year Factory Protection Plans available
- Remote monitoring and diagnostic capabilities
- Integrated synchronization and protection
- Reliable – tens of millions of run hours and counting



C30



C65



C65 ICHP



C65 CARB



HAZARDOUS LOCATIONS

Model	Fuels ⁽⁵⁾	Power Output ⁽¹⁾	Electrical Efficiency	Exhaust Gas Flow		Exhaust Temperature		Net Heat Rate		Dimensions ⁽²⁾ (W x D x H)	
		kW	%	kg/s	lbm/s	C°	F°	MJ/kWh	btu/kWh	m	in
GASEOUS FUELS ⁽³⁾											
C30 LP	NG	28	25	0.31	0.68	275	530	13.8	13,100	0.76 x 1.5 x 1.8	30 x 60 x 70
C30 HP	NG, P, LG, DG	30	26	0.31	0.68	275	530	13.8	13,100	0.76 x 1.5 x 1.8	30 x 60 x 70
C30 HZLC ⁽⁴⁾	NG	30	26	0.32	0.70	275	530	13.8	13,100	0.87 x 2.9 x 2.2	34 x 112 x 85
C65	NG, P	65	29	0.49	1.08	309	588	12.4	11,800	0.76 x 1.9 x 1.8	30 x 77 x 76
C65 ICHP	NG, P, LG, DG	65	29	0.49	1.08	309	588	12.4	11,800	0.76 x 2.2 x 2.4	30 x 87 x 93
C65 CARB	NG	65	28	0.51	1.13	311	592	12.9	12,200	0.76 x 2.2 x 2.6	30 x 87 x 103
C65 CARB	LG, DG	65	29	0.49	1.08	309	588	12.4	11,800	0.76 x 2.2 x 2.6	30 x 77 x 85
C65 HZLC ⁽⁴⁾	NG	65	29	0.50	1.09	325	617	12.9	12,200	0.87 x 3.2 x 2.3	35 x 128 x 90
C200 LP	NG	190	31	1.3	2.9	280	535	11.6	11,000	1.7 x 3.8 x 2.5	67 x 150 x 98
C200 HP	NG, P, LG, DG	200	33	1.3	2.9	280	535	10.9	10,300	1.7 x 3.8 x 2.5	67 x 150 x 98
C200 HZLC ⁽⁴⁾	NG	200	33	1.3	2.9	280	535	10.9	10,300	1.9 x 3.2 x 3.1	74 x 126 x 122
C600 LP	NG	570	31	4.0	8.8	280	535	11.6	11,000	2.4 x 9.1 x 2.9	96 x 360 x 114
C600 HP	NG, P, LG, DG	600	33	4.0	8.8	280	535	10.9	10,300	2.4 x 9.1 x 2.9	96 x 360 x 114
C800 LP	NG	760	31	5.3	11.7	280	535	11.6	11,000	2.4 x 9.1 x 2.9	96 x 360 x 114
C800 HP	NG, P, LG, DG	800	33	5.3	11.7	280	535	10.9	10,300	2.4 x 9.1 x 2.9	96 x 360 x 114
C1000 LP	NG	950	31	6.7	14.7	280	535	11.6	11,000	2.4 x 9.1 x 2.9	96 x 360 x 114
C1000 HP	NG, P, LG, DG	1000	33	6.7	14.7	280	535	10.9	10,300	2.4 x 9.1 x 2.9	96 x 360 x 114
LIQUID FUELS ⁽⁵⁾											
C30	D, A, K	29	25	0.31	0.69	275	530	14.4	13,700	0.76 x 1.5 x 1.9	30 x 60 x 70
C65	D, A, K	65	29	0.49	1.08	309	588	12.4	11,800	0.76 x 1.9 x 1.8	30 x 77 x 76
C65 ICHP	D, A, K	65	29	0.49	1.08	309	588	12.4	11,800	0.76 x 2.2 x 2.4	30 x 87 x 93
C200	D	190	30	1.3	2.9	280	535	10.9	10,300	1.7 x 3.8 x 2.5	67 x 150 x 98

⁽¹⁾ Nominal full power performance at ISO conditions: 59° F, 14.696 psia, 60% RH

⁽²⁾ Height dimensions are to the roofline. Exhaust outlet can extend up to 7 inches above the roofline.

⁽³⁾ Models available to operate on these different fuels: NG – Natural Gas; P – Propane; LG – Landfill Gas; DG – Digester Gas

⁽⁴⁾ Hazardous Location units suitable for use in potentially explosive atmospheres (UL Class I, Division 2 or Atex Class I, Zone 2)

⁽⁵⁾ Models available to operate on these different fuels: D – Diesel; A – Aviation; K – Kerosene

Specifications are not warranted and are subject to change without notice.



C200



C1000

State of direct fuel cell/turbine systems development[☆]

Hossein Ghezel-Ayagh*, Jim Walzak, Dilip Patel, Joseph Daly,
Hans Maru, Robert Sanderson, William Livingood

FuelCell Energy, Inc., 3 Great Pasture Road, Danbury, CT 06813, USA

Received 30 November 2004; received in revised form 24 December 2004; accepted 24 December 2004
Available online 13 March 2005

Abstract

FuelCell Energy Inc. (FCE) is actively developing fuel cell/gas turbine hybrid systems, DFC/T®, for generation of clean electric power with very high efficiencies. The gas turbine extends the high efficiency of the fuel cell without the need for supplementary fuel. Key features of the DFC/T system include: electrical efficiencies of up to 75% on natural gas (60% on coal gas), minimal emissions, simple design, reduced carbon dioxide release to the environment, and potential cost competitiveness with existing combined cycle power plants. FCE successfully completed sub-MW scale proof-of-concept tests (pre-alpha DFC/T hybrid power plant). The tests demonstrated that the concept results in higher power plant efficiency. A small packaged natural gas fueled sub-MW unit is being developed for demonstrations (alpha and beta units). Also, the preliminary design of a 40 MW power plant including the key equipment layout and the site plan was completed.

© 2005 Elsevier B.V. All rights reserved.

Keywords: Carbonate fuel cell; Internal reforming fuel cell; Gas turbine; Hybrid power plant; Multi-MW plant design; MCFC

1. Introduction

In recent years, there has been a surge of interest in the integration of the fuel cells with gas turbines for electric power generation. The premise of these power cycles are ultra high efficiency and very low emissions. Among various types of fuel cells, the high temperature type (>600 °C), including solid oxide fuel cell (SOFC) and molten carbonate fuel cell (MCFC), is suitable for integration with gas turbines [1]. The gas turbines being mechanical energy conversion devices operate more efficiently at higher temperatures (turbine inlet). The hybrid fuel cell/gas turbine systems using SOFC [2] and MCFC [3] have been studied and optimized for performance.

FCE's DFC/T hybrid system concept is based on integration of the company's internal reforming Direct FuelCell® [4,5] with an indirectly heated gas turbine to supplement fuel cell generated power. The fuel cell plays the key role by producing the larger share of the power (>80%). The gas turbine

is utilized for generation of additional power by recovering the fuel cell byproduct heat in a Brayton cycle, as well as for providing the air for fuel cell operation. The power plant design consists of a novel waste heat recovery approach for extraction of heat from the fuel cell exhaust [6]. Because of the indirect heat transfer to the turbine expander and absence of a combustor, NO_x is not generated by the gas turbine.

One of the key features of DFC/T concept is the independent (uncoupled) operating pressure of the fuel cell and turbine. Hence, the system works very efficiently with a wide range of air compression ratios (3–15). Typically, small-scale gas turbines (micro-turbines) use a low compression ratio (3–4), while the MW-size units are designed for high compression ratios (7–15). The DFC/T system design is suitable over a range of applications from sub-MW industrial to medium scale (MW) distributed generation to large central station plants. The concept also features adeptness to the existing industrial frame gas turbines. Based on these features, FCE embarked on the proof-of-concept tests integrating a fuel cell stack with a micro-turbine. The results of these tests were also used to provide the design (mechanical and control) information for development of multi-MW scale power plants. The current Vision 21 project is intended to move

[☆] This paper was presented at the 2004 Fuel Cell Seminar, San Antonio, TX, USA.

* Corresponding author. Tel.: +1 203 825 6048; fax: +1 203 825 6273.

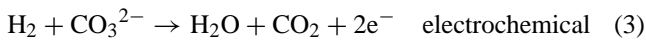
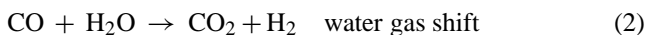
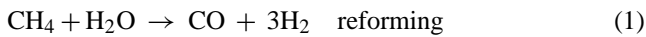
E-mail address: hghezel@fce.com (H. Ghezel-Ayagh).

forward the development of multi-MW power plants for the wholesale market.

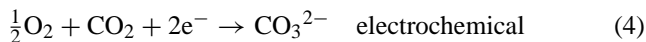
2. System description

The DFC/T system concept is schematically shown in Fig. 1. The system includes a heat recovery unit (HRU) consisting of a series of heat exchangers arranged to maximize the heat recovery from the cathode exhaust gas. The HRU has a dual functionality of preparing the anode gas, and also, transferring a portion of system exhaust heat to the gas turbine air (in low temperature recuperator, LTR). The preparation of anode gas includes humidification of natural gas by the feed water, and preheating of the anode gas to the fuel cell operating temperature. The humidification process provides the steam needed for the reforming of natural gas. Typically a steam-to-carbon ratio of two and higher is required for steam reformation of natural gas to prevent carbon formation. The mixed fuel and steam are preheated to the temperature of about 550 °C prior to entering the fuel cell anode. The methane in the natural gas is steam reformed in the direct carbonate fuel cell (internal reforming) to hydrogen, which is the primary fuel for the fuel cell. The fuel cell reactions are:

Anode



Cathode



At the anode, hydrogen is electrochemically reacted producing dc electricity, and CO₂ and water vapor as byproducts. The availability of water vapor at anode as a product of electrochemical reaction helps drive the reforming reaction

to completion and minimizes the need for feed water to the system. The anode exhaust containing some unreacted fuel is mixed with air and then oxidized completely in a catalytic oxidizer.

In the turbine cycle, air is compressed to the operating pressure of the gas turbine and heated in the LTR using waste heat from the fuel cell. The compressed air is then heated further to the operating temperature of the gas turbine expander by a high temperature recuperator (HTR) located between the oxidizer and fuel cell (cathode). The hot compressed air is expanded in the turbine providing additional electricity. The expanded air then flows into the oxidizer. The oxidizer exhaust, containing excess air, flows into HTR, and subsequently into the fuel cell cathode. At the cathode, oxygen (in the air) and CO₂ (from the anode exhaust) are reacted to complete the fuel cell electrochemical reaction. The heat generated in the fuel cell as the byproduct of the electrochemical reaction is utilized partly to support the endothermic (methane) reforming reaction. The thermal integration of the fuel cell electrochemical and methane reforming reactions offered by the internal reforming direct fuel cell enhances the fuel cell electrical efficiency while helping in the thermal management of fuel cell stack/module. The cathode exhaust, containing the heat from fuel cell, provides the heat for preheating the air (in LTR) and fuel, and for generation of steam in HRU before exiting from the power plant.

3. Proof-of-concept tests

The focus of proof-of-concept tests was on the verification of the DFC/T concept, the developmental testing of critical system components and acquiring design information for development of power plant products. The first series of tests involved integration of a 250 kW (full-size) DFC stack with a modified Capstone Simple Cycle Model 330 micro-turbine. The micro-turbine was constructed with a compressed air exhaust port and expander inlet pipe to provide flow connections

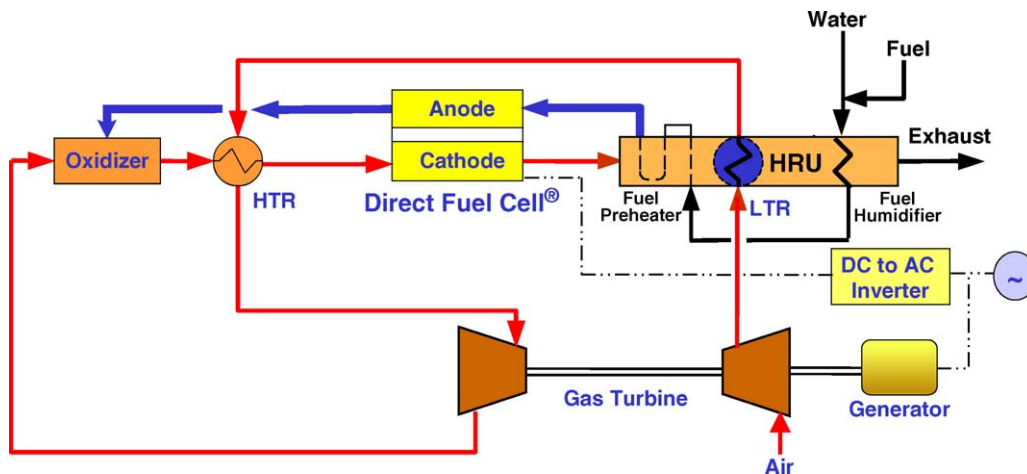


Fig. 1. DFC/T[®] ultra high efficiency system concept: fuel cell byproduct heat is utilized in gas turbine to supplement fuel cell power.

to the fuel cell system. An air blower was also included in the power plant, which increased the flexibility of operation for the testing purposes. The power plant was capable of operating in dual modes: fuel cell/turbine integrated mode and fuel cell only mode. The dual mode capability was used to evaluate the benefits of the DFC/T cycle over the fuel cell-only cycle. The results of the first phase of tests have previously been presented and published [7,8]. The dual mode operation confirmed that greater efficiencies could be obtained by integration of micro-turbine with the fuel cell. As micro-turbine with higher airflow became available, the next phase of tests were conducted after replacing Capstone Model 330 with Capstone C60. These tests also benefited from the next generation of full-size fuel cell stack. Fig. 2 shows a picture of the DFC/T power plant facility with the C60 micro-turbine integrated in the fuel cell system. Fig. 3 shows a simplified process flow sheet for the sub-MW DFC/T power plant, including a typical set of process operational data. Three heat recuperators for indirect heating of air from the compressor side of the micro-turbine were included. The anode exhaust oxidizer included a high temperature catalytic section.

The proof-of-concept test was completed verifying the DFC/T concept. The world's first grid-connected fuel cell/turbine hybrid system operated for >6600 h. Thermal management of the system was confirmed by increasing micro-turbine expander inlet temperature while controlling the fuel cell operating temperature. The control strategies were refined based on the operational experience. The tests successfully demonstrated the ability of the control system to follow prescribed load ramps and to respond to abrupt utility grid outages. The system trip/emergency shutdown scenarios were tested successfully. The power plant operation was



Fig. 2. Sub-MW DFC/T hybrid power plant facility: full-size DFC stack was integrated with capstone C60 micro-turbine.

demonstrated using the micro-turbine as the only source of fresh air supply to the system. The operational tests, as well as the tests of the power plant heat-up during the process and control checkout of the balance-of-plant (BOP), confirmed the stable and well-controlled operation of the DFC/T power plant with the micro-turbine. NO_x emission levels of less than 0.25 ppm were achieved. Computer simulation of the power plant including mass and energy balances was utilized as analytical tool during the testing period. The BOP equipment and the micro-turbine performance were monitored and eval-

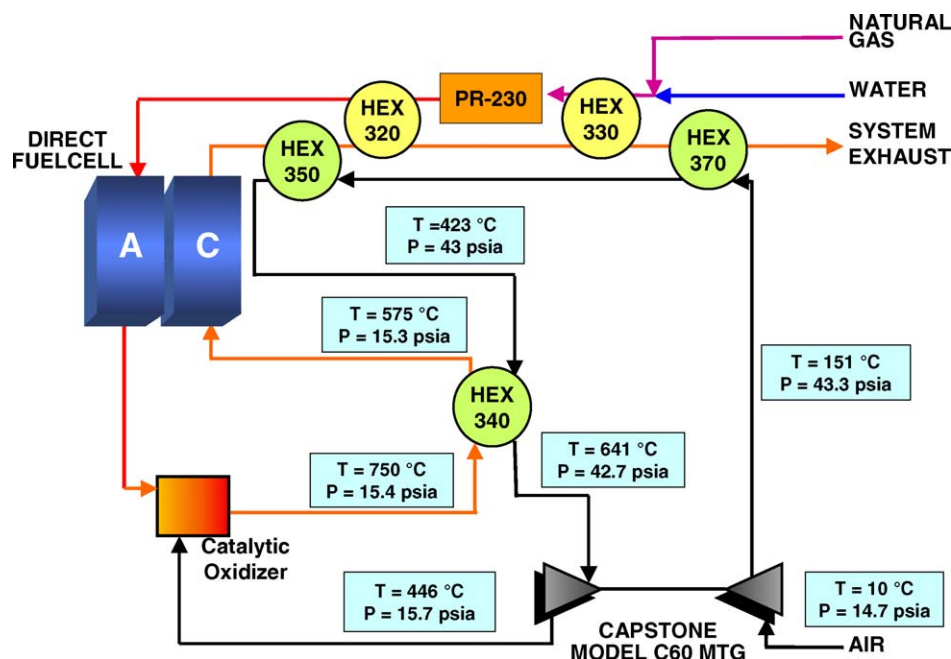


Fig. 3. Sub-MW DFC/T hybrid power plant facility process flow diagram: a typical set of operational data are included.

uated. The heat transfer coefficients for the heat exchangers were analyzed against the vendor supplied information. The heat losses from the pipes and equipment in the power plant test facility were estimated. The results of the sub-MW system tests have indicated that effective recuperation of heat to the gas turbine and minimization of the heat loss from the BOP equipment are important factors in the design of DFC/T power plants.

4. Sub-MW power plant design and demonstrations

Demonstration of DFC/T system configuration in sub-MW class power plant units for distributed generation is the next step in evolution of the hybrid systems. FuelCell Energy has planned to build and test a packaged DFC/T power plant at its facility in Danbury, CT (alpha unit), and then demonstrate the second DFC/T power plant (beta unit) in Montana. These DFC/T sub-MW plants will demonstrate grid-connected operations, help assess the efficiency potential of the sub-MW plants and provide valuable data on integration and operation of DFC/T power plants under laboratory and field conditions.

The preliminary design of the sub-MW packaged demonstration unit has been completed. Steady-state mass and energy balances for the power plant were performed for various modes of operation; including start-up, standby, and full load operation; using the CHEMCAD process simulation software. The process equipment specifications were prepared and issued to original equipment manufacturers (OEM) and suppliers for quotation. A process flow diagram of the power plant including major operating equipment along with the plant start-up equipment was generated. The design modifications of existing DFC300A fuel cell module for application to the DFC300/T system were completed. A safety review of the DFC300T system was conducted based on the Hazop methodology utilized widely by the process industries. A set of piping and instrumentation diagrams (P&IDs), with instrument and equipment design information, was also prepared

incorporating design information and recommendations from sub-MW proof-of-concept test results, DFC300 product data and the Hazop safety review mentioned above. Suppliers for key equipment such as micro-turbine, recuperators and anode gas oxidizer have been selected. Three-dimensional equipment (process, utility and other) and piping layout drawings were prepared using the intergraph plant design software. Pipe stress analysis was completed using Caesar II software, generating specifications for expansion joints and pipe supports. Specifications for all valves including safety valves and pressure regulators were prepared, and bids were solicited from the suppliers. Design parameters and specifications have been developed for key instrument and control equipment. All major equipment and instrument items have been ordered. The procurement is in progress.

A preliminary review of potential demonstration sites in Montana for the beta sub-MW unit was completed. Two venues in Montana, including the Engineering/Physical Science Building at Montana State University (Bozeman, MT) and the Deaconess Billings Clinic (Billings, MT), were investigated. Both sites were found to be suitable for the demonstration.

5. Multi-MW power plant design

The baseline DFC/T configuration included a high temperature recuperator. The multi-MW power plant performance (power output and efficiency) estimates for the near, intermediate and long-term systems, based on this configuration, are presented in Table 1. For comparison, performance estimates for the DFC-only systems are also shown in the table. Based on the comparison, the integration of the fuel cell with turbine in a hybrid system offers significant improvement in power plant electrical efficiency. The mid-term and long-term estimates are both based on improved fuel cell performance expected with fuel cell developments. The long-term system, in addition, employs an advanced gas turbine featuring in-

Table 1
Multi-MW DFC/T power plant (baseline configuration) performance projections

	Near-term		Mid-term		Long-term
	DFC	DFC/T hybrid	Improved DFC	DFC/T hybrid with improved DFC	DFC/T hybrid with intercooled & re-heat gas turbine
Fuel cell					
dc power out (MW)	12.0	12.0	16.8	16.8	33.5
ac power out, gross (MW)	11.3	11.3	16.4	16.3	32.7
Gas turbine					
Expander power (MW)		7.9		8.7	20.7
Compressor power (MW)		(5.3)		(5.9)	(10.9)
Net ac out (MW)		2.5		2.6	9.3
Air blower power (MW)	(0.3)		(0.3)		
Auxiliary power consumption (MW)	(0.1)	(0.1)	(0.1)	(0.1)	(0.2)
Net power output (MW)	11.0	13.7	15.9	18.8	41.8
Efficiency (%) (LHV natural gas)	49.9	62.0	57.0	67.0	74.6

Hybrid system has potentially significant efficiency gain over DFC-only system.

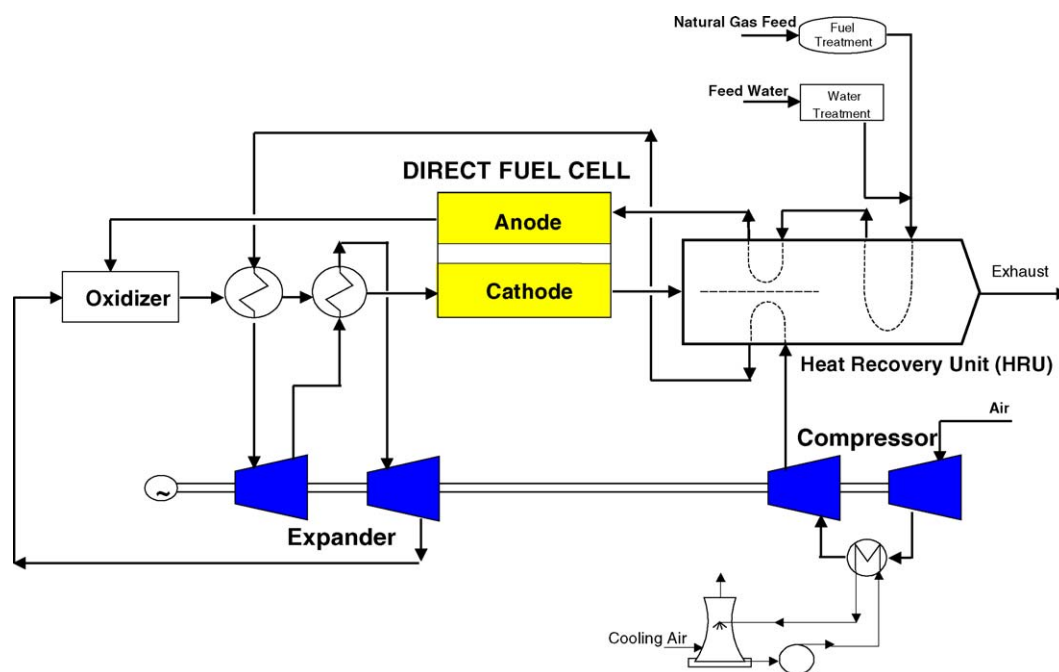


Fig. 4. Process flow diagram of the long-term multi-MW DFC/T hybrid system: system features an advanced gas turbine with intercooled and re-heat cycle.

tercooled and reheat cycle that might be available in future with gas turbine developments. Fig. 4 shows the process flow diagram of the system. The long-term system has a potential to offer system electrical efficiency approaching 75% (LHV natural gas).

The preliminary design of a 40 MW power plant for near-term application was completed. The design is based on a scalable approach using FCE's existing M-10 (MW-scale) fuel cell modules in a cluster arrangement. The fuel cell cluster design has five M-10 modules in a cluster with common distribution piping for the fuel and oxidant gases. Based on the scalable overall plant design concept, the plant is arranged in three sections in addition to the centralized equipment. Each section consists of two clusters of fuel cell modules together with supporting equipment. The centralized equipment, which supports all three sections, includes a gas turbine, an anode gas oxidizer and other common site equipment such as a fuel clean-up subsystem and a water treatment subsystem.

The process flow diagrams with process controls for normal operation and start-up heating were generated. Steady-state mass and energy balances for the power plant were completed for various modes of operation; including start-up, standby, and full load operation. The performance of the 40 MW power plant estimated based on near-term fuel cell performance and a commercially available gas turbine is presented in Table 2. Specifications were prepared for key pieces of equipment and subsystems. Potential suppliers were contacted, and preliminary configuration information and cost estimates were obtained. The gas turbine selected for the 40 MW plant design is a Man Turbo Model 1304-11. Man Turbo's THM heavy-duty gas turbine features a rugged

industrial design. Key characteristics of the gas turbine include: pressure ratio of eight and turbine inlet temperature of 1800 °F. The fuel clean-up subsystem is a centralized desulfurizer for the natural gas fuel, which uses activated carbon in an epoxy lined carbon steel vessel. Electrical one-line diagrams were prepared for the power generation and auxiliary power needs. The power conditioning system (PCS) is designed to convert the 300 VDC from the fuel cells to 13.8 kV and is modular. A PCS module supports each fuel cell cluster. The 6000 kW modular unit is a packaged assembly that includes IGBT-based inverters and a step-up transformer. The central control system for the plant is designed to coordinate the output of the three plant sections (six PCS modules). It provides operational sequence control for plant start-up heating, on-load operation, and normal and emergency shutdowns.

An overall layout/plot plan of the 40 MW plant is shown in Fig. 5. The site is approximately 273' × 325' in size. The

Table 2
Forty-megawatt DFC/T hybrid power plant performance (estimate)

Fuel cell	
dc power output (MW)	36.1
ac power output (MW)	34.3
Gas turbine	
Expander power (MW)	21.8
Compressor power (MW)	(10.4)
Net ac power (MW)	10.8
Plant parasitic load	
Anode gas compressor (MW)	(3.6)
Other auxiliary loads (MW)	(0.8)
Net power output (MW)	40.8
Efficiency (%) (LHV of natural gas)	61.8

An electrical efficiency of 62% is expected in a near-term system.

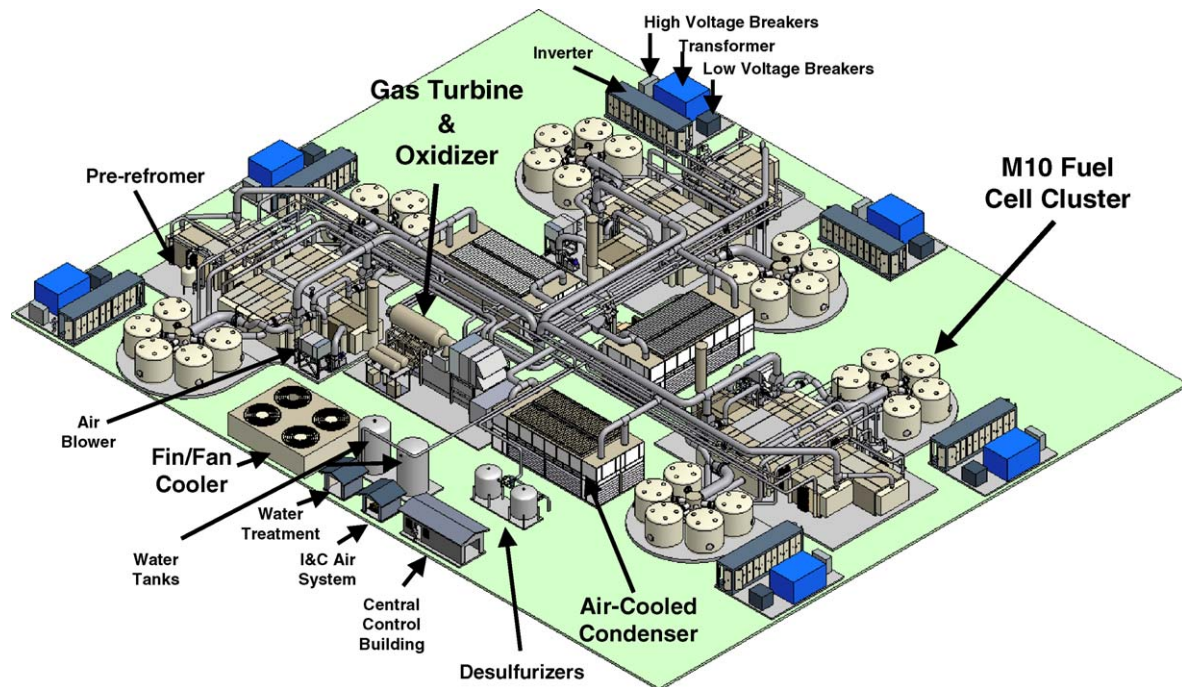


Fig. 5. Forty megawatt plant layout/plot plan: power plant is divided into three sections, each containing a pair of fuel cell module clusters.

arrangement of equipment on the site is designed to provide easy access to the equipment for maintenance and replacement, and minimize the length for the largest process piping. Design of the site arrangement included sizing of all the process piping and the development of process pressure profiles consistent with performance estimates. Thermal insulation requirements were established for all the process piping based on a surface touch temperature limit criteria. A computer model was developed for detailed design of the piping system including pipe sizes and insulation thickness requirements.

6. Conclusions

The proof-of-concept test of the DFC/T system in the sub-MW power plant facility was completed achieving the milestone of being the world's first grid-connected hybrid fuel cell/gas turbine power plant. Thermal management of the system was confirmed. The control strategies were refined. System trip/emergency shutdown scenarios were tested successfully. Power plant operation, using a microturbine as the only source of fresh air supply to the system, was demonstrated.

The preliminary design of the sub-MW hybrid packaged unit (for alpha demonstration) has been completed. Design modifications to the existing DFC-300A fuel cell module for its application to the DFC300/T unit were completed. A Hazop safety review of the DFC300/T system was completed and a set of P&IDs was refined. All major equipment and instrumentation items have been ordered. Procurement of parts and system components is in progress.

A scalable approach for the multi-MW plant design based on fuel cell clusters of the existing 1 MW (M-10) modules has been developed. Preliminary design for the 40 MW DFC/T hybrid system using a commercially available gas turbine was completed. The system electrical efficiency (LHV) based on near-term fuel cell performance was estimated to be 62%. Process flow diagrams with equipment and controls for operation and start-up have been prepared. Major equipment specifications were prepared and vendor quotes were solicited. Electrical one-line diagrams have been generated. Plant pipe sizing and insulation requirements were determined. Major equipment layouts and power plant plot plans have been generated.

Acknowledgements

The development of Direct Fuel Cell[®]/Turbine hybrid power system is being performed as a cost-shared Vision 21 project supported by the US Department of Energy through the National Energy Technology Laboratory (NETL) under contract DE-FC26-00NT40798. The technical guidance of Mr. Norman Holcombe, the DOE Contracting Officer's Representative (COR) of NETL is acknowledged.

References

- [1] M.C. Williams, J.P. Strakey, S.C. Singhal, U.S. distributed generation fuel cell program, *J. Power Sources* 131 (May (1–2)) (2004) 79–85.
- [2] Y. Yi, A.D. Rao, J. Brouwer, G.S. Samuelsen, Analysis and optimization of a solid oxide fuel cell and intercooled gas turbine

- (SOFC–ICGT) hybrid cycle, *J. Power Sources* 132 (May (1–2)) (2004) 77–85.
- [3] P. Lunghi, R. Bove, U. Desideri, Analysis and optimization of hybrid MCFC gas turbines plants, *J. Power Sources* 118 (May (1–2)) (2003) 108–117.
- [4] J. Doyon, M. Farooque, H. Maru, The direct fuelcell stack engineering, *J. Power Sources* 118 (May (1–2)) (2003) 8–13.
- [5] M. Farooque, H. Ghezel-Ayagh, Molten carbonate fuel cells and systems, system design, part 7, in: W. Vielstich, A. Lamm, H. Gasteiger (Eds.), *Handbook of Fuel Cells, Fundamentals Technology and Applications*, vol. 4. Fuel Cell Technology and Applications, Part 2, John Wiley and Sons, LTD., 2003, pp. 942–968 (Chapter 68, ISBN 0-471-40026-9).
- [6] H. Ghezel-Ayagh, A.J. Leo, R. Sanderson, High-Efficiency Fuel Cell System, U.S. Patent No. 6,365,290 (April 2002).
- [7] H. Ghezel-Ayagh, H. Maru, Direct fuel cell/turbine system for ultra high efficiency power generation, in: 2002 Fuel Cell Seminar, Palm Springs, CA November 18–21, 2002.
- [8] H. Ghezel-Ayagh, J.M. Daly, Z. Wang, Advances in direct fuel cell/gas turbine power plants, in: *Proceedings of ASME/IGTI Turbo Expo*, 2003 (ASME Paper GT 2003-38941).



Performance comparison of three solid oxide fuel cell power systems

Junxi Jia^{1,*}, Abuliti Abudula², Liming Wei³ and Yue Shi¹

¹College of Power and Energy Engineering, Harbin Engineering University, Harbin 150001, China

²North Japan New Energy Research Center, Hirosaki University, Aomori 030-0813, Japan

³School of Electric and Electronic Information Engineering, Jilin Architectural and Civil Engineering Institute, Changchun 130021, China

SUMMARY

An energy analysis of three typical solid oxide fuel cell (SOFC) power systems fed by methane is carried out with detailed thermodynamic model. Simple SOFC system, hybrid SOFC-gas turbine (GT) power system, and SOFC-GT-steam turbine (ST) power system are compared. The influences of air ratio and operative pressure on the performance of SOFC power systems are investigated. The net system electric efficiency and cogeneration efficiency of these power systems are given by the calculation model. The results show that internal reforming SOFC power system can achieve an electrical efficiency of more than 49% and a system cogeneration efficiency including waste heat recovery of 77%. For SOFC-GT system, the electrical efficiency and cogeneration efficiency are 61% and 80%, respectively. Although SOFC-GT-ST system is more complicated and has high investment costs, the electrical efficiency of it is close to that of SOFC-GT system. Copyright © 2013 John Wiley & Sons, Ltd.

KEY WORDS

solid oxide fuel cell; hybrid power system; electric efficiency

Correspondence

*Junxi Jia, College of Power and Energy Engineering, Harbin Engineering University, Harbin 150001, China.

†E-mail: jjajunxi99@sohu.com

Received 6 September 2012; Revised 8 November 2012; Accepted 11 November 2012

1. INTRODUCTION

Conventional energy conversion systems using fossil fuels are known by their negative impact through greenhouse gas emissions and air pollution, and these impacts will increase as an energy demand increases. These impacts can be reduced or eliminated by using an alternative conversion technology like solid oxide fuel cell (SOFC) to generate heat and power as needed for different applications.

SOFC converts the chemical energy of the fuel directly to electrical energy. It can achieve high electrical efficiencies and is a highly environmentally benign method of electric power production [1].

Hydrogen is the most commonly used fuel in the fuel cell technology, but natural gas, biomass gasification synthesis gas, and petroleum-based fuel can also be used. SOFCs, because of their high operating temperatures, do not require pure hydrogen as fuel, exhibiting a high fuel flexibility, which is a major advantage concerning the high cost of hydrogen production [2–4].

The high operating temperature of SOFC gives good possibilities for cogeneration applications. There have

been numerous models developed to simulate performance of SOFC power systems [5–24]; the features of these models are different.

Some simple SOFC system can be used for residential scales power applications. Bedringas *et al.* [5] have reported that a system electrical efficiency near 60% could be achieved for a SOFC system with external reforming. Chan *et al.* [6] presented a discussion of simple SOFC system without gas turbine (GT) fed by hydrogen and methane, respectively, and results shows both a H₂-fed system and a CH₄-fed system can achieve an electrical efficiency of more than 50%.

Jia *et al.* [7] have analyzed the effects of gas recycle on performance of SOFC power systems. Results show that internal reforming SOFC power system can achieve an electrical efficiency of more than 44% and a system cogeneration efficiency including waste heat recovery of 68%.

Some models available in the literatures [8–24] focus on complicated hybrid SOFC and GT power system.

The works of literatures [8–10] examined the effects of operating pressure, steam-to-carbon ration, and fuel flow rate on performance of SOFC-GT power systems. Refs. [11–18] address a full and partial load analysis of hybrid SOFC-GT

power plant. Electric efficiencies of these hybrid systems are higher than 60% at design point and also very high at part load condition.

Yi *et al.* [19] introduced a SOFC and intercooled GT hybrid cycle, and system electrical efficiency is even higher than 75% when operating pressure is 50 bar, and an excess air in the SOFC is low.

Duan *et al.* [20] and Odukoya *et al.* [21] studied the SOFC–micro GT hybrid power system. Their research results show that turbine inlet temperature is a key parameter that limits the electrical efficiency of hybrid power system. Increasing of fuel utilization factor is an effective measure to improve the performance of hybrid system. Both the electrical efficiency of hybrid power system and turbine inlet temperature reduce with the increase of the ratio of steam to carbon.

A good air conditioning system is one of the key features of energy-saving building. The SOFC integration system, which combines heat, power, and cold, is more attractive to building services designers [22–24]. Malico *et al.* [22] designed a trigeneration system using a high-temperature fuel cell. VELumani *et al.* [23] analyzed a hybrid-combined heat and power system. The system considers the coupling of a SOFC stack, microturbine, and a single effect absorption cooling system. Results show that the electric efficiency could rise above 60%. If waste heat is utilized to provide heating or cooling, the thermal efficiency of the system can go above 70%. Akkaya *et al.* [24] presented an energetic performance analysis for a combined power generation system consisting of a SOFC and an organic Rankine cycle (ORC). First, Law efficiency is increased about 14–25% by recovering SOFC waste heat through ORC based on investigated design parameter conditions.

Many cogeneration system concepts [5–24] are conceivable with SOFC as mentioned above; they can be divided into three categories. Simple SOFC system can be used for residential scales power applications, integrating GTs into large SOFC plants (SOFC-GT), which is considered competitive in the market of distributed power supply and hybrid power system consisting of SOFC, GT, and steam turbine (ST). As few of the papers mentioned above compared and analyzed all three SOFC power systems together, this study aims to investigate the performance assessment of these power systems. A mathematical model of the internal-reforming SOFC, which is the heart of the system, has been developed that takes into account the influence of cell operative pressure, air ratio, etc. These three typical SOFC power systems mentioned above are compared by energy analysis. The irreversibility of each system is discussed; then, the possibilities for improvements are made.

2. SYSTEM CONFIGURATIONS AND DESCRIPTION

Figure 1 shows a simple SOFC system with heat recovery. Methane fuel enters the plant and is compressed to the system pressure requirements and preheated to a temperature

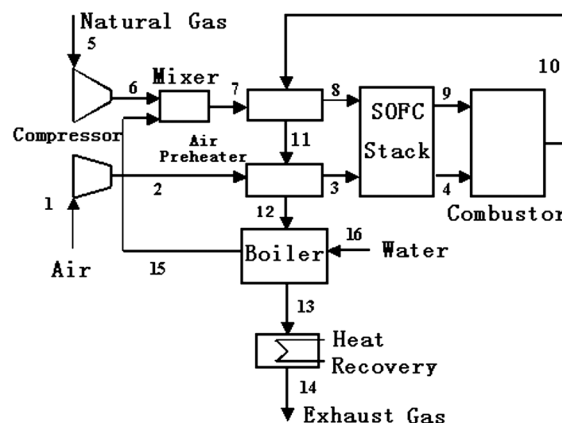


Figure 1. Configuration of simple SOFC power system.

below the cell-stack operating temperature about 850 °C. Air is pressurized and preheated to a temperature approximately below the cell-stack temperature before admittance into the SOFC stack. Methane and oxygen are channeled through the anode and cathode compartments, respectively. Methane is internally reformed in the anode compartment, and hydrogen-rich gas is produced. Oxygen in the air fed to the cathode accepts electrons from external circuit to form oxygen ions. The ions are conducted through the solid electrolyte to the anode. At the fuel electrode, the ions combine with hydrogen in the fuel to form water. Electrons flow from the anode through the external circuit back to the cathode. Since the electrochemical is exothermic, the cell produces heat as well as electricity. After exiting the cell, the residual fuel and excess air mix and react in the combustor. The combusted exhaust gases then flow through two heat exchangers to preheat the fuel and air. The exhaust gases then go into the boiler to produce superheated steam. The steam is mixed with methane then delivered to the preheater. The heat recovery is used to collect the useful heat, which is similar to that in a cogeneration plant. The system exhaust gases exit the system near 80 °C.

In contrast to the system in Figure 1, for SOFC-GT power systems shown in Figure 2, the high temperature and pressure effluent from the combustor is expanded through GT to generate the mechanical power, which is used to generate the electrical power. Then, the turbine exhaust is provided to heat the fuel and air.

The SOFC-GT-ST power system is shown in Figure 3; the electrical power is generated not only by the SOFC and GT, but also by the ST.

3. SYSTEM MODELING

3.1. SOFC model

In general, the ideal reversible potential of H₂-O₂ SOFC can be calculated by the Nernst equation:

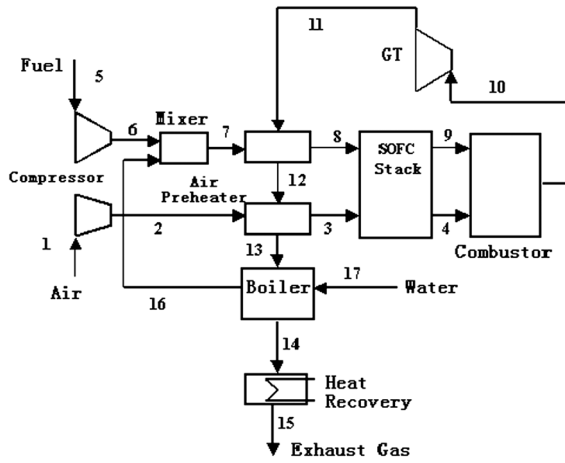


Figure 2. Configuration of SOFC-GT power system.

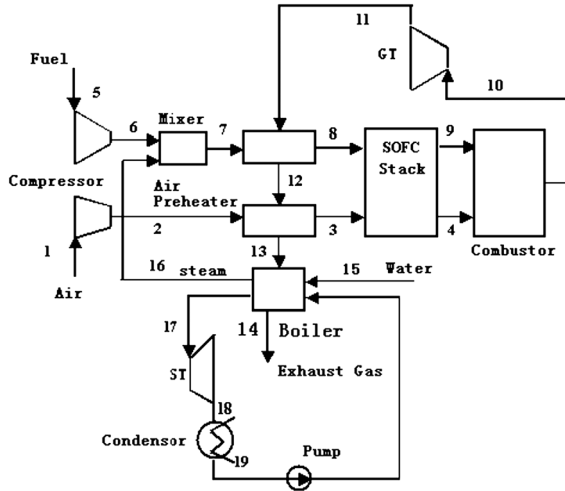


Figure 3. Configuration of SOFC-GT-ST power system.

$$E_0 = \frac{-\Delta G_0}{2F} + \frac{RT}{2F} \ln \frac{p_{H_2} \cdot (p_{O_2})^{1/2}}{p_{H_2O}} \quad (1)$$

Nernst potential is reduced to the terminal voltage by the sum of the local voltage polarizations. The three polarizations are ohmic, activation, and concentration polarization. Therefore, the cell terminal voltage is given:

$$V = E_0 - \eta_{act,a} - \eta_{act,c} - \eta_{ohm} - \eta_{con} \quad (2)$$

where V is the cell potential.

3.1.1. Activation polarization

The development of electrochemical reaction requires overcoming an activation energy barrier. The electrode potential to overcome this activation energy is called the activation polarization. This phenomenon can be described by the Butler-Volmer equation

$$i = i_0 \left\{ \exp \left(\frac{\alpha z F \eta_{act}}{RT} \right) - \exp \left[\frac{-(1-\alpha) z F \eta_{act}}{RT} \right] \right\} \quad (3)$$

where α is the transfer coefficient, z is the number of electrons participating in the electrode reaction, F is the Faraday constant, and i_0 is the exchange current density that can be calculated as

$$i_{0,a} = \gamma_a \left(\frac{p_{H_2}}{p_{0,a}} \right) \left(\frac{p_{H_2O}}{p_{0,a}} \right) \exp \left(-\frac{E_{act,a}}{RT} \right) \quad (4)$$

$$i_{0,c} = \gamma_c \left(\frac{p_{O_2}}{p_{0,c}} \right)^{0.25} \exp \left(-\frac{E_{act,c}}{RT} \right) \quad (5)$$

Values for γ_a , γ_c , $E_{act,a}$, and $E_{act,c}$ could be found in literature[25].

3.1.2. Ohmic polarization

Ohmic losses occur because of resistance resulting from the flow of ions in the electrolyte and the flow of electrons through the electrode.

Ohmic polarization is expressed by Ohm's law:

$$\eta_{ohm} = i \sum R_i \quad (6)$$

where $R_i = \rho_i \delta_i$ is the ohmic resistance of anode, cathode, and electrolyte, δ_i is the corresponding thickness of them, and ρ_i is the material resistivity, which is the strong function of temperature. Both ρ_i and δ_i are given in Table I [26].

3.1.3. Concentration polarization

The electrode concentration overpotential considers the difference in gas concentrations between the electrode-electrolyte interface and the bulk.

In this paper, the overall concentration overpotential calculation is simplified assuming a constant value for the limiting current density and implementing the Fick's law.

$$\eta = \frac{RT}{2F} \ln \left(1 - \frac{i}{i_L} \right) \quad (7)$$

3.1.4. Electrochemical reaction

In the SOFC, the overall electrochemical is as follows, which is significantly exothermic.

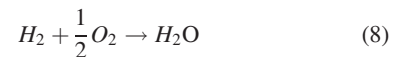
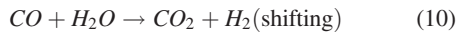
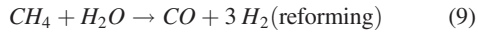


Table I. Properties of SOFC components.

	ρ_i (Ωcm)	δ_i (cm)
Cathode	$0.008114 \exp(600/T)$	0.200
Electrolyte	$0.00294 \exp(10350/T)$	0.004
Anode	$0.00298 \exp(-1392/T)$	0.015
Interconnection	—	0.01

For a methane-fed SOFC system, either internal or external reforming is needed. In order to reduce cost of an expensive external reformer and the cooling air flowrate for the fuel cell stack, the use of internal reforming is adopted. The usual high operating temperature of SOFC allows sustaining the reforming process. Therefore, methane is reformed to produce hydrogen according to the high endothermic reaction



From Eqs. (9) and (10), it is clear that these processes require steam. This can be produced externally by a boiler or by a heat recovery of exhaust gases from the combustor or the GT.

Assuming the reforming and shifting reactions at chemical equilibrium, the equilibrium constants can be calculated from the partial pressures of the reactants and products.

$$K_{PR} = \frac{P_{\text{H}_2}^3 P_{\text{CO}}}{P_{\text{CH}_4} P_{\text{H}_2\text{O}}}(\text{reforming}) \quad (11)$$

$$K_{PS} = \frac{P_{\text{H}_2} P_{\text{CO}_2}}{P_{\text{CO}} P_{\text{H}_2\text{O}}}(\text{shifting}) \quad (12)$$

where the equilibrium constants K_{PR} and K_{PS} have been correlated to the temperature.

$$\log K_p = AT^4 + BT^3 + CT^2 + DT + E \quad (13)$$

where the constant values are listed in Table II [8,9].

Assuming that x , y are the molar flow rates of CH_4 and CO , respectively, participating in the reactions, then the equilibrium constants of the reactions can be derived by

$$K_{PR} = \frac{\left(\frac{H_2^{in} + 3x + y - z}{n_{\text{tot}}^{in} + 2x}\right)^3 \left(\frac{CO^{in} + x - y}{n_{\text{tot}}^{in} + 2x}\right) P^2}{\left(\frac{CH_4^{in} - x}{n_{\text{tot}}^{in} + 2x}\right) \left(\frac{H_2O^{in} - x - y + z}{n_{\text{tot}}^{in} + 2x}\right)} \quad (14)$$

$$K_{PS} = \frac{(CO_2^{in} + y)(H_2^{in} + 3x + y - z)}{(CO^{in} + x - y)(H_2O^{in} - x - y + z)} \quad (15)$$

Table II. Values of equilibrium constants of reforming and shifting reactions.

	Reforming	Shifting
A	-2.63121×10^{-11}	5.47301×10^{-11}
B	1.24065×10^{-7}	-2.57479×10^{-7}
C	-2.25232×10^{-7}	4.63742×10^{-7}
D	1.95028×10^{-1}	-3.91500×10^{-1}
E	-66.1395	13.2097

where superscript *in* is inlet. The term n_{tot}^{in} is the total mole flow rates of the inlet gas mixture including the methane and the steam vapor.

The reaction rate z is determined by the Faraday's Law.

$$z = I/(2F) \quad (16)$$

When the temperature is known, the equilibrium constants can be calculated from Eq. (13), and unknowns x and y are given by solving Eqs. (14) and (15) using a numerical calculated method at given inlet conditions of the flow.

The electric power produced is given by

$$W_{\text{SOFC}} = IV \quad (17)$$

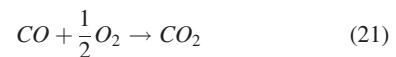
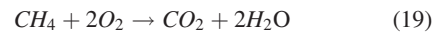
The equation for the energy balance of SOFC is

$$\sum_i H_i^{in} + \sum_k R_k(-\Delta H_k) = W_{\text{SOFC}} + \sum_i H_i^{out} \quad (18)$$

The energy balance includes the electrical power W_{SOFC} and the enthalpy changes of the chemical and electrochemical reactions and gives the evaluation of the average temperature of the stack.

3.2. Combustor model

Residual fuel (hydrogen, methane, carbon monoxide) from anode outlet stream reacts with the excess air of the cathode outlet stream. Combustion reactions, assumed at chemical equilibrium and driven into completion:



Assuming the process is adiabatic, the combustor outlet temperature is calculated on the energy balance.

3.3. Heat exchanger model

Two heat exchangers have been used for preheating fuel and air in this work. Both heat exchangers are assumed to be counter-flow exchangers. Computation of the heat exchange between the hot and cold fluids is based on the energy balance expressed as follows:

$$\Delta H = m_c C_{p,c}(T_{c,o} - T_{c,i}) = m_h C_{p,h}(T_{h,i} - T_{c,o}) \quad (22)$$

$$\Delta H = UA\Delta T_m \quad (23)$$

Here, subscripts 'c' and 'h' stand for the cold and hot side energy balance, U is the overall heat-transfer coefficient, A is the heat-exchange area, and ΔT_m is the log mean temperature difference.

3.4. Compressor and GT models

To simplify the study, it is assumed that the GT and compressor work at their respective designed condition under steady-state operation. A set of operating parameters and the assumed efficiencies are given in Table III. Once the pressure ratio is given, the outlet temperature of the compressor and GT is given as:

$$\frac{T_{COM,out}}{T_{COM,in}} = \frac{T_{GT,in}}{T_{GT,out}} = \pi^{\frac{k-1}{k}} \quad (24)$$

Then, the compressor work and GT output can be obtained, respectively,

$$W_{COM} = \frac{1}{\eta_{COM,s}} [H(T_{COM,out}) - H(T_{COM,in})] \quad (25)$$

$$W_{GT} = \eta_{GT,s} [H(T_{GT,in}) - H(T_{GT,out})] \quad (26)$$

where, η_s is adiabatic efficiency given in Table III.

3.5. Net power output and process heat

Net power of the system is given by

$$W_{net} = W_{SOFC} + (W_{GT} - W_{COM}) + W_{ST} \quad (27)$$

The electrical efficiency is defined as the ratio of the electrical power output to the LHV of the fuel, which is expressed as

$$\eta_{ele} = W_{net}/Q_{LHV} \quad (28)$$

where Q_{LHV} is the lower heating value of the fuel.

The total efficiency is defined as the ratio of the sum of the net electrical power and the heat recovery to the LHV of the fuel, which is defined as:

$$\eta_{tot} = (W_{net} + Q_{recovery})/Q_{LHV} \quad (29)$$

Table III. Setting values of parameters.

Parameter	Setting value
Compressor adiabatic efficiency	70%
Gas turbine adiabatic efficiency	85%
Mechanical efficiency	99.7%
Inverter efficiency	98%
Fuel cell press drop	3%
Preheater press drop	3%
Combustor press drop	3%
Boiler efficiency	90%
Steam turbine efficiency	90%
Steam cycle pressure	12.7 bar
Steam turbine inlet temperature	613 K
Condenser pressure of the steam cycle	0.05 bar

The heat recovery is referred to the amount of energy that is obtainable from the exhaust which can be used to produce steam or hot water for industrial and commercial applications.

4. RESULT AND DISCUSSION

The key parameter in SOFC computation is the operating temperature which is dependent on various operating and design data. The electrochemical model is solved with a tentative temperature. The electrochemical model determines terminal voltage and electric power. The energy balance (Eq. (18)) accepts these results from electrochemical model and calculates the temperature of SOFC. The temperature is applied to the electrochemical model for the next calculation of cell terminal voltage and power until the convergence is obtained.

For the whole system model, since the calculation of heat exchanger need the heating fluid parameters (such as the exit gas temperature of the combustor), which are not known at the beginning of the simulation, a set of initial parameters has to be assumed in order to run the system model until convergence is met eventually. A set of operating parameters and the assumed efficiencies of the system components are given in Table III. The simulations were done using Matlab 7.0.

The simulated V–I curve is compared with the experimental data in reference [27] in Figure 4. The relative deviation between the calculated voltage and experimental voltage is less than 5%, which shows that the present model is reliable.

4.1. The simple SOFC power system

In this study, the pressure ratio of both compressors is set to 1.28, the fuel flow rate to 5.72 mol/s, and the air flow rate to 185.22 mol/s.

The simulated pressure, temperature, and molar composition at each state-point of the system shown in Figure 1 are listed in Table IV.

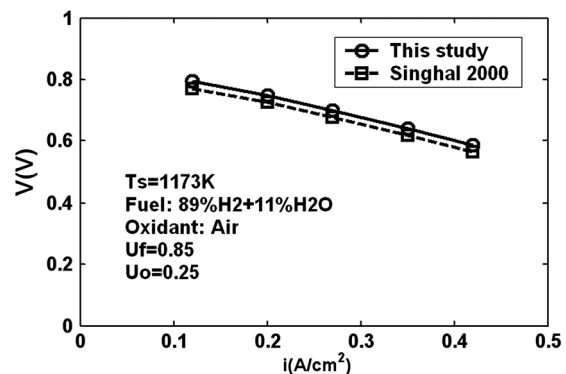


Figure 4. Prediction and experiment results of cell voltage vs. current density.

Table IV. State-points main properties for simple SOFC power system.

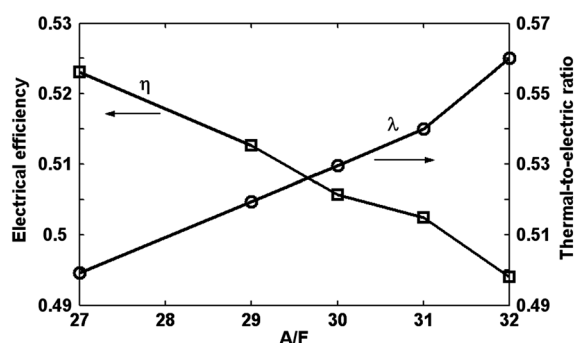
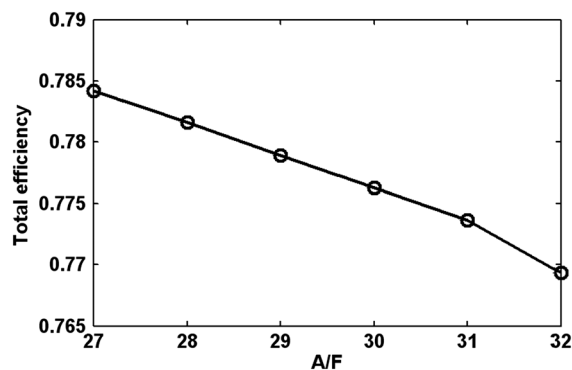
	T(K)	H ₂ (%)	H ₂ O(%)	O ₂ (%)	N ₂ (%)	CH ₄ (%)	CO ₂ (%)	CO(%)
1	298	0	0	21.00	79.00	0	0	0
2	321	0	0	21.00	79.00	0	0	0
3	973	0	0	21.00	79.00	0	0	0
4	1127	0	0	16.62	83.38	0	0	0
5	295	0	0	0	0	100	0	0
6	327	0	0	0	0	100	0	0
7	370	0	66.67	0	0	33.33	0	0
8	823	0	66.67	0	0	33.33	0	0
9	1127	11.62	68.38	0	0	0	17.46	2.54
10	1231	0	11.31	13.57	72.30	0	2.83	0
11	1186	0	11.31	13.57	72.30	0	2.83	0
12	640	0	11.31	13.57	72.30	0	2.83	0
13	557	0	11.31	13.57	72.30	0	2.83	0
14	353	0	11.31	13.57	72.30	0	2.83	0
15	393	0	100	0	0	0	0	0
16	298	0	100	0	0	0	0	0

The results of the simulation show that the waste heat recovered is 1264.1 kW. The net electrical power output (W_{net}) of the plant is 2268.65 kW. The thermal-to-electric ratio is 0.56. The electrical and total efficiencies of the plant are 49% and 77%.

The irreversibility in the combustor is low because the inlet temperature is high and there is little fuel left. The most irreversibility process occurs in the air preheater because the air flow rate and temperature differences are large. Here, a large amount of heat equal to about 1.55 times the power output of the fuel cell is transferred to the entering air. However, the excess air is needed to provide air-cooling in SOFC, and excess air reduces the temperature gradient and makes the cell temperature more uniform [28,29].

The influence of the ratio of the air flow rate to the fuel flow rate (A/F) on the thermal-to-electric ratio, electrical efficiency, and system total efficiency is shown in Figures 5 and 6, respectively.

When the flow rate of air decreased, the heat requirement is reduced. Therefore, the irreversibility is

**Figure 5.** Effect of A/F on electrical efficiency and the thermal-to-electric ratio.**Figure 6.** Effect of A/F on system total efficiency.

reduced, too. When the A/F decreases from 32 to 27, the electrical efficiency increases from 49% to 52%.

4.2. The SOFC-GT power system

In order to decrease the irreversibility resulting from high air flow rate and large temperature difference between the cold fluid and the hot exhaust gas in the preheater, the lower air flow rate is adopted, and the temperature of hot exhaust gas is decreased after entering the GT to produce the mechanical power. That is the SOFC-GT power system shown in Figure 2.

In this particular case study, the pressure ratio of both compressors is set to 8, the fuel flow rate is 5.72 mol/s, and the ratio of air flow rate to the fuel flow rate (A/F) is set as 27.

The results of the simulation of temperature, pressure, and composition at each node of the system are listed in Table V. Some results relating to system performance are listed in Table VI.

Table V. State-points main properties for SOFC-GT power system.

	T(K)	P(bar)	H ₂ (%)	H ₂ O(%)	O ₂ (%)	N ₂ (%)	CH ₄ (%)	CO ₂ (%)	CO (%)
1	298	1	0	0	21.00	79.00	0	0	0
2	580	8	0	0	21.00	79.00	0	0	0
3	928	7.76	0	0	21.00	79.00	0	0	0
4	1091	7.53	0	0	15.69	84.31	0	0	0
5	295	1	0	0	0	0	100	0	0
6	580	8	0	0	0	0	100	0	0
7	580	7.76	0	66.67	0	0	33.33	0	0
8	923	7.53	0	66.67	0	0	33.33	0	0
9	1091	7.53	11.64	68.36	0	0	0	17.62	2.38
10	1271	7.3	0	13.34	12.23	71.10	0	3.34	0
11	976	2.54	0	11.31	13.57	72.30	0	2.83	0
12	930	2.46	0	11.31	13.57	72.30	0	2.83	0
13	631	2.40	0	11.31	13.57	72.30	0	2.83	0
14	518	2.32	0	11.31	13.57	72.30	0	2.83	0
15	353	2.25	0	100	0	0	0	0	0
16	580	8	0	100	0	0	0	0	0
17	298	1.03	0	100	0	0	0	0	0

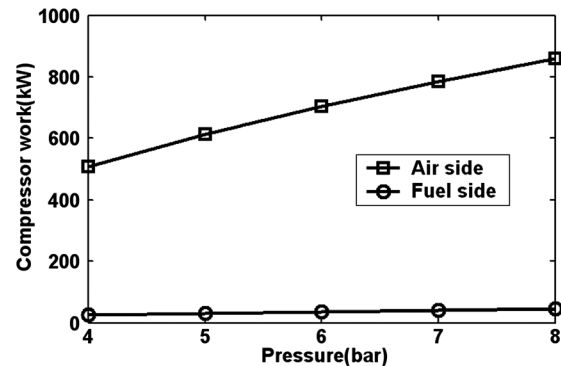
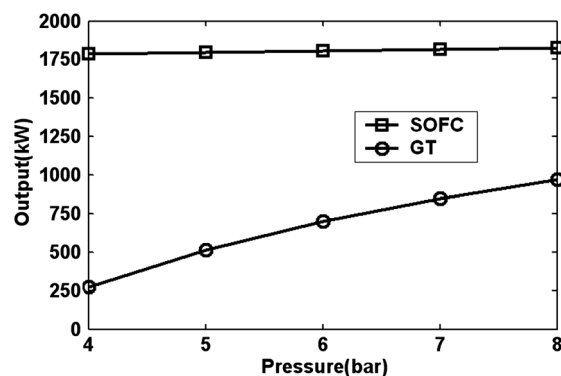
Table VI. Main results of the simulation for the SOFC-GT power system.

Parameter	Value
Compressor work (air side)	857.667 kW
Compressor work (fuel side)	45.024 kW
GT power output	968.246 kW
SOFC stack power	1791.44 kW
Net power output	1857 kW
Waste heat recovery	587.655 kW
Electrical efficiency	60.65%
Total efficiency	79.84%

Compared to the simple SOFC power system, the combustion products flow through the GT, and the mechanical power is produced, then the temperature of the gas is lowered. The outlet flow (11-Point in Figure 2) in SOFC-GT power system has a lower temperature than that (10-Point in Figure 1) in simple SOFC power system. Then, the temperature difference in air preheater becomes small, so the irreversibility is decreased obviously. More chemical energy is translated into electric and mechanical power instead of heat energy to heat the cooling air. The net electrical power output of the plant is 1857 kW. The heat recovery is 588 kW. The ratio of the heat energy to the electric power is 0.31, which is far less than that of simple SOFC power system.

The effect of operating pressure on compressors work, SOFC and GT output power, heat recovery, and efficiency is shown in Figures 7–10, respectively.

Although increase of flow pressure in fuel and air required more work given to compressor shown in Figure 8, the improvement in overall useful energy output from the SOFC and GT overweighs the extra work required and results in the decrease of heat recovery; the electrical efficiency is enhanced ultimately.

**Figure 7.** Effect of operating pressure on compressors work.**Figure 8.** Effect of operating pressure on SOFC and GT power output.

4.3. The SOFC-GT-ST power system

In order to utilize exhaust gas further, the ST is added to SOFC-GT power system to produce mechanical

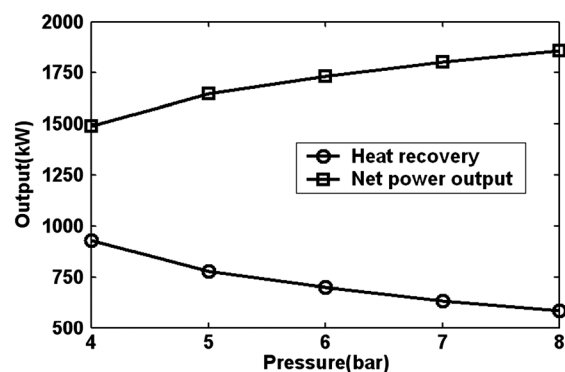


Figure 9. Effect of operating pressure on heat recovery and net power output.

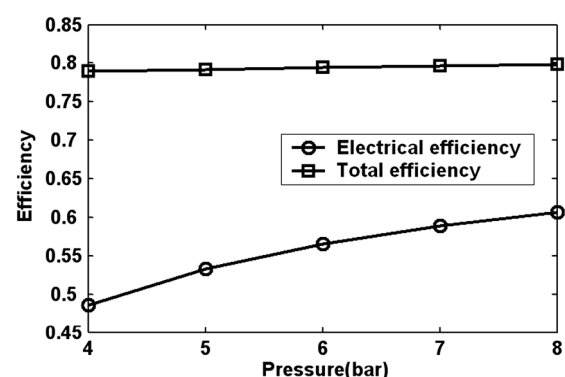


Figure 10. Effect of operating pressure on efficiency.

power, which is the SOFC-GT-ST power system shown in Figure 3.

The hot steam at combustor outlet has been utilized first to produce mechanical power in GT and then to generate superheated vapor in a boiler.

In this study, the pressure ratio of both compressors is set to 12.7, the pressure ratio of GT is 2.83, the fuel flow rate to 7.627 mol/s, and the ratio of air flow rate to the fuel flow rate (A/F) is set as 27. The ST inlet temperature and pressure are fixed at 613 K and 12.7 bar. The condenser pressure of the steam cycle is 0.05 bar. The ST efficiency is 90%. The boiler efficiency is set as 90%.

The calculated temperature and pressure at each node of the system in Figure 3 are listed in Table VII. The performance of SOFC-GT-ST system is listed in Table VIII.

Although the ST is adopted to produce the mechanical power in steam cycle (Rankine Cycle), the results show that the use of complex ST plant is not very useful as supposed. It is because of two reasons. The first reason is the hot exhaust leaving from the GT has to keep a relatively high temperature to heat the cold steam to become the superheated vapor, which limits the GT capacity to produce mechanical power. The power share coming from the GT in SOFC-GT-ST is less than that in SOFC-GT system. The

Table VII. State-points main properties for SOFC-GT-ST power system.

	T(K)	P(bar)
1	298	1
2	669	12.7
3	923	12.3
4	1112	12.03
5	298	1
6	669	12.7
7	638	12.3
8	928	12.5
9	1112	12.03
10	1238	11.3
11	968	4
12	930	3.92
13	709	3.84
14	353	3.76
15	298	1
16	613	12.7
17	613	12.7
18	306	0.05
19	306	0.05

Table VIII. Main results of the simulation for SOFC-GT-ST power system.

Parameter	Value
Compressor work (air side)	2273.49 kW
Compressor work (fuel side)	124.83 kW
GT power output	2186.31 kW
SOFC stack power	3499.94 kW
Net power output	1857 kW
Electrical efficiency	60.40%

second reason is the temperature difference between the cold steam and hot exhaust is large in boiler; therefore, its irreversibility is high.

Although the ST produces the mechanical power combining with the GT in SOFC-GT-ST, the effect of the decrease of the power from the GT and increase of irreversibility in the boiler overweighs the amount of power from the ST; thus, the total electrical efficiency is even lower than that of SOFC-GT power system slightly. At the same time, ST makes the system more complicated and more expensive.

Performance comparisons of five SOFC system designs are shown in Figure 11.

Case (1): simple SOFC power system, $A/F = 32$,

Case (2): simple SOFC power system, $A/F = 27$,

Case (3): SOFC-GT power system, $A/F = 27$, operating pressure = 6 bar,

Case (4): SOFC-GT power system, $A/F = 27$, operating pressure = 8 bar,

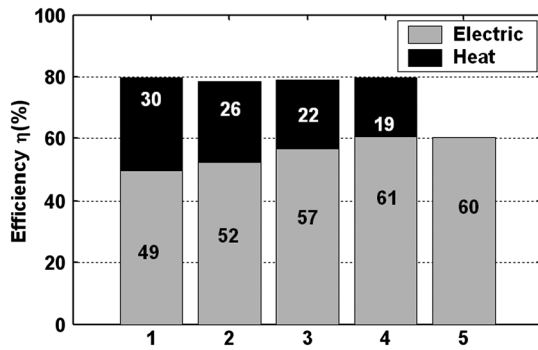


Figure 11. Electric efficiency and total efficiency for five discussed cases.

Case(5): SOFC-GT-ST power system, A/F=27, operation pressure=12.7 bar,

5. CONCLUSIONS

In the present paper, three typical SOFC power systems fed by methane are compared by energetic analysis. Simulations reveal that efficiencies of 49% electric and 77% cogenerative are feasible for simple SOFC system in residential-scale applications. Decreasing excess air in the SOFC has a positive effect on the electric and total efficiency.

It is possible for a hybrid SOFC-GT power system to achieve an electrical efficiency greater than 60%, and a total efficiency near 80%. Increasing in operating pressure increases the electrical efficiency. However, the total efficiency increases slightly as the pressure increases.

The efficiency of SOFC-GT-ST is close to that of SOFC-GT power system. Although the power output of exhaust gases shows some improvement through the ST, the decrease of power output from the GT overweighs the advantages. At the same time, ST adds complexity, control needs, and potential high costs of the whole system.

NOMENCLATURE

A	= area (m ²)
A/F	= molar air–fuel ratio
C _p	= specific heat at constant pressure (J/mol K)
E _{act}	= activation energy (J/mol)
E ₀	= reversible cell potential (V)
F	= Faraday constant, 96485C/mol
ΔG	= change in Gibbs free energy (J/mol)
H	= enthalpy (J/mol)
ΔH	= enthalpy change of reaction (J/mol)
i	= current density (A/m ²)
i ₀	= exchange current density (A/m ²)
i _L	= limiting current density (A/m ²)
I	= current (A)

GT	= gas turbine
K	= equilibrium constant
LHV	= lower heating value (J/mol)
m	= molar flow rate (mol/s)
P	= pressure (bar)
ST	= steam turbine
R	= universal gas constant, 8.314 J/(mol K)
R _i	= ohmic resistant (Ωcm ²)
R _k	= reaction rate (mol s ⁻¹)
T	= temperature (K)
V	= terminal voltage (V)
U _f	= fuel utilization
U _o	= oxidant utilization
W	= electrical power (W)
z	= H ₂ reacted moles (mol s ⁻¹)
Z	= electrons transferred per reaction

Greek Letters

α	= transfer coefficient
ρ	= specific resistivity (Ωcm)
δ	= thickness (cm)
η	= polarization (V)
η	= efficiency

Subscripts

a	= anode
act	= activation polarization
c	= cathode
com	= compressor
con	= concentration polarization
ohm	= ohm polarization
R	= reforming reaction
S	= shifting reaction
tur	= turbine

ACKNOWLEDGEMENTS

The authors acknowledge the financial support provided by Centre College Primary Scientific Research Item Funds(HEUCF 100303).

REFERENCES

1. Akkaya AV. Electrochemical model for performance analysis of a tubular SOFC. *International Journal of Energy Research* 2007; **31**:79–98.
2. Bang-Moller C, Rokni M. Thermodynamic performance study of biomass gasification, solid oxide fuel cell and micro gas turbine hybrid systems. *Energy Conversion and Management* 2010; **51**:2339–2330.

3. Ghosh S, De S. Exergy analysis of a cogeneration plant using coal gasification and solid oxide fuel cell. *International Journal of Energy Research* 2006; **30**:647–658.
4. McIlveen-Wright DR, Moglie M, Rezvani S, Huang Y, Anderson M, Redpath D, Dave A, Hewitt NJ. A techno-economic analysis of biomass gasifiers integrated with high and intermediate temperature solid oxide fuel cells. *International Journal of Energy Research* 2011; **35**:1037–1047.
5. Bedringas KW, Ertesvag IS. Exergy analysis of solid oxide fuel cell (SOFC) systems. *Energy* 1997; **22**:403–412.
6. Chan SH, Low CF, Ding OL. Energy and exergy analysis of simple solid oxide fuel cell power systems. *Journal of Power Sources* 2002; **103**:188–200.
7. Jia J, Li Q, Luo M, Wei L, Abuliti A. Effects of gas recycle on performance of solid oxide fuel cell power systems. *Energy* 2011; **36**:1068–1075.
8. Massardo AF, Lubelli F. Internal reforming solid oxide fuel cell-gas turbine combined cycles. *Journal of Engineering for Gas Turbines and Power* 2000; **122**:27–35.
9. Chan SH, Ho HK, Tian Y. Modelling of simple hybrid solid oxide fuel cell and gas turbine power plant. *Journal of Power Sources* 2002; **109**:111–120.
10. Suther T, Fung AS, Koksall M, Zabihian F. Effects of operating and design parameters on the performance of a solid oxide fuel cell–gas turbine system. *International Journal of Energy Research* 2011; **35**:616–632.
11. Campanari S. Full load and part-load performance prediction for integrated SOFC and microturbine systems. *Journal of Engineering for Gas Turbine and Power* 2000; **122**:239–246.
12. Costanmagna P, Magistri L, Massardo AF. Design and part-load performance of a hybrid system based on a solid oxide fuel reactor and a micro gas turbine. *Journal of Power Sources* 2001; **96**:352–368.
13. Chan SH, Ho HK, Tian Y. Modelling for part-load operation of solid oxide fuel cell-gas turbine hybrid power plant. *Journal of Power Sources* 2003; **144**:213–227.
14. Calise F, Palombo A, Vanoli L. Design and partial load exergy analysis of hybrid SOFC-GT power plant. *Journal of Power Sources* 2006; **158**:225–244.
15. Calise F, Dentice M, Palombo A, Vanoli L. Simulation and exergy analysis of a hybrid Solid Oxide Fuel Cell(SOFC)-Gas Turbine System. *Energy* 2006; **31**:3278–3299.
16. Cocco D, Tola V. Externally reformed solid oxide fuel cell-micro-gas turbine (SOFC-MIT) hybrid systems fueled by methanol and di-methyl-ether (DME). *Energy* 2009; **34**:2124–2130.
17. Traverso A, Magistri L, Massardo AF. Turbomachinery for the air management and energy recovery in fuel cell gas turbine hybrid systems. *Energy* 2010; **35**:764–777.
18. Komatsu Y, Kimijima S, Szmyd JS. Performance analysis for the part-load operation of a solid oxide fuel cell-micro gas turbine hybrid system. *Energy* 2010; **35**:982–988.
19. Yi Y, Rao AD, Brouwer J, Scott G. Analysis and optimization of a solid oxide fuel cell and intercooled gas turbine (SOFC-ICGT) hybrid cycle. *Journal of Power Sources* 2004; **132**:77–85.
20. Duan L, He B, Yang Y. Parameter optimization study on SOFC-MGT hybrid power system. *International Journal of Energy Research* 2011; **35**:721–732.
21. Odukoya A, Carretero JA, Reddy BV. Thermodynamic optimization of solid oxide fuel cell-based combined cycle cogeneration plant. *International Journal of Energy Research* 2011; **35**:1399–1411.
22. Malico I, Carvalhinho AP, Tenreiro J. Design of a trigeneration system using a high-temperature fuel cell. *International Journal of Energy Research* 2009; **33**:144–151.
23. Velumani S, Guzma CE, Peniche R, Vega R. Proposal of a hybrid CHP system: SOFC/microturbine/absorption chiller. *International Journal of Energy Research* 2010; **34**:1088–1095.
24. Akkaya AV, Sahin B. A study on performance of solid oxide fuel cell-organic Rankine cycle combined system. *International Journal of Energy Research* 2009; **33**:553–564.
25. Paola C, Kaspar H. Modeling of solid oxide heat exchanger integrated stacks and simulation at high fuel utilization. *Journal of the Electrochemical Society* 1998; **145**:3995–4007.
26. Norman F, William JW, Jack W. A mathematical model of a solid oxide fuel cell. *Journal of the Electrochemical Society* 1995; **42**:3792–3800.
27. Singhal SC. Advances in solid oxide fuel cell technology [J]. *Solid State Ionics* 2000; **135**:305–313.
28. Jia J, Abuliti A, Wei L, Jiang R, Shen S. A mathematical model of a tubular solid oxide fuel cell with specified combustion zone. *Journal of Power Sources* 2007; **171**:696–705.
29. Jia J, Jiang R, Shen S, Abuliti A. Effect of operation parameters on performance of tubular solid oxide fuel cell. *AIChE Journal* 2008; **54**:554–564.



An optimal configuration for a solid oxide fuel cell-gas turbine (SOFC-GT) hybrid system based on thermo-economic modelling

Jamasb Pirkandi*, Mostafa Mahmoodi, Mohammad Ommian

Department of Aerospace Engineering, Malek Ashtar University of Technology, Tehran, 15875-1774, Iran

ARTICLE INFO

Article history:

Received 22 June 2016

Received in revised form

4 January 2017

Accepted 4 January 2017

Available online 9 January 2017

Keywords:

Hybrid system

Solid oxide fuel cell

Gas turbine

Optimal configuration

Thermo-economic model

ABSTRACT

The aim of this research is to present an optimal configuration for solid oxide fuel cell-gas turbine hybrid systems based on thermo-economic modelling. To this end, four different designs of direct hybrid systems with pressurized and atmospheric fuel cells have been presented. In the first two designs, one stack fuel cells has been used in the hybrid system, and in the other designs, two stack fuel cells have been utilized. By examining four hybrid system, it was found that hybrid system with one pressurized fuel cell hybrid system is better than the other. The advantages of this system include its lower irreversibility rate, low purchase, low installation and startup costs, and the adequate price of its generated electricity. Results show that the hybrid system with one atmospheric fuel cell has a low electrical efficiency, high irreversibility rate; and also the price of its generated electricity is higher than that of the other proposed systems. Conversely, the hybrid systems with two fuel cells, in spite of enjoying a high efficiency, are not cost-effective and economical. The findings indicate that the total efficiency of 64% and electrical efficiency of 51% was achieved for optimal hybrid system. Also, the thermo-economic analyses show that the generated electricity price is about USD 11.6 cents/kWh based on the Lazareto's model and USD 18.5 cents/kWh based on the total revenue requirement model. The purchase, installation and startup cost of this hybrid system is about \$1692/kW; which is almost twice the cost of a gas turbine unit.

© 2017 Elsevier Ltd. All rights reserved.

1. Introduction

In light of the growing consumption of energy in the world, the priorities have shifted to the use of novel techniques and systems of energy production with high efficiency and low emission. The fuel cell technology, in which hydrogen generates electricity and heat through a series of electrochemical reactions with oxygen, is considered to be one of the best electricity generation mechanisms of the future (Hall and Kerr, 2003). The heat obtained from the electrochemical reactions of a high-temperature fuel cell can be used in an appropriate heat engine in order to improve its overall performance. Considering the above mentioned, many researchers have become interested in combining the fuel cells with various power generation systems. The resulting hybrid systems enjoy a high efficiency; and many researchers as well as manufacturing companies are trying to commercialize these systems and also to increase their efficiency and power production capacity

(Kuchonthara et al., 2003).

Hybrid systems are power generation systems in which a heat engine such as gas turbine (GT), steam turbine, Stirling engine, etc. is combined with a non-heat engine like a fuel cell. The mentioned hybrid systems consist of a fuel cell as the high temperature source of gas turbine cycle. However, if required; the combustion chamber is added to the cycle. In fact the combustion chamber of the gas turbine engine has been replaced with SOFC. A gas turbine can be directly or indirectly connected to the SOFC. When the same operating fluid passes through the fuel cell and the lower cycle, the considered system is called a hybrid system with direct thermal contact (Zhang et al., 2010; Brouwer, 2006). In hybrid systems with indirect thermal contact, different operating fluids pass through the fuel cell and lower cycle, and these two cycles exchange their heat via a heat exchanger. Solid oxide fuel cells (SOFC) are the type of cells with high working temperatures, and they are better suited for use in hybrid power generation systems. These cells always produce considerable quantities of high-quality heat and energy. Many researchers have recently focused on finding the best way of using this heat. The combination of solid oxide fuel cells with various types of turbines and micro gas turbines has been frequently used in electricity generation systems (Buonomano et al., 2015).

* Corresponding author. Tel.: +98 2122945141; fax: +98 2122935341.

E-mail addresses: j.pirkandi@dena.kntu.ac.ir (J. Pirkandi), mostafamahmoodi@mut.ac.ir (M. Mahmoodi), m.ommian@gmail.com (M. Ommian).

Nomenclature		ν	specific volume (m^3/kmol)
		τ	average annual time at nominal capacity
		<i>Subscripts</i>	
A	Area (m^2)	a	air
CC_L	levelized capital investment cost (\$)	ab	afterburner
\dot{C}_P	rate of power generation cost (\$/h)	an	anode
\dot{C}_F	rate of fuel cost (\$/h)	c	compressor
E	reversible voltage of fuel cell (V)	ca	cathode
\dot{E}	rate of exergy (W/h)	cell	fuel cell
F	faraday's constant (96,485 C/mol)	f	fuel
FC_L	levelized fuel cost (\$)	g	gas
h	enthalpy (kJ/kmol)	gen	generation
i	current density (A/m^2)	in	inlet
I	current (A)	inv	inverter
\dot{I}	rate of irreversibility (W/h)	out	exit
n	molar flow rate (kmol/s)	rec	recuperator
OMC_L	levelized operating and maintenance cost (\$)	surr	surrounding
P	pressure (kPa)	th	thermal
r_p	pressure ratio	tot	total
Q	heat generation rate (kW)	w	water
Ru	universal gas constant (8.314 J/mol.K)	wp	water pump
S	entropy (kJ/kmol.K)		
T	temperature (K)	<i>Acronyms</i>	
W	electrical power (kW)	GT	Gas Turbine
\dot{Z}^{CI}	initial capital investment cost (\$/h)	LHV	Low Heating Value (kJ/kmol)
\dot{Z}^{OM}	operating and maintenance cost (\$/h)	SOFC	Solid Oxide Fuel Cell
<i>Greek letters</i>		TRR	Total Revenue Requirement cost (\$)
η	efficiency		

With regards to the working pressure, the solid oxide fuel cells used in this type of hybrid systems (direct thermal contact) are divided into two types: pressurized, and atmospheric. In the pressurized type, the fuel cell is situated between compressor and turbine, and it has a high working pressure. In the atmospheric type, the fuel cell is located downstream of the turbine, and the turbine's outflowing gasses enter it at low pressure (about the pressure of the atmosphere). The fuel cell used in pressurized systems is often subjected to a specific pressure, which increases its output power but, accordingly, creates more challenges in the design and control of the system. In this approach, because of the high pressure produced in the fuel cell, its casing has to be securely sealed. To overcome this problem, atmospheric type fuel cells are used in the hybrid systems. These systems pose much less of a hazard by keeping the fuel cells at atmospheric pressure. In this system, the air flowing into the fuel cell is taken from the turbine's exhaust gasses. If the cell has a high working temperature or the gas turbine has a high expansion percentage, it will be difficult to achieve the minimum working temperature needed at the input of this type of fuel cell.

A review of the former research works indicates that in recent years numerous researchers have worked on the direct combination of gas turbines and fuel cells under pressure, and that the atmospheric systems have attracted less of an attention. The investigations show that generally one stack fuel cell has been used in the structure of most hybrid systems. Also, the examined works indicate that the hybrid systems have been explored more from thermodynamic and exergy perspectives, and that the researchers have focused less on economic analyses. Considering the above-mentioned notions, the main objective of this research is to introduce and present several different configurations for direct type hybrid systems of gas turbine and fuel cell, and to analyse them on

the basis of thermo-economic modelling.

Araki et al. (2006) investigated a hybrid power generation system consisting of two high-temperature and low-temperature solid oxide fuel cell stacks. Musa and Paepe (2008) studied the performances of hybrid cycles with two high-temperature and medium-temperature solid oxide fuel cells. Cheddie (2010) proposed SOFC for integration into a 10 MW gas turbine power plant, operating at 30% efficiency. The power output of the hybrid plant is 37 MW at 66.2% efficiency. A thermo-economic model predicts a payback period of less than four years. Tarroja et al. (2010) studied a SOFC-GT hybrid system, explored the different methods of preheating the cathode's inflowing air, e.g. using a blower or injector, and compared the results with those of a system with a single heat exchanger. Facchinetti et al. (2014) analysed the design and optimization of a SOFC-GT hybrid cycle with a new configuration, which had been considered for use in residential buildings. Arsalis (2007, 2008) investigated four different steam turbine cycles. The models have been developed to function both at design and off-design conditions. Cheddie and Murray (2010a, b); Cheddie et al. (2011) proposed direct, semi-direct and indirectly coupled of SOFC and a 10 MW power plant. Lorenzo and Fragiaco (2015) formulated zero-dimensional and stationary simulation model of an SOFC system fed by syngas in cogenerate arrangement and implemented in the Matlab environment by which the SOFC system performances were evaluated. Ebrahimi and Moradpoor (2016) proposed a novel cycle combining three technologies of solid oxide fuel cell, micro gas turbine, and organic Rankine cycle to produce power in micro scale. Meratizaman et al. (2014) considered integration of MED with SOFC-GT power cycle in 300–1000 kW (size of SOFC). Saisirirat (2015) simulated a detailed thermodynamic model of SOFC and gas turbine hybrid system and few configurations of the combined or hybrid cycles are proposed and analysed.

Buonomano et al. (2015) presented a comprehensive review of the possible layout configurations of hybrid power plants based on the integration of solid oxide fuel cells and gas turbine technologies. These researchers have employed simple economic models in their investigations in order to determine the price of the generated electricity, and their considered hybrid systems have included gas turbines and pressurized fuel cells.

In view of the above information, in this study, contrary to most of the former works in which a simple system configuration has been analysed, four different hybrid system configurations with pressurized and atmospheric fuel cells are investigated. In two of the analysed configurations, two fuel cell stacks have been used, and their results have been compared with those of simpler models. Since the fuel cell, as one of the main components of these types of hybrid systems, plays a significant role in the generation of power, this research has attempted to separately explore the electrochemical and thermal performances of the fuel cell. Contrary to most of the previous research works, the working temperature of the cell has not been assumed as constant in this investigation, but has been computed for different working conditions. In the economic analyses performed in this research, two simple economic models and the total revenue requirements (TRR) method have been used to determine the price of the generated electricity and the other relevant expenses. The TRR model is an accurate and complete model for economic analyses and it can calculate all the capital investment and current costs of a system (Bejan et al., 1996). In this paper System performance Criteria such as power, efficiency, emission rate, irreversibility and price of electricity was investigated simultaneously.

2. The proposed hybrid systems

Hybrid systems can be divided into two categories: direct and indirect. The selection of a SOFC/GT layout depend on several design parameters, such as operating temperature and pressure of the SOFC stack, type of fuel, type of Brayton cycle and so on. During the past few years researchers developed a plurality of SOFC/GT configurations, aiming at improving the electrical efficiency and/or to reduce capital costs. In fact, the selecting a configuration is one of the key steps before designing a hybrid system. This study presents four configurations of SOFC/GT hybrid system and discusses why one configuration is better than the other.

In this section, four direct types of hybrid systems with different configurations have been presented. In the first and second

configurations, one fuel cell has been used; while in the other two configurations, two cells have been used. In order to present the governing equations, it is necessary to introduce a basic cycle.

2.1. The direct hybrid system with one pressurized fuel cell

Fig. 1 illustrates a direct type hybrid system of gas turbine and solid oxide fuel cell, as the basic hybrid system. As this figure indicates, in this hybrid system, one stack fuel cell at the upstream of turbine has been used. According to the investigations, in most of the performed research works on hybrid systems, this design scheme has been explored and analysed.

The proposed system comprises a stack of solid oxide fuel cell with internal reforming, afterburner chamber, gas turbine, air compressor, fuel compressor, water pump and three recuperators. The air and natural gas used in the system are first compressed by some compressors and by passing through the air and fuel recuperators, are warmed before entering the cell. Natural gas, after entering the fuel cell, is reformed at the anode section and is produced pure hydrogen. The hydrogen obtained from natural gas reacts with the existing oxygen in the air, which has passed through another recuperator and entered the fuel cell. Considering the exothermic nature of the electrochemical reaction in the fuel cell, a portion of the heat generated from this reaction is used to reform the natural gas utilized in the process, another portion enters the surrounding environment and the remaining portion of the heat warms up the internal gasses and the gasses exiting the fuel cell. The reaction between hydrogen and oxygen in the cell produces substantial electrical power, which increases the efficiency of the hybrid system. The fuel cell's exhaust gasses that were not used in the reforming reaction enter the afterburner chamber, where they react with each other. The output products of the afterburner chamber then enter the gas turbine and produce mechanical work through expansion. Finally, the hot exhaust gasses of the turbine enter the three recuperators. The first two recuperators are used to preheat the air and fuel that enter the cell, and the third recuperator is used to generate thermal energy.

2.2. The direct hybrid system with one atmospheric fuel cell

The second proposed system is a direct hybrid system with an atmospheric fuel cell. As is observed in Fig. 2, in this type of hybrid system, the fuel cell is situated at the downstream of turbine and its working pressure is about the pressure of atmosphere. The gasses

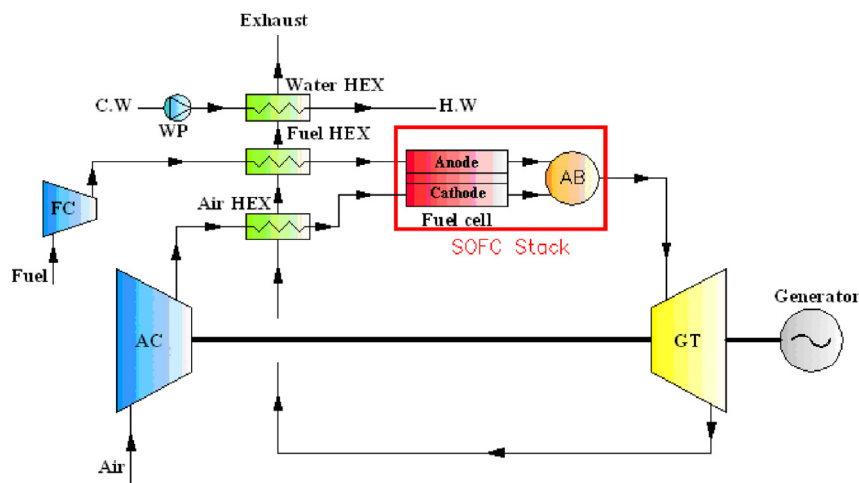


Fig. 1. The direct hybrid system with one pressurized fuel cell (first design).

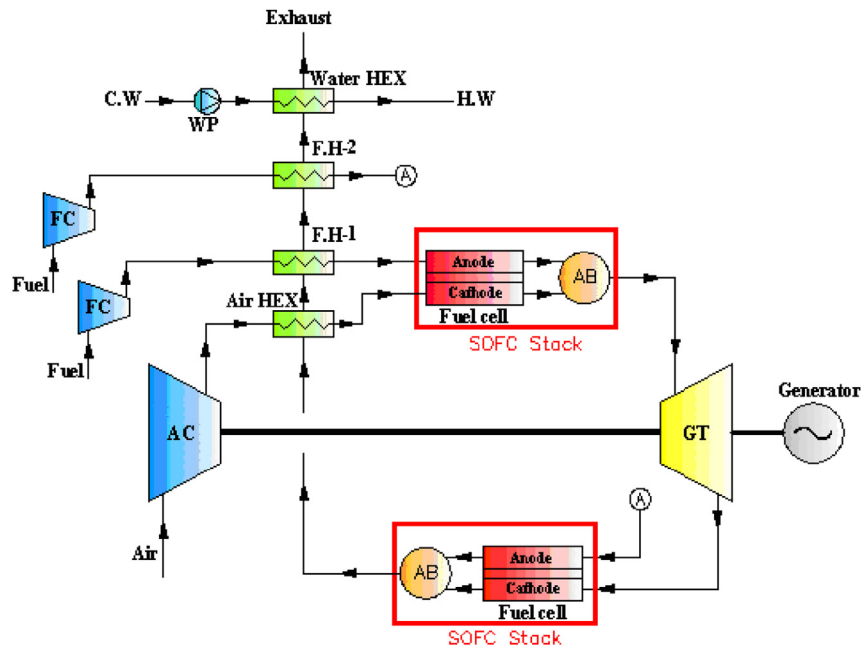


Fig. 4. The direct hybrid system with one pressurized and one atmospheric fuel cell (fourth design).

exiting the afterburner chamber then enter the turbine and generate power. Also, the turbine's exhaust gasses enter the cathode section of the atmospheric fuel cell and along with the fuel injected into the anode section supply another portion of the hybrid system's generated power. Similar to the pressurized fuel cell, the gasses not utilized in the atmospheric cell enter the second afterburner chamber and, after participating in a high-temperature chemical reaction, are conveyed to the heat exchangers. The hot exhaust gasses of the afterburner chamber also enter the heat exchangers in order to warm up the air, fuel and water used in the hybrid system; and after exchanging their heat, these gasses are discharged into the surrounding environment (see Fig. 5).

In this paper, Criteria for selection of optimum system were high power and efficiency and low emission rate, irreversibility and price of electricity. The results of the optimal mode for each configuration are not stated in this article. Optimal results obtained are presented in tables and for each state three criteria include good, moderate and poor was defined. Criteria have the same weight. System that has the highest score was selected as an appropriate configuration. Survey of all the criteria have not been addressed in any article. The main objective of this paper is to investigate the four different configurations and identify the disadvantages and capabilities of each one. This type of work has been done for the first time. Previous articles usually evaluate pressurized hybrid system with one fuel cell. The main variables in this paper include: Power, Compressor pressure ratio, Electrical efficiency, Irreversibility rate, Emission, Electricity generation price, Purchase, installation and start-up cost.

3. Assumption

The following assumptions have been considered in modelling and analysing the introduced hybrid systems:

- Gas leakage from inside the system to the outside has been ignored.
- A stable fluid flow has been considered in all the cycle components.

- The distribution of temperature, pressure and chemical components within the fuel cell has been disregarded.
- A constant voltage has been considered for the cells of the fuel cell.
- It has been assumed that the fuel inside the fuel cell converts to hydrogen through internal reforming.
- The fuel utilized in the system contains 97% methane, 1.5% carbon dioxide and 1.5% nitrogen. Also, the air used in the system contains 21% oxygen and 79% nitrogen.
- In this research, air and fuel enter the system under standard conditions and at identical temperatures and pressures (temperature of 25 °C and pressure of 1 bar).

4. Governing equations

In this section, the governing equations of the problem have been presented in three separate areas comprising the thermodynamic, exergy and economic equations. Due to the similar components used in all four proposed designs, the first design including the direct hybrid system with one pressurized fuel cell is chosen as the main design, and its relevant equations are presented.

4.1. Thermodynamic equations

4.1.1. Air and fuel compressor

According to thermodynamic equations, the temperature of the compressor's outflow gasses and the real work needed by the compressor can be determined (Haseli and Dincer, 2008). It should be mentioned that due to the dependency of the isentropic efficiency on the compressor's pressure ratio and because of the fluctuations of this efficiency with pressure variations, polytropic efficiency has been used in system analysis instead of isentropic efficiency. (Haseli and Dincer, 2008).

$$\dot{W}_{c,a} = \dot{n}_{c,a} \cdot (\bar{h}_{out(c,a)} - \bar{h}_{in(c,a)}) \quad (1)$$

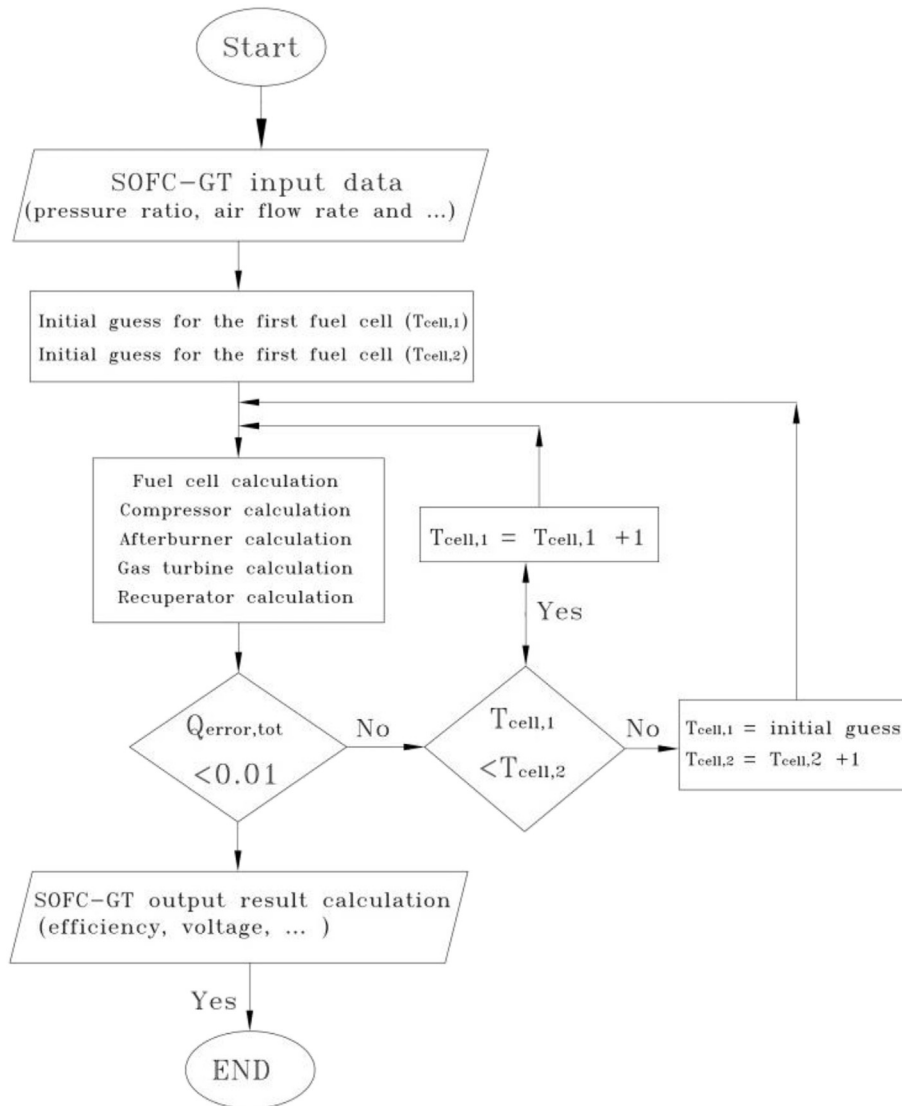


Fig. 5. Flowchart of SOFC-GT modelling.

$$\dot{S}_{gen(c,a)} = \dot{n}_{c,a} \cdot (\bar{s}_{out(c,a)} - \bar{s}_{in(c,a)}) \quad (2)$$

where subscript (c,a) is the air compressor and this relationship is used for fuel compressor with subscript (c,f).

4.1.2. Afterburner and combustion chamber

Since only a portion of the fuel and air that enter the system are used up in the fuel cell, an afterburner chamber is necessary for the cycle. All reactions are exothermic, and they raise the temperature of the gasses that exit the afterburner chamber (Haseli and Dincer, 2008).

$$\dot{n}_{in,ab} \bar{h}_{in,ab} - \dot{n}_{out,ab} \bar{h}_{out,ab} - \dot{Q}_{loss,ab} = 0 \quad (3)$$

$$\dot{Q}_{loss,ab} = \dot{n}_{f,ab} \times (1 - \eta_{ab}) \times LHV \quad (4)$$

$$\eta_{ab} = f_{theoretical}/f_{actual} \quad (5)$$

$$\dot{S}_{gen,ab} = \dot{n}_{out,ab} \bar{s}_{out,ab} - \dot{n}_{in,ab} \bar{s}_{in,ab} + \frac{\dot{Q}_{loss,ab}}{T_{surr}} \quad (6)$$

4.1.3. Turbine

As was previously mentioned, the polytropic efficiency has been used instead of the isentropic efficiency (Haseli and Dincer, 2008).

$$\dot{W}_{GT} = \dot{n}_{GT} (\bar{h}_{in,GT} - \bar{h}_{out,GT}) \quad (7)$$

$$\dot{S}_{gen,GT} = \dot{n}_{GT} (\bar{s}_{out,GT} - \bar{s}_{in,GT}) \quad (8)$$

4.1.4. Fuel cell

The general solutions for the conservation of mass and energy equations of the fuel cell require the evaluation of the voltage and current generated in the cell. (Chan et al., 2002).

The full procedures for computing the cell voltage loss have

been presented in (Chan et al., 2002; Pirkandi et al., 2012; Volkan, 2007).

Due to the high operating temperatures of solid oxide fuel cells, the fuel needed by the cell can be produced within the cell from hydrocarbons such as natural gas. In this paper, a fuel cell with direct internal reforming has been used, in which the heat released from the electrochemical reaction of electrodes is utilized to carry out the endothermic reforming reaction. In computing the temperature of the gasses released from the fuel cell stack, the three heat sources in the cell should be taken into consideration. Since the reforming reaction in the cell is endothermic and the shifting and electrochemical reactions are exothermic, the net heat transfer of the solid oxide fuel cell will be obtained from the differences between the heating values of the above three reactions. The heating values resulting from the reforming (\dot{Q}_r), shifting (\dot{Q}_{sh}) and electrochemical (\dot{Q}_{elec}) reactions are obtained by means of Equations (9) through (11) (Chan et al., 2002).

$$\dot{Q}_r = x(\bar{h}_{CO} + 3\bar{h}_{H_2} - \bar{h}_{CH_4} - \bar{h}_{H_2O}) \quad (9)$$

$$\dot{Q}_{sh} = y(\bar{h}_{CO_2} + \bar{h}_{H_2} - \bar{h}_{CO} - \bar{h}_{H_2O}) \quad (10)$$

$$\dot{Q}_{elec} = zT\Delta S - I\Delta V_{loss} \quad (11)$$

$$\dot{Q}_{net} = \dot{Q}_{elec} + \dot{Q}_{sh} - \dot{Q}_r \quad (12)$$

With regards to Eq. (13), a portion of this residual net heat is used to raise the temperature of the cell's internal and outflowing gasses (\dot{Q}') and another portion enters the surrounding environment (\dot{Q}_{surr}).

$$\dot{Q}_{net} = \dot{Q}' + \dot{Q}_{surr} \quad (13)$$

In a real condition, the processes implemented in a fuel cell cannot be considered as adiabatic whatsoever; and always there is some heat loss to the surrounding atmosphere. By considering this problem as an ideal case, it is assumed that the fuel cell is internally adiabatic and that the net residual heat is used to raise the temperature of the cell's internal and outflowing gasses (\dot{Q}''). In this case, by considering the same temperature for the gasses exiting from the anode and cathode, Eq. (14) is obtained. In this equation, $\Delta h_{an,in}$ and $\Delta h_{ca,in}$ denote the enthalpy changes of reactants, and $\Delta h_{an,out}$, $\Delta h_{ca,out}$ indicate the enthalpy changes of products at the anode and cathode (Pirkandi et al., 2012).

$$\dot{Q}'' = \Delta h_{ca,in} + \Delta h_{ca,out} + \Delta h_{an,in} + \Delta h_{an,out} \quad (14)$$

To compute the temperature of the fuel cell's outflowing gasses, an iteration algorithm has been employed, and the convergence criterion has been considered as Eq. (15).

$$Q_{error} = \left| \frac{\dot{Q}'' - \dot{Q}'}{\dot{Q}'} \right| < 0.01 \quad (15)$$

After calculating the output temperature, Eq. (16) can be used to determine the amount of heat loss in the fuel cell.

$$\dot{n}_{ca,in}\bar{h}_{ca,in} + \dot{n}_{an,in}\bar{h}_{an,in} = \dot{n}_{ca,out}\bar{h}_{ca,out} + \dot{n}_{an,out}\bar{h}_{an,out} + \dot{Q}_{surr} + \dot{W}_{SOFC} \quad (16)$$

4.1.5. Recuperator

The temperatures of the gasses exiting from the first three recuperators are calculated based on their effectiveness (Haseli et al., 2008). Eqs. (17) and (18) have been used to compute the useful heating load in the last recuperator, by considering the efficiency of this recuperator.

$$\dot{Q}_{rec,g} = \epsilon_{rec,w}\dot{n}_g(\bar{h}_{in,rec} - \bar{h}_{out,rec}) \quad (17)$$

$$\dot{Q}_{rec,w} = \dot{n}_w\bar{C}_p(T_{out,w} - T_{in,w}) \quad (18)$$

By using Eq. (18), the quantity of warm water needed for the heating units in the cogeneration system (\dot{n}_w) can be determined. In this research, the temperature of the warm water coming out of the recuperator has been considered as 90° C. The amount of heating load obtained from the last recuperator is used to calculate the total thermal efficiency of the system (Haseli et al., 2008).

$$\dot{S}_{gen,rec} = \dot{n}_a(\bar{s}_{out,a} - \bar{s}_{in,a}) - \dot{n}_g(\bar{s}_{in,g} - \bar{s}_{out,g}) \quad (19)$$

4.1.6. Pump

The required pump work is obtained from Eq. (20).

$$\dot{W}_{wp} = \dot{n}_w v_w (P_{out,w} - P_{in,w}) \quad (20)$$

After exchanging its heat in the heating units, the warm water flowing out of the pump is again returned to the power generation system for reheating. (Pirkandi et al., 2012).

$$\dot{S}_{gen,wp} = \dot{n}_w(\bar{s}_{out,w} - \bar{s}_{in,w}) \quad (21)$$

4.1.7. Hybrid system

By considering the whole hybrid system as a control volume, it's electrical, thermal, total, and exergy efficiencies will be obtained. (Pirkandi et al., 2012).

$$\eta_{ele} = \frac{\dot{W}_{net}}{\dot{n}_f LHV} \quad (22)$$

$$\eta_{exergy} = \frac{\dot{W}_{net} + \dot{E}_{out,w}}{\dot{E}_{in,a} + \dot{E}_{in,f} + \dot{E}_{in,w}} \quad (23)$$

The net power output of the system is equal to the sum of the net power outputs of fuel cell and turbine, and also the energy input of the system is equal to the sum of the energies released by the utilization of fuel in the cell and afterburner chamber (Pirkandi et al., 2012).

$$\dot{W}_{net} = (\dot{W}_{AC-tot})_{SOFC} + (\dot{W}_{AC-net})_{GT} \quad (24)$$

$$(\dot{W}_{AC,net})_{GT} = (\dot{W}_{DC,net}) \times \eta_{inv,gen} - \dot{W}_{wp} - \dot{W}_{c,air} - \dot{W}_{c,fuel} \quad (25)$$

In Eq. (25), the term of $\eta_{inv,gen}$ is the direct-to-alternating current conversion factor of the micro turbine generator.

4.2. The exergy equations

A subject arising from the second law of thermodynamics is the method of exergy analysis in system modelling (Kotas, 1995; Haseli

et al., 2008). The rates of destroyed exergy and lost exergy and the irreversibility rate in the whole proposed system can be obtained from Equations (26) through (28):

$$\dot{E}_{destroyed, sys} = \dot{E}_{in,a} + \dot{E}_{in,f} + \dot{E}_{in,w} - \dot{W}_{net} - \dot{E}_{out,w} - \dot{E}_{out,gas} \quad (26)$$

$$\dot{E}_{lost,sys} = \dot{E}_{out,gas} \quad (27)$$

$$\dot{I}_{tot} = \dot{E}_{destroyed,sys} + \dot{E}_{lost,sys} \quad (28)$$

4.3. The economic equations

In order to economically optimize the energy systems, it is necessary to compare the annual expenses associated with investment, fuel, operating and maintenance. The above items are ideally considered and summarized in Eq. (29), which expresses a cost balance for the whole system (Bejan et al., 1996).

$$\dot{C}_{p,tot} = \dot{C}_{F,tot} + \dot{Z}_{tot}^{CI} + \dot{Z}_{tot}^{OM} \quad (29)$$

The sum of the expenses associated with the initial capital investment and repair and maintenance is expressed as a single parameter (\dot{Z}), according to Eq. (30) (Bejan et al., 1996).

$$\dot{Z} = \dot{Z}_{tot}^{CI} + \dot{Z}_{tot}^{OM} \quad (30)$$

In this research, the generated electricity and the natural gas have been considered as the output product and the consumed fuel of the hybrid system. Eq. (31) is the objective function in the optimization problem, in which the electricity generation cost must be minimized. In Eq. (31), c_p denotes the cost of generated electricity per unit Giga Joule.

$$c_p = \frac{\dot{C}_{F,tot} + \dot{Z}_{tot}^{CI} + \dot{Z}_{tot}^{OM}}{\dot{W}_{net}} \quad (31)$$

Usually, in thermoeconomic analysis, especially the analysis of large and complex systems, the economic modelling is the hardest part. The validity of a thermoeconomic analysis depends to a large extent on the accurate computation of \dot{Z} by the considered economic model (Bejan et al., 1996).

Considering the above notions, the simple economic model of Lazaretto and the total revenue requirement method have been used for the economic analyses performed in this research.

4.3.1. Lazaretto's simple economic model

This model is one of the simplest economic models, and it has been presented by professor Lazaretto of the University of Milan. In this model, the sum of the initial capital investment and the operating and maintenance costs has been formulated according to Eq. (32) (Bejan et al., 1996).

$$\dot{Z}_k = CRF \frac{\Phi_r}{3600 N} PEC_k \left[\frac{\$}{s} \right] \quad (32)$$

In the above equation, PEC_k is the initial purchase cost of the k th equipment (which is calculated based on the thermodynamic parameters (Santin et al., 2010)), Φ_r is the operating and maintenance cost (1.06–1.1), N is the total annual operating hours of the system under full load (85% of total work capacity, and equal to 7446 h), and CRF is the capital recovery factor. The capital recovery factor, as has been indicated in Eq. (33), is itself a function of the interest rate

(i) and the number of years the machineries have been in operation (n), and it is calculated based on the values of these two parameters (Bejan et al., 1996). In thermoeconomic analyses, the CRF normally has a range of 0.147–0.18. In Eq. (33), the interest rate or the discount factor has been considered in the range of 0.1–0.12.

$$CRF = \frac{i(1+i)^n}{(1+i)^n - 1} \quad (33)$$

4.3.2. The economic model of the total revenue requirement method

The total revenue requirement approach has been used in this section for the economic analysis of the system. In this method, based on the economic hypotheses, the equipment and land purchase costs, cost of engineering services, facilities construction cost, fuel cost, repair, maintenance costs and so on are computed and levelized on an annual basis over the system's operating period (Bejan et al., 1996). In this model, the sum of the initial capital investment cost and the costs associated with operating and maintenance has been expressed by Eq. (34) (Bejan et al., 1996).

$$\dot{Z}_k = \frac{CC_L + OMC_L}{\tau} \times \frac{PEC_k}{\sum_k PEC_k} \quad (34)$$

$$CC_L = TRR_L - FC_L - OMC_L \quad (35)$$

The levelized annual total revenue requirement (TRR_L) is determined by applying the capital recovery factor and the discount factor, according to Eq. (36) (Bejan et al., 1996):

$$TRR_L = CRF \sum_{j=1}^n \frac{TRR_j}{(1+i)^j} \quad (36)$$

In the above equation, TRR_j is the total revenue requirement in the j th year of system operation; and the detailed procedure regarding its computation has been given in (Cheddie and Murray, 2010a). After determining the mentioned costs according to Eqs. (37) through (39), the annual price of electricity generated by the system and the annual levelized costs are computed (Cheddie and Murray, 2010a).

$$\dot{Z}_{tot} = \dot{Z}_{tot}^{CI} + \dot{Z}_{tot}^{OM} = \frac{CC_L + OMC_L}{\tau} \quad (37)$$

$$\dot{C}_{p,tot} = \frac{CC_L + OMC_L + FC_L}{\tau} = \frac{TRR_L}{\tau} \quad (38)$$

$$c_p = \frac{TRR_L}{\tau \times \dot{W}_{tot}} \quad (39)$$

The purchase, installation, and start-up costs of a power generation unit are obtained by Eq. (40).

$$c_{pp} = \frac{PEC_{tot} + 0.46PEC_{tot}}{\dot{W}_{tot}} \quad (40)$$

5. The solution method

In view of the equations mentioned in the preceding sections, a computer program has been written for analysing the problem. The first part of this computer code contains the combined system's input information including its working pressure and the flow rates

of air and fuel entering the system. At this point, because of the cell's working temperature not being constant, an arbitrary cell temperature is initially guessed. Using this guesstimated cell temperature, in the next step, the nonlinear reforming and electrochemical equations along with the cell's thermal equations are solved simultaneously, and the desired outcomes including the amounts of produced chemical components and the values of temperature, voltage loss, real voltage, current, power, efficiency, and other considered parameters in the fuel cell are obtained. The equations of the other system components are also analysed along with the fuel cell equations. After analysing the whole system, the new cell temperature is determined by considering the given conditions. In case the convergence condition of the cycle is not fulfilled, the analysis will be repeated with a new temperature. Following the thermodynamic analyses, economic analyses are also carried out for the system in the final section.

6. Validation

To validate the prepared computer code, the system introduced by (Shirazi et al., 2010) has been modelled and its findings have been compared with the results obtained from the present code. The close agreement between these results in Table 1 validates the present method and the developed code. In the performed modelling, the cell's working temperature and the temperature of the turbine's inflowing gasses have been considered as 1175 and 1457.2 K. The slight discrepancy between the results of the written code and those of Shirazi is due to the way by which the cell's concentration voltage loss is calculated. Shirazi et al. had assumed a constant limit current density in calculating this voltage loss; while in the present research, the amount of limit current density has been computed.

7. Results

The fuel cell used in this research is of the tubular solid oxide type (similar to the model manufactured by the Siemens-Westinghouse Co.) (Ciesar, 2001), and its specifications along with its other constant parameters have been presented in Table 2. Also, the constant parameters used for the equipment of the hybrid system have been considered based on the sample analysed in

Table 1
Comparing the results of the present code with the numerical results of (Shirazi et al., 2010).

Parameters	(Shirazi et al., 2010) Results	Present Work
Fuel Cell Voltage (V)	0.729	0.735
Air Compressor Work (kW)	303.8	302
Fuel Compressor Work (kW)	27.1	26.5
Net. Turbine Work (kW)	376.8	377.2
Net. Fuel Cell Work (kW)	1738.04	1741
Heat Regeneration (kW)	727	725.8
Electrical Efficiency (%)	61.3	62.2
Total Efficiency (%)	82.1	83.5

Table 2

Assumed parameters of the fuel cell (Ciesar, 2001).

Parameter	Amount of assumed
Length of each cell	150 cm
Diameter of each cell	2.2 cm
Number of cell	5133
Fuel Utilization Ratio	0.85
Fuel cell pressure loss	4%
Inventor efficiency	89%

(Haseli and Dincer, 2008).

In the following, the performances of the four proposed hybrid systems have been compared. For a better evaluation, this comparison has been carried out for two cases. In the first case, the same area has been considered for the stack of fuel cells used in all the proposed configurations and in the second case, the area of the fuel cells used in the systems with two stacks of cells has been halved. The electrical efficiency, price of the generated electricity, and the purchase, installation and start-up cost of the hybrid systems are the parameters examined in this section. In all the analyses of this section, the temperature of the inflowing turbine gasses has been assumed as 1200 °C.

7.1. Using fuel cells with the same cell area in all the considered design configurations

In this section, the same selected cell areas have been considered for all the fuel cells in the four hybrid systems. The diagrams comparing the performances of all four hybrid systems in this case have been presented in Figs. 6 through 10. As is observed in Fig. 6, the electrical efficiency of the hybrid systems with two fuel cells is higher than that of single-cell systems. The results show that the fourth design enjoys the highest electrical efficiency (55%) and the second design has the least efficiency (49%).

The other important parameter that should be considered in the analysis of energy systems is their irreversibility rate. Systems with the least irreversibility rates have an adequate performance and are preferred over the other system designs. As is observed in Fig. 7, the least irreversibility rates are associated with the hybrid systems

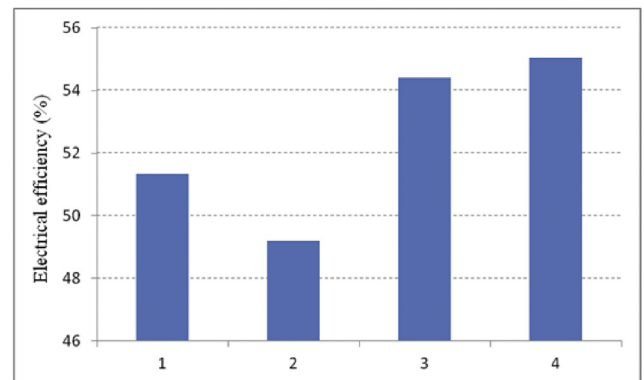


Fig. 6. Comparing the electrical efficiencies of various hybrid systems.

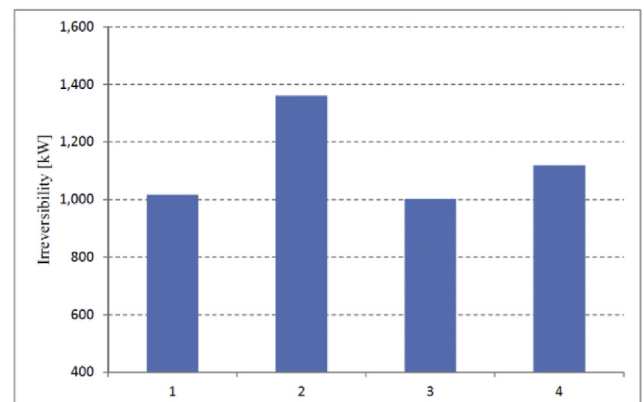


Fig. 7. Comparing the irreversibility rates of various hybrid systems.

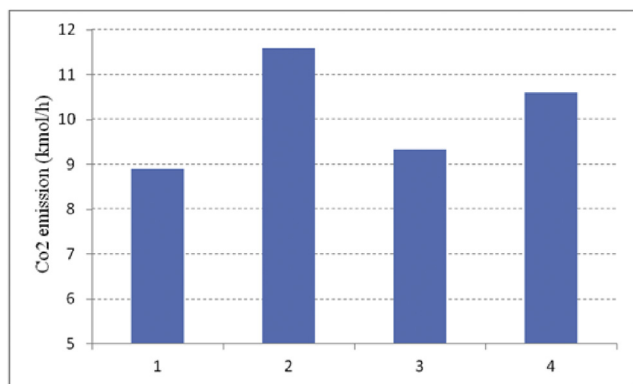


Fig. 8. Comparing the amounts of emission produced by various hybrid systems.

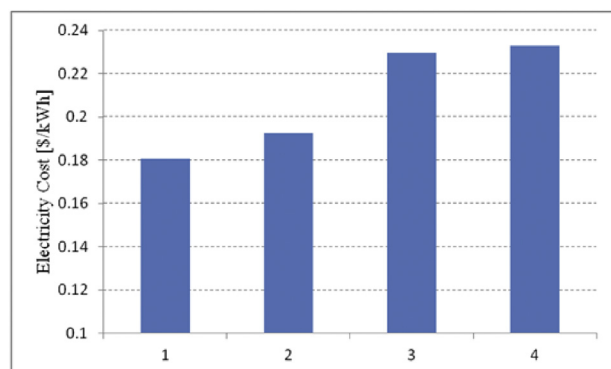


Fig. 9. Comparing the prices of the electricity generated by various hybrid systems.

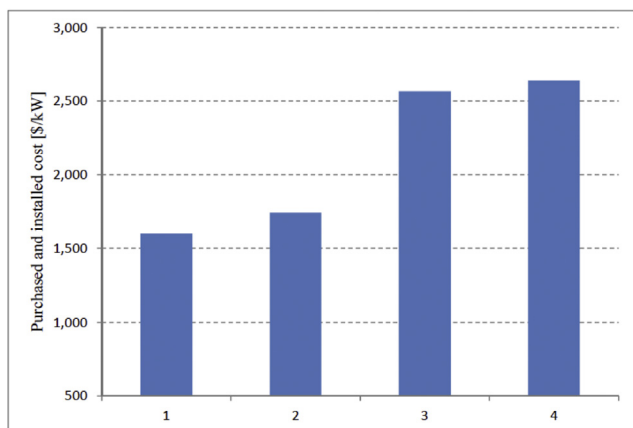


Fig. 10. Comparing the purchase, installation and start-up costs of various hybrid systems.

with pressurized fuel cells (first and third designs). According to this figure, the second configuration has the greatest irreversibility rate and is considered as an inefficient design. Regarding the emission levels produced by various hybrid systems, the systems with pressurized fuel cells have a better performance.

Another important parameter in choosing an optimal system is its low price of generated electricity and the low initial costs associated with equipment purchase, installation and start-up. In this regard, the economic performances of the four proposed designs have been compared in Figs. 9 and 10. As is observed in these two figures, considering the similarity of fuel cell stacks in the proposed schemes, the price of electricity generated by them and also their purchase, installation and start-up cost in the third and fourth designs are high. These configurations, despite having a higher electrical efficiency, are not cost-effective economically. The findings indicate that for each kilowatt of generated electricity, the equipment purchase, installation and start-up cost for hybrid systems with two fuel cells is about \$1000 higher than that for single-cell hybrid systems; and the main reason for this is the use of two

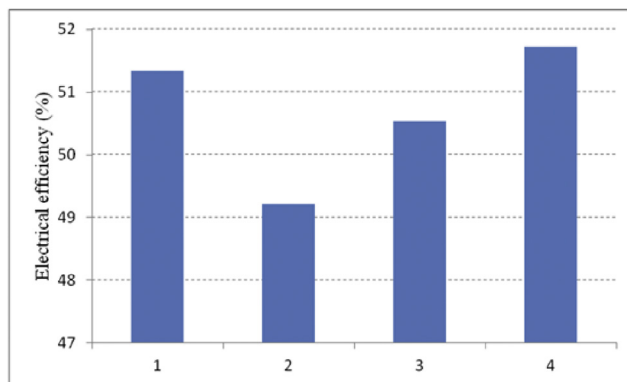


Fig. 11. Comparing the electrical efficiencies of various hybrid systems.

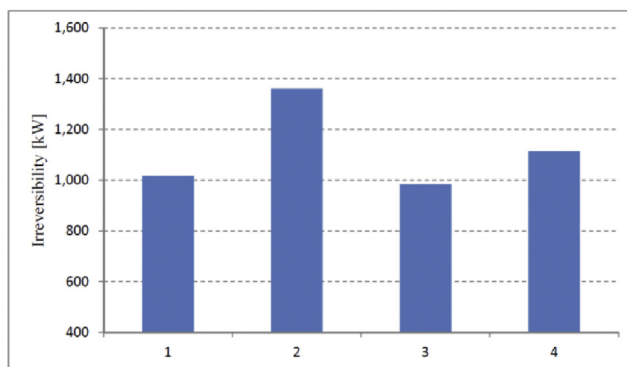


Fig. 12. Comparing the irreversibility rates of various hybrid systems.

Table 3

Comparing the performances of the direct hybrid systems with a constant cell area.

Design configuration	1	2	3	4
System layout	Direct with one pressurized fuel cell	Direct with one atmospheric fuel cell	Direct with two pressurized fuel cell	Direct with one pressurized and one atmospheric fuel cell
Electrical efficiency	o	—	+	+
Irreversibility rate	+	—	+	o
Emission	+	—	+	o
Electricity generation price	+	o	—	—
Purchase, installation and start-up cost	+	o	—	—

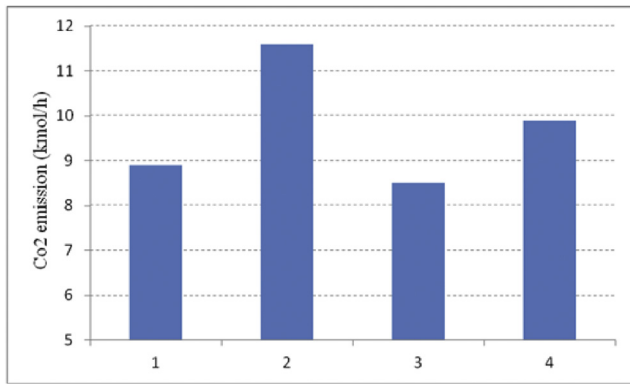


Fig. 13. Comparing the amounts of emission produced by various hybrid systems.

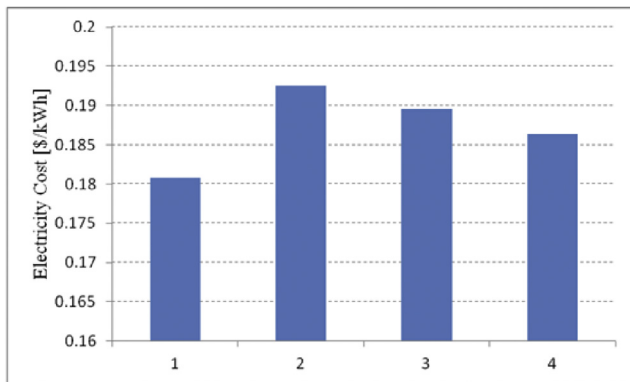


Fig. 14. Comparing the prices of electricity generated by various hybrid systems.

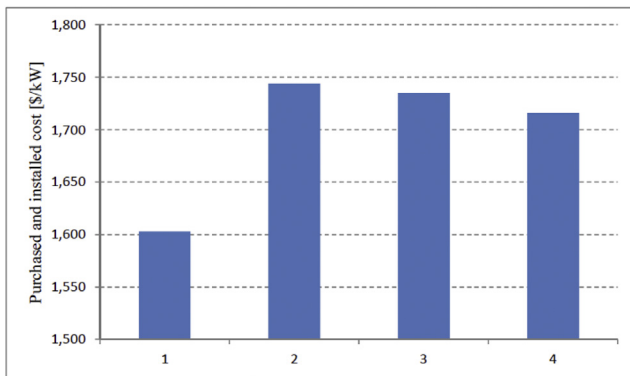


Fig. 15. Comparing the purchase, installation and start-up costs of various hybrid systems.

fuel cells in the structure of the former hybrid systems.

The results of this section have been summarized in Table 3. The performance of each system has been indicated by one of the three grades: appropriate (+), acceptable (O) and inappropriate (–). As is observed in this table, the first, third, fourth and second design configurations constitute the optimal hybrid systems in that order. In case of using the same fuel cells in all four design schemes, the direct hybrid system with one pressurized cell will generally have an appropriate performance. The findings indicate that the third and fourth designs, despite having a high efficiency, are not cost-effective, since they use two fuel cells in their configuration. In the next section, by reducing the areas of the fuel cells used in these two designs, the performances of all the direct hybrid systems are re-evaluated.

7.2. Using fuel cells with a reduced cell area in the third and fourth design schemes

As was mentioned in the preceding section, one of the major drawbacks of hybrid systems with two fuel cells is the high price of electricity generated by them and also the high initial costs associated with the equipment purchase, installation and start-up of these systems. In this section, instead of using two high-capacity fuel cell stacks, two cells with lower capacities have been used in the third and fourth designs. The performance diagrams pertaining to all four hybrid systems have been compared in Figs. 11 through 15. As is observed, by reducing the areas of the fuel cells, the electricity generation cost and also the purchase, installation and start-up cost of the third and fourth designs diminish considerably. The findings indicate that with regards to the 50% reduction in the capacity of the fuel cells in the mentioned designs, the first configuration is still economically attractive and has a low electricity generation price and secondary costs. Reducing the capacities of the fuel cells in the third and fourth designs causes another important drawback: the reduction of the electrical efficiency of the system. Another point which is again observed in this section is the inefficiency of the second design. The direct hybrid system with one atmospheric fuel cell has a low electrical efficiency and irreversibility rate and high emission, and the price of the electricity generated by this system is higher compared to the other proposed systems.

The results of this section have been presented in Table 4. As is observed, the first, fourth, third and second design configurations are sequentially ranked as the optimal hybrid systems.

In view of the obtained results, it can be concluded that the direct hybrid system with one pressurized fuel cell enjoys the highest performance among the other hybrid systems. A lower emission, smaller irreversibility rate, low purchase, installation and start-up cost and a suitable price of generated electricity are the advantages of this system. Among the four introduced systems, the

Table 4

Comparing the performances of the direct hybrid systems with optimized cell areas.

Design configuration	1	2	3	4
System layout	Direct with one pressurized fuel cell	Direct with one atmospheric fuel cell	Direct with two pressurized fuel cell	Direct with one pressurized and one atmospheric fuel cell
Electrical efficiency	+	–	o	+
Irreversibility rate	+	–	+	o
Emission	+	–	+	o
Electricity generation price	+	–	o	o
Purchase, installation and start-up cost	+	–	–	o

direct hybrid system with one atmospheric fuel cell is the least efficient system.

8. Conclusion

In investigating the four types of direct hybrid systems it was found that the direct hybrid system with one pressurized fuel cell performs better than the other hybrid systems. The advantages of this system include lower emission, smaller irreversibility rate, lower equipment purchase, installation and start-up costs, and adequate price of generated electricity. The direct hybrid system with one atmospheric fuel cell has a low electrical efficiency and irreversibility rate and high emission, and its electricity generation cost is higher than that of the other proposed systems. Despite having a higher electrical efficiency, the third and fourth configurations are not economically cost-effective, and their equipment purchase, installation and start-up costs as well as the price of electricity generated by them are higher. The main reason is the use of two fuel cells in the configuration of the hybrid system. The obtained results indicate that by reducing the areas of the fuel cells, the price of the generated electricity and the relevant expenses can be reduced to some extent. The obtained results indicate that the total efficiency and electrical efficiency of the direct hybrid system with a pressurized fuel cell are roughly 64% and 51%, respectively. Close to 80% of the hybrid system's power is supplied by the fuel cell. Thermo-economic analysis results also show that the price of the generated electricity is about USD 11.6 cents/kWh, based on the simple Lazaretto model, and USD 18.5 cents/kWh, based on the complete economic model of TRR. Also, the purchase, installation and start-up cost of the hybrid system is about \$1692/kW, which is almost twice the cost of a gas turbine unit.

References

- Araki, T., Ohba, T., Takezawa, Sh., Onda, K., Sakaki, Y., 2006. Cycle analysis of planar SOFC power generation with serial connection of low and high temperature SOFCs. *J. Power Sources* 158, 52–59.
- Arsalis, A., 2008. Thermo-economic modeling and parametric study of hybrid SOFC–gas turbine–steam turbine power plants ranging from 1.5 to 10 MW. *J. Power Sources* 181, 313–326.
- Arsalis, A., 2007. Thermo-economic Modeling and Parametric Study of Hybrid Solid Oxide Fuel Cell – Gas Turbine – Steam Turbine Power Plants Ranging from 1.5 MW to 10 MW. M.Sc. thesis. Virginia Polytechnic Institute and State University.
- Bejan, A., Tsatsaronis, G., Moran, M., 1996. Thermal design and Optimization. John Wiley & Sons, Canada.
- Brouwer, J., 2006. Hybrid Gas Turbine Fuel Cell Systems. National Fuel Cell Research Center, University of California. See also URL: <http://www.nfrcr.uci.edu>.
- Buonomano, A., Calise, F., Dentice, M., Palombo, A., Vicidomini, M., 2015. Hybrid solid oxide fuel cell-gas turbine systems for combined heat and power. *J. Appl. Energy* 156, 32–85.
- Chan, S.H., Ho, H.K., Tian, Y., 2002. Modeling of simple hybrid solid oxide fuel cell and gas turbine power plant. *J. Power Sources* 109, 111–120.
- Cheddie, D.F., Murray, R., 2010a. Thermo-economic modeling of a solid oxide fuel cell/gas turbine power plant with semi-direct coupling and anode recycling. *J. Hydrogen Energy* 35, 11208–11215.
- Cheddie, D.F., 2011. Thermo - economic optimization of an indirectly coupled solid oxide fuel cell/gas turbine hybrid power plant. *J. Hydrogen Energy* 36, 1702–1709.
- Cheddie, D.F., Murray, R., 2010b. Thermo-economic modeling of an indirectly coupled solid oxide fuel cell/gas turbine hybrid power plant. *J. Power Sources* 195, 8134–8140.
- Ciesar, J.A., 2001. Hybrid Systems Development by the Siemens Westinghouse Power Corporation. Presented by Siemens Westinghouse Power Corporation. Natural Gas/Renewable Energy Hybrids Workshop. United State department of energy, Pennsylvania.
- Cheddie, Denver F., 2010. Integration of a solid oxide fuel cell into A 10 MW gas turbine power plant. *J. Energies* 3, 754–769.
- Ebrahimi, M., Moradpoor, I., 2016. Combined solid oxide fuel cell, micro-gas turbine and organic Rankine cycle for power generation (SOFC–MGT–ORC). *J. Energy Convers. Manag.* 116, 120–133.
- Facchinetti, E., Favrat, D., Marechal, F., 2014. Design and optimization of an innovative solid oxide fuel cell–gas turbine hybrid cycle for small scale distributed generation. *J. Fuel Cells* 14 (4), 595–606.
- Hall, J., Kerr, R., 2003. Innovation dynamics and environmental technologies: the emergence of fuel cell technology. *J. Clean. Prod.* 11, 459–471.
- Haseli, Y., Dincer, I., 2008. Thermodynamic modeling of a gas turbine cycle combined with a solid oxide fuel cell. *J. Hydrogen Energy* 33 (20), 5811–5822.
- Haseli, Y., Dincer, I., Naterer, G.F., 2008. Thermodynamic analysis of a combined gas turbine power system with a solid oxide fuel cell through exergy. *J. Thermochim. Acta* 480, 1–9.
- Kotas, T., 1995. The Exergy Method of Thermal Plant Analysis. Krieger Publishing Company, USA, Florida.
- Kuchonthara, P., Bhattacharya, S., Tsutsumi, A., 2003. Combinations of solid oxide fuel cell and several enhanced gas turbine cycles. *J. Power Sources* 124, 65–75.
- Lorenzo, G., Fragiocomo, P., 2015. Energy analysis of an SOFC system fed by syngas. *J. Energy Convers. Manag.* 93, 175–186.
- Meratizaman, M., Monadizadeh, S., Amidpour, M., 2014. Techno-economic assessment of high efficient energy production (SOFC–GT) for residential application from natural gas. *J. Nat. Gas Sci. Eng.* 21, 118–133.
- Musa, A., Paape, M., 2008. Performance of combined internally reformed intermediate high temperature SOFC cycle compared to internally reformed two-staged intermediate temperature SOFC cycle. *J. Hydrogen Energy* 33, 4665–4672.
- Pirkandi, J., Ghassemi, M., Hamed, M.H., Mohammadi, R., 2012. Electrochemical and thermodynamic modeling of a CHP system using tubular solid oxide fuel cell (SOFC–CHP). *J. Clean. Prod.* 29–30, 151–162.
- Saisirirat, P., 2015. The solid oxide fuel cell (SOFC) and gas turbine (GT) hybrid system numerical model. *J. Energy Proced.* 79, 845–850.
- Santin, M., Traverso, A., Magistri, L., Massardo, A., 2010. Thermoeconomic analysis of SOFC–GT hybrid systems fed by liquid fuels. *J. Energy* 35, 1077–1083.
- Shirazi, A., Aminyavari, M., Najafi, B., Rinaldi, F., Razaghi, M., 2010. Thermal-economic-environmental analysis and multi-objective optimization of an internal-reforming solid oxide fuel cell-gas turbine hybrid system. *J. Hydrogen Energy* 37, 19111–19124.
- Tarroja, A., Muelle, R.F., Maclay, J., Brouwe, J., 2010. Parametric thermodynamic analysis of a solid oxide fuel cell gas turbine system design space. *J. Eng. Gas Turbines Power* 132, 72301–723011.
- Volkan, A., 2007. Electrochemical model for performance analysis of a tubular SOFC. *J. Energy Res.* 31, 79–98.
- Zhang, X., Chan, S.H., Li, G., Ho, H.K., Li, J., Feng, Z., 2010. A review of integration strategies for solid oxide fuel cells. *J. Power Sources* 195, 685–702.